Development and application of luminescence dating of cobbles from glaciofluvial sediments

Geraint Thomas-Howard Jenkins

Abstract

The aim of this thesis is to develop and test the luminescence dating of cobbles from glaciofluvial sediments. In recent years luminescence dating has increasingly been applied to date glaciofluvial sediments, but uncertainties about the degree of bleaching of the luminescence signal make dating challenging. Sub-surface luminescence measurements from cobbles from well-bleached environments are able to confirm that the cobbles were well-bleached at deposition. Having this confirmation when studying heterogeneously bleached environments would be a significant advantage.

Bleaching experiments are undertaken to assess if numerical models of bleaching with depth are correct in nature. Measurements confirm that as the length of exposure increases the luminescence signal is reset to greater depths. Cobbles obtained from Orrisdale Head, Isle of Man, show significant sub-surface bleaching, with rock slices to depths of 12 mm into the cobble sub-surface having been completely bleached at deposition. Fading-corrected $IRSL_{50}$ ages (20.7 ± 1.3 ka) agree with independent age control at the site. One cobble also appears to show both the advance (26.2 ± 0.3 ka) and retreat of the Irish Sea Ice Stream. A major advantage of applying luminescence dating to cobbles instead of sand-sized grains is that at depths of > 2 mm into the cobble 92 % of the dose rate comes from the cobble itself and this makes luminescence ages insensitive to water content.

In further tests of this approach, cobbles from two locations in north Wales show limited sub-surface bleaching, however the $IRSL_{50}$ ages from the surface slices agree with independent age control. Following the trial at locations with independent age control, cobbles are obtained from a deposit at Bridgwalton which marks the furthest extent of a separate ice lobe which occupied the Cheshire-Shropshire basin. The $IRSL_{50}$ age (25.3 ± 1.6 ka) gives the first depositional age for this location and shows that the Last Glacial Maximum (LGM) at this site is synchronous with that observed for the Irish Sea ice stream at the Scilly Isles. Luminescence dating of cobbles has an enormous potential in providing accurate and robust ages for glaciofluvial sediments that are challenging to date.

Acknowledgments

The research conducted for this PhD was supported by an Aberystwyth University DCDS Scholarship which the student is eternally grateful for,

Firstly, I would like to thank Professor Geoff Duller. His application to research was something that I had not experienced before, and the opportunity to learn from this has been invaluable. Maybe I will appreciate this even more when I have moved on…. I would also like to thank Professor Neil Glasser who provided fantastic feedback throughout my project. It was his book (Glacial Geology) that started my interest ~ 8 years ago in everything glacial and rocky. Also, many thanks go to Professor Helen Roberts who provided fantastic feedback and has always worked to ensure that my research has been as rigorous as possible.

Outside of my direct supervision I have to thank Professor Richard Chiverrell for his fantastic guidance in-field, Dr Rachel Smedley for her experience in all things PhD and glacial and Hollie Wynne for all of her help (and patience) in the laboratory.

I have to thank Debra Colarossi, Melissa Chapot, Robyn Pinder, Svenja Riedesel, Xianjiao Ou and countless other individuals who I have probably over looked (and of course Anna Bowen) who have all made my postgraduate experience (outside of supervisory meetings) an enjoyable one.

Last, but not least – I would like to thank my wife, mother, father and sister. If I have had many sleepless nights, I dread to think how many I've caused for them….

Contents

List of Figures

List of Tables

Let us probe the silent places, let us seek what luck betide us;
Let us journey to a lonely land I know.
There's a whisper on the night-wind, there's a star agleam to guide us,
And the Wild is calling, calling . . . let us go.

1. Introduction & Literature Review

1.1. Introduction to thesis

Reconstructing the former positions and timing of past ice sheets is essential. This is because information recorded in the palaeo record can inform present day predictions of ice mass loss and ice dynamics of large ice sheets such as Antarctica and Greenland (Stokes and Clark, 2001). Geomorphological and sedimentological investigations, however, need to be coupled with a reliable chronological technique to establish the precise timings of advance and recession. Providing accurate retreat ages can be difficult for glacial sediments, partly due to the lack of organic material for radiocarbon dating (Fuchs and Owen, 2008). The dating of inorganic material (sand grains) using luminescence dating can circumvent this issue, however, many challenges still remain, including the fact that, generally, only a small proportion of the sediment grains measured are exposed to daylight sufficiently at deposition to completely reset the luminescence signal (Duller, 2006).

However, instead of using sand-sized grains a novel approach is to use large clasts (or cobbles) to provide depositional ages. This approach has the advantage that measurements at different depths into the cobble sub-surface can show if the sample was completely bleached at deposition and thereby gives greater confidence in the ages

produced (Sohbati *et al*., 2012a; 2012b; Sohbati *et al*., 2015). In some circumstances it has even been shown that measurements of luminescence at different depths can reveal multiple episodes of bleaching and burial and record multiple geomorphological events (Freiesleben *et al*., 2015). In glacial environments, where heterogeneous bleaching is likely to be a problem, the ability to determine whether a cobble was completely bleached, prior to burial, offers an advantage over sand-sized luminescence dating.

This thesis aims to build on previous cobble luminescence dating research (which has largely focused on single samples from well-bleached environments) to assess if cobbles can be used to reliably date glacial deposits, and if so, if cobbles can provide any advantages compared with luminescence dating based on sand-sized grains. This study, therefore, aims to be the first to date glacial sediments using cobbles. This research comes at a time when the NERC funded consortium BRITICE-CHRONO is establishing the retreat ages for large swathes of the British-Irish Ice Sheet (e.g. Evans *et al*., 2017; Smedley *et al*., 2017a) and drawing on the geochronological technique of luminescence dating of glaciofluvial sand-sized sediments.

1.2. Literature review

1.2.1. Luminescence dating

Luminescence dating is a geochronological technique which records the last time that mineral grains (primarily quartz and feldspar) were exposed to daylight (Duller, 2008a; Rhodes, 2011). When mineral grains become buried they then store energy from ionising radiation within their crystalline structures and release this when stimulated by light (or heat). Measurements of the emitted luminescence signal from the minerals can then be used to establish the total amount of stored energy (equivalent dose) and when this is divided by the amount of radiation delivered to the dosimeter annually (dose rate)

this will give the amount of time which the mineral has been receiving radiation (and, therefore, the burial period).

$$\text{Age (years)} = \frac{\text{Equivalent dose } (D_e) \text{ (Gy)}}{\text{Dose rate (Gy/year)}} \qquad \text{(Equation 1.1)}$$

Energy is stored within minerals when electrons become trapped at defect sites within the crystalline structures (Duller, 2008a). Such defects can be either structural or chemical impurities within the crystal (Preusser *et al*., 2009). An energy-level diagram is illustrated in Figure 1.1 and shows the processes occurring within the crystal. Radiation interacts with the crystal and provides energy to electrons which then become raised into the conduction band ('Irradiation' stage in Figure 1.1; Duller, 2008a). Following movement through the conduction band they can then become trapped in 'trapping centres' (T_1 and T_2 on Figure 1.1). At a later time, electrons can be released (stage (iii) in Figure 1.1) and this results in a loss of energy which can be emitted in the form of a photon of light.

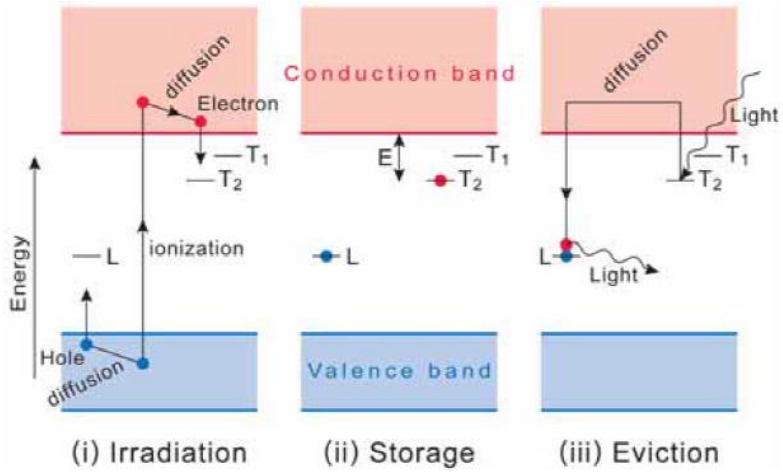

Figure 1.1. Energy schematic illustrating (i) the effect of radiation interacting with the mineral (and crystal structure) which results in the excitation of electrons into the conduction band. (ii) Electrons then become trapped at defect sites (T_1 and T_2), (iii) the crystal is then stimulated and releases electrons. These then recombine with holes at luminescence centres and emit photons of light (Duller, 2008a).

Once a stimulating light is turned on, traps are emptied and the recorded signal decreases, showing a 'decay curve'. A preheat to the sample is applied before optical stimulation and this is necessary because preheating removes the unstable signal (those higher up the energy level diagram (e.g. T_1 in Figure 1.1), and allows subsequent luminescence measurements to just sample electrons from more stable traps (Duller, 2008a).

To establish a depositional age it is essential that the dosimeter (i.e. the mineral grain) is exposed prior to becoming buried so that electrons trapped within the crystalline structure are emptied and this can occur through heating, light exposure and even pressure (resulting from the subglacial pressure upon mineral grains beneath a glacier) (Bateman *et al*., 2012; 2018).

Once sediment grains (the dosimeter) are buried they become exposed to natural ionizing radiation from the surrounding environment and this results in charge accumulating within the minerals. Ionizing radiation to the samples is associated with the decay of K, Rb, U and Th and also the contribution from cosmic rays. The dose delivered to the sediment grains is dependent on the concentrations of K, Rb, U and Th not only in the surrounding environment, but also from the individual mineral grains themselves (in the case of feldspars). The rate of radiation from the surrounding environment and individual mineral grains can be determined in the laboratory and is termed the dose-rate (and is measured in Grays per thousand years (Gy/ka) (Equation 1.1)). Following collection and sample preparation the mineral grains are then stimulated in the laboratory to measure the amount of trapped charge within the mineral grains. The stimulation by light results in electrons being evicted from traps and some recombine with trapped holes at the luminescence centres which produces a photon of light. The various steps involved in establishing a luminescence age are illustrated in Figure 1.2.

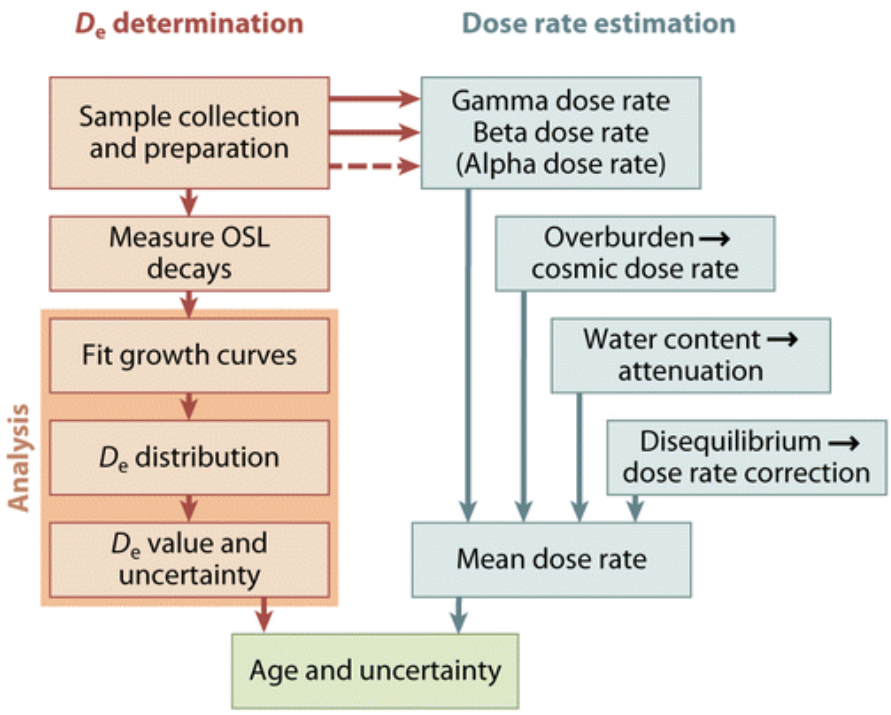

Figure 1.2. Illustration of the steps required to establish an OSL ages (Rhodes, 2011) with D_e determination illustrated in the left column and dose rate estimation in the right column.

1.2.2. Feldspars and anomalous fading

As previously outlined, the two primary minerals used in the luminescence dating of sediments are quartz and feldspar (Duller, 2008a). Typically quartz minerals have been measured and this is due to the stability of the luminescence signal (Duller, 2008a), however, recent corrections for the anomalous fading of feldspars, and the discovery of a more stable feldspar signal has resulted in an increase in interest in the use of feldspars (Thomsen *et al*., 2008; Buylaert *et al*., 2009). One benefit of using feldspars is that the mineral is generally more sensitive (the amount of luminescence emitted per unit of dose) than quartz. Single quartz grains from glaciofluvial sediments from Chile investigated by Duller (2006) showed that only ~ 0.5 % of grains could be detected whereas those

measured by Smedley *et al*. (2016) for single grains of feldspar show that 6 – 30 % of the total number of grains analysed were used to provide equivalent doses.

Challenges of using feldspar minerals in luminescence dating however include the stability of the signal and the decreased sensitivity. Feldspar minerals suffer from the effects of anomalous fading whereby the signal can deplete athermally over time (Wintle, 1973). This means that when the feldspar mineral grains are buried and accumulating charge due to environmental radiation, some of this signal is lost, even from traps where kinetics suggest that they should be stable over hundreds, thousands or millions of years. Jain and Ankjærgaard (2011) have built upon previous investigations (Poolton *et al*., 2002) of instability within feldspar minerals and have produced a model to explain feldspar luminescence (Figure 1.3) which differs from the model given in Figure 1.1. The feldspar model proposes that unstable signals are a result of ground-state tunnelling (Transition A in Figure 1.3) whereby electron-hole recombination occurs during burial of the mineral grains and does not involve excitation of charge out of the traps and into the conduction band and this is the process responsible for anomalous fading. Infra-red (IR) stimulation in the laboratory results in a transition to the excited state and from this state it is possible that rapid recombination of electron-hole pairs occurs (Transition B in Figure 1.3). This means that pairs that would normally take longer time periods to recombine can do so whilst stimulating with IR.

If rates of fading can be quantified then it is plausible that corrections can be made for the unstable part of the IRSL signal. As fading occurs logarithmically, over time, measurements can be made in the laboratory and then extrapolated over geological timescales (Huntley and Lamothe, 2001). The loss of signal due to fading is given as a g-value (%/decade) and is normalised to 2 days (Auclair *et al*., 2003). Fading is measured by irradiating samples and storing for different time periods (Figure 1.4).

To minimise the effect of anomalous fading, Thomsen *et al*. (2008) proposed making a second IR stimulation at a higher temperature (following initial IR stimulation) which excites remaining electrons into higher states (Transition C in Figure 1.3) and they can then access distant hole traps (Thomsen *et al*., 2008). This distance ensures that the probability of recombination when buried (fading) is significantly reduced (Figure 1.3). Thomsen *et al*. (2008) and Buylaert *et al*. (2012) have shown that an initial infrared (IR) stimulation, followed by a high-temperature post IR IRSL stimulation alleviates the problems associated with anomalous fading, leading to lower g-values (Figure 1.4). However, one drawback is that the post-IR IRSL signal is less sensitive to bleaching than the $IRSL_{50}$ signal (Figure 1.5) which is a potential challenge when using the post-IR IRSL method for dating poorly-bleached sediments.

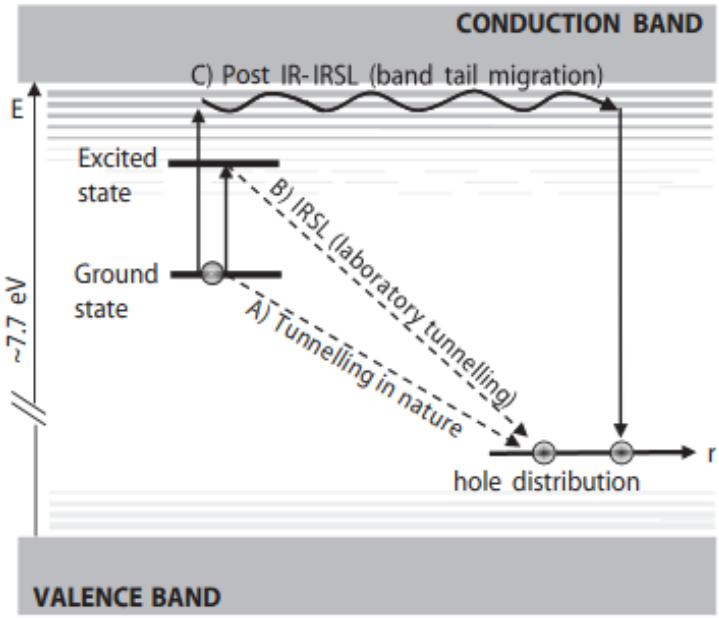

Figure 1.3. Schematic of the model for feldspar luminescence (Buylaert *et al*., 2012) illustrating 3 possible ways in which charge in the ground state of a trap may move to recombine with a hole and generate luminescence (A, B and C).

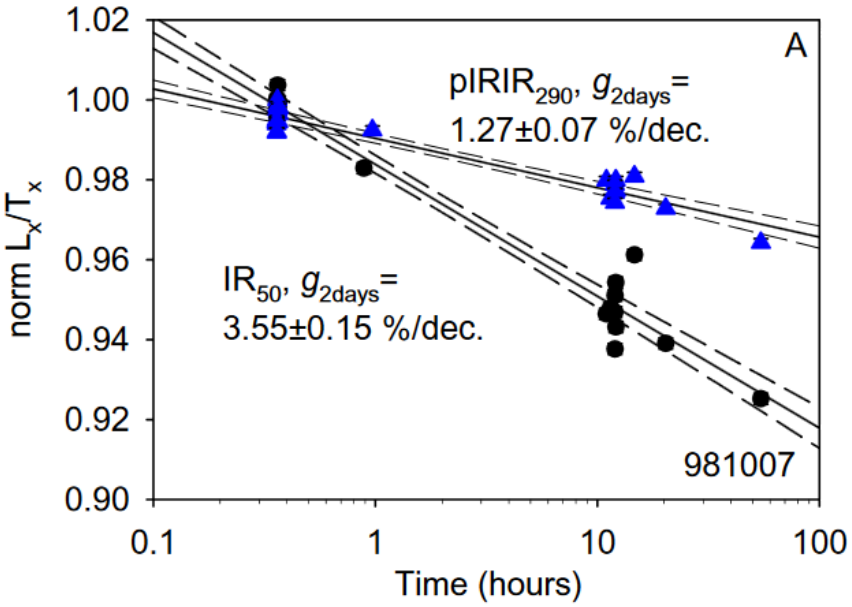

Figure 1.4. Example of g-value measurements made by Buylaert *et al.* (2012) for the $IRSL_{50}$ (black circles) and the post-IR $IRSL_{290}$ signals (blue triangle) on a single aliquot. The data shows that the g-value for the $IRSL_{50}$ signal is greater (3.55 ± 0.15 %/decade) (due to athermal loss) compared to the lower g-value for the more stable post-IR $IRSL_{290}$ signal (1.27 ± 0.07 %/decade).

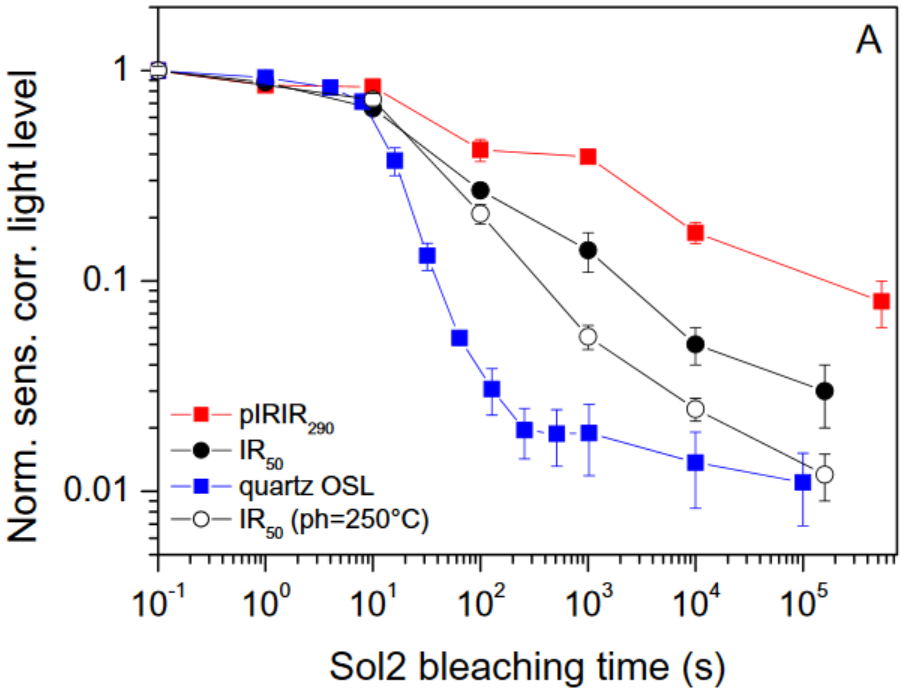

Figure 1.5. Example of changes in the bleaching rates between quartz, $IRSL_{50}$ and post-IR $IRSL_{290}$ signals (Buylaert *et al.*, 2012). Here, the remaining normalised luminescence signal is illustrated against time within a solar simulator and this shows that quartz bleaches quicker than both the $IRSL_{50}$ and post-IR $IRSL_{290}$ signals.

1.2.3. Luminescence dating of glaciofluvial sediments and the associated challenges

Luminescence dating using sand-sized grains of quartz or feldspar has been applied in recent years and many of the ages that have been determined underpin our understanding of ice sheet dynamics (Svendsen *et al*., 2004; Thomas *et al*., 2006a; Smedley *et al*., 2016; Smedley *et al*., 2017a). However, the application of luminescence dating to glaciofluvial sediments is challenging due to the decreased likelihood of sufficient bleaching of the mineral grains during glacial transportation processes (Duller, 1994; Duller, 2008b). However, from the range of glacial systems, glaciofluvial or proglacial outwash are the most likely environments to provide well-bleached sediment and, therefore, research has been focused here (Richards *et al*., 2000; Duller, 2006). The turbulence and turbidity of glaciofluvial channels has been cited as a primary cause for a lack of well-bleached material (Gemmell, 1997; Thrasher *et al*., 2009a), however some grains transported at the top of the water column may have been well-bleached. This potentially results in the production of a heterogeneously bleached sediment. To increase the likelihood of obtaining well-bleached sediment Thrasher *et al*. (2009a) suggested a lithofacies approach to sampling glaciofluvial sediments. This method aims to identify sedimentary units which were most likely to have been exposed during transportation and deposition (Thrasher *et al*., 2009a) and can work in tandem with single-grain analysis to identify the well-bleached portion within glaciofluvial sediments. In this study, glaciofluvial sediments were targeted from the range of glacial deposits and, in addition to this, gravel bar-top lithofacies are targeted during sampling to maximise the opportunity for bleaching of cobbles. It has also been shown that reducing the size of the aliquot can aid in dating heterogeneously-bleached environments (Duller, 2008b).

A range of models have been proposed for isolating populations of equivalent doses in heterogeneously-bleached environments (Galbraith *et al*., 1999). It has been

shown that the Minimum Age Model (MAM) is most appropriate for samples that were partially bleached at deposition (Galbraith and Roberts, 2012; Smedley *et al*., 2016). The MAM uses a truncated lower end of the D_e distribution and considers those grains to be well-bleached. An example of the use of the MAM is given by Smedley *et al*. (2016) who applied the MAM to establish equivalent doses for glacial sediments from Lago Buenos Aires, Patagonia. Figure 1.6 illustrates the range in D_e values measured for single grains of feldspar from the glacial environment, given in a radial plot, with the grey highlighted area showing the MAM D_e values. In Figure 1.6 the D_e measured from the MAM used only the 20 % brightest grains (closed triangles). When applying the MAM, however, it is required to define an overdispersion value (*sigma b*) to account for the degree of spread in the well-bleached dataset. This is an important value as *sigma b* defines the width of the normal distribution of the well-bleached population. This means that overestimation of *sigma b* can result in an overestimation of D_e (and therefore age) of the sample. Defining overdispersion can be difficult for glacial sediments and this is due to the fact that overdispersion values should be representative of a sample of the same age.

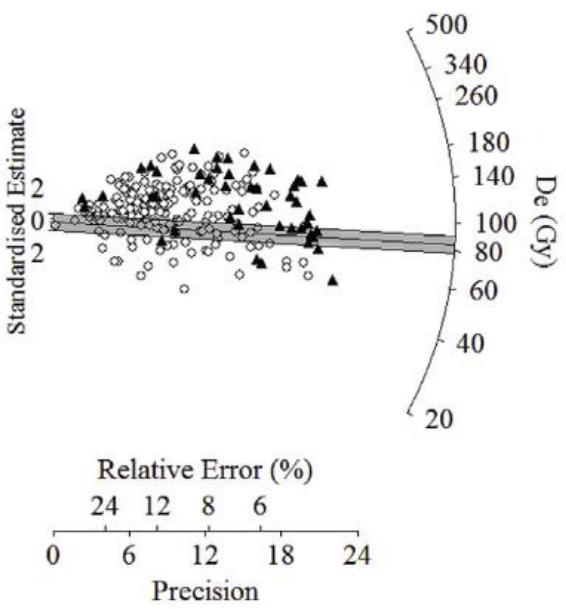

Figure 1.6. Example of a feldspar single-grain D_e distribution from a glacial sediment (Smedley *et al*., 2016) with the MAM (grey highlighted area) used to obtain a value of D_e for the brightest grains only (closed triangles).

Another challenge of dating glacial sediments is that the former water content is difficult to estimate. This is important in glacial environments whereby stagnant ice can persist. It has been shown that a 1 % difference in water content results in ~ 1 % difference in the OSL age (Fuchs and Owen, 2008) and therefore estimations of water content are important.

1.3. Luminescence dating of rocks

Daylight bleaching of mineral grains has formed the basis of luminescence dating of sediments since 1979 (Wintle and Huntley, 1979) and is applied to grains ranging from a few micrometres in diameter to several hundred micrometres. In such applications it is assumed that light is able to pass through the entire grain during bleaching in nature. Where mineral grains are still part of a solid rock those at the surface would be assumed

to bleach in the same way. However, measurements have only recently been undertaken for the sub-surface and an insight into how light penetrates has only just been established.

Measurements have been undertaken by Richards (1994) who analysed quartzite stone tools that were exposed, then subsequently buried, from the Diring Yuriakh site, Siberia, Russia. Richards (1994) looked at quartz grains, layer-by-layer, with depth, into a stone tool and showed that the luminescence signal was reset, with depth. Liritzis (2011) provides a review of the use of luminescence signals from rocks, mainly for use in dating dressed stone surfaces. The use of rocks in luminescence dating has focused on two methods, and these are both outlined below.

1.3.1. Exposure luminescence dating

Firstly the penetration of light into a rock sub-surface that is exposed at the time of sampling can be measured and the subsequent modelling of the normalised luminescence signal (L_n/T_n ratio) depth profiles are compared to profiles from a known-age exposure (OSL surface exposure dating) (Lehmann *et al*., 2018). The amount of time that a rock surface has been exposed at the Earth's surface can be investigated through surface exposure dating using luminescence (e.g. Lehmann *et al*., 2018). As previously outlined, surface exposure dating differs from 'standard' luminescence dating techniques. In this case, the bleaching profile (the depth to which light interaction occurs) of mineral grains at and beneath the surface of a rock is investigated. Therefore, changes in the amount of trapped charge with depth into the rock surface are examined (Figure 1.7).

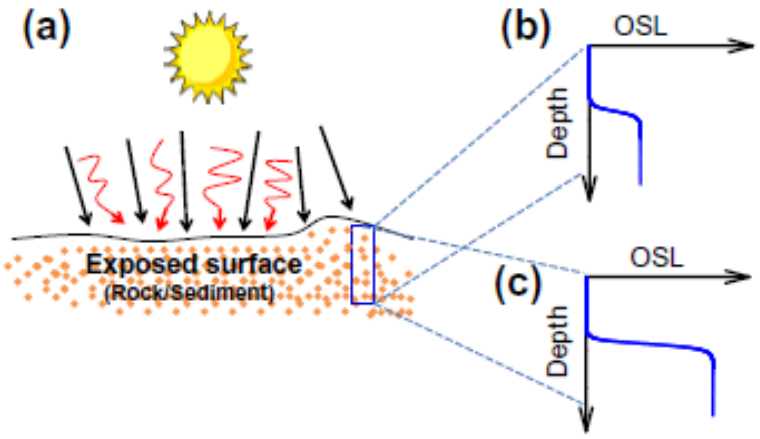

Figure 1.7. (a) Schematic of the concept of surface exposure luminescence dating. Black arrows indicate an input of ionizing radiation and the red arrows indicate bleaching of the mineral particles. (b) Illustrates an example of a luminescence-depth profile from a material that was reset at a previous event, and (c) illustrating the bleaching of mineral grains from an initial saturated state (Sohbati *et al*., 2012b).

Within the solid rock, latent luminescence accumulates over time, since initial formation of the rock. This latent luminescence accumulates in response to the natural ionizing radiation from the radioactive isotopes in the ^{232}Th, ^{238}U, ^{235}U and ^{40}K series. For typical quartz dose rates it will take ~ 100 – 200 ka for trapped charge to reach saturation (Wintle and Murray, 2006). Therefore, the luminescence signal in most bedrock samples will be saturated before being exposed at or near to the Earth's surface. The exposure of this solid rock at the Earth's surface (due to subaerial erosion of overlying bedrock) results in the removal of latent luminescence and a resetting of the luminescence signal. With increased exposure time this 'zeroing' of the luminescence signal will occur to greater depths. A model of light penetration in a naturally exposed granite cobble has been proposed by Sohbati *et al*. (2012c)

$$L = L_0 e^{-\overline{\sigma\varphi_0} t e^{-\mu x}} \quad \text{(Equation 1.2)}$$

here L_0 is the maximum luminescence signal intensity at saturation, L is the luminescence remaining at depth (x) after an exposure time (t), σ is the photoionisation cross section

and φ_0 is the photon flux at the rock surface with μ the attenuation coefficient as light penetrates the rock. Figure 1.8 illustrates the modelled evolution of a bleaching profile into a rock sub-surface following varying periods of exposure.

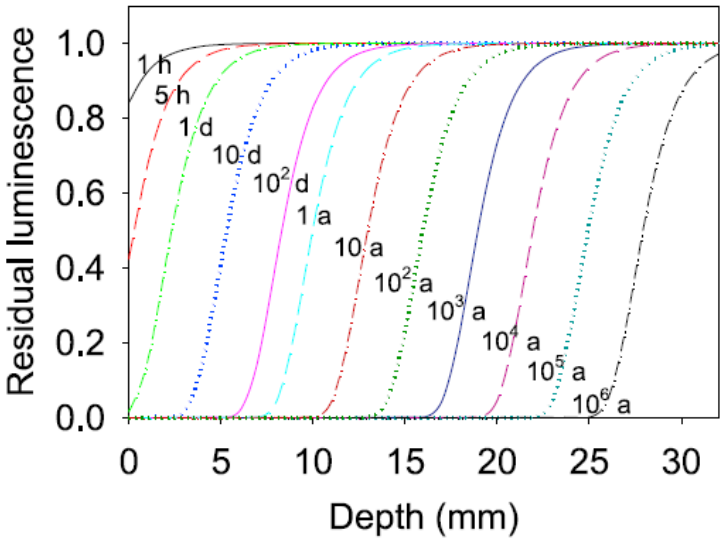

Figure 1.8. Profile of the residual luminescence signal existing at varying exposure times (from 1 hour to 1 million years). The depth of signal resetting illustrates the amount of time that the surface has been exposed (Sohbati *et al*., 2012c).

1.3.1.1. Previous applications of surface exposure luminescence dating and development of the technique

Pioneering research in developing the surface exposure luminescence dating technique was undertaken by Sohbati *et al*. (2012a) who determined the exposure ages for rock art found on sandstone in the Canyonlands National Park, Utah, USA. In this pioneering study, problems in model parameter estimation were overcome. This was undertaken through analysing the sub-surface L_n/T_n patterns of a local road-cut exposure, of a known-age, to allow calibration of the bleaching properties of the lithology. Sohbati *et al*. (2012a) analysed quartz grains within the sandstone to a depth of > 10 mm in three different samples. The OSL-depth profile of the known age sample (exposed 80 years

before time of study) was modelled firstly to estimate material dependent parameters within the mathematical model (Equation 1.2). The friable sandstone was abraded in 1 mm increments and the quartz grains were measured to obtain the luminescence signal with depth. The sensitivity-corrected natural OSL signals (L_n/T_n) were plotted against depth into the rock samples (Figure 1.9). Multigrain aliquots were undertaken for each point and the points present in Figure 1.9 are averages of at least 3 aliquots. The data points presented follow trends expected by the physical model and calibration with a known-age sample resulted in the calculation of exposure ages for the two samples at 127 ± 11 years and 713 ± 61 years. This study relies upon the known-age exposure of the sample from the road cut which allows a calibration of the luminescence-depth signal however this provides a challenge for areas where this may not be known.

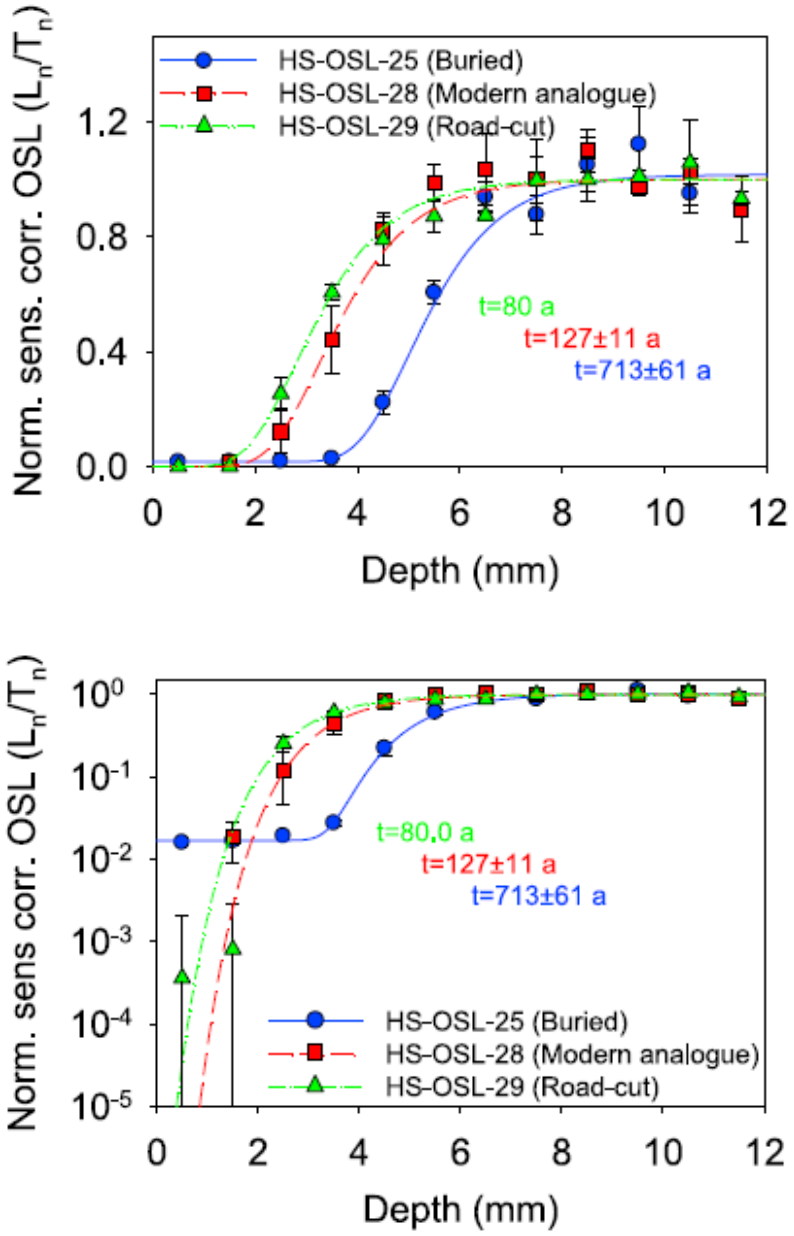

Figure 1.9. Bleaching with depth model fitted to data points obtained for the 3 different samples by Sohbati *et al*. (2012a) with sensitivity-corrected OSL signals (L_n/T_n) plotted against depth (above) and on a logarithmic scale (below). The logarithmic scale of sensitivity-corrected OSL illustrates a burial, following exposure, for HS-OSL-25 as indicated by the regrowth of the luminescence signal.

1.3.2. Luminescence dating of buried cobbles

The second scenario is the bleaching of the luminescence signal into the rock (or cobble) sub-surfaces then the reburial of the cobble and the regrowth of the luminescence

signal (to allow D_e determinations - but with a sub-surface bleaching profile still encoded). The sub-surface profiles can then show if the cobble was completely bleached (in addition to the burial ages) and a numerical model can be fitted to establish the exposure length (Chapot *et al*., 2012; Sohbati *et al*., 2011; Sohbati *et al*., 2012a; Freiesleben *et al*., 2015). As previously outlined, the dating of cobbles within glaciofluvial sediments (as undertaken within this project) differs from surface exposure dating. Cobbles may have been exposed at the time of deposition, and their sub-surface bleached. Following this the cobbles become buried and the luminescence signal starts to rebuild. The sub-surface bleaching profile can then be analysed to assess if the cobble was completely bleached before burial.

1.3.2.1. Previous applications of cobble luminescence dating and development of the technique

The relatively novel cobble luminescence dating technique has been applied at a number of locations to help address a range of environmental questions (including at archaeological settings and fluvial deposits) (Liritzis *et al*., 1997; Habermann *et al*., 2000; Polikreti, 2007; Sohbati *et al*., 2011; Sohbati *et al*., 2012a). In addition to this, the cobble luminescence dating technique has been applied to a variety of lithologies, including quartzites, gneiss and granites. A number of examples are discussed below.

Freiesleben *et al*. (2015) established the depositional age for a granite cobble found in an archaeological site near Aarhus, Denmark, using the sub-surface rock slices which showed signs of being completely bleached (the flat area before the development of the bleaching profile (60 – 70 mm into the cobble in Figure 1.10)). Intact granite slices were taken from granite cores and were placed onto the luminescence readers directly, as opposed to disaggregated material which has been used in other studies (e.g. Sohbati

et al., 2012a). Feldspar minerals were analysed using a high temperature post IR-$IRSL_{290}$ protocol. Sensitivity-corrected luminescence L_n/T_n profiles with depth were produced (Figure 1.10). Ages were determined for the burial of the cobble using the $IRSL_{50}$ signal (1.73 ± 0.16 ka). In addition to these measurements, the exact same cobble had been exposed at its surface, and the L_n/T_n measurements, with depth, allowed a calibration of the mathematical parameters, so that a numerical model could be fitted to confirm the well-bleached context of the cobble. The surface of the granitic clast was interpreted to have been exposed during occupation of the archaeological site, with markings on the clast interpreted as whetstone abrasions. This is confirmed by model fitting for the surface of the clast which produced a burial age of ~ 1.3 ka, with the granite clast buried following abandonment of the settlement. A third outcome from the study was that a theoretical model was developed to describe multiple exposure and burial events (Figure 1.11). Figure 1.11 also illustrates the regrowth of the luminescence signal once a bleached cobble surface becomes buried. Equivalent doses are then measured from the regrown area of the bleaching curve (see arrows in Figure 1.11).

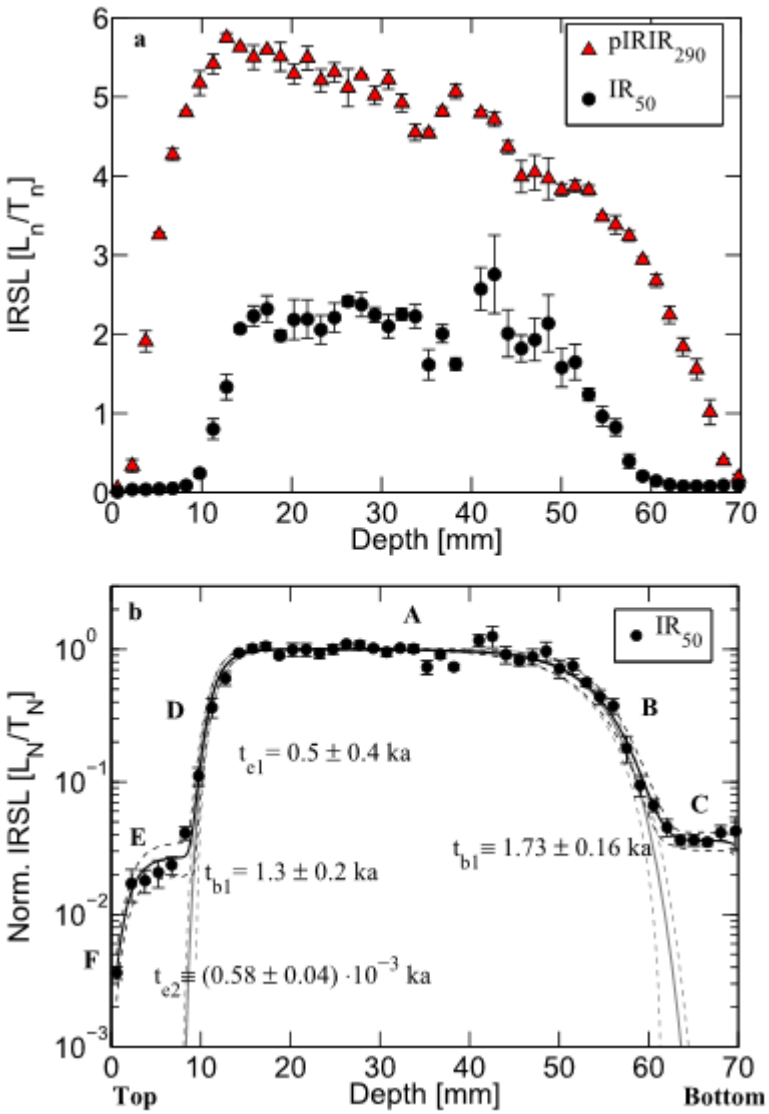

Figure 1.10. Luminescence-depth profiles for the $IRSL_{50}$ and post-IR $IRSL_{290}$ signal (upper figure) and a logarithmic scale of normalised luminescence (bottom figure) with each data point an average of 3 rock slice measurements. The solid line represents the model fitting which was used to verify ages established from $IRSL_{50}$ measurements (Freiesleben *et al.*, 2015).

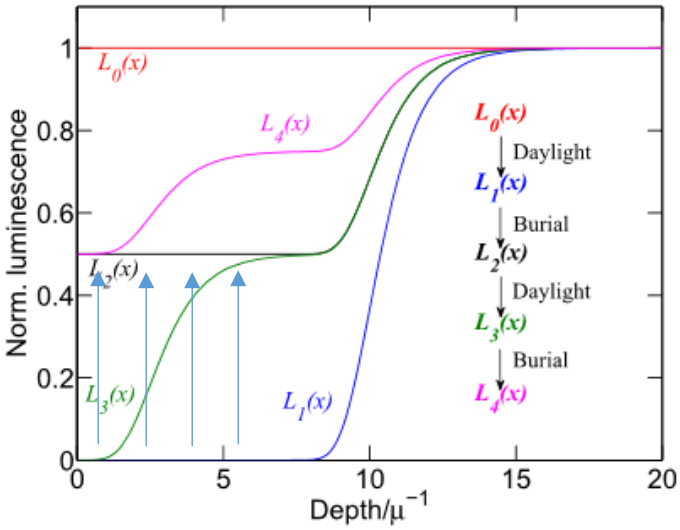

Figure 1.11. Model of normalised luminescence-depth profiles for 4 separate exposure and burial events. This figure illustrates the decrease in trapped charge from an initial saturated state with repeated exposure events resulting in a reduction in trapped charge from a lower 'plateau' of luminescence signal (Freiesleben *et al*., 2015). Blue arrows indicate the area of signal regrowth from which D_e measurements are made.

Simms *et al*. (2011) undertook a different approach, and investigated the depositional age of the underside (but the surface slice *only*) of cobbles within three raised beaches on the South Shetland Islands, Antarctic Peninsula (Figure 1.12). Luminescence measurements were undertaken on quartz which was obtained by slicing 1 mm thick slices, crushing and sieving the sediment to obtain the required grain sizes. Ages for 8 samples from the 3 raised beaches ranged from ~ 2 ka to 200 years, and were consistent with radiocarbon measurements at the location (Simms *et al*., 2011; Figure 1.13). Challenges encountered in this investigation included the low quartz luminescence sensitivity and the contamination of the quartz signal with feldspar minerals present within the rock samples. Additionally, there was no confirmation that the cobbles were completely bleached by analysing their sub-surfaces.

Figure 1.12. Image of the raised beaches on the South Shetland Islands, Antarctica, which were used to obtain granite cobbles from (Simms *et al*., 2011).

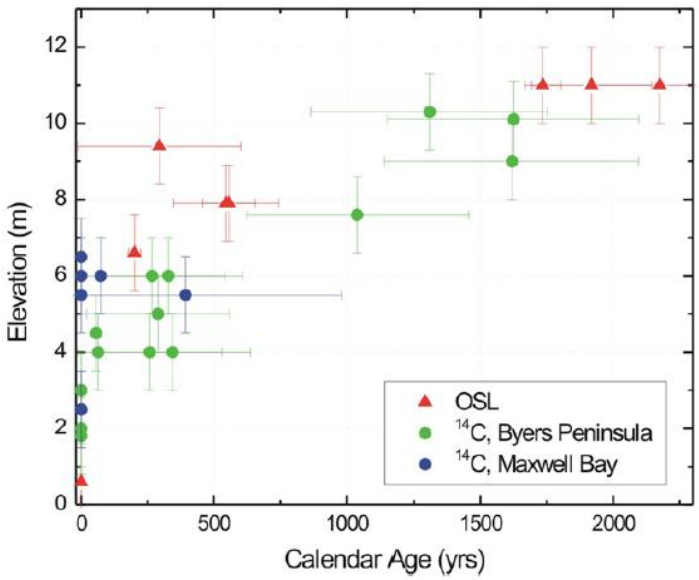

Figure 1.13. Quartz luminescence ages taken from the surface of granite cobbles (red triangles) in comparison to radiocarbon ages for three separate raised beaches (Simms *et al*., 2011).

The burial age of alluvially deposited quartzite cobbles at an archaeological site in Portugal was investigated by Sohbati *et al*. (2012b). Measurements were undertaken on rock slices and large aliquots of quartz grains taken from the buried quartzite rock

surface (Figure 1.14). In addition to analysing the surface slice to establish a depositional age, bleaching occurred to a depth of ~ 3 mm into the cobble surface and illustrates that the clast was well bleached before burial (Figure 1.15). An age of ~ 45 ka was produced from intact rock slices from one cobble and was consistent with independent control for the site. Independent age control was provided by the luminescence dating of sediment of the underlying sediment facies (Sohbati *et al*., 2012b). However, a second buried clast gave a younger age indicating a resetting event in the range of 25 – 14 ka. Such investigations illustrate the importance of buried cobble ages and that the cobble sub-surfaces may indicate if the cobble was completely bleached.

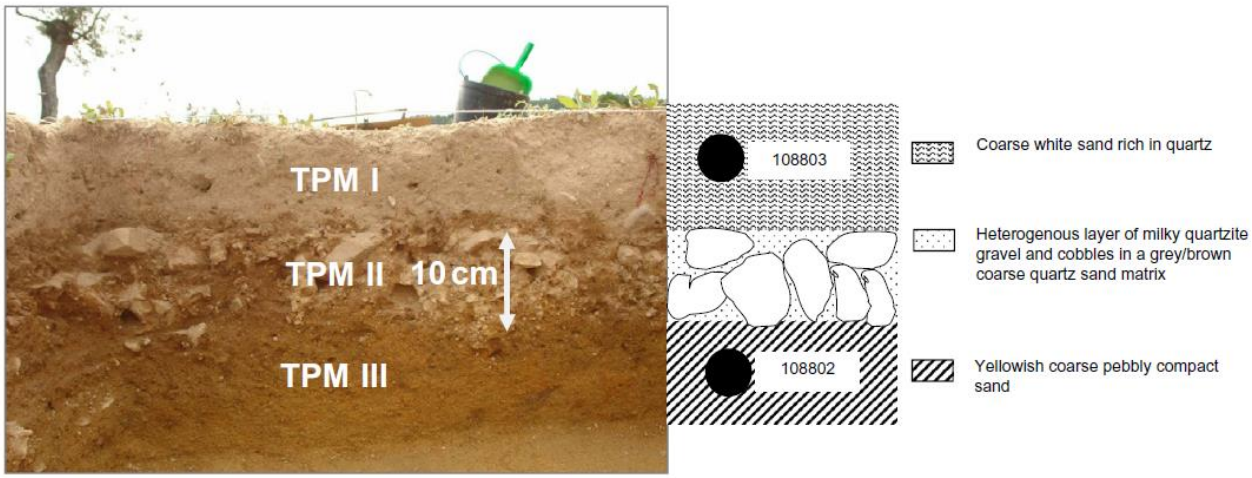

Figure 1.14. Sedimentary units containing the buried cobble investigated by Sohbati *et al*. (2012b) at an archaeological site in Portugal.

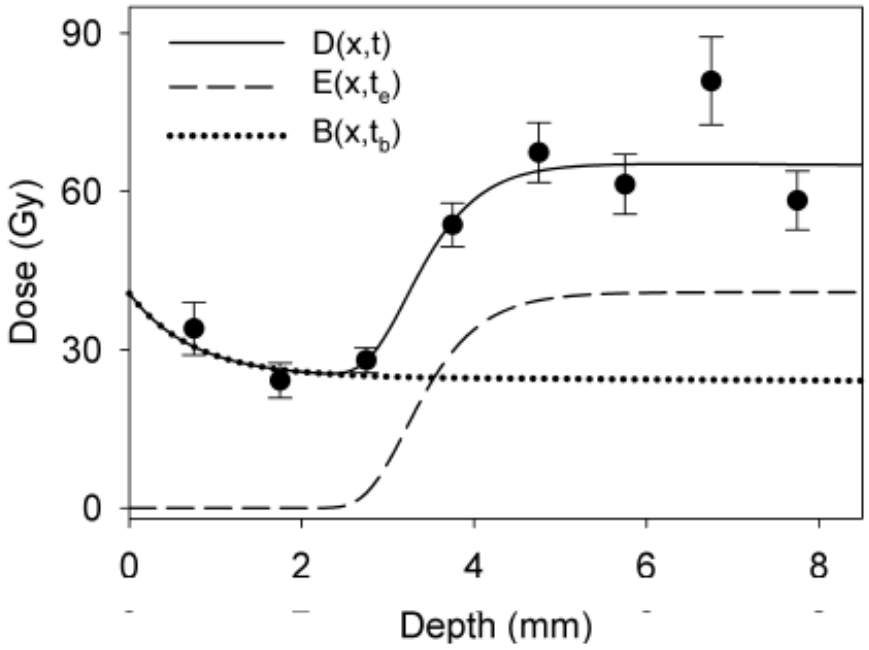

Figure 1.15. Example of the luminescence-depth profile below the surface of the buried quartzite clast which illustrates that the cobble was well-bleached before deposition (Sohbati *et al*., 2012b). The solid line represents a model fitted to the data points, with the dashed line illustrating the change of dose with depth. The dotted line shows the accumulation of dose inside the cobble during burial.

The burial age of a granite cobble emplaced in a pavement at a prehistoric cult site in the Negev Desert, Israel, has also been investigated using cobble luminescence dating (Sohbati *et al*., 2015). Sohbati *et al*. (2015) analysed the surface, and subsequently the sub-surface, of a single granite cobble, in addition to the sediment buried beneath this (to provide a check to the cobble ages). A post-IR $IRSL_{225}$ protocol was used on rock slices, taken from the surface and sub-surface of a granite cobble. The dose rate to the cobble and sediment was measured using high-resolution gamma spectrometry. Quartz and $IRSL_{50}$ ages from the underlying sediment and the $IRSL_{50}$ and post-IR $IRSL_{225}$ ages from rock slices were consistent, and give an age of ~ 4.2 ka (Sohbati *et al*., 2015). A bleaching profile, beneath the cobble surface was produced and shows that the cobble was well-bleached (due to the consistently low L_n/T_n ratios over a depth of ~ 10 mm) (Figure 1.16). This study links the sub-surface luminescence ages to an independent

check of sediment luminescence dating, however, it is noted that this sample was taken from a known well-bleached environment. Therefore, questions still remain regarding the potential for extensive sub-surface bleaching in heterogeneously bleached glacial deposits.

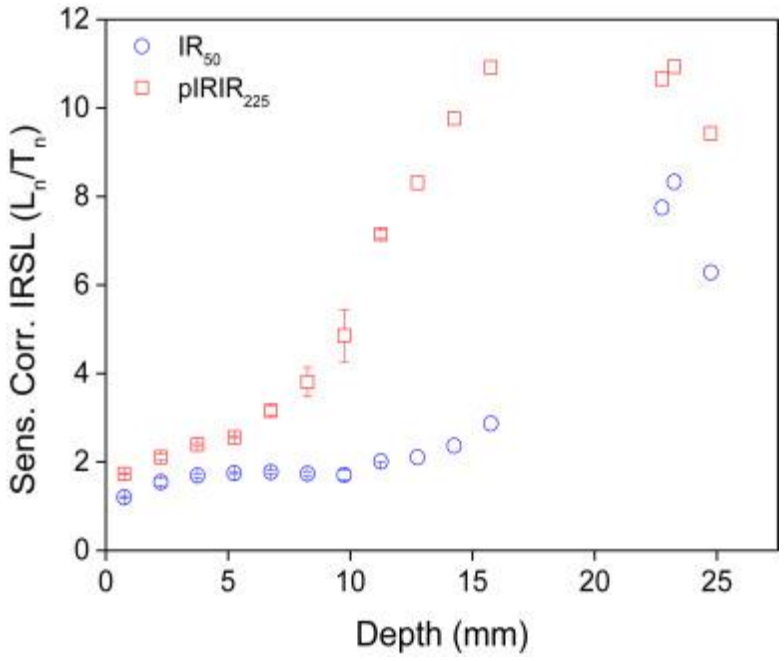

Figure 1.16. L_n/T_n ratios, with depth, into the buried face of a single granite cobble. The difference between the $IRSL_{50}$ and post-IR $IRSL_{225}$ bleaching profiles is illustrated (Sohbati *et al*., 2015).

1.4. Research aims and objectives

The overarching aim of this thesis is to establish if cobbles can be used to accurately date the deposition and burial of glaciofluvial deposits. This is split into a number of discrete objectives, which are outlined below:

Objective 1: Verify bleaching models of changes in luminescence, with depth, into a cobble sub-surface by using a non-exposed cobble and exposing this for increasing time periods and observing the development of the bleaching profile (see Chapter 4)

Objective 2: Testing cobble luminescence dating at a location with a well-developed independent age control (checking the range of bleaching across a population of cobbles, and observing sub-surface luminescence measurements) (see Chapter 5).

Objective 3: Testing the replicability of cobble luminescence dating at another retreat location with independent age control (do cobbles behave the same at this additional location?) (see Chapter 6).

Objective 4: Establish if the cobble dating luminescence technique can constrain a location that marks the furthest extent of the British-Irish Ice Sheet, in a location with no independent age control and marks the furthest extent of the only land-terminating ice stream of the British Irish Ice Sheet (see Chapter 7).

2. Study Sites & Sampling Strategy

2.1. Introduction

This chapter outlines the sites studied and provides information on the British-Irish Ice Sheet (BIIS) and the Irish Sea Ice Stream. Justification is also provided as to why the locations were selected for sample collection. Sedimentary descriptions and images are provided for each location and in addition to this the strategies employed during sampling at each site are also provided.

2.2. The British-Irish Ice Sheet (BIIS)

The Last Glacial Maximum (LGM) of the BIIS occurred at ~ 27 ka BP (Hubbard *et al*., 2009; Clark *et al*., 2012). In recent years the extent of the BIIS has been revised from ~ 357,000 km^2 to 840,000 km^2 with the BIIS covering areas of current sea-floor and continental shelves (Clark *et al*., 2012). The BIIS had ice accumulation centres over Scotland, north England, central Wales and central Ireland (Hubbard *et al*., 2009) and had significant ice loss margins in the Irish Sea, North Sea and Atlantic coast with ice streams extending to the continental shelf edge (Figure 2.1). The majority of retreat of the BIIS occurred by drainage through such ice streams, until the ice margins stepped onto land, which is likely to have then changed the processes of ice loss (Clark *et al*.,

2012). Due to the large ice loss of the BIIS through ice streams, the BIIS becomes a useful analogue for changes in the West Antarctic Ice Sheet today. A key area of loss for the BIIS was through the Irish Sea ice stream, which extended through the Irish Sea Basin into the Celtic deep and to the edge of the continental shelf.

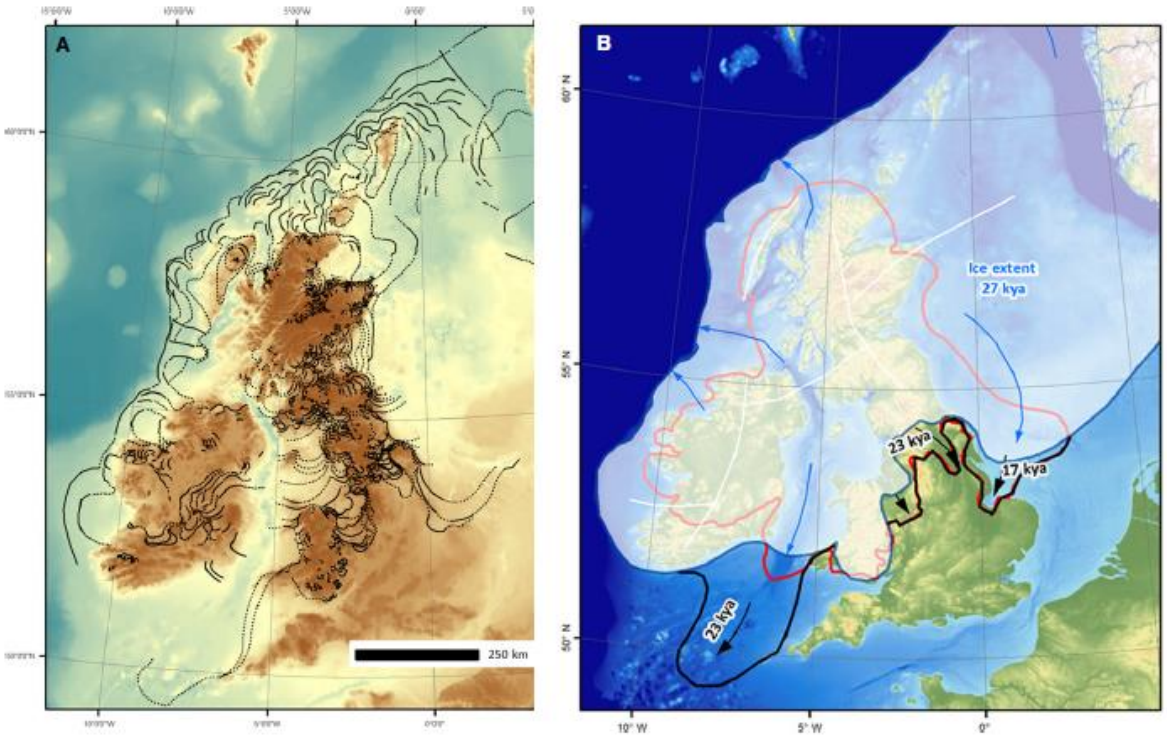

Figure 2.1. (a) Reconstruction of the pattern of retreat of the BIIS inferred from geomorphological evidence and (b) an overview of the maximum ice-sheet extent (Clark *et al*., 2018) with the redlines in (b) showing the previous interpretation of ice sheet extent by Bowen *et al*. (1986).

2.3. Irish Sea Ice Stream

The Irish Sea Ice Stream was the largest ice stream to drain the BIIS (Chiverrell *et al*., 2013) (Figure 2.2). The Irish Sea ice stream was a grounded, largely marine-terminating ice mass which reached its furthest extent south of the Isles of Scilly (Scourse, 1991; Smedley *et al*., 2017a) and this is the furthest south that the BIIS extended. The ice stream was nourished by separate onshore ice caps from Wales,

Ireland, northern England and Scotland. Streaming of the Irish Sea ice stream has been observed from sea-bed landforms, including subglacial bedforms observed off Anglesey, Wales (Van Landeghem *et al*., 2009) which showed converging flow into the north Irish Sea Basin.

Extensive geochronological analysis of the retreat of the Irish Sea ice stream has been undertaken. This includes radiocarbon dating, luminescence dating and cosmogenic nuclide dating (Thrasher *et al*., 2009a; McCarroll *et al*., 2010; Chiverrell *et al*., 2013). Radiocarbon analysis has either focused on material from warm stages that bracket deposits or dating of marine shells found within glacigenic sediments (McCabe *et al*., 2007; Chiverrell *et al*., 2013). This is due to the general lack of organic material in the glacial settings. OSL dates for the Irish Sea ice stream have been given from small aliquots and single-grains of quartz (Thrasher *et al*., 2009a; Smedley *et al*., 2017a), however, luminescence dating has had to contend with the possibility that the sediments were poorly bleached at deposition. Cosmogenic nuclide dating of the Irish Sea ice stream has targeted quartz-rich rock types for ^{10}Be dating and volcanic lithologies for ^{36}Cl exposure dating (McCarroll *et al*., 2010; Chiverrell *et al*., 2013).

Bayesian modelling of radiocarbon, luminescence and cosmogenic ages of the retreating Irish Sea ice stream was undertaken by Chiverrell *et al*. (2013). This Bayesian model (Figure 2.2) synthesises data along 650 km of ice retreat and covering a period of 8000 years. The furthest extent of the Irish Sea ice stream was recorded at 25.3 – 24.5 ka, with rapid decay following this and resulting from climatic warming (Chiverrell *et al*., 2013). Retreat of the Irish Sea ice stream was uneven, with initial rapid retreat occurring at ~ 550 m a^{-1}. This then slowed as the ice stream entered constrained areas between southern Ireland and Pembrokeshire at ~ 23.7 – 22.9 ka to ~ 100 ma^{-1}. The final phase of ice retreat identified for the ice stream was at the northern extent of the Isle of

Man, and gives a final deglaciation age of the Irish Sea Basin at ~ 17.8 – 16.9 ka. In addition to the Bayesian modelling provided by Chiverrell *et al*. (2013), recent analysis by Smedley *et al*. (2017a) confirms the depositional ages of outwash sediments, using OSL, at the Isles of Scilly, with the furthest extent of the ISIS at 25.5 ± 1.5 ka. It is evident that given the well-constrained retreat of the Irish Sea ice stream that this sector of the BIIS provides valuable opportunities to test our novel luminescence dating technique.

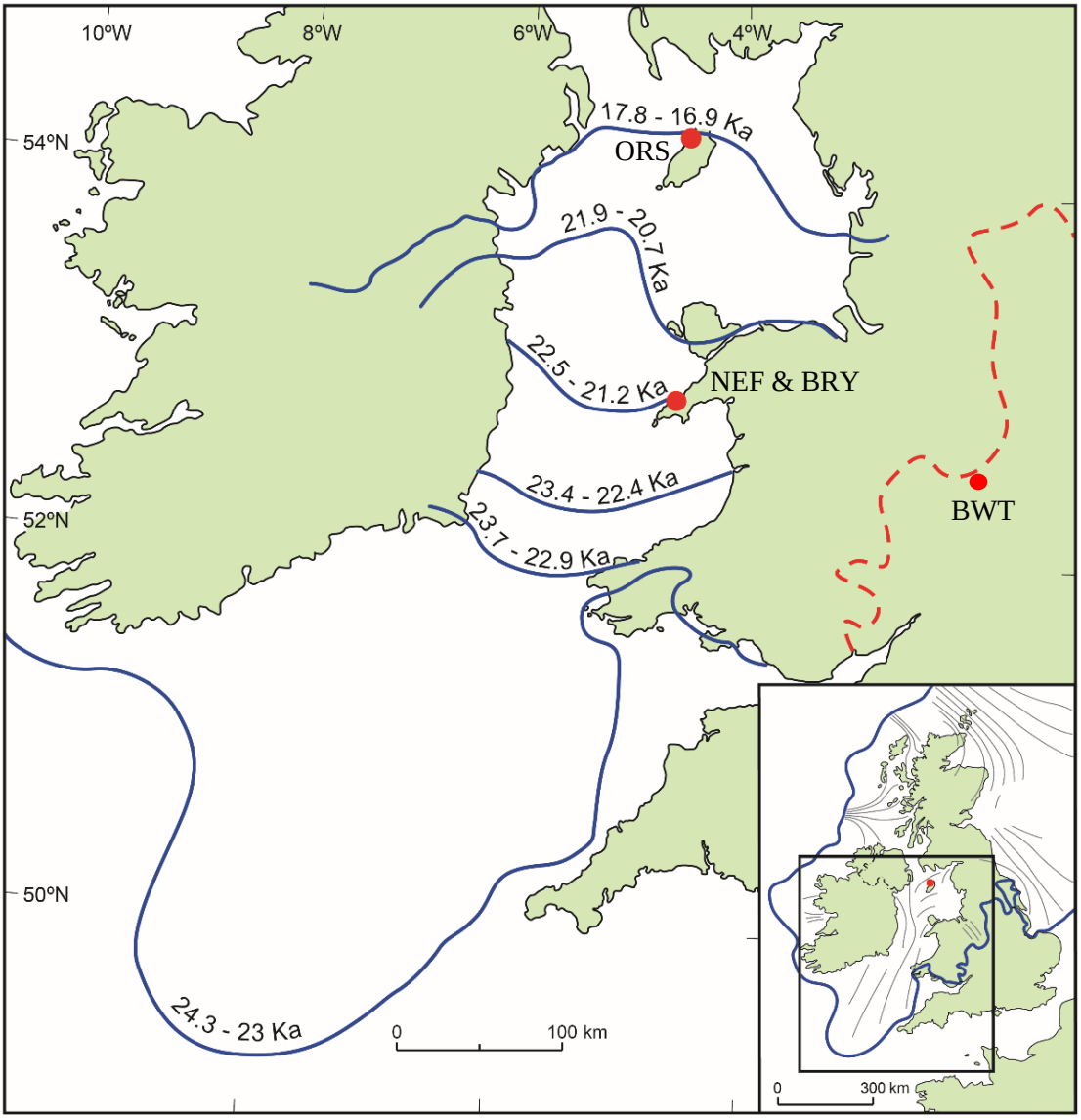

Figure 2.2. Bayesian modelled retreat ages and ice margin positions of the Irish Sea ice stream (after Chiverrell *et al*. 2013) and ice margins and ice stream flow lines of a LGM BIIS (inset). The red dots indicate the location of Orrisdale Head (ORS), Nefyn and Bryn-yr-Eryr (NEF) and Bridgwalton (BWT) studied in this thesis.

2.4. Site selection and independent age control

The two locations were selected to undertake the testing of this novel luminescence cobble dating technique due to the independent age control available, from multiple geochronological techniques and due to the abundance of glaciofluvial sediment exposures. For Orrisdale Head, independent ages include radiocarbon ages from marine microfauna at Killard Point, Ireland (McCabe *et al*., 2007), quartz optically stimulated luminescence (OSL) ages at Orrisdale Head (Thrasher *et al*., 2009a) and cosmogenic radionuclide ages from ice-moulded bedrock at Holyhead Mountain, north Wales (McCarroll *et al*., 2010). All of these sites are located along a retreat sequence of the Irish Sea ice stream (Figure 2.2) and as previously outlined, the ages have been combined in a Bayesian model by Chiverrell *et al.* (2013). A series of retreat limits have been proposed by Chiverrell *et al*. (2013) extending from south of the Isles of Scilly at 24.3 – 23.0 ka to a margin lying south of Killard Point, immediately north of Orrisdale Head and south of the Lake District at 17.8 – 16.9 ka. The two margins that bracket the site at Orrisdale Head are ~ 70 km to the south at 21.9 – 20.7 ka and to the north at 17.8 - 16.9 ka (Figure 2.2). Chiverrell *et al*. (2018) have added 11 single grain quartz OSL ages and 8 cosmogenic isotope ages to further define the ice retreat sequence in the northern Irish Sea Basin, and using a Bayesian model were able to constrain deglaciation of the Isle of Man before 18.9 ± 1.0 ka. This chronology is similar to, but refines previous Bayesian modelling of the ice retreat dynamics (Chiverrell *et al.*, 2013) and also suggests that the small aliquot OSL ages (Thrasher *et al.*, 2009a) for the Orrisdale ice marginal complex underestimate the age by 2 - 6 ka.

The Llyn Peninsula is also an ideal location for the testing of a novel chronological technique as independent age control is available from multiple

geochronological techniques, including cosmogenic radionuclide ages from ice-scoured bedrock at Mottee Stone, Ireland (Bowen *et al*., 2002), the Wicklow Mountains, Ireland (Ballantyne *et al*., 2006) Holyhead Mountain, Anglesey (McCarroll *et al*., 2010) and OSL ages from Nefyn, Llŷn Peninsula (Thrasher *et al*., 2009a). As at Orrisdale Head, all of these sites are located along a retreat sequence of the Irish Sea ice stream (Figure 2.2) and as previously outlined, the ages have been combined in a Bayesian model by Chiverrell *et al.* (2013). The coastal sections of the north Llŷn Peninsula lie on the edge of a retreat phase given by Chiverrell *et al*. (2013), and are located between the ages of 22.5 – 20.7 ka. In addition to these modelled ages by Chiverrell *et al*. (2013) recent luminescence and cosmogenic nuclide ages have been produced for the Llyn Peninsula by Smedley *et al*. (2017b) and Bayesian modelled ages give retreat along the Llyn Peninsula from 24 – 20 ka. It is clear that this section of the Irish Sea ice stream is very well constrained and provides an excellent opportunity to replicate cobble luminescence dating at this location.

Finally, Bridgwalton, Shropshire, was selected due to the limited independent age control which provides an opportunity to trial this cobble luminescence dating technique at a location where the depositional age is unknown. Further details about each site are given in the following sections.

2.5. The Isle of Man

The Isle of Man occupies a vital position recording the dynamics of palaeo-ice stream and ice-sheet processes in the northern Irish Sea Basin. Ice entered the basin from both Scotland and the English Lake District and inundated the island as it continued to extend into the south of the Irish Sea basin (McCarroll *et al*., 2010). The majority of

glacial sediments on the Isle of Man relate to the final phase of recession (Thomas *et al*., 2004) and this, therefore, provides the opportunity to assess deglaciation dynamics and processes.

An indication that the entirety of the Isle of Man was overrun with ice is the presence and orientation of striations, in addition to the extensive glacial sediment deposits (Figure 2.3). The Quaternary glacial deposits of the Isle of Man are generally divided into two suites, which are the 'local' and 'foreign' origin groups. The local, 'high-level' suite is composed of diamict, with thinner beds of gravel which sit on top of bedrock and all sediments contain the local Manx and Dalby group lithologies (Chiverrell *et al*., 2013). The 'foreign' or 'low-level' sediment deposits contain exclusively erratic material, with rock types from the Southern Uplands and western Scotland. These deposits are found only in the north of the island, and on some parts of the island periphery (Chiverrell *et al*., 2013). The 'foreign' glacial sediments to the north of the island, including the field-site of Orrisdale Head, include glacial sediments and features such as large moraine ridges, ice-disintegration topography and ice-frontal alluvial fans and sandur systems deposits (Figure 2.3).

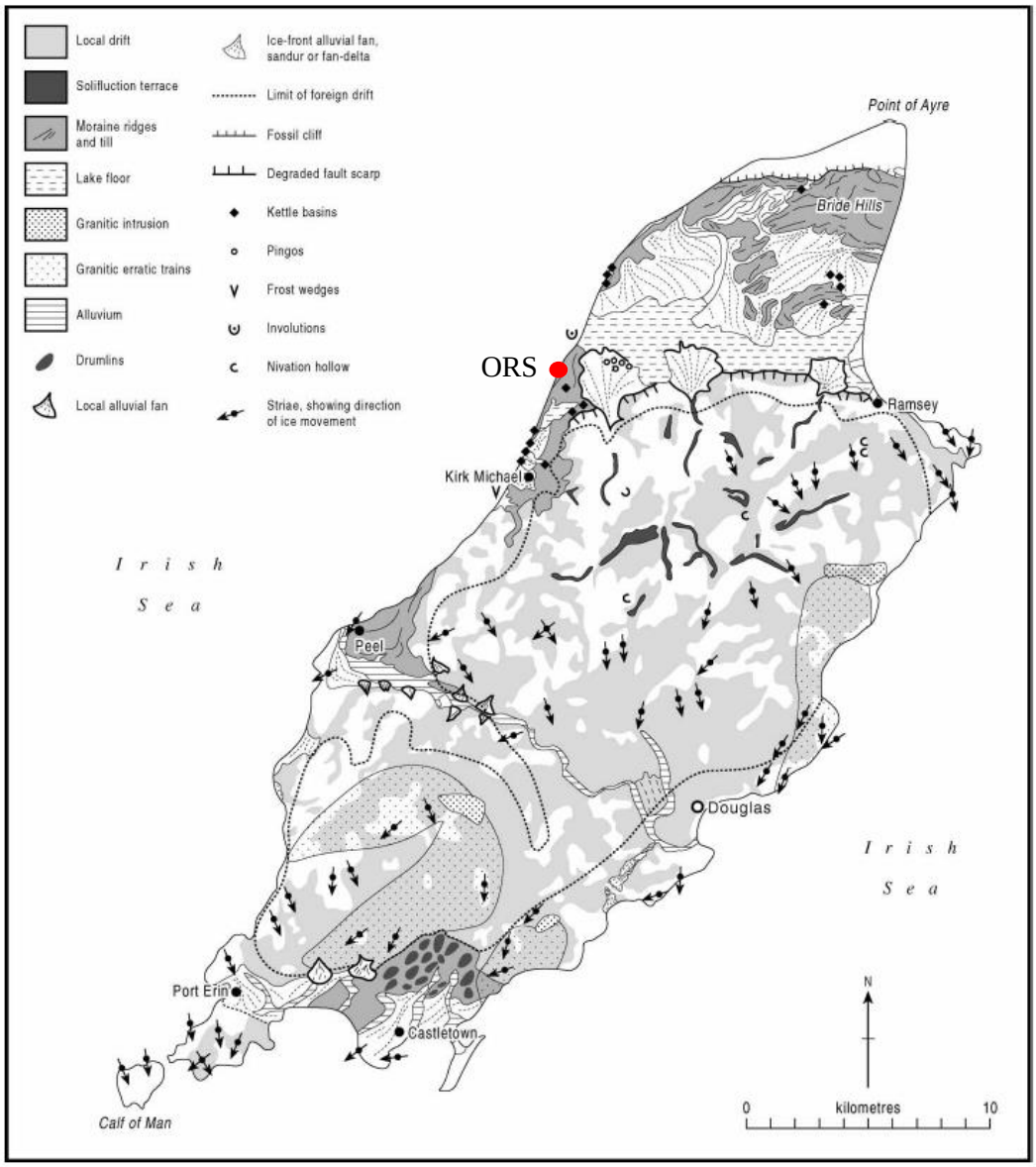

Figure 2.3. Geomorphological and sedimentological map of the Isle of Man, including the location and sedimentary deposits sampled in this study (Orrisdale Head) (Roberts *et al*., 2007).

2.5.1. Orrisdale Head, Isle of Man

The study site at Orrisdale Head, on the Isle of Man (Figure 2.2; 2.3), is an ice-marginal sandur system, deposited during final deglaciation of the Irish Sea ice stream and is exposed along coastal sections (Thrasher *et al*., 2009a). Orrisdale Head forms part of an 8 km long coastal section, giving near continuous exposure of glaciofluvial deposits in cliffs up to 9 m in height. The sedimentary exposures at Orrisdale Head have been

extensively mapped by Thomas *et al*. (2006b) and subsequently re-drafted by Thrasher *et al*. (2009a) (Figure 2.4). The sedimentology of the Orrisdale Head exposure has been interpreted to illustrate a series of fining-up cycles from bar core gravels (Gm / Gp lithofacies) through to finely laminated bar-top sand deposits (Fl lithofacies) (Figure 2.5). Both ice-proximal and ice-distal deposits have also been identified. Optically stimulated luminescence measurements on small-aliquot quartz samples, was undertaken by Thrasher *et al*. (2009a) at Orrisdale Head. Thrasher *et al*. (2009a) targeted ice-distal sediments, from a range of sand lithofacies, however the quartz equivalent dose (D_e) distributions were wide and positively skewed and indicated heterogeneous bleaching in the environment (Thrasher *et al*., 2009a). However, the application of a Minimum Age Model (MAM) allowed the calculation of equivalent dose distributions and quartz samples produced ages from ~ 14 – 26 ka and are included in the Bayesian model of Chiverrell *et al*. (2013).

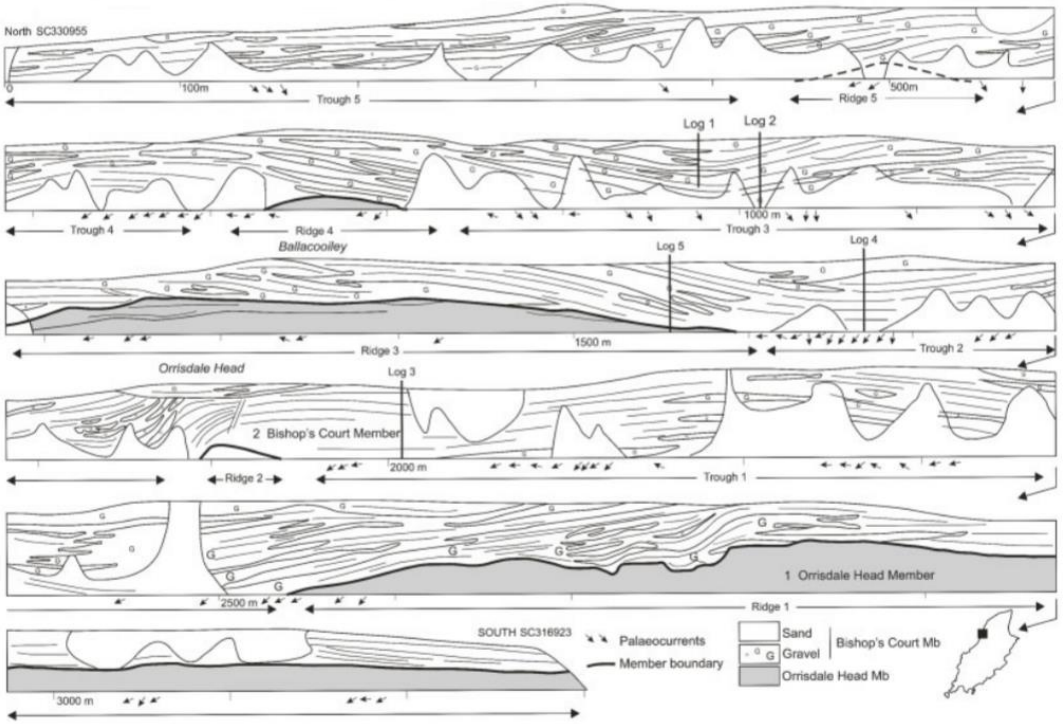

Figure 2.4. Sedimentary coastal exposures at Orrisdale Head, mapped by Thomas *et al*. (2006b) and re-drawn by Thrasher *et al*. (2009a) illustrating the large lateral extends of sands and gravels deposited in an ice-marginal sandur system.

At 54.319416ºN 4.5727167ºW a series of gravel bars, fining upwards into sand units are seen and are indicative of deposition in a sandur with repeated packages superimposed upon one another (Figure 2.4). Four gravel packages (ORS01, 02, 03, 04) lying within 20 m of each other laterally and between ~ 3 and 7 m below the current surface were sampled. Stratified planar crossbeds of gravel (Gp) and massive, matrix-supported gravel lithofacies (Gms) were targeted (Figure 2.6) as it is thought that they represent bar or sandur surfaces, thus maximising the probability that clasts were exposed to daylight at deposition.

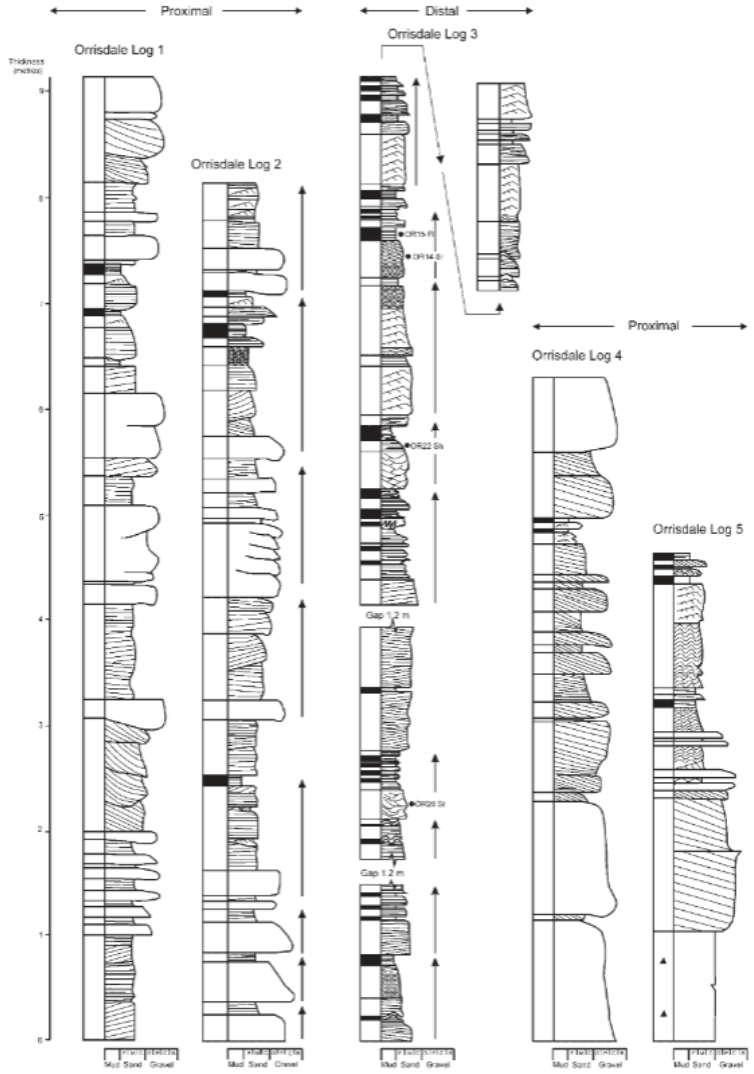

Figure 2.5. Sedimentary logs produced by Thrasher *et al*. (2009a) for sections of the Orrisdale Head exposure (see log positions in Figure 2.4). These also illustrate the location of the luminescence samples, all within ice-distal locations (in contrast to the ice-proximal cobble samples obtained in this study).

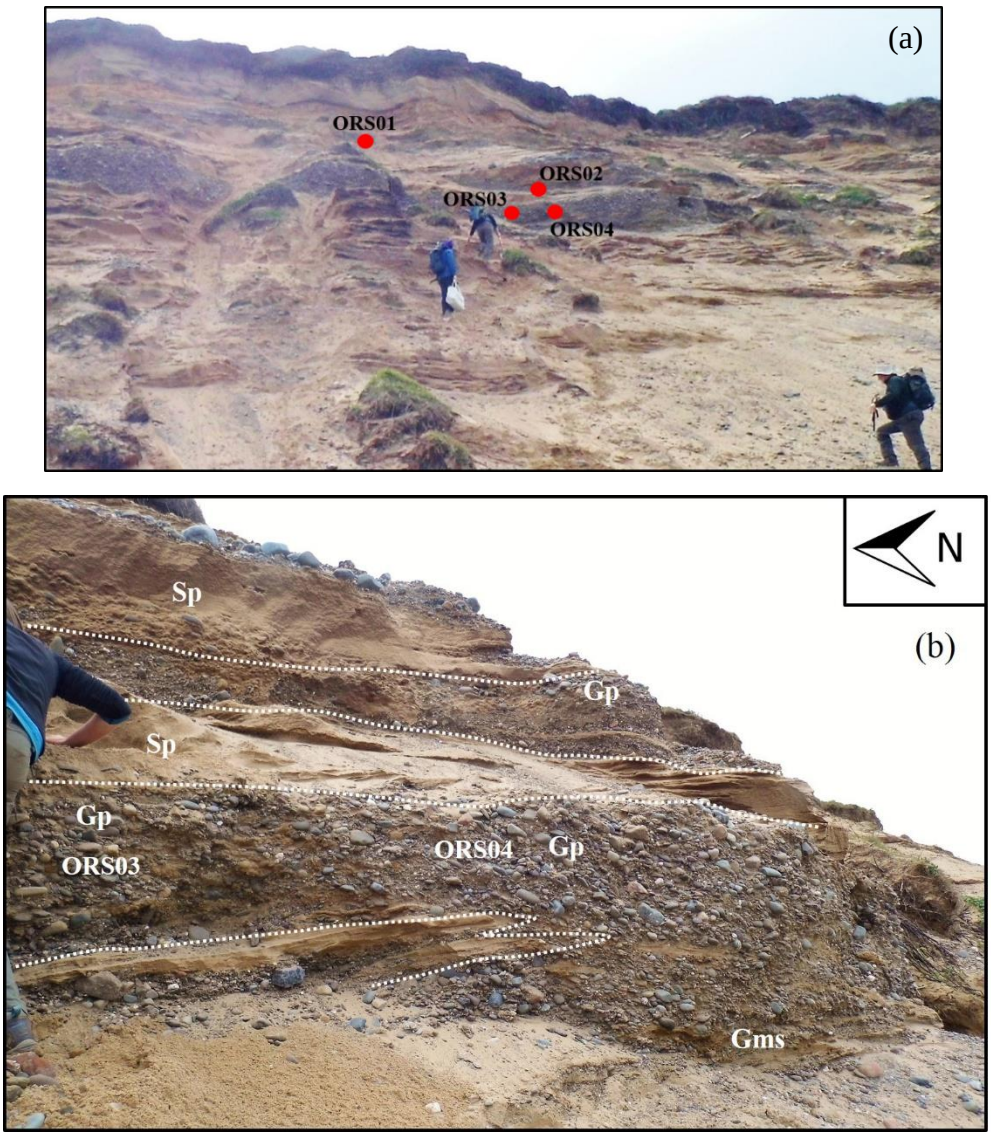

Figure 2.6. (a) Photograph of the coastal glaciofluvial sediment exposure at Orrisdale Head, taken from the beach foreshore, with the location of 4 sampled gravel units illustrated (ORS01 - 04). (b) Example image of the stratified planar cross beds (Gp) and massive, matrix-supported (Gms) gravel lithofacies exposed at Orrisdale Head.

2.6. Llŷn Peninsula, north-west Wales

The Llŷn Peninsula, north-west Wales, occupies a vital position for assessing the recession of the Irish Sea ice stream, as, similar to the Isle of Man, it records terrestrial final-phase recession (Thomas and Chiverrell, 2007). The Llŷn Peninsula is also ideally placed as it is located ~ 150 km south of the Isle of Man, and, therefore, provides the opportunity to investigate retreat of the ice stream along the Irish Sea basin (Figure 2.2).

The Llŷn Peninsula and adjacent parts of Anglesey record the eastern margin of the Irish Sea ice stream, which would have flowed south into the Irish Sea Basin, and would have coupled with ice radiating from the adjacent Welsh Ice Sheet (Thomas and Chiverrell, 2007). Thomas and Chiverrell (2007) identified key sediment-landform assemblages associated with the ice stream across the Llŷn Peninsula (Figure 2.7), and includes drumlin swarms and subglacial erosional assemblages, associated with subglacial ice stream conditions. Ice stream-marginal assemblages were also identified and include glaciotectonised push moraines and intervening sandur troughs. Ice stream-marginal assemblages also extended to freely expanding proglacial sandur and delta deposits. A key feature of most ice-marginal assemblages, across the Llŷn Peninsula, is the record of oscillatory behaviour of the Irish Sea ice stream. Readvance phases of the Irish Sea ice stream were identified by push moraines and glaciotectonised sandur sediments, such as those at Dinas Dinlle (Thomas and Chiverrell, 2007). The coastal sites, Nefyn and Bryn-yr-Eryr investigated below are located along the northern coast of the Llŷn Peninsula and are related to the 'IVb' phase of glacial-landform assemblages given by Thomas and Chiverrell (2007).

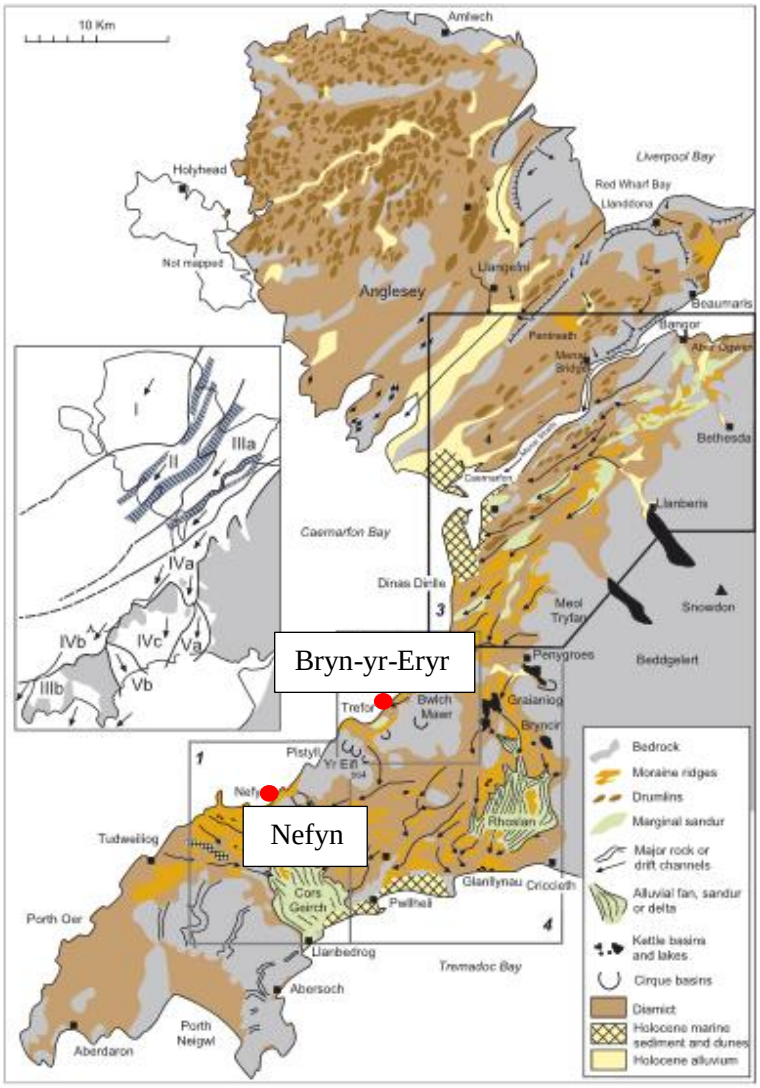

Figure 2.7. Geomorphological map of the Llŷn Peninsula and Anglesey (Thomas and Chiverrell, 2007) illustrating summary ice flow directions and an inset of the main landform-assemblage types. The location of one of the sampled locations (Nefyn) is also included and is of the 'IVb' landform assemblage type (see inset).

2.6.1. Nefyn

The first of two locations from which samples were collected along the Llŷn Peninsula (Figure 2.2) is the coastal exposures of Irish Sea ice stream retreat glaciofluvial sediments at Nefyn, which have been described by Thomas and Chiverrell (2007). As previously outlined in Section 2.5, Nefyn was selected due to the independent age control available through Bayesian modelling of multiple chronological techniques (Chiverrell

et al., 2013). These give bracketing margins for the Llyn Peninsula at 22.5 – 20.7 ka (Figure 2.2). The sedimentology at Nefyn is more complex than that observed at Orrisdale Head on the Isle of Man, whereby the sediments at Nefyn illustrate three discrete depositional glaciofluvial packages (Figure 2.8). The first, lowest unit, in the Nefyn section is defined as Sequence A by Thomas and Chiverrell (2007) with Sequence A2 an upward-fining succession from massive to planar cross-bedded pebble gravel (Thomas and Chiverrell, 2007) and the A2 package is interpreted as proglacial sandur deposited during retreat (Figure 2.8). Sequence B lies unconformably on top of sequence A and contains upward-fining successions from gravel (cross-stratified pebble gravel, passing upwards into massive pebble gravel and then into cross-bedded cobble gravel) into sand (Thomas and Chiverrell, 2007). Sequence B is interpreted by Thomas and Chiverrell (2007) as a large clastic wedge which thickens at an ice-contact slope indicating deposition in an ice-front alluvial fan. The third, and final sequence, Sequence C, is a fan-shaped wedge containing sand and gravels and interpreted as final abandonment of the ice-frontal alluvial fan, as this sequence fines upwards into mud deposits (Thomas and Chiverrell, 2007). Despite the different sequences described, all of these related to final deglaciation of the ice stream, with the transition from Sequence A to B illustrating localised readvance (Thomas and Chiverrell, 2007).

At 52.939600^{o}N 4.5209303^{o}W, the surface of a planar gravel bar located in a section with multiple gravel packages indicative of sandur deposition was targeted and samples NEF01 and NEF02 were taken within the same unit and within ~ 5 m laterally of each other (Figure 2.9). Both NEF01 and NEF02 were taken from Sequence A (A2) as described by Thomas and Chiverrell (2007). At 52.938840^{o}N 4.5230064^{o}W, ~ 200 m along the coastal exposures from samples NEF01-2, samples were taken from gravel

units from Sequence C (NEF03) and Sequence B (NEF04) as both Sequence C and B are exposed, vertically, within the same exposure (Figure 2.9).

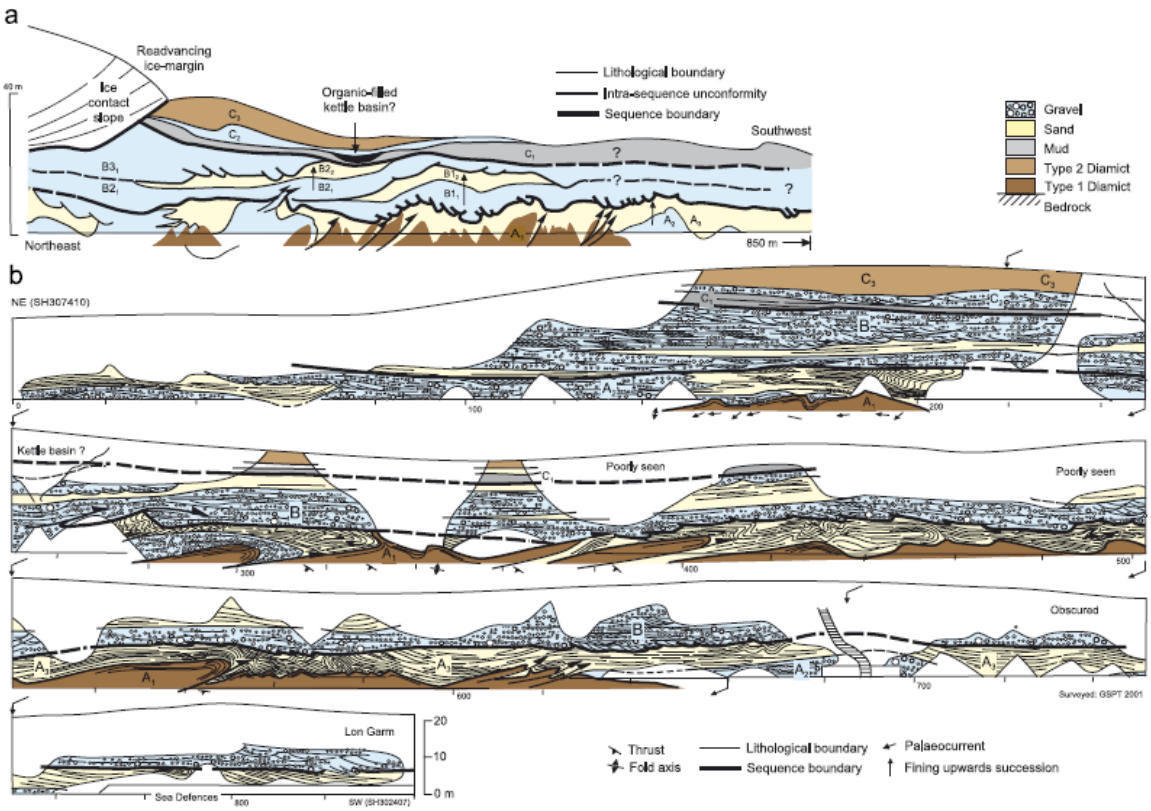

Figure 2.8. Sedimentary architecture of the exposures at Nefyn, north Wales (b) by Thomas and Chiverrell (2007) and reconstruction of the 3 depositional sequences (a) with a retreating ice-margin. The sedimentary architecture illustrates the lateral extent of Sequence A, B and C, and illustrates the occurrence of both B and C sequences in the same exposures.

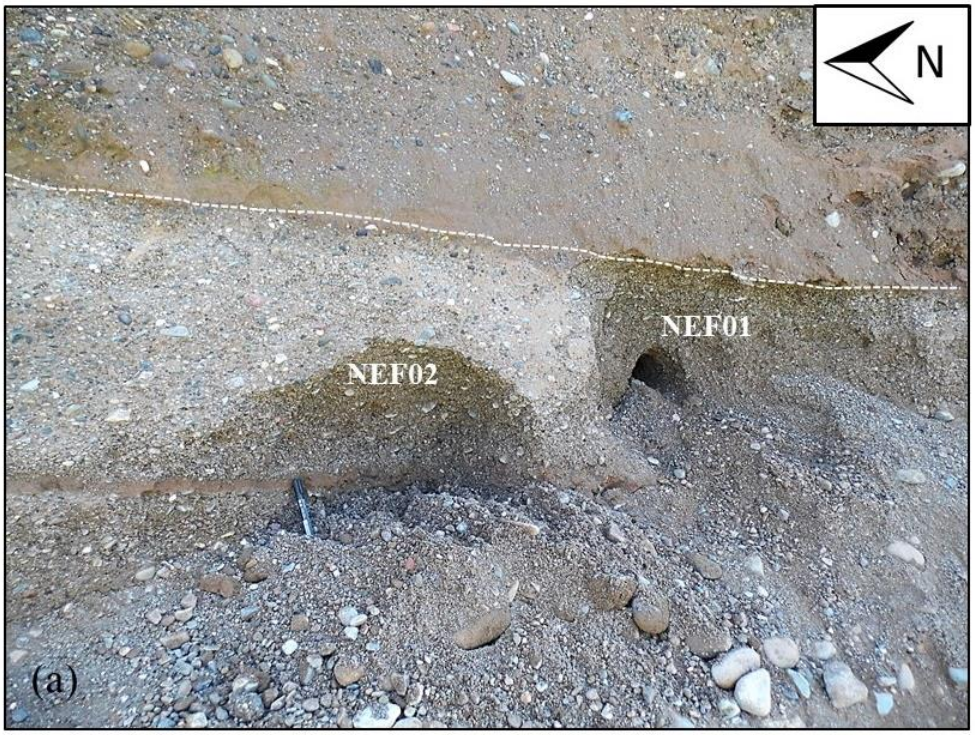
N
NEF01
NEF02
(a)


N
NEF03
(b)

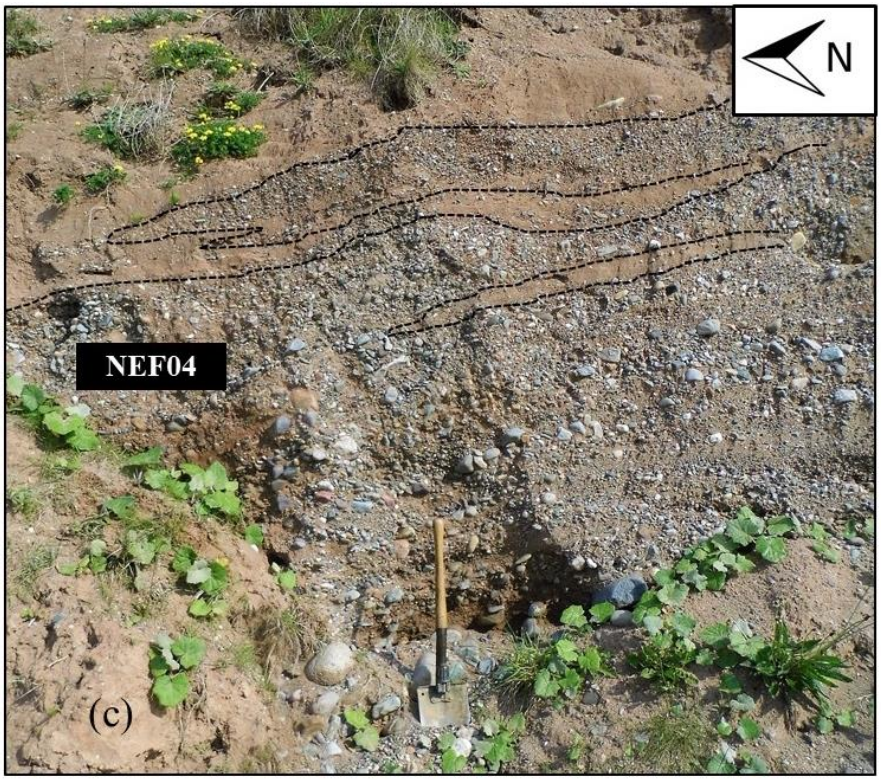

Figure 2.9. Photographs of the coastal exposures at Nefyn for the samples NEF01-2 (a), NEF03 (b) and NEF04 (c).

2.6.2. Bryn-yr-Eryr

The sediments exposed at Bryn-yr-Eryr, on the Llŷn Peninsula are interpreted to have been deposited in a sandur environment (Thomas and Chiverrell, 2007) and are located ~ 10 km north-east of Nefyn (Figure 2.7). As was the case at Nefyn, independent age control is available, and the same bracketing ages apply at Bryn-yr-Eryr as those at Nefyn (provided by Chiverrell *et al*., 2013) with bracketing ages to the south at 22.5 ka and to the north at 20.7 ka (Figure 2.2). The sediments at Bryn-yr-Eryr are exposed for ~ 1.5 km along the coast and consist of gravels, sands and diamicts. The gravel lithofacies at Bryn-yr-Eryr have been identified as the 'G2' gravel assemblage (Thomas and Chiverrell, 2007) and are stacked, massive and planar cross-bedded gravel, occasionally divided by laminated sand facies (Figure 2.10). This 'G2' lithofacies at Bryn-yr-Eryr is

similar in depositional environment (proximal facies generated by repeated meltwater cycles) to the proximal sandur deposits at Orrisdale Head, Isle of Man.

At 53.005365°N 4.3997937°W the ‘G2’ gravel sediments are exposed and occur as massive gravels with interbedded sands (Figure 2.11). All samples were obtained from this location (BRY01, 02, 03) and all within ~ 10 m laterally of each other (Figure 2.11) and ~ 8 m below the current land surface. The surface of bedded gravel lithofacies were targeted and this was undertaken, as at other locations, to maximise the probability that clasts were exposed to daylight at deposition.

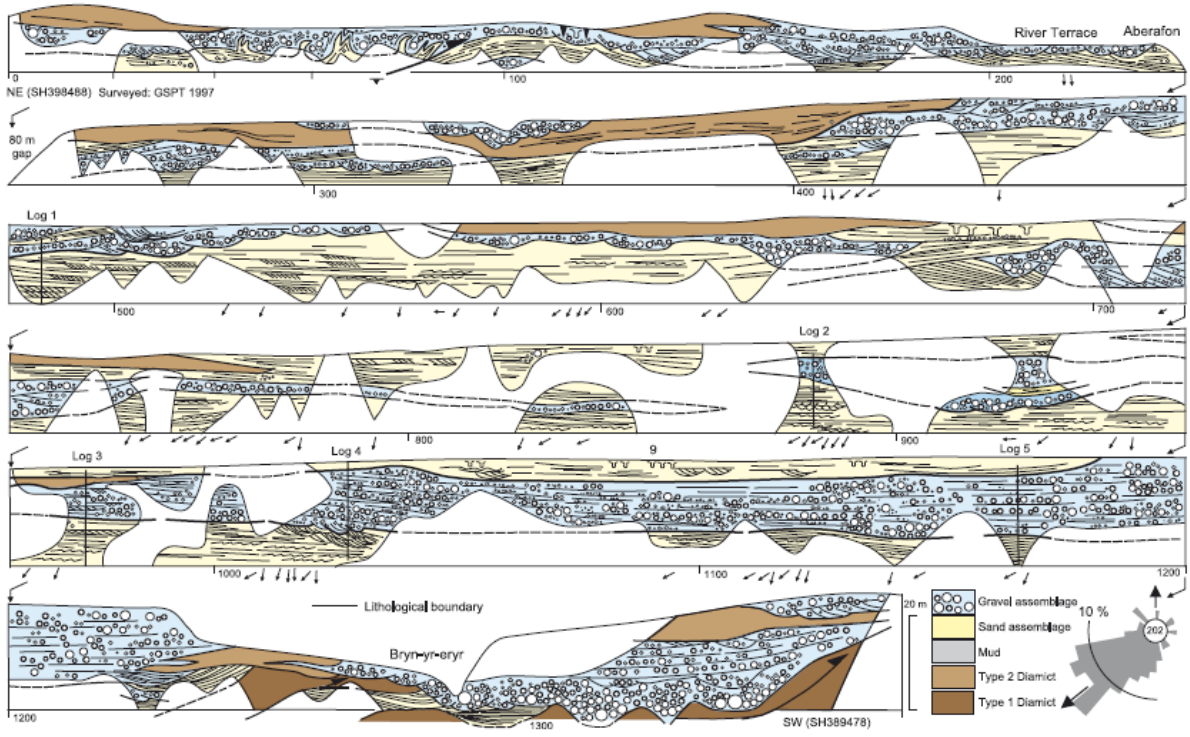

Figure 2.10. Illustration of the diamict, sand and gravel lithofacies exposed along the coastal from Aberafon to Bryn-yr-Eryr (Thomas and Chiverrell, 2007).

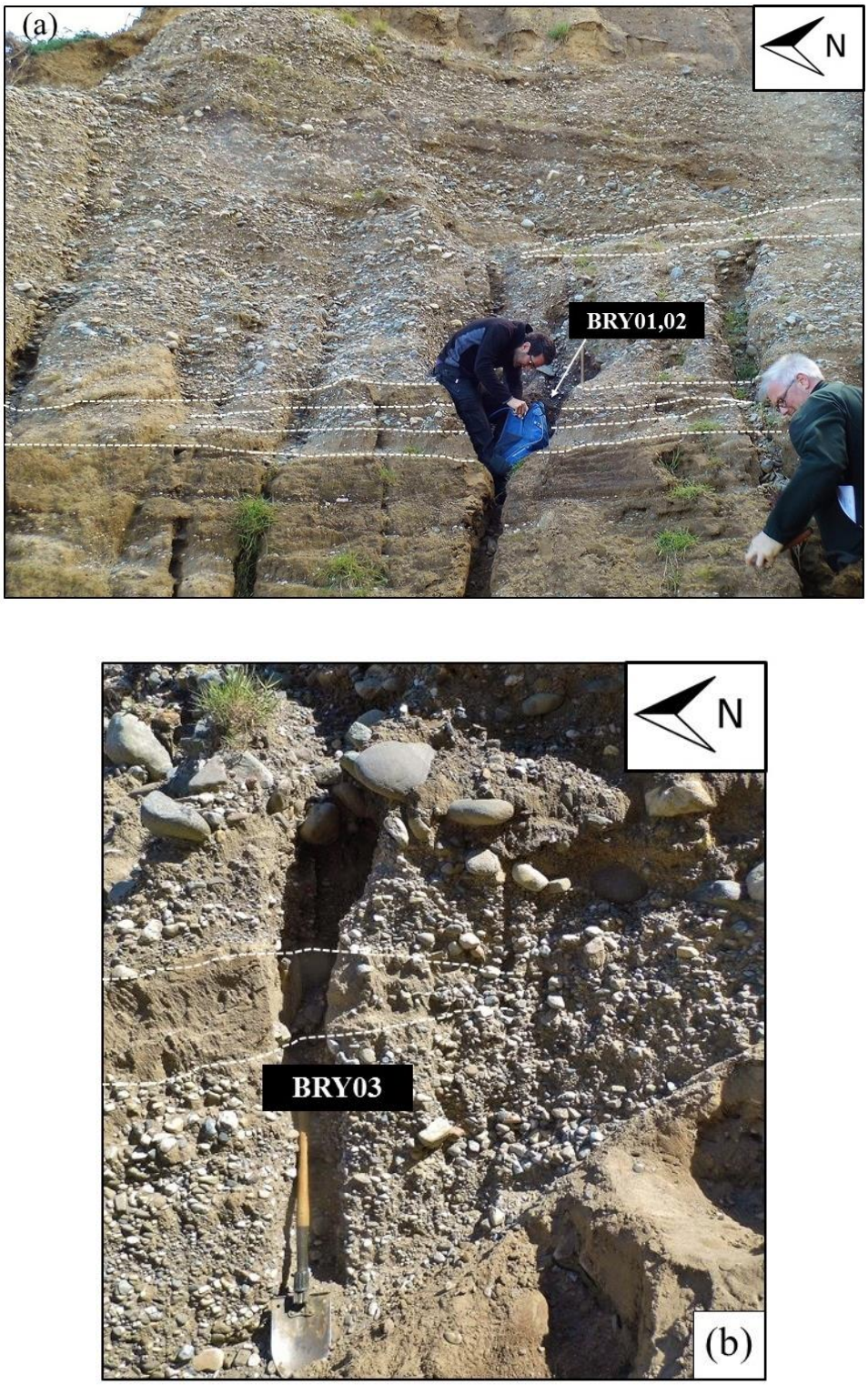

Figure 2.11. Photographs of the coastal sediment exposures at Bryn-yr-Eryr taken from the foreshore of the beach. The location of the first two samples is illustrated (a) along with the third sampling location (BRY03), which was located ~ 10 m laterally from the first site (b). These images illustrate the massive, occasionally inter-bedded sand and gravel lithofacies at Bryn-yr-Eryr.

2.7. Cheshire-Shropshire Lowlands

The Cheshire-Shropshire lowlands would have experienced maximum ice stream coverage at sometime between ~ 28 – 18 ka (Chiverrell and Thomas, 2010) whereby a separate independent ice lobe from the Irish Sea ice stream flowed southward into the Cheshire-Shropshire lowlands (Figure 2.2; 2.12). The Cheshire-Shropshire lowlands marks a position of on-shore glacial maximum extent (Figure 2.2; 2.12) and this ice lobe also coalesced with the Welsh Ice Cap to the west (Jansson and Glasser, 2005; Chiverrell and Thomas, 2010). Large and prominent moraines are apparent in the Cheshire-Shropshire lowlands and are associated with a series of outwash deposits and lacustrine sediments showing punctuated retreat through the basin (Evans *et al*., 2005; Thomas, 1989). The ice stream in the Cheshire-Shropshire Lowlands is interpreted to have reached the 'Wolverhampton Line' as illustrated by the position of the 'Whitchurch' moraine (Chiverrell and Thomas, 2010). A location in the Cheshire-Shropshire lowlands was selected due to the lack of independent age control in general for the entire ice stream (in comparison to the Irish Sea Ice Stream within the Irish Sea Basin) and due to the lack of independent age control for the LGM furthest extent. In addition to this, a comparison of ages to the Irish Sea ice stream within the Irish Sea Basin can be drawn.

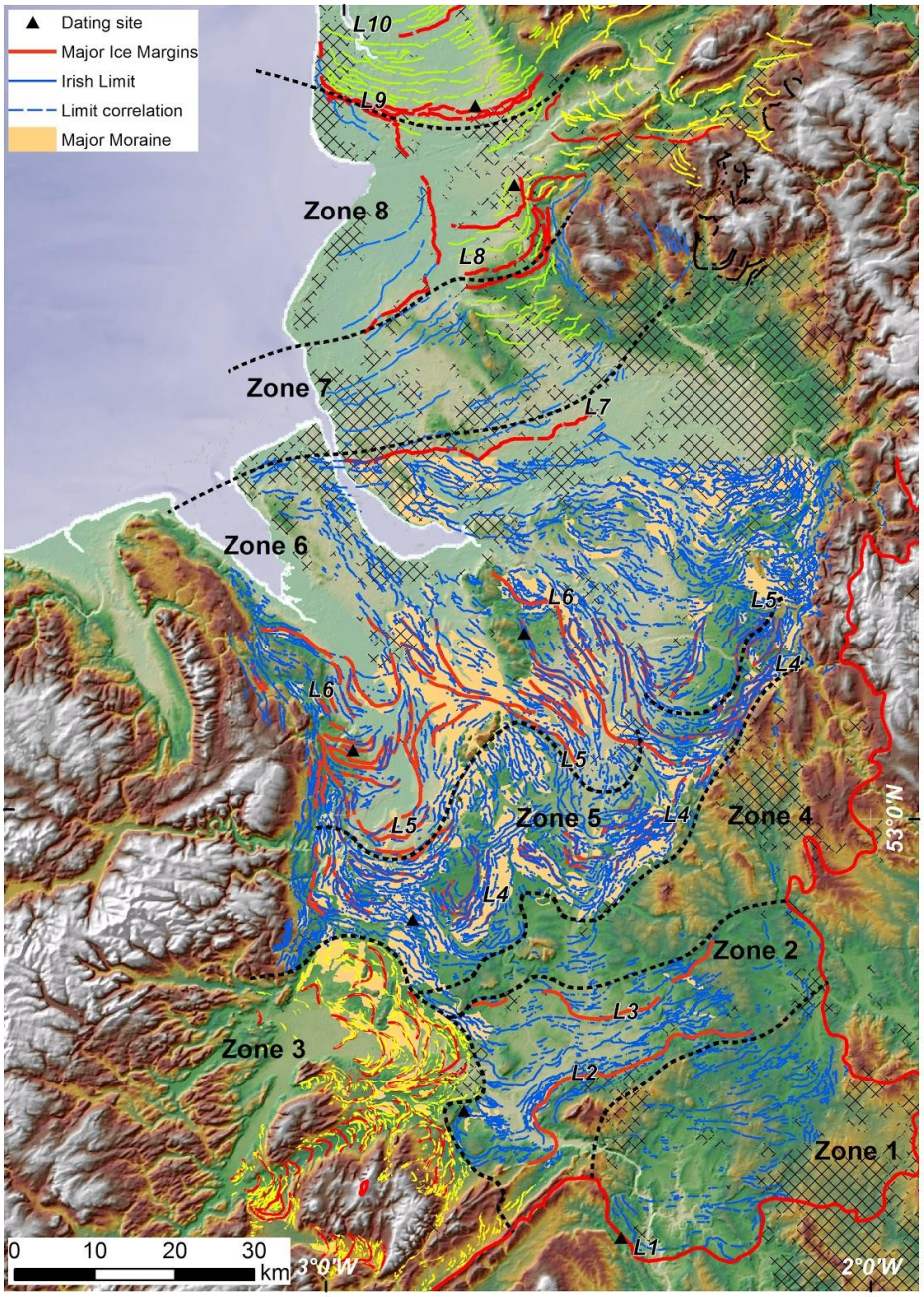

Figure 2.12. Retreat stages (with zone 1 illustrating the furthest extent) for the ice lobe which occupied the Cheshire-Shropshire basin (Chiverrell *et al*., in prep) with label L1 illustrating the location of Bridgwalton relative to the entire ice lobe.

2.7.1. Bridgwalton, Shropshire

The study site at Bridgwalton, Shropshire (Figure 2.2; 2.12), has received little attention and there is currently no published investigations of the sediment deposits. The

sediments at Bridgwalton were deposited in a deltaic environment, during the maximum extent of the ice stream that occupied the Cheshire-Shropshire lowlands. Bridgwalton was selected as the location records the maximum extent of the ice stream and also records on-shore ice stream termination at the LGM. In addition to this, Bridgwalton was selected due to the lack of chronological constraints. The two previous locations (Isle of Man and Llŷn Peninsula) had extensive independent age control available, through numerous geochronological techniques. However, due to the lack of independent ages at Bridgwalton, the application of this novel technique aims to provide the first reliable ages for the glaciofluvial sediments, following the trial application at well-constrained locations.

Bridgwalton, Shropshire, is a glacial deposit exposed in a commercial quarry, with numerous worked sediment faces across a range of depths within the quarry. The sedimentology at Bridgwalton illustrates a well-developed sequence of foreset bedding with sand and gravel lithofacies and a coarse gravel lithofacies capping the underlying foresets. The sand and gravel deposited in the foreset beds would have cycled through sandur deposits before deltaic deposition, thus improving the chance that cobbles were exposed prior to deposition. The Bridgwalton deposits currently have no independent age control. At 52.529290^{o}N 2.4629867^{o}W a series of gravel bars capping a foreset delta deposit are seen and three gravel packages were targeted from this for sampling (BWT01, 02, 03). The first gravel package (BWT01) was obtained ~ 10 m laterally and ~ 5 m below the other two (BWT02, 03) (Figure 2.13).

Figure 2.13. Photograph of two locations sampled at Bridgwalton (BWT02, 03) with both samples located towards the surface of the gravel bar to maximise the probability that cobbles were bleached at deposition.

2.8. Sample Selection

At all 4 sites, clasts were collected whilst using a black, light-tight plastic sheet held against the sediment exposure. Cobbles were identified in the sediment with the help of a red LED head torch, with b-axes varying from ~ 10 – 3.5 cm, and these were collected into light tight bags. Cobbles to a minimum size of ~ 3.5 cm were collected due to the difficulty in obtaining rock slices and estimations of dose rates in smaller material. The orientation of each clast was recorded by marking the upper and lower surfaces. Approximately 45 clasts of varying lithologies were obtained from the gravel lithofacies at Orrisdale Head. In addition to collecting cobbles from the four gravel packages (ORS01-04), two samples of the matrix from each gravel package were collected for

dosimetry and combined to give a single representative sample of the matrix for each package (samples OH01, 02, 03, 04). The gamma dose rate for each gravel package was also measured in situ using an Ortec DigiDART and a 2 inch NaI (Tl) crystal. Due to the successful sampling at Orrisdale, similar protocols were applied at Nefyn, whereby 30 granite clasts were obtained, and granite cobbles were targeted specifically due to the collection and analysis of cobbles from Orrisdale. In contrast to Orrisdale, however, four samples of the matrix were collected, instead of two, in an attempt to provide a more reliable measurement of the surrounding dose rate. At Bryn-yr-Eryr ~ 30 granite clasts were obtained using a black, light-tight plastic sheet which was held against the sediment exposures. Finally, at Bridgwalton, 20 granite cobbles were obtained from the gravel packages and were collected into light-tight bags. Along with the three gravel packages sampled, 4 samples of the matrix for dosimetry measurements were obtained from each gravel package and combined to give a single representative sample of the matrix for each package (samples BWT01, 02, 03). At all locations well-rounded cobbles were obtained and this was due to the well-sorted and highly eroded material within glacial sandur environments.

2.9. Summary

This chapter outlined the study locations selected, with Orrisdale Head, Isle of Man and Nefyn and Bryn-yr-Eryr, north Wales selected due to the extensive independent age control. This allows the trial application of this novel technique. Following application to two well-constrained locations, the analysis of Bridgwalton, Shropshire, provides the opportunity to establish the first age constraints for the site. In addition to this, this section outlines the methods applied during sampling and the best-practises for obtaining cobbles for luminescence dating.

3. Sample Preparation, Measurement and Dosimetry

3.1. Sample preparation

Previous luminescence studies of rocks (e.g. Chapot *et al*., 2012) have obtained sediment grains from rock samples by abrading the material, however, the crystalline lithologies analysed here would result in the breaking of individual grains during abrasion. In addition to this, it is unclear how many individual grains may provide a luminescence signal, and, therefore, keeping individual grains in-situ may be advantageous. Other studies (Sohbati *et al*., 2012a; Freiesleben *et al*., 2015; Sohbati *et al*., 2015) have measured the luminescence signal from in-tact, whole rock slices, taken from rock cores extracted from the cobbles themselves. Typically these have been ~ 1.5 mm thick and provide the opportunity for measuring a small number of grains in-situ.

Following the collection of cobbles into light-tight bags in the field (see Section 2.4.2), the samples were then opened under subdued red light in the laboratory. Rock cores of ~ 8 mm in diameter and of varying lengths (up to ~ 20 mm long) were obtained from cobbles, using a water-cooled, low-speed diamond-tipped drill (Figure 3.1). Where possible, triplicate cores were taken adjacent to each other, to provide multiple measurements of L_n/T_n and equivalent doses. Rock cores were placed into a chuck holder with a micrometre providing accurate measurements of depth into the rock core. The rock

cores were then sliced, using a Buehler IsoMet 11-4254 water-cooled, diamond-edged wafering blade (0.3 mm blade thickness) (Figure 3.2), and produced rock slices of 0.7 mm (0.71 ± 0.19 mm (n = 116)) in thickness (Figure 3.3). Rock slices were cut thinner in this study than previous studies (e.g. Freiesleben *et al*., 2015) so as to provide more luminescence measurements, over the same depth scales. A challenge does exist regarding the slicing of rock slices at the surface of the cobbles. This is because the natural micro topography of the surface slice results in splitting of slices. Therefore, rock slices from the surface are generally thicker (~ 1.2 mm) than those below the surface. The granite rock slices were washed in distilled water in an ultrasonic bath for 15 minutes to remove rock powder that was produced during the drilling and slicing process. The clean rock slices were dried and subsequently placed into steel planchettes for luminescence measurements, ensuring that the upper-face of the rock slices were placed facing upwards, ensuring that measurements focus on the surface of the rock slice. To establish an age for each location (e.g. Orrisdale Head) the average age is taken from the population of all rock slices that show consistent ages and the uncertainty given is the standard deviation of the population of consistent ages.

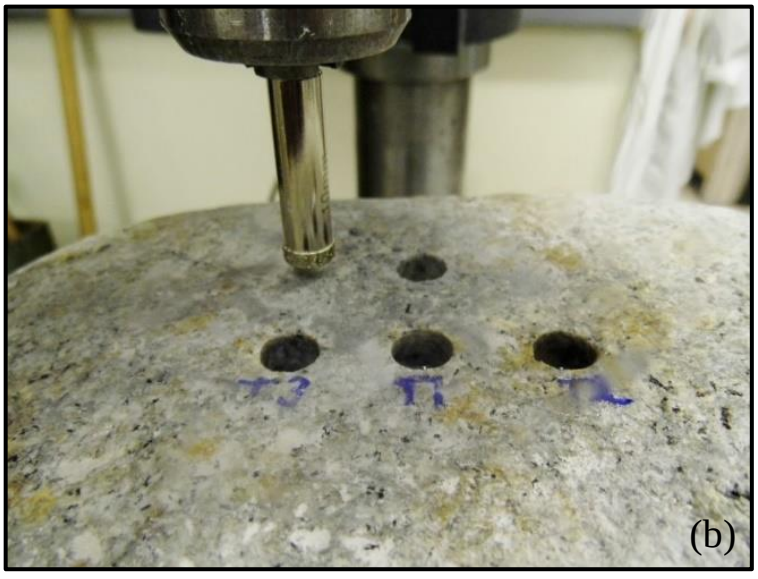

Figure 3.1. An experimental, test granite cobble placed on the drill-press platform following drilling (a) and a detailed image of the diamond-tipped drill bit used to obtain cores from the granite cobbles (b). Smaller cobbles are held in-placed upon the drilling platform using a detachable vice, as required.

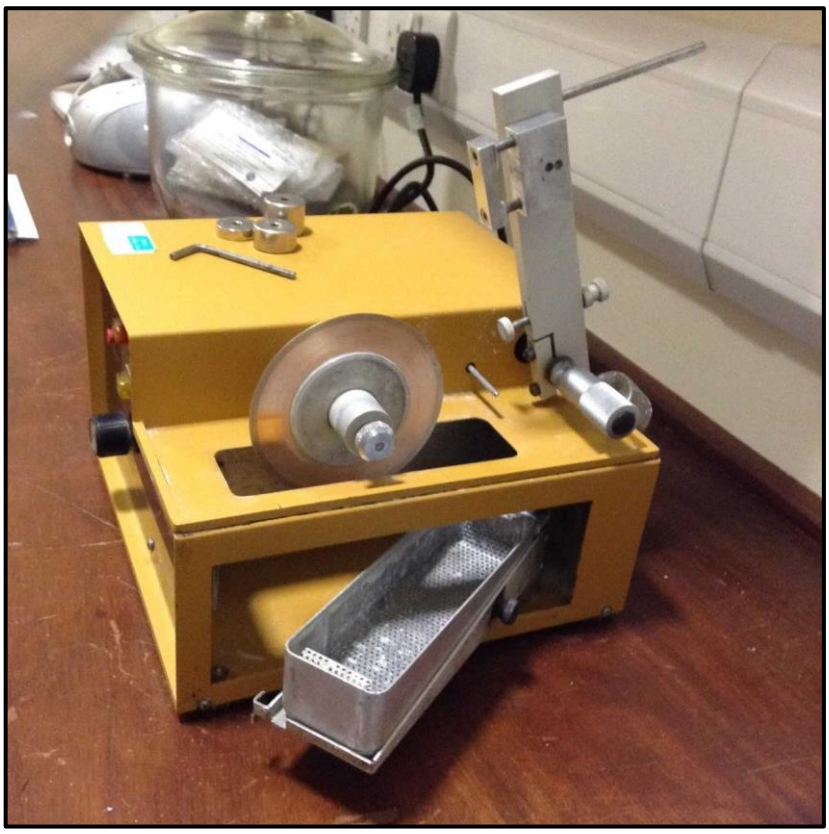

Figure 3.2. Image of the Buehler IsoMet 11-4254 used to obtain rock slices, with the water-cooled, diamond-edged wafering blade installed. Additional weights can be added to the slicing arm to alter the speed of the slicing process.

3.2. Luminescence procedures and measurement protocols

Known radiation doses must be provided in the laboratory to make accurate luminescence measurements (Aitken, 1985; Hansen *et al*., 2015). This is undertaken by using an absolutely known reference source to provide a calibration of the radiation source on the luminescence reader when analysing separated mineral grains. It has been shown that different grain sizes can result in a different dose rate to the sample (Wintle and Aitken, 1977; Armitage and Bailey, 2005) (Figure 3.4; 3.5). For the calibration of the beta source to rock slices in this study, a vein quartz cobble (ORS01-5) was obtained from Orrisdale Head, Isle of Man and from this cobble 12 rock slices were produced with thicknesses of 0.75 ± 0.1 mm.

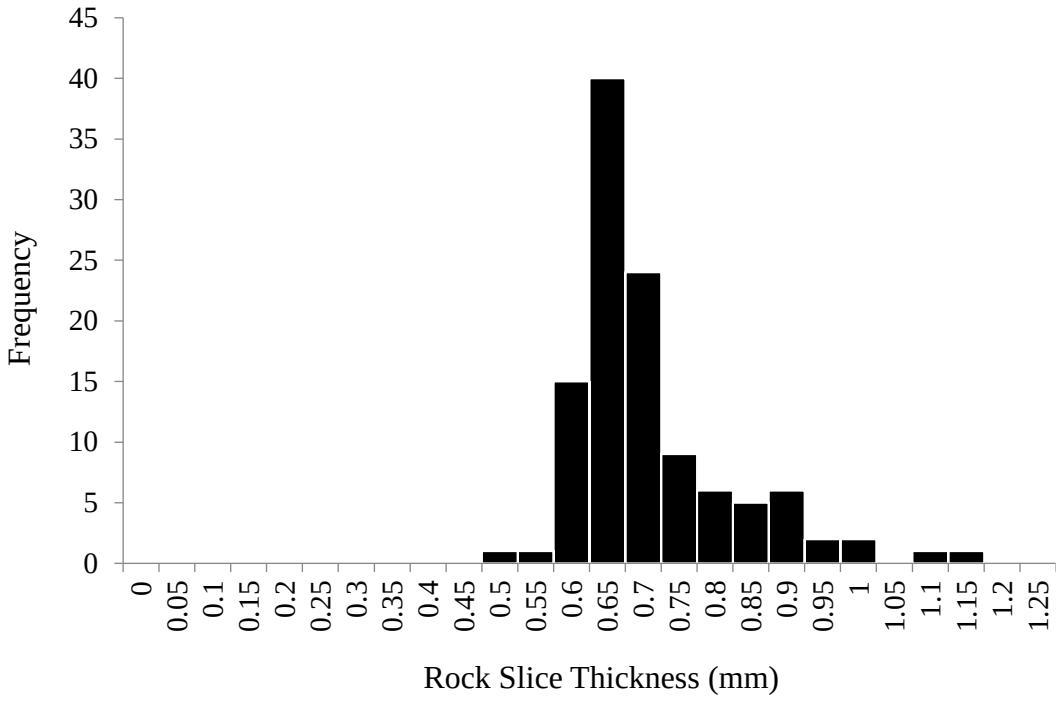

Figure 3.3. Rock slice thicknesses for 116 individual slices with an average thickness of 0.71 ± 0.19 mm.

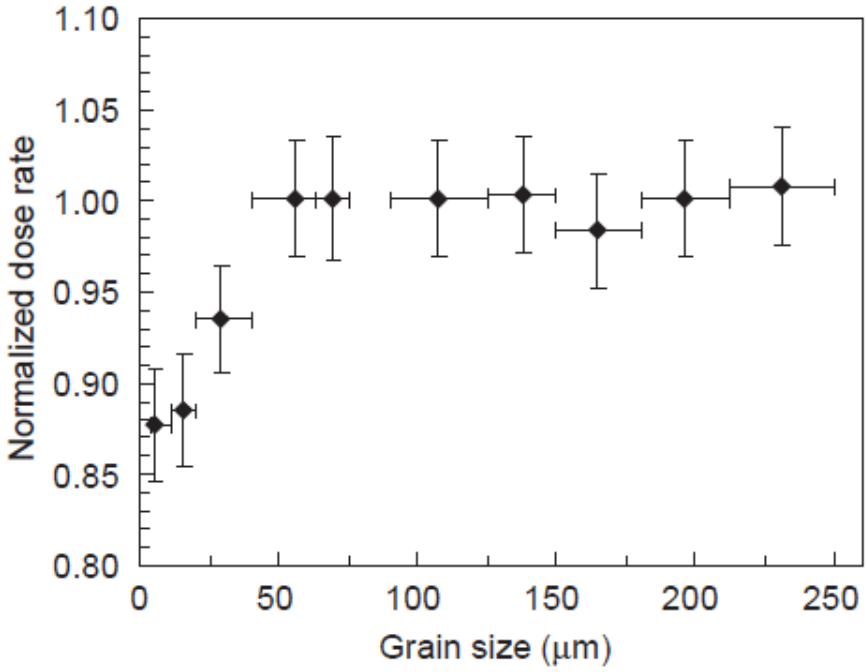

Figure 3.4. Normalised dose rates plotted against changes in grain size by Armitage and Bailey (2005) illustrating a lower dose rate for grain sizes up to ~ 50 µm.

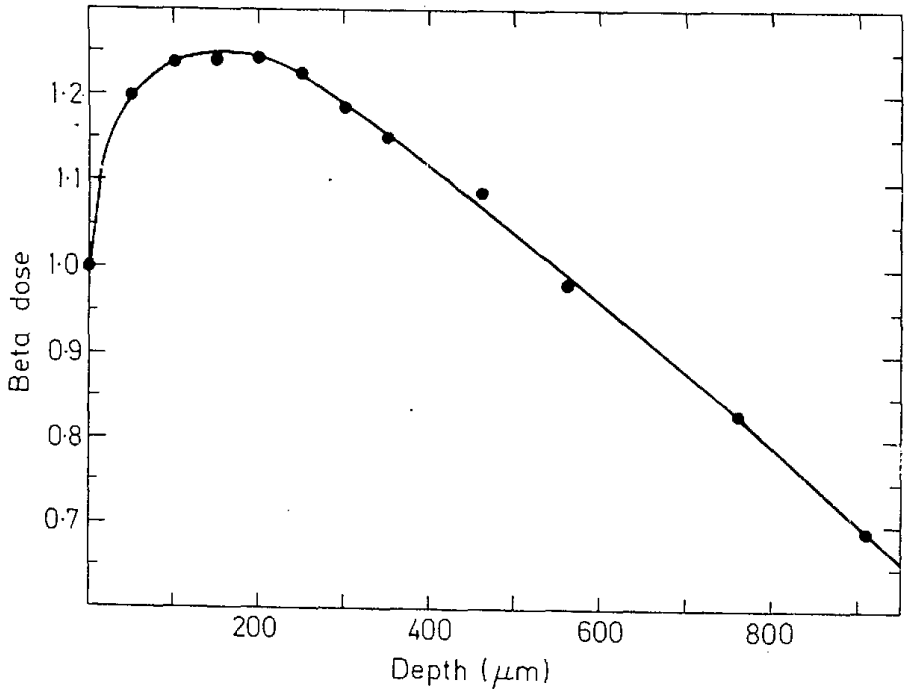

Figure 3.5. Beta dose rate within a slice as a function of depth (for material with a density and beta absorption characteristics as aluminium (and therefore quartz). The data points were obtained by irradiating fine-grains deposited onto a 0.45 mm thick aluminium disc with aluminium absorber of the indicated thickness interposed (Aitken, 1985).

The optically stimulated luminescence signal from these quartz slices was sensitised and stabilised by giving repeated cycles of irradiation (42.9 Gy) and heating (up to 500^{o}C) in order to provide a reproducible material for calibration. A dose of 4.90 Gy was given using a calibrated ^{137}Cs gamma source at DTU, Denmark, in a scatter free geometry. The rock slices were returned to Aberystwyth and measured using blue LEDs to stimulate OSL and a single-aliquot regenerative dose protocol. Due to the change in thickness of rock slices, placed in steel planchettes in comparison to sand-sized sediment the dose rate to rock slices changed from 0.036 Gy/s (used for coarse grain sediment) to 0.031 Gy/s and all subsequent measurements on rock slices were corrected for this change in dose-rate.

All luminescence measurements used a Risø TL/OSL reader (Bøtter-Jensen *et al.*, 2003) (originally manufactured in 1989 but refurbished with new electronics and optical

stimulation head in 2010 - Model TL/OSL-DA-20). Infrared stimulation (880 nm) was achieved with 22 TSFF5210 LEDs delivering 160 mW/cm^2 at the sample and photon detection was undertaken with a 2 mm thick Schott BG39, Corning 7-59 and Neutral Density 2.0 filter (when intense signal) combination with an EMI 9635QA photomultiplier tube. Beta irradiation used a calibrated ^{90}Sr/^{90}Y source mounted on the reader.

A post-IR IRSL$_{225}$ SAR protocol based on the approach of Buylaert *et al*. (2009) was used to measure the signal from granite rock slices (Table 3.1). A slower heating rate (1^{o}C/s) than normal was used with preheats held for 100s instead of the more common 60s, and the sample was held at its measurement temperature of 50^{o}C or 225^{o}C for 100s before IR stimulation began. These changes were made to reduce the impact of thermal lag within the rock slices. All pre-heat and stimulation steps within the SAR protocol were carried out in a nitrogen atmosphere.

Table 3.1. Modified Single Aliquot Regenerative dose (SAR) procedure used to measure granite rock slices.

Step	***Description***	***Signal***
1	No dose in cycle 1 – different regenerative doses in later cycles	
2	Preheat to 250^{o}C at 1^{o}C/s and hold for 100 s	
3	Heat to 50^{o}C at 1^{o}C/s, pause for 100 s, and measure IRSL for 200 s	Lx_{50}
4	Heat to 225^{o}C at 1^{o}C/s, pause for 100 s, and measure IRSL for 200 s	Lx_{225}
5	Test dose (34 Gy)	
6	Preheat to 250^{o}C at 1^{o}C/s and hold for 100 s	
7	Heat to 50^{o}C at 1^{o}C/s, pause for 100 s, and measure IRSL for 200 s	Tx_{50}
8	Heat to 225^{o}C at 1^{o}C/s, pause for 100 s, and measure IRSL for 200 s	Tx_{225}
9	Heat to 280^{o}C at 1^{o}C/s, pause for 100 s, and measure IRSL for 200 s	
10	Repeat cycles 1 – 9 for different regenerative doses	

3.3 Dosimetry

The environmental dose rate to rock slices originates from radionuclides in the surrounding matrix, the cobble itself and from cosmic rays. Therefore, to make dosimetry measurements a sample from the cobble and the surrounding matrix were required. A sample of each cobble and a sample of the surrounding matrix were milled to a fine powder prior to dosimetry measurements. To obtain material for milling from the cobbles, a larger core than normal was taken from the cobbles, using a 30 mm diameter diamond-tipped drill core. The material extracted from this larger core was then milled to a fine powder.

Dose rates were determined from thick source alpha counting (using a Daybreak 583 instrument) and beta counting (using a Risø GM-25-5 instrument; Bøtter-Jensen and Mejdahl, 1988). TSAC was used to calculate the U and Th concentrations (Table 3.2b), and a combination of beta counting and TSAC were used to calculate the K concentration (Duller *et al*., 2015). The U, Th and K concentrations were then combined to establish the external gamma dose rate with the conversion factors of Guérin *et al*. (2011). In-situ measurements of the external gamma contribution (Table 3.2a) were also made. In previous studies the water content of the cobble itself has been assumed to be negligible (e.g. Sohbati *et al*., 2015). In this study a water content of < 0.1 % was measured for sample ORS04–1 confirming that the water content of the cobble was indeed negligible.

3.3.1. Thick source alpha counting (TSAC)

Thick source alpha counting (TSAC) was used to calculate the U and Th concentrations using a Daybreak 583 alpha counter. A pair counting method was used in this study, as outlined in Appendix J of Aitken (1985). A scintillation of light is produced when an alpha particle interacts with the zinc sulphide screen and is detected using a

photomultiplier. Before a powdered portion of the sample is measured, the background for two zinc sulphide screens is measured. The powdered samples were spread over a zinc sulphide screen in a Perspex holder and placed into the alpha counter.

3.3.2. Beta counting

Beta counting was undertaken on a Risø GM-25-5- beta counter. The same samples were used for beta counting as were used for alpha counting. Three milled powder samples were packed into plastic pots and sealed with plastic film. Samples were then placed into a slide which is fed into the beta counter, with five positions allowing three measurements of the sample and two standard samples. Standard samples consisted of one pot of powder from a Shap granite and one magnesium oxide (MgO) with known dose rates.

3.3.3. In-field gamma spectrometry

In-field gamma spectrometry measurements were made following sampling of the lithofacies, with a hole bored using a hand auger to a depth of ~ 30 cm into the facies. Measurements were undertaken for 60 minutes to allow the accurate capture of the gamma field. In-field gamma measurements were made using an Ortec DigiDART gamma spectrometer equipped with a 2 inch NaI (Tl) crystal. The in-field gamma spectrometer is calibrated using a set of radioactively doped blocks at Oxford University (Rhodes and Schwenninger, 2007).

3.3.4. Internal dose rate of feldspar grains in rock slices

The internal beta dose rate from K-feldspar grains was calculated assuming a 12.5 % K content (Huntley and Baril, 1997). The internal potassium content of k-feldspar

grains was not measured directly in this study and this was due to the rock slices not being disaggregated for measurement. An internal K content of 12.5 % was assumed following similar assumptions used in sand-sized luminescence dating, whereby the internal K content is not measured, but assumed at 12.5 %. In addition to this, it has been shown (Huntley and Baril, 1997) that feldspar grains with the highest K content dominate the luminescence signal. It is clear, as outlined above, that the internal K content is challenging to determine and similar protocols have been applied in other cobble-dating studies (Freiesleben *et al*., 2015; Sohbati *et al*., 2015). The internal beta dose rate contributes significantly to the overall dose rate whereby at depths of 2 mm or more into the cobble (for cobble ORS04-1-A), the internal beta dose arising from K in the feldspar grains is 33 % of the total dose rate. The sizes of feldspar grains within the rock slices were measured using a digital hand-lens from cobbles at each location. For cobble ORS04-1-A grain sizes ranged from 320 – 1500 μm and gave a mean value of 647 ± 235 μm. The internal beta dose rate calculated for this grain size was 2.250 ± 0.702 Gy/ka (Table 3a). Grain sizes were measured from cobbles at each location and, therefore, altered the internal dose rate for each study site.

3.3.5. Cosmic dose rate

The cosmic dose rate contribution to the overall environmental dose rate is relatively small, however this is still accounted for here in the total environmental dose rate. The dose rate contribution from cosmic radiation was calculated following Prescott and Hutton (1994) and is presented in Table 3.2a. The depth of each sample was estimated in-field and was measured from the sample to the assumed past land surface as opposed to the present-day top of the section.

3.3.6. Water content

To measure the saturated water contents for the surrounding matrix, the sediment was packed into tights and weighed. Then, the sediment was placed into a beaker of water until completely saturated. The saturated tights were then suspended and were interpreted to be entirely saturated when individual drops of water fell from the sample at time intervals of 1 minute. The saturated sediment was then weighed before being placed into the oven for several days. Estimating the water content over the entire burial period for a sample is difficult due to the possibility for the water content fluctuating across this time. Measurements of water contents of the sediment are required to calculate the correct dose rates to the rock slices. Saturated water contents were measured in the laboratory and gave saturated values of 15 ± 5 %. In addition to this, a water content of 27 % was applied for samples at Bridgwalton, following the process outlined in Chiverrell *et al*. (in prep) and based on water content estimations for sand-sized material from the same location.

3.4. Modelling the dose rate with depth into cobble sub-surfaces

The sources of radiation to individual rock slices comes from alpha, beta and gamma dose rates from the cobble itself, beta and gamma dose rates from the sediment matrix, internal beta dose rates from the grains themselves and cosmic rays (Figure 3.6). The interaction of two materials (cobble and matrix), with different dose-rates, means that numerical modelling is required to establish the dose rate at a specific depth into one of the materials. Dose rates need to be calculated at specific depths, into the cobble sub-surfaces. Freiesleben *et al*. (2015) calculated the variation of dose rate with depth into a cobble, making use of the approach outlined by Aitken (1985, Appendix H). In Freiesleben *et al.* (2015), the cobble was part of a rubble layer, and the calculations

assumed that the cobble was part of a flat layer, of thickness *h* and of infinite lateral extent.

Equation 3.1 describes the variation in the beta dose rate with depth (*x*) into a cobble sub-surface that is buried within a sediment matrix.

$$\dot{D}(x)_{\beta}^{\text{Cobble}} = \dot{D}_{\text{Rock},\beta}^{\text{inf}}\left[1 - 0.5\left(e^{-bx} + e^{-b(h-x)}\right)\right] + \dot{D}_{\text{Sed},\beta}^{\text{inf}} 0.5\left(e^{-bx} + e^{-b(h-x)}\right). \quad (3.1)$$

In this equation, *b* is the beta attenuation factor (1.9 mm^{-1} following Sohbati *et al*., 2012c) and $\dot{D}_{\text{Rock},\beta}^{\text{inf}}$ and $\dot{D}_{\text{Sed},\beta}^{\text{inf}}$ are the infinite matrix beta dose rates for the cobble and sediment (Table 3a). For cobbles that are typically ~ 40 - 90 mm in diameter, the approximation of Freiesleben *et al*. (2015) is appropriate for the beta dose rate. An equation of the same form is used for the gamma contribution $\left(\dot{D}(x)_{\gamma}^{\text{Cobble}}\right)$ but with an attenuation factor of 0.01 mm^{-1} (Sohbati *et al*., 2015). For the alpha contribution to the equation ($\dot{D}(x)_{a}^{\text{Cobble}}$), the sediment alpha contribution is ignored. This is due to the short distances (~ 10 μm) travelled by alpha particles, meaning that the alpha contribution from the sediment would only impact upon the uppermost surface of the uppermost rock slice. The dose rate at a specific depth (*x*) is then calculated by summing the alpha ($\dot{D}(x)_{a}^{\text{Cobble}}$), beta ($\dot{D}(x)_{\beta}^{\text{Cobble}}$) and gamma $\left(\dot{D}(x)_{\gamma}^{\text{Cobble}}\right)$ contributions, the internal beta dose, and the cosmic ray dose.

Following the method outlined above, the dose rates were established using TSAC, beta counting and in-field gamma spectrometry to provide the total dose rate. An example of changes in dose rates, with depth into a cobble, is illustrated in Figure 3.7. The dose rate to feldspar grains in rock slices in core ORS04-1-A vary from 5.37 ± 0.72 Gy/ka at the surface of the cobble to 6.78 ± 0.75 Gy/ka inside the cobble (see Figure 3.7).

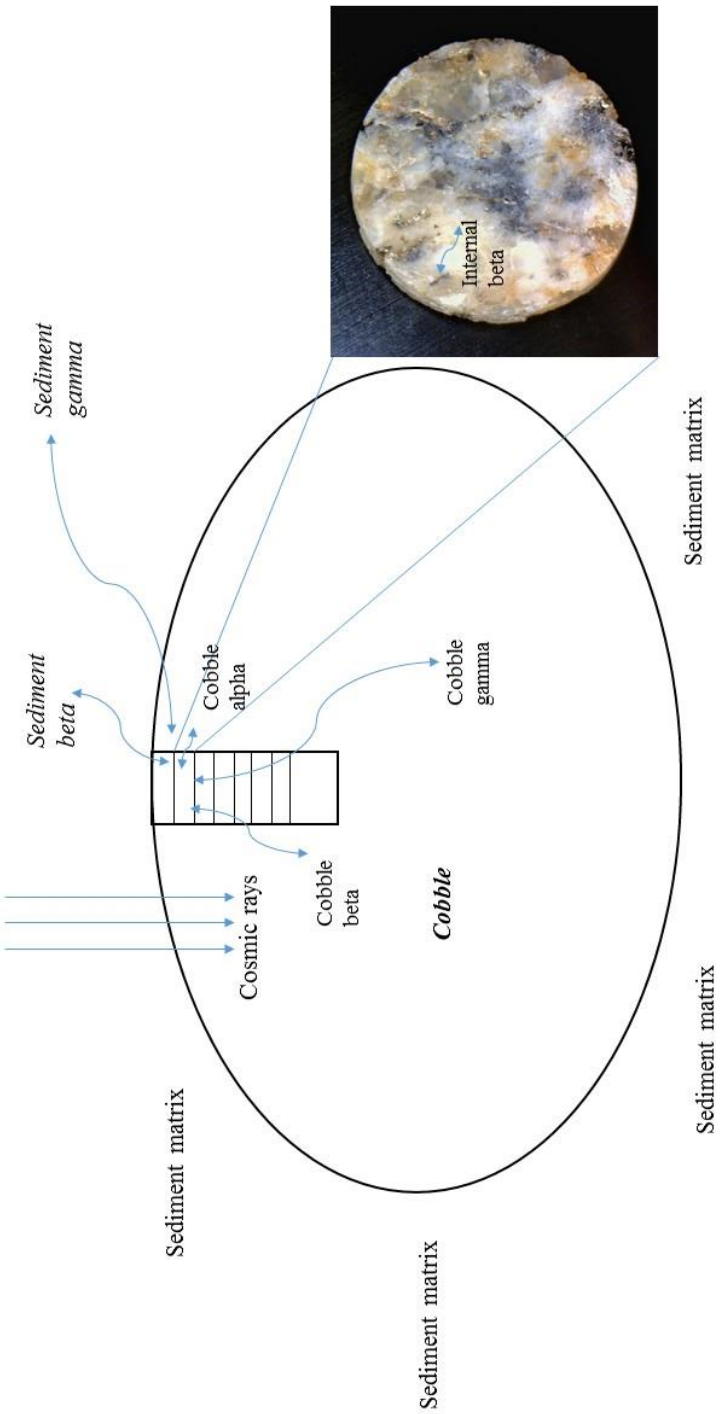

Figure 3.6. Schematic of the cobble and sediment matrix and the various dose rate contributions from both materials.

The example shows the dose rate changes rapidly in the outer 2 mm of the cobble due to the large difference in the beta dose rate from the matrix and the cobble and the limited penetration of beta particles (Figure 3.7). For cobble ORS04-1-A the gamma dose varies little with depth, and is much lower (0.31 ± 0.02 Gy/ka at the cobble surface) than the beta dose.

At depths of 2 mm or more into cobble ORS04-1-A, the internal beta dose arising from K in the feldspar grains is 33 % of the total dose rate, and the external beta dose to the grains arising from the cobble is 53 % of the total dose rate. When this is combined with the gamma dose arising from the cobble itself, this means that 93 % of the total dose rate arises from the cobble itself at depths ≥ 2 mm below the surface. This dose rate is insensitive to the water content of the matrix, and also to potential changes due to post-depositional migration of radionuclides (Olley *et al*., 1997), and hence studying cobbles offers major advantages compared to more conventional dating using finer sediments. The dose rate situation is also similar at Bridgwalton, whereby at depths of > 2 mm the dose rate is 89 % independent of the dose rate from the surrounding sediment matrix (and therefore the water content).

However, care must be taken when assessing the dose rate to the outermost ~ 2 mm of the cobbles because the dose rate changes rapidly through this upper layer (i.e. the outer 1 or 2 slices in this study, Figure 3.7), meaning that small uncertainties in the assessment of the depth will result in uncertainties in the dose rate (cf. Simkins *et al*., 2016); to circumvent these challenges, the outer ~2 mm of the cobbles should be avoided where possible. However, this is largely dependent upon the level of sub-surface bleaching in the samples.

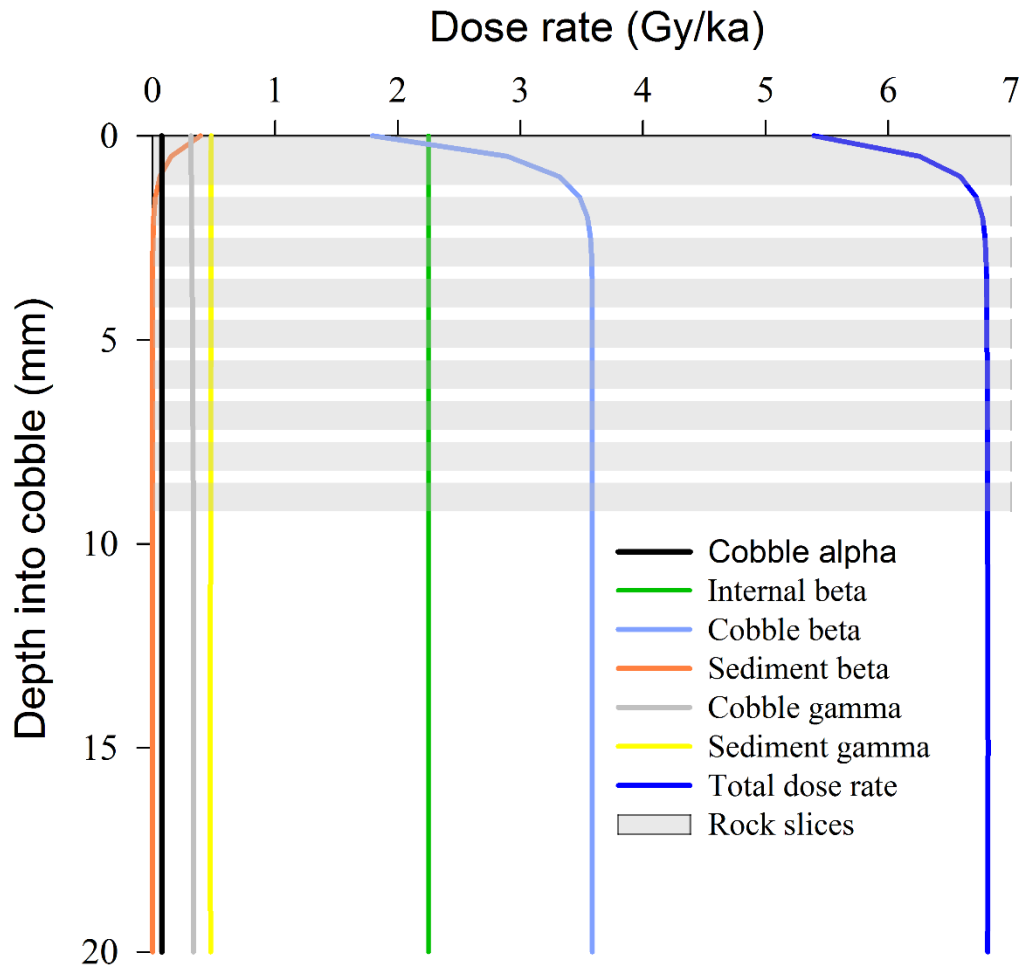

Figure 3.7. Dose rate variations with depth into the sub-surface of core ORS04-1-A, with increasing distance from the cobble surface-sediment matrix interface.

3.5. Environmental dosimetry data

Environmental dosimetry data for all locations studied within this thesis are outlined in Tables 3.2a and 3.2b. Contributions to the total environmental dose rate to feldspar minerals come from an external alpha dose rate, external beta dose rate, internal beta dose rate, external gamma dose rate and the cosmic dose rate. As shown in the previous section, these measurements are undertaken for both the cobble itself, and the surrounding sediment matrix and modelled using equations outlined in Section 3.2.7. The dose rate, with depth into the cobble sub-surface, was calculated for each individual

cobble analysed, due to the changes in dosimetry between the individual cobbles (Tables 3.2a, b).

Table 3.2a. Measured dosimetry data for all cobble and matrix samples studied

				Attenuated and water corrected dose rates				
Sample name	***Sample type***	***TSAC (cts/ks/cm^2)***	***Infinite beta dose rate (Gy/ka)***	***Beta (Gy/ka)***	***Gamma (Gy/ka)***	***In-situ gamma (Gy/ka)***	***Cosmic (Gy/ka)***	***Internal beta (Gy/ka)***
OH02	Matrix	0.375 ± 0.007	1.383 ± 0.047	0.861 ± 0.079	0.621 ± 0.045	0.687 ± 0.035	-	-
OH04	Matrix	0.305 ± 0.006	1.257 ± 0.044	0.782 ± 0.072	0.549 ± 0.040	0.799 ± 0.040	-	-
ORS02-1	Cobble	1.840 ± 0.032	4.454 ± 0.142	3.292 ± 0.243	3.029 ± 0.200	-	0.104 ± 0.05	2.250 ± 0.702
ORS04-1	Cobble	1.080 ± 0.019	4.852 ± 0.154	3.586 ± 0.265	2.406 ± 0.131	-	0.094 ± 0.05	2.250 ± 0.702
ORS04-3	Cobble	1.460 ± 0.023	5.215 ± 0.166	3.854 ± 0.285	2.643 ± 0.131	-	0.094 ± 0.05	2.250 ± 0.702
NEF03	Matrix	0.473 ± 0.007	1.897 ± 0.063	1.312 ± 0.092	0.892 ± 0.062	1.044 ± 0.052	-	-
NEF04	Matrix	0.495 ± 0.007	1.949 ± 0.060	1.348 ± 0.093	0.820 ± 0.041	0.700 ± 0.049	-	-
NEF03-2	Cobble	1.480 ± 0.024	2.844 ± 0.088	2.335 ± 0.103	2.042 ± 0.151	-	0.070 ± 0.03	1.399 ± 0.367
NEF04-1	Cobble	0.594 ± 0.011	3.871 ± 0.124	3.179 ± 0.143	1.708 ± 0.077	-	0.070 ± 0.03	1.399 ± 0.367
NEF04-3	Cobble	0.837 ± 0.015	2.764 ± 0.090	2.270 ± 0.103	1.598 ± 0.101	-	0.070 ± 0.03	1.399 ± 0.367
BRY01	Matrix	0.617 ± 0.009	2.502 ± 0.078	1.776 ± 0.119	1.052 ± 0.062	1.232 ± 0.074	-	-
BRY02	Matrix	0.482 ± 0.007	1.832 ± 0.061	1.300 ± 0.089	1.144 ± 0.057	0.977 ± 0.068	-	-
BRY01-1	Cobble	0.584 ± 0.011	3.869 ± 0.124	3.261 ± 0.138	1.718 ± 0.079	-	0.070 ± 0.03	1.189 ± 0.328
BRY02-2	Cobble	0.860 ± 0.015	4.512 ± 0.144	3.803 ± 0.161	2.187 ± 0.111	-	0.070 ± 0.03	1.189 ± 0.328
BRY02-4	Cobble	0.607 ± 0.009	3.290 ± 0.106	2.773 ± 0.118	1.498 ± 0.061	-	0.070 ± 0.03	1.189 ± 0.328
BRY02-6	Cobble	0.805 ± 0.010	4.364 ± 0.139	3.678 ± 0.156	2.045 ± 0.077	-	0.070 ± 0.03	1.189 ± 0.328
BRY03-1	Cobble	0.776 ± 0.010	4.349 ± 0.139	3.666 ± 0.155	1.965 ± 0.143	-	0.070 ± 0.03	1.189 ± 0.328
BRY03-2	Cobble	0.733 ± 0.012	4.276 ± 0.136	3.160 ± 0.234	2.002 ± 0.860	-	0.070 ± 0.03	1.189 ± 0.328
BWT03	Matrix	0.361 ± 0.006	0.971 ± 0.035	0.554 ± 0.056	0.576 ± 0.038	0.753 ± 0.038	-	-
BWT03-1	Cobble	0.504 ± 0.011	3.604 ± 0.115	2.749 ± 0.240	1.537 ± 0.069	-	0.070 ± 0.03	2.000 ± 0.849

Table 3.2b. Dosimetry data calculated for all cobble and matrix samples studied

Sample name	***Sample type***	***Cobble Size (mm) (a:b:c)***	***Depth (m)***	***K (%)***	***U (ppm)***	***Th (ppm)***
OH02	Matrix	-	-	0.62 ± 0.05	1.09 ± 0.18	4.49 ± 0.58
OH04	Matrix	-	-	0.55 ± 0.04	1.33 ± 0.16	4.15 ± 0.52
ORS02-1	Cobble	86:57:56	6	3.03 ± 0.20	6.65 ± 1.11	29.66 ± 3.72
ORS04-1	Cobble	60:32:30	7	2.41 ± 0.13	4.67 ± 0.60	14.85 ± 2.00
ORS04-3	Cobble	73:39:38	7	2.64 ± 0.13	8.97 ± 0.60	10.76 ± 1.98
NEF03	Matrix	-	-	1.74 ± 0.08	2.55 ± 0.17	4.76 ± 0.56
NEF04	Matrix	-	-	1.78 ± 0.08	2.54 ± 0.18	5.41 ± 0.61
NEF03-2	Cobble	70:59:36	10	1.69 ± 0.20	7.28 ± 0.74	17.14 ± 2.45
NEF04-1	Cobble	62:42:37	10	4.12 ± 0.17	2.43 ± 0.32	8.64 ± 1.01
NEF04-3	Cobble	49:41:37	10	2.45 ± 0.15	2.96 ± 0.48	13.76 ± 1.56
BRY01	Matrix	-	-	2.32 ± 0.11	3.05 ± 0.26	7.12 ± 0.86
BRY02	Matrix	-	-	1.67 ± 0.09	2.25 ± 0.20	6.03 ± 0.68
BRY01-1	Cobble	69:57:40	10	4.13 ± 0.17	2.10 ± 0.34	9.45 ± 1.13
BRY02-2	Cobble	53:39:32	10	4.63 ± 0.21	2.72 ± 0.50	15.24 ± 1.68
BRY02-4	Cobble	40:35:34	10	3.33 ± 0.14	3.04 ± 0.26	6.90 ± 0.85
BRY02-6	Cobble	54:40:32	10	4.46 ± 0.18	3.20 ± 0.31	12.01 ± 1.05
BRY03-1	Cobble	61:39:38	10	4.43 ± 0.22	3.50 ± 0.29	10.15 ± 0.97
BRY03-2	Cobble	45:44:36	10	4.48 ± 0.18	2.25 ± 0.36	13.23 ± 1.22
BWT03	Matrix	-	-	0.74 ± 0.05	1.78 ± 0.16	4.17 ± 0.53
BWT03-1	Cobble	51:43:30	10	3.87 ± 0.16	2.23 ± 0.29	6.75 ± 0.97

4. Experimental bleaching of rock slices and cobble sub-surfaces

4.1. Introduction

A fundamental aspect of using cobbles in luminescence dating is the penetration of light into the cobble and the impact that this has upon the luminescence signal. Three different experiments are described in this chapter which aims to increase our knowledge in this area. The first is to investigate the bleaching of the $IRSL_{50}$ and post-IR $IRSL_{225}$ signal from single slices of granite, using the solar simulator (Section 4.2). The second experiment is to use the same light source for a cobble and investigate how bleaching proceeds at different depths (Section 4.3). Finally, the pattern of bleaching observed from a cobble exposed to natural sunlight is examined (Section 4.4).

4.2. Experiment 1: bleaching of individual rock slices

Previous studies have shown that the $IRSL_{50}$ signal bleaches more quickly than the post-IR $IRSL_{225}$ signal (Buylaert *et al*., 2012; Colarossi *et al*., 2015). Colarossi *et al*. (2015) measured changes in the normalised luminescence signal for quartz and feldspar, with the difference in bleaching between the $IRSL_{50}$ and post-IR IRSL signals also measured. Measurements of bleaching are undertaken for this study because (1) no mineral separation has been undertaken, and therefore the IRSL signal could come from

a variety of minerals. (2) The rock slices are considerably thicker (~ 700 µm) (about 3 – 6 times thicker) than sediment grains. Three rock slices were taken from cobble ORS02-1 (F-11, 12, 13) which is a cobble that was buried in the glacial sediments at Orrisdale Head, Isle of Man (Figure 4.1). These rock slices were bleached thoroughly and stabilised prior to the experiment by giving successive irradiation and stimulations (3 cycles of the SAR sequence outlined in Table 3.1). A dose of 43 Gy was then given before bleaching for a given time period (and repeated for each bleaching experiment). These 3 individual rock slices were bleached for periods of up to 1 week in the SOL-2 solar simulator. Measurements on the rock slices used for bleaching experiments used the sequence outlined in Section 3.3 (Table 3.1), however, only the natural signal was measured along with 1 test dose (43 Gy). The data (Figure 4.2) for given bleaching times was then normalised to the value given for a measurement following zero exposure and each data point for a given time of bleaching is an average of the three L_n/T_n values (one from each rock slice).

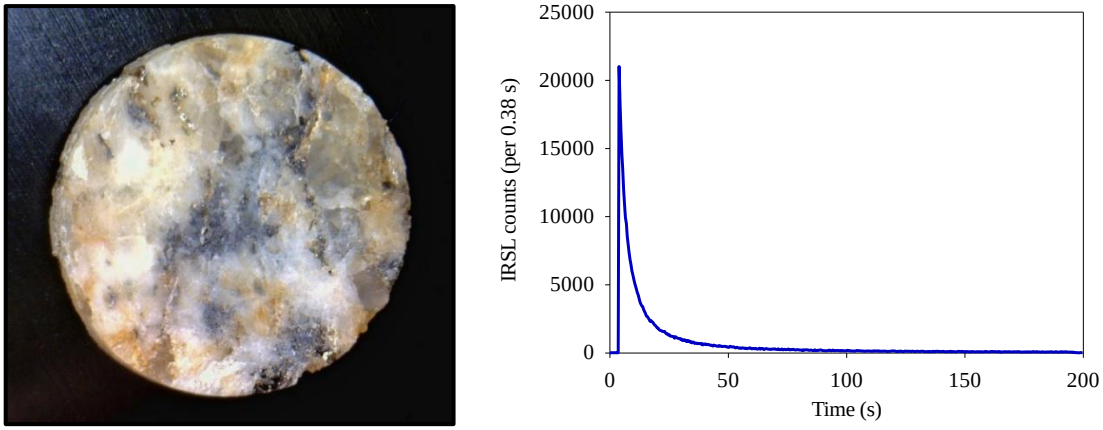

Figure 4.1. Digital microscope image of rock slice ORS02-1-F-11 and a decay curve for the same rock slice for the $IRSL_{50}$ signal following a given test dose of 43 Gy (with a neutral density 2.0 filter also installed). L_n/T_n measurements were established by integrating the signal over the first 9 channels and for the background, the last 50 channels.

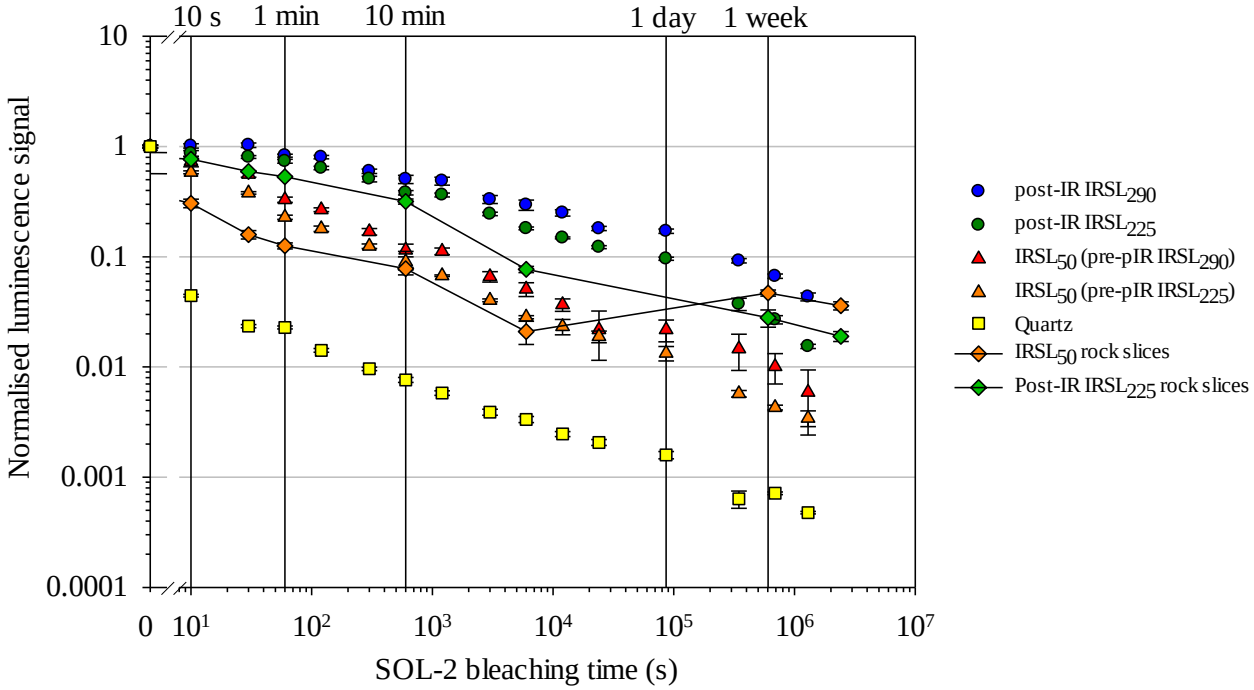

Figure 4.2. Changes in normalised luminescence over time for rock slices (with a line fit) and in comparison to bleaching of quartz and feldspar grains by Colarossi *et al*. (2015). The data without a line fit are those measured by Colarossi *et al*. (2015). Each data point in Figure 4.2 is the average of 3 rock slices.

Patterns in the normalised luminescence signal, over time, show a general agreement with the data given by Colarossi *et al*. (2015). The post-IR IRSL$_{225}$ signal shows excellent agreement with measurements on sand-sized feldspar by Colarossi *et al*. (2015). This shows that the post-IR IRSL$_{225}$ signal, originating from thicker, unseparated rock slices bleaches in a similar fashion to separated, thinner sediment grains. However, although a general agreement between the data sets exist, there appears to be some data points which show different bleaching for the same signals given for sediment samples. The IRSL$_{50}$ signal at 10 seconds, 30 seconds and 1 minute bleaches quicker than the IRSL$_{50}$ observed by Colarossi *et al*. (2015), however, after 10 minutes, the remaining IRSL$_{50}$ signal agrees with that observed by Colarossi *et al*. (2015). This could potentially be a result of the difficulty of bleaching rock slices for such a short period of time in the SOL-2 solar simulator. The most noticeable change is the IRSL$_{50}$ signal in rock slices following 1 week of bleaching in the SOL2. For the 1 and 2 week measurements, the

$IRSL_{50}$ signal remaining is higher than that after 3 days. Furthermore a greater proportion of the $IRSL_{50}$ signal remains than the post-IR $IRSL_{225}$ signal, with the $IRSL_{50}$ signal higher than that observed by Colarossi *et al*. (2015). It is unclear why this remaining luminescence is present for the $IRSL_{50}$ signal and could potentially be a result of rock slices being turned over during the transportation process (meaning that the other side of the rock slice was stimulated). Further data on bleaching of slices will be presented in Section 4.3.3.

4.3. Experiment 2: Bleaching as a function of depth into a saturated cobble sub-surface

At the time of experimental construction, bleaching with depth into a rock sub-surface had only been modelled by Sohbati *et al*. (2012c) with no extensive experimental measurements undertaken on characterising the extent and shape of bleaching profiles. A bleaching model has been proposed by Sohbati *et al*. (2012c) (Equation 4.1) which uses a double exponential function of exposure time and depth is used to describe the decrease in luminescence into a granite sub-surface (Figure 4.3).

$$L(x) = e^{-t\overline{\sigma\varphi_0}(e^{-\mu x})} \qquad \text{(Equation 4.1)}$$

Here, L is the luminescence signal at depth x, with the parameters t the time of exposure, φ is the light intensity and σ is the photoionization cross section. Finally, μ (mm^{-1}) is the attenuation coefficient of the light through the rock.

An early attempt of measuring bleaching with depth was undertaken by Simms *et al*. (2011), who measured the remaining luminescence signal from quartz, with depth into a rock sub-surface, following 1 hour of exposure to daylight. Although a different mineral was used to that studied in this thesis, and different approaches to the bleaching

experiment were undertaken, this experiment shows that after ~ 1 hour of natural bleaching, the luminescence signal is at least partially reset to a depth of ~ 5 mm (Figure 4.4). However, the experiment by Simms *et al*. (2010) illustrates only one time period of bleaching, and the luminescence signal is not completely reset for the surface slice.

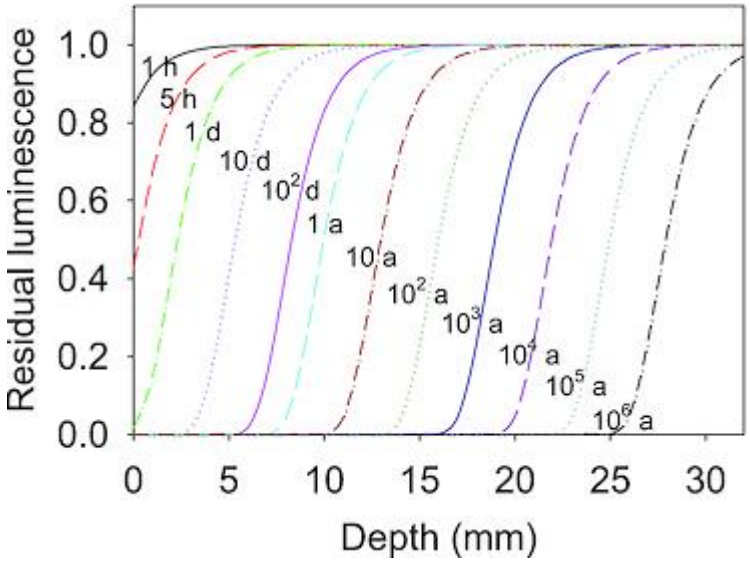

Figure 4.3. Profiles of residual luminescence with depth after given periods of daylight exposure as predicted by the model given by Sohbati *et al*. (2012c) (Equation 4.1). This model does not include any term to describe the growth of luminescence over long periods of time due to natural ionizing radiation.

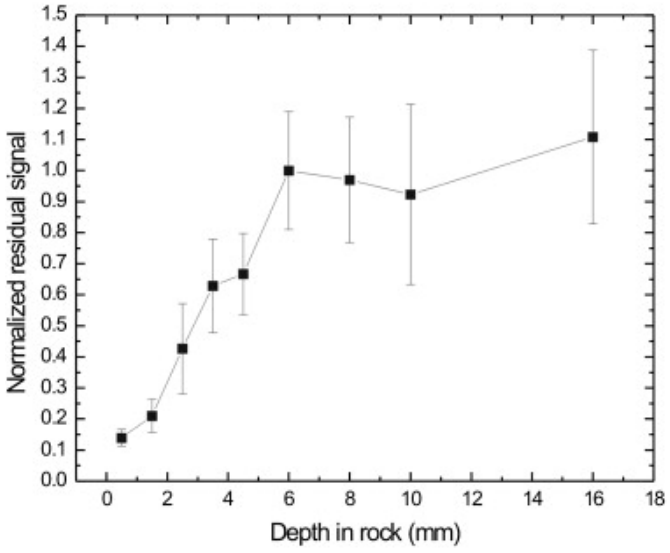

Figure 4.4. Normalised OSL signal, with depth, for quartz minerals into a granite sub-surface (Simms *et al*., 2011).

To undertake bleaching experiments a granite cobble (of dimensions 22:12:10 cm) was obtained from the beach foreshore at Aberystwyth (Figure 4.5). This cobble was cut in half to expose the non-bleached interior of the cobble using a diamond-edge wafering blade. To check weather any bleaching had occurred in the interior of the cobble (> 2 cm deep into the cobble) a core was taken following the slicing of the cobble, and this shows that no sub-surface bleaching had occurred (due to the lack of any bleaching profiles) see Figure 4.6 (with a bleaching time of zero). The cobble half was then placed into the SOL2 solar-simulator for various periods of time, up to ~ 1 week of bleaching (10,080 minutes) (see Figure 4.6).

Figure 4.5. Image of the sliced cobble half showing the un-exposed interior (with the black line illustrating the areas avoided due to potential light penetration when the cobble was exposed. Red squares illustrate the location of cores obtained from the cobble half with one hole (to the right of the picture) showing the last obtained core (for 1 week of bleaching in the SOL-2 solar simulator). The first core taken from this cobble illustrated that the centre of the cobble half had not been bleached.

For the experiment here, 1 core is taken for each time period with cores taken following bleaching periods of zero, 5 minutes, 10 minutes, 40 minutes, 80 minutes, 160 minutes, 640 minutes, 1280 minutes (~ 1 day), 2560 minutes (~ 2 days), 5120 minutes (~ 3.5 days) and for 1 week of exposure in the SOL-2 solar simulator. Figure 4.6 shows the uncorrected L_n/T_n ratios for each individual core for both the $IRSL_{50}$ and post-IR $IRSL_{225}$ signals.

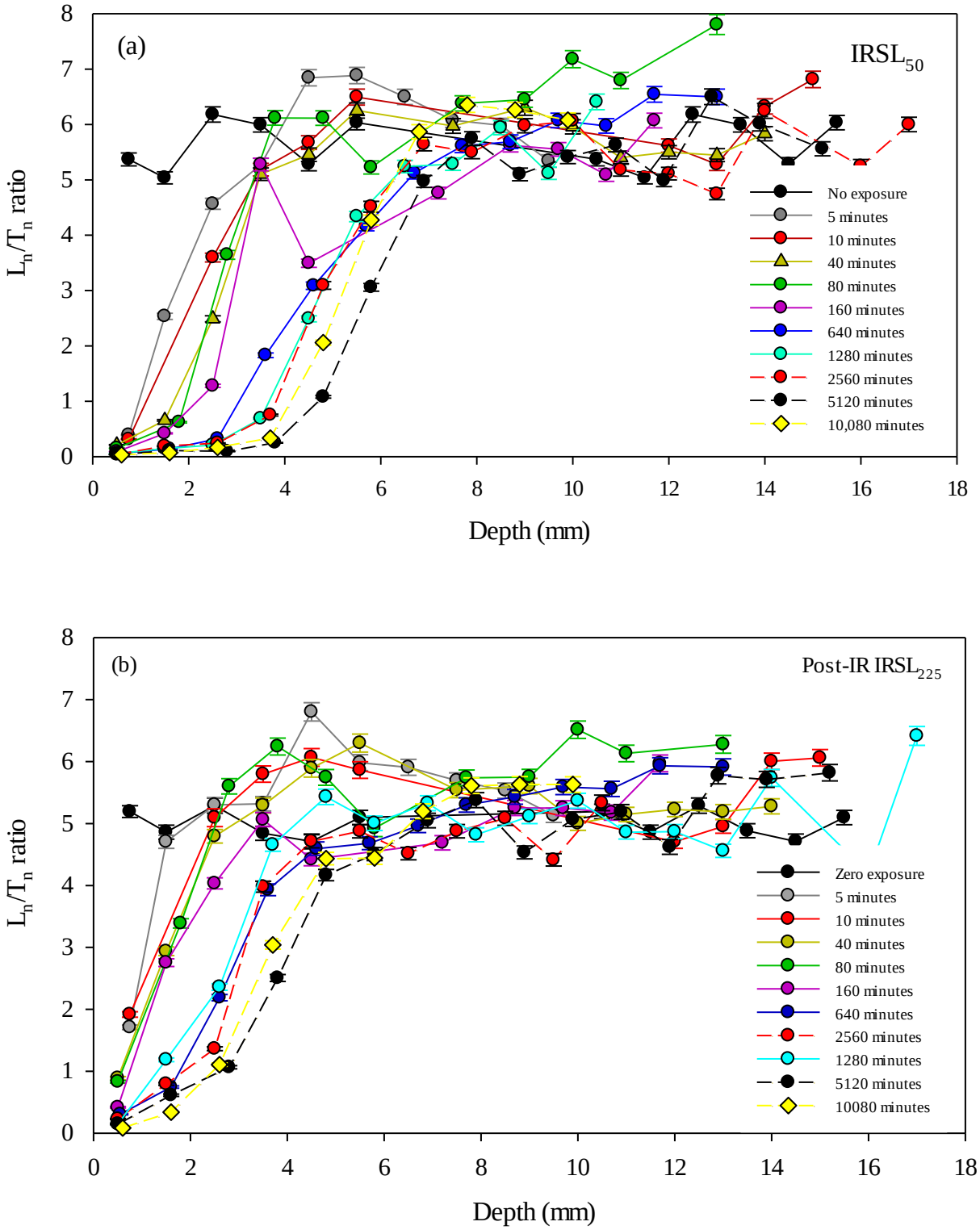

Figure 4.6. Non-normalised $IRSL_{50}$ (a) and post-IR $IRSL_{225}$ (b) L_n/T_n ratios for each time period of bleaching, with depth. The saturated L_n/T_n ratios are illustrated here and show consistent values between cores and with depth.

4.3.1. Bleaching of the $IRSL_{50}$ signal with depth

Figure 4.7 illustrates the change in the normalised $IRSL_{50}$ signal, with depth, up to a time period of 10,080 minutes (~ 1 week). To normalise the data, each individual core was normalised to its saturated $IRSL_{50}$ L_n/T_n values (those that plateau following the initial bleaching period). The data in Figure 4.7 are then fitted using the model (Equation 4.1) of Sohbati *et al*. (2012c). Fitting of the model by Sohbati *et al*. (2012c) to the L_n/T_n values was undertaken in the software package Sigmaplot 12.5. The parameters $-t\overline{\sigma\varphi_0}$ (the luminescence decay rate) given in Equation 4.1 were combined to reduce the variables within the model.

It is clear from the L_n/T_n ratios, with depth, for the zero exposure, that the interior of the cobble had not been bleached, as was expected. This is shown by no decrease in the average L_n/T_n ratio at the surface of the cobble and the normalised luminescence signal remaining at ~ 1 throughout the entire depth (Figure 4.7). After exposure in the SOL2 of 5 minutes only ~ 6 % of the $IRSL_{50}$ signal remains in the surface slice, showing the rapid decrease in signal for the surface slice. For 5 minutes of exposure, by ~ 1.5 mm into the sub-surface, ~ 40 % of the $IRSL_{50}$ signal remains. This again shows a rapid resetting of the luminescence signal in the upper surface slices for the $IRSL_{50}$ signal. Following 80 minutes of bleaching in the SOL2 solar simulator, only ~ 9 % of the $IRSL_{50}$ signal remains at a depth of 1.8 mm and by 2.8 mm only ~ 55 % of the $IRSL_{50}$ signal remains. The bleaching then continues, with depth, for periods of times up to 1 week of bleaching in the SOL2 solar simulator and after 1 week of exposure, the $IRSL_{50}$ signal is almost entirely reset to a depth of ~ 4 mm. The development of the resetting of the luminescence signal, with depth, shows a monotonic pattern of bleaching. There are some exceptions to this, whereby after 1 week of bleaching, the luminescence signal is not reset to greater depths than the earlier exposure of 5120 minutes. This, however, may be due

to the fact that individual cores can vary in mineralogical content and this has also been shown by Ou *et al*. (2018).

The model (Equation 4.1) from Sohbati *et al*. (2012c) generally fits well to the L_n/T_n data measured in the bleaching experiment (Figure 4.7). However, there are some exceptions to this, and this is primarily focused around the surface slices, whereby the model of Sohbati *et al*. (2012c) predicts total bleaching, but the measured L_n/T_n values show some remaining residual luminescence signal (e.g. 1 week of bleaching (10,080 minutes) in Figure 4.7). This was also observed by Ou *et al*. (2018). This indicates that a remaining residual signal exists for the upper slices measured in the bleaching experiment. In addition to this, Figure 4.7 shows that the shape of the remaining normalised luminescence signal, with depth, varies between rock cores taken from the same cobble (μ) (for example, 5 minutes of bleaching in the SOL2 shows a steeper curve than that observed for 640 minutes (Figure 4.7)). This shows a deviation from the predicted bleaching, over time, illustrated by Sohbati *et al*. (2012c) shown in Figure 4.3 and this change in the shape of the bleaching curve (the attenuation coefficient of the light through the rock) is attributed to the potential for small changes in the mineralogical content between different rock cores from the same cobble.

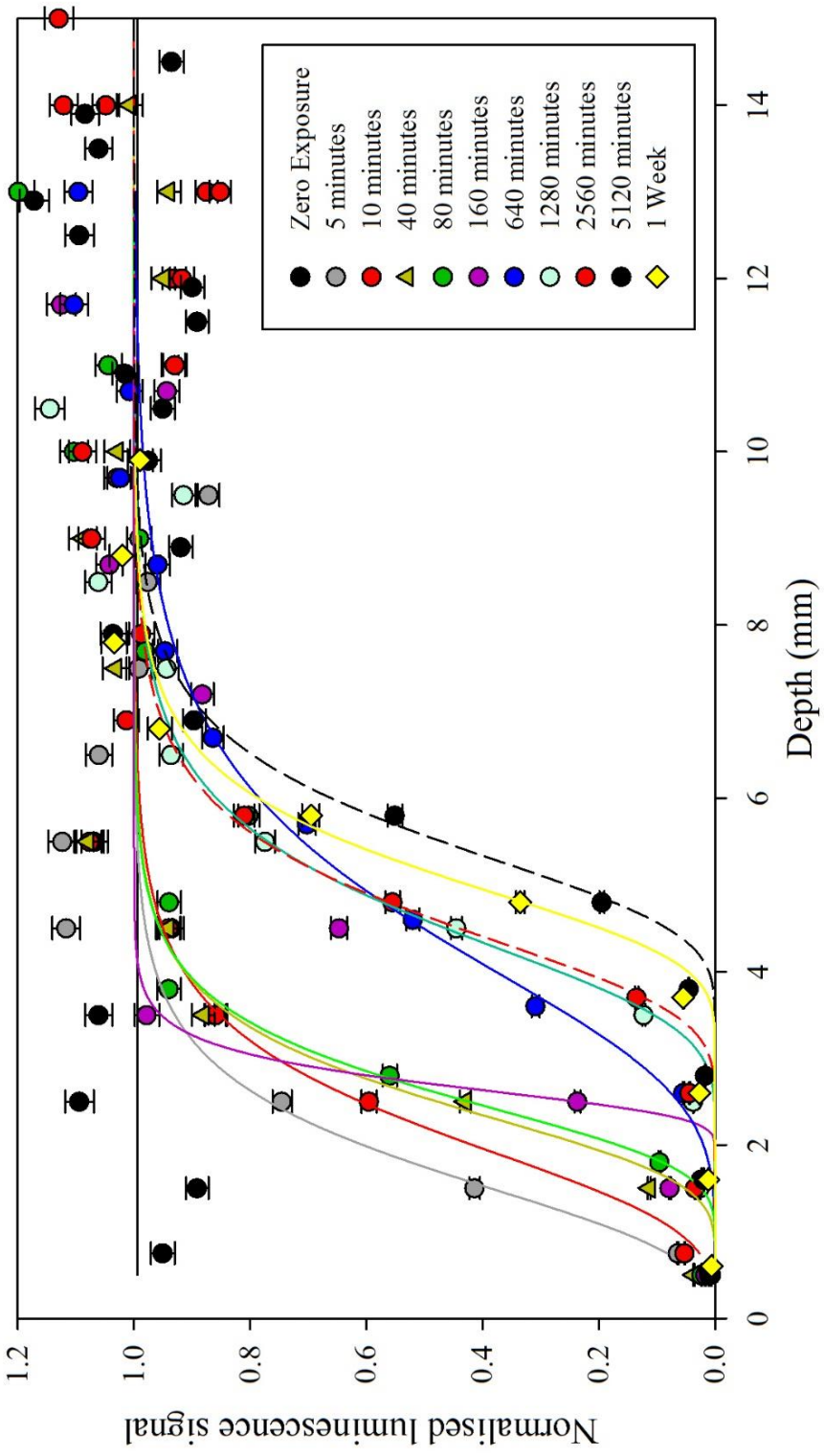

Figure 4.7. Normalised L_n/T_n values for all cores for the $IRSL_{50}$ signal from zero exposure, to a time of ~ 1 week of exposure.

4.3.2. Bleaching of the post-IR IRSL$_{225}$ signal with depth

Figure 4.8 illustrates the change in the normalised post-IR IRSL$_{225}$ signal, with depth, up to a time period of ~ 1 week. As was the case for the IRSL$_{50}$ signal, it is clear from the L_n/T_n ratios, with depth, for the zero exposure, that the cobble had not been bleached, as was expected. From zero exposure to the first time period of exposure of 5 minutes, ~ 30 % of the post-IR IRSL$_{225}$ signal remains un-bleached, which is in contrast to the 6 % remaining for the IRSL$_{50}$ signal. Such a difference in bleaching is expected, following measurements made in Section 4.2 which illustrates that the IRSL$_{50}$ signal bleaches quicker than the post-IR IRSL$_{225}$ signal. For 5 minutes of bleaching, for the post-IR IRSL$_{225}$ signal some interaction with the next slice, at a depth of 1.5 mm occurs, with 82 % of the post-IR IRSL$_{225}$ signal remaining. The decrease in the post-IR IRSL$_{225}$ signal continues across the bleaching periods, when, at 80 minutes of bleaching in the SOL2 solar simulator, only ~ 14 % of the post-IR IRSL$_{225}$ signal remains for the surface slice and ~ 60 % remains for the next slice. Following 10,080 minutes of bleaching, the post-IR IRSL$_{225}$ signal becomes much lower for the first two slices, and also continues for the third, fourth and fifth slices into the cobble sub-surface**.**

As is the case for the IRSL$_{50}$ L_n/T_n with depth data measured during this experiment, the model of Sohbati *et al*. (2012c) generally fits well to the post-IR IRSL$_{225}$ data points. The post-IR IRSL$_{225}$ signal is reduced to greater depths, for greater time periods of exposure, and follows a similar pattern of bleaching predicted by the model. However, there are some exceptions to this and this is shown following 1280 minutes of bleaching in the SOL2.

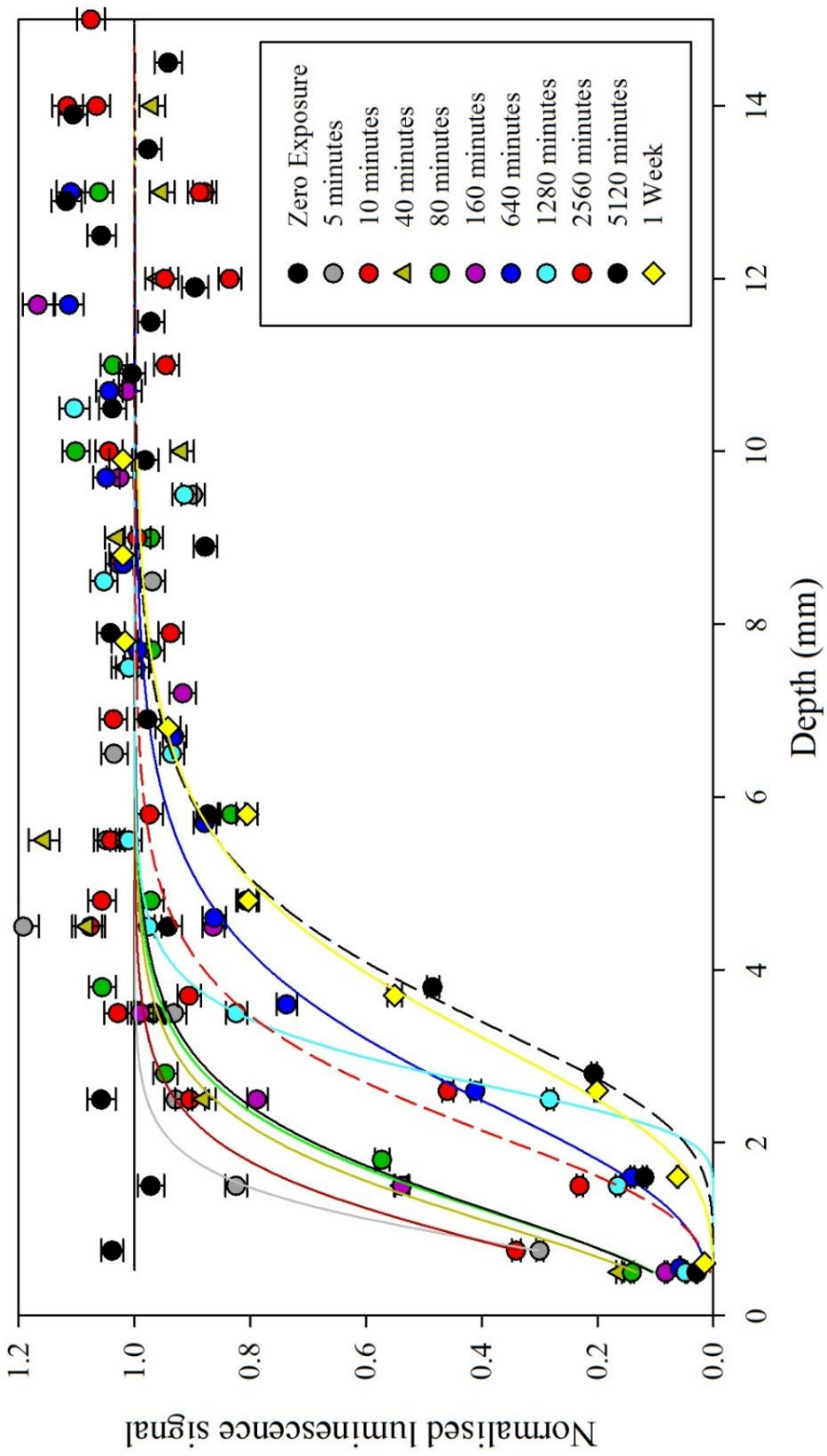

Figure 4.8. Normalised L_n/T_n values for all cores for the post-IR $IRSL_{225}$ signal with depth.

The L_n/T_n ratios shows a gradual increase for the upper three rock slices, whereas the model by Sohbati *et al*. (2012c) predicts that the signal is completely reset at this stage. Additionally, the shape of the curves also varies, for different time periods of exposure, in a similar fashion to that observed for the $IRSL_{50}$ signal. The variability observed between the model fitting and the measured L_n/T_n values is interpreted to be as a result of the variability of the natural samples with changes in the mineralogical content potentially impacting upon the depth, and shape, of bleaching profiles.

Similar patterns of changes in the $IRSL_{50}$ and post-IR $IRSL_{225}$ signal, with depth, into a granite cobble, are illustrated by Ou *et al*. (2018) who shows that after 92 days of natural exposure the $IRSL_{50}$ signal is reduced by 50 % down to depths of ~ 4 – 5 mm (Figure 4.9). This also shows how effective the SOL2 solar simulator is at resetting the IRSL signal in comparison to natural sunlight.

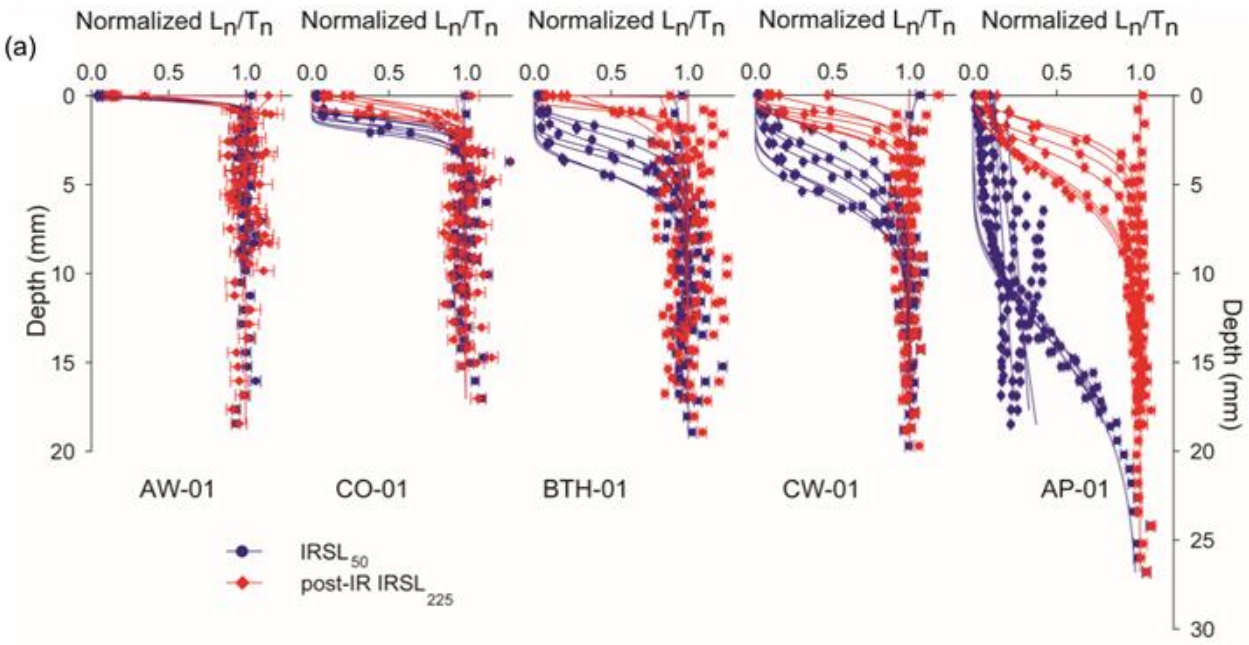

Figure 4.9. Bleaching with depth into different rock types measured by Ou *et al*. (2018) ranging from dark coloured to light coloured rock types (left to right). Two granite cobbles are illustrated here (BTH-01 and CW-01) and show bleaching up to periods of 91 days.

4.3.3. Bleaching of the surface slices

Because measurements of changes in luminescence over time were made for Experiment 2, discussed above, this means that the surface slices, from the cores that provided sub-surface information, can be used to check the measurements made in Experiment 1 (Section 4.2) which looks at the surface slices only. The normalised changes in luminescence over time for the surface slices from Experiment 2 are shown in Figure 4.10 with all measurements normalised to the initial non-exposed surface slice. The measurements of changes in luminescence over time show that the resetting of the luminescence signal from rock slices taken from the surface of cores generally agrees with the same measurements from rock slices in Experiment 1 (see Section 4.2). However, the $IRSL_{50}$ measurements do not agree with the $IRSL_{50}$ values for rock slices from Experiment 1. The $IRSL_{50}$ bleaching values for 1 week, however, agree with those shown by Colarossi *et al*. (2015).

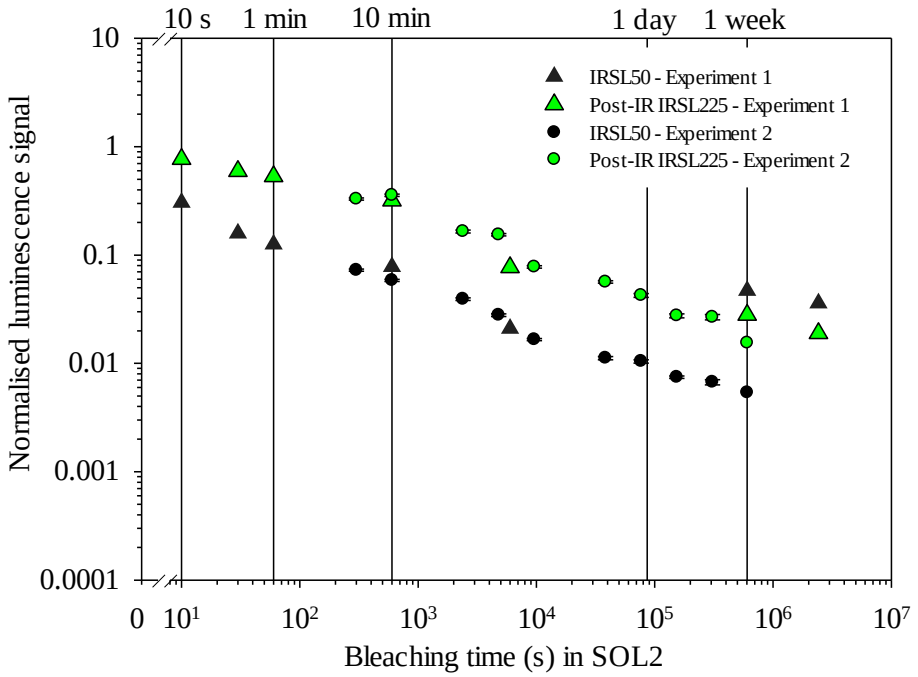

Figure 4.10. Comparison of changes in normalised luminescence over time for three rock slices, taken from a buried glaciofluvial cobble at Orrisdale Head and bleached in the SOL-2 solar simulator for different periods of time.

4.4. Experiment 3: Comparison of experimental bleaching to a naturally exposed cobble

A cobble which was exposed on the beach foreshore at Orrisdale Head, Isle of Man, is compared here to the profiles observed during the laboratory bleaching experiments, so as to observe potential bleaching extents of the naturally exposed cobble. Figure 4.11 illustrates the initial zero exposure (natural signal, unbleached) and the exposure of 2560 minutes from Experiment 2. As described above, this shows the $IRSL_{50}$ signal remaining low to a depth of ~ 3.5 mm and the post-IR $IRSL_{225}$ signal increases from the first to second slices into the sub-surface. Figure 4.12 shows L_n/T_n with depth for a cobble that was exposed on the foreshore of Orrisdale Head, Isle of Man. The exposure length of the cobble on the beach foreshore at Orrisdale Head is unknown, however, it was interpreted that the cobble had been exposed for a significant period due to its position on the beach foreshore and incorporated into the beach deposits. The orientation of the clast was not recorded. Duplicate cores were taken from cobble ORS00-1, with cores ORS00-1-B and ORS00-1-C taken adjacent to each other. These cores were then sliced entirely, following the process outlined in Section 3.1.1 and the L_n/T_n ratios were measured following the same protocol in Section 3.2 (Table 3.1). The sub-surface plot at Orrisdale Head shows that the $IRSL_{50}$ signal is very similar, with depth, to that observed in the bleaching experiment and this is also the case for the post-IR $IRSL_{225}$ signal. This may indicate that the cobble was exposed for similar or great time lengths than the bleaching experiment (2560 minutes) or there is a large variation in the lithology between the two rock types, thus allowing greater resetting of the luminescence signal, with depth (Ou *et al*., 2018). The model fitting of Sohbati *et al*. (2012c) also fits the L_n/T_n values, with depth, for the naturally exposed cobble, and in addition to this, the slope of

the bleaching profile (Figure 4.12) appears similar to that observed for the bleaching experiment (Figure 4.11).

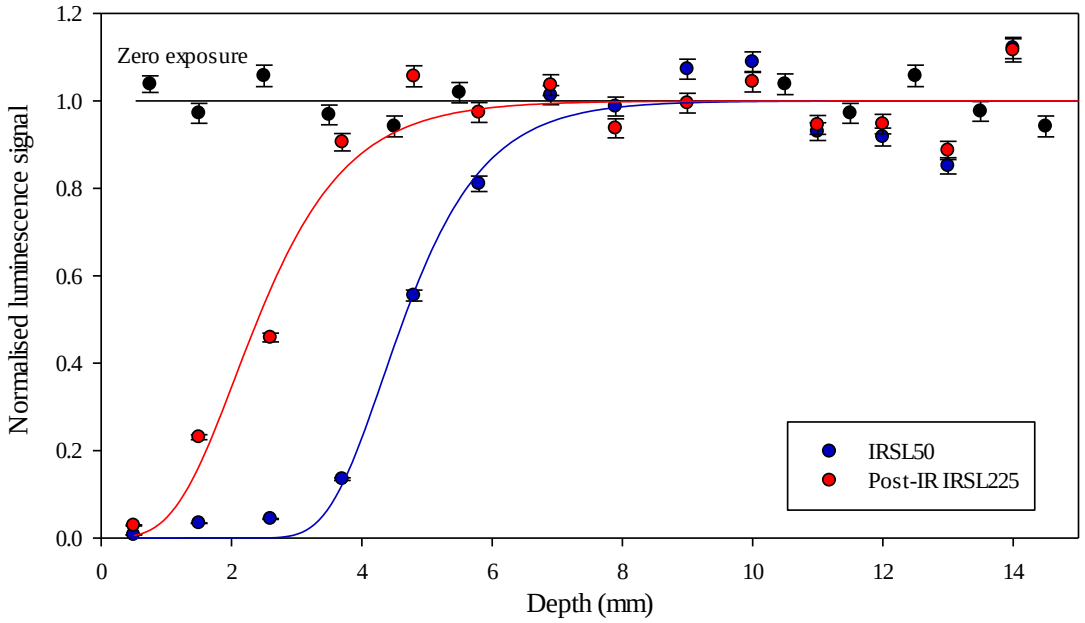

Figure 4.11. Normalised L_n/T_n measurements for zero exposure and following 2560 minutes of exposure. The black line illustrates zero exposure from the $IRSL_{50}$ signal.

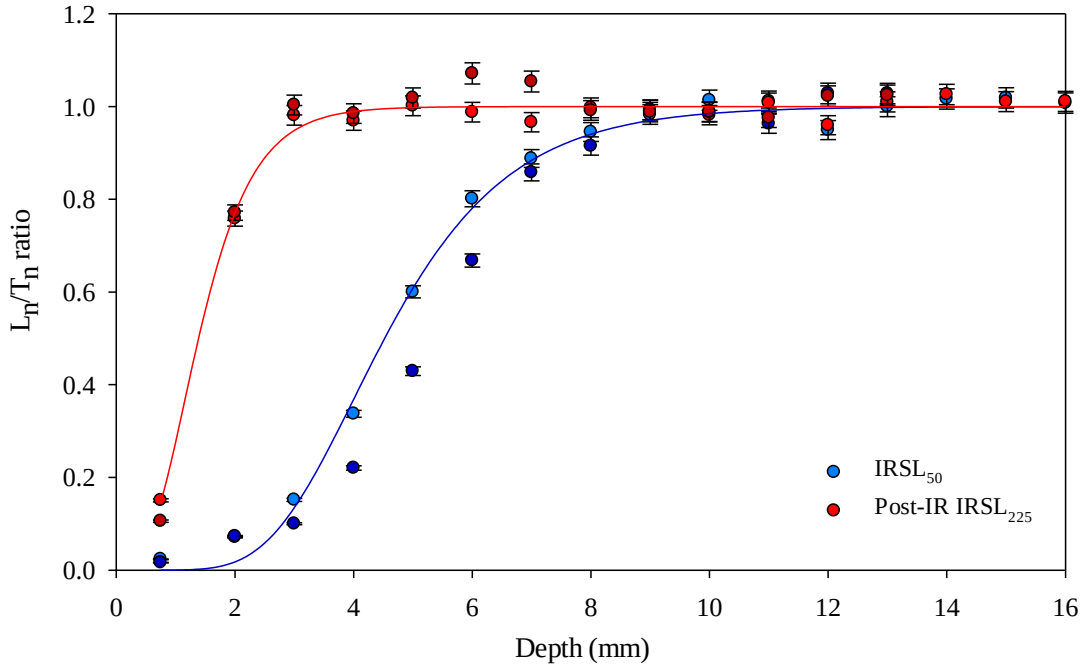

Figure 4.12. Example of changes in the natural luminescence signal, to a depth of ~ 16 mm, for two cores taken from the exposed cobble from Orrisdale Head. The solid lines illustrates the fitting of a bleaching model used by Sohbati *et al*. (2012c).

4.5. Conclusions

Measurements of changes in L_n/T_n, over time, for 3 rock slices taken from a cobble from Orrisdale Head, Isle of Man, shows that bleaching of rock slices generally agree with the data of Colarossi *et al*. (2015) and this shows that the thicker, unseparated feldspar minerals in rock slices bleach at the same rates as sediment grains (Experiment 1). Bleaching with depth experiments (Experiment 2) show that following an initial exposure of 5 minutes in the SOL2 solar simulator, most of the $IRSL_{50}$ signal is removed from the surface slice. Then, following 1 week of bleaching in the SOL2, the $IRSL_{50}$ signal is completely reset up to a depth of ~ 4 mm. The $IRSL_{50}$ signal bleaches deeper, for the same time-scales, than the post-IR $IRSL_{225}$ signal. However, following 1 week of bleaching, the post-IR $IRSL_{225}$ signal is reset for the upper few mm. A bleaching model (Sohbati *et al*., 2012c) fits the L_n/T_n values with depth, with the exception to this being the upper few rock slices, which show that the luminescence signal is not completely reset (but is predicted to happen by the bleaching model). The bleaching profiles progress monotonically with depth, over time, and the shape of the bleaching profile remain similar. These measurements also show how effective the SOL2 solar simulator is at resetting the $IRSL_{50}$ signal compared to naturally exposed samples (Ou *et al*., 2018). Additionally, L_n/T_n measurements from rock slices from the surface of cores used for a depth bleaching experiment show that signal bleaching for both the $IRSL_{50}$ and post-IR $IRSL_{225}$ signals match that of Colarossi *et al*. (2015) up to a period of 1 week. Finally, in Experiment 3, a naturally exposed cobble taken from the foreshore of Orrisdale Head was analysed, and the model of Sohbati *et al*. (2012c) fits the natural L_n/T_n values with depth well.

5. Testing cobble luminescence dating at a location with independent age control (Orrisdale Head, Isle of Man)

5.1. Introduction

This chapter investigates whether buried cobbles can be used to date glaciofluvial sediments. In addition to this, this chapter explores whether cobbles record the extent of bleaching at deposition in a heterogeneously bleached environment. The site selected for the trial application at Orrisdale Head, Isle of Man, has been outlined in Section 2.4.1 and is an ice-marginal sandur deposited during final deglaciation of the Irish Sea ice stream. Previous studies have generally focused on single cobbles from well-bleached environments (Freiesleben *et al*., 2015; Sohbati *et al*., 2015) (see Section 1.3) and therefore the challenges associated with identifying those cobbles which have been bleached at deposition in a heterogeneously-bleached environment are also discussed. As previously outlined (Section 1.3) an advantage of using cobbles for luminescence dating is that the amount of bleaching that occurred before burial can be established (but this has only been tested in known well-bleached environments). Knowing if the cobble was completely bleached or not would offer a significant advantage over sand-sized luminescence dating. Luminescence ages from cobbles, therefore, could provide more accurate ages (than sand-sized luminescence dating) for retreat of the Irish Sea Ice Stream. Data and interpretations contained in this Chapter have been published and can be found within Appendix A of this thesis.

5.2. Did the bleaching of cobbles occur?

Forty-five different cobbles were obtained from Orrisdale Head using the sampling process outlined in Section 2.4.2. However, this section will focus on 10 granite cobbles and this is because the other lithologies (sandstones and quartz) were too friable and yielded very little luminescence signal. As an example, a single quartz slice from Orrisdale Head, Isle of Man gave < 1,000 OSL counts (per 0.38s) with no discernible decay in the signal following this. It was clear from this, therefore, that as initially expected, the quartz rock slices were not suitable for such measurements. As previously mentioned, other studies have focused on single cobbles (Freiesleben *et al*., 2015; Sohbati *et al*., 2015), however, in this study a larger population of cobbles was obtained (n = 10) and, therefore, a method of rapidly identifying those cobbles that have been bleached the most is required. A core was taken from each cobble, using the process outlined in Section 3.1.1. A single slice was cut from the surface of each core and the natural luminescence signals (L_n/T_n ratios) were measured for the $IRSL_{50}$ and post-IR $IRSL_{225}$ signals (Figure 5.1). The $IRSL_{50}$ and post-IR $IRSL_{225}$ signals were measured using a single cycle of the measurement procedure (Table 3.1) to provide a rapid way of measuring the differences in bleaching between the cobbles.

In order to assess how L_n/T_n ratios (and therefore bleaching) may change across the same cobble, or from different faces of the same cobble, multiple rock cores were obtained from the same cobbles. Although the orientations (marking of the upper-face and lower-face) of the cobbles were measured when collected (see Section 2.4.2) it is not known, in this environmental setting, if the upper-face of the cobbles recorded at deposition would be the best bleached. This is due to the potential for multiple bleaching and transportation events within a glacial sandur deposit. Therefore, to ensure that the correct areas were targeted, the L_n/T_n ratios from different faces of the cobbles were

taken. Such single-cobble analysis has not been previously analysed in cobble-dating studies. In addition to the 10 rock slices taken from the surface of the 10 different cobbles, 13 rock cores were taken from different faces of the same cobbles. Figure 5.1 shows the L_n/T_n ratios for the 10 different cobbles, with a total of 23 different surface slices taken.

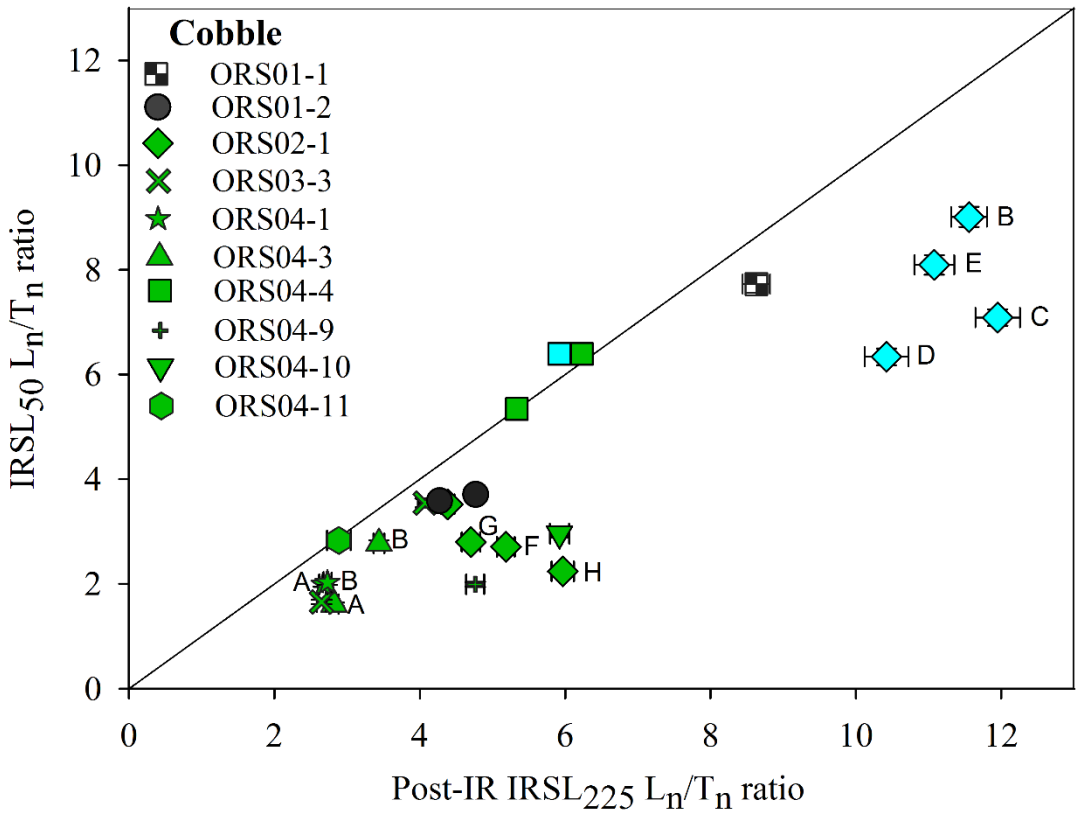

Figure 5.1. Surface slice L_n/T_n ratios for 23 different rock slices, from 10 different granite cobbles with the top (upper-face), side and bottom (lower-face) of the cobbles illustrated. Two cobbles with low L_n/T_n ratios, one cobble with an intermediate L_n/T_n ratio and one cobble with a high L_n/T_n ratio are labelled and their natural luminescence intensity, as a function of depth, are described below (Section 5.3.2). Green symbols illustrate the upper-face, black symbols illustrate the side-faces and blue symbols illustrate the bottom-faces of the cobbles.

The L_n/T_n ratios from the 23 different rock slices (from 10 different cobbles) cover a wide range, from 1.61 ± 0.04 to 9.01 ± 0.19 for the $IRSL_{50}$ signal and 2.65 ± 0.06 to 11.95 ± 0.31 for the post-IR $IRSL_{225}$ signal when using a 34 Gy test dose. The

measured $IRSL_{50}$ L_n/T_n ratios are also generally lower than the post-IR $IRSL_{225}$ L_n/T_n ratios due to the $IRSL_{50}$ signal suffering from anomalous fading (Thomsen *et al*., 2008) and the more rapid bleaching rate of the $IRSL_{50}$ signal (Colarossi *et al*., 2015). This range in L_n/T_n ratios is interpreted to show the difference in the exposure to daylight at deposition and is the first illustration of a range of bleaching exposures for buried cobbles. The analysis of multiple cobbles from a heterogeneously bleached environment therefore shows a range in bleaching of the cobbles (as it does for sand-sized material) and contrasts previous investigations of cobbles (Sohbati *et al*., 2015) that analyse single cobbles from well-bleached archaeological environments.

A large difference in the L_n/T_n ratios from one face of a cobble to another is also observed within Figure 5.1. This is illustrated by the cobble ORS02-1, with an L_n/T_n ratio of 2.70 ± 0.04 for the top of the cobble and 9.01 ± 0.19 for the bottom of the cobble for the $IRSL_{50}$ signal and 5.18 ± 0.12 for the top of the cobble and 11.55 ± 2.46 for the bottom for the post-IR $IRSL_{225}$ signal. This again shows a range in bleaching, not only between individual cobbles but across the same cobble. In Figure 5.1 the upper-face of the cobbles (as recorded at sampling) are plotted in green, with the side-faces of the cobbles in black and the bottom-faces of the cobbles in blue. Even from this small data set, it appears that the top of the cobbles were better bleached than the bottom. This implies that bleaching occurred at final deposition, as opposed to multiple bleaching and transportation events of the cobble within the glacial sandur deposit. Slices taken from duplicate cores, adjacent to each other (within < 1 cm), show consistent L_n/T_n values and shows that bleaching was consistent for the same area of the cobble face. This is shown by ORS04-1-A and ORS04-1-B which are two rock slices which have been obtained from cores adjacent to each other. ORS04-1-A has an $IRSL_{50}$ L_n/T_n ratio of 1.99 ± 0.04 and a post-IR $IRSL_{225}$ L_n/T_n ratio of 2.67 ± 0.06 whilst ORS04-1-B has an $IRSL_{50}$ L_n/T_n ratio of

2.03 ± 0.04 and a post-IR IRSL225 L_n/T_n ratio of 2.73 ± 0.06. This consistency between rock slices allows for duplicate and triplicate measurements and will potentially allow for the averaging of multiple equivalent doses at a later stage.

It is apparent, therefore, that there was a range in bleaching observed for the 10 granite cobbles from Orrisdale Head. In addition to this, it is clear that the top of the cobbles were better bleached than the sides or bottom of the cobbles. The natural luminescence intensity, as a function of depth, is investigated below, and focuses on two cobbles with low surface L_n/T_n ratios, one with an intermediate L_n/T_n value and one with a high L_n/T_n value.

5.3. Sub-surface luminescence measurements for buried glaciofluvial cobbles

Following measurement of the L_n/T_n ratios for all of the granite cobble surfaces (see Section 5.2) to determine the range in bleaching between the cobbles and L_n/T_n measurements for an exposed granite cobble, the bleaching into the cobble sub-surfaces is then investigated. The L_n/T_n information, with depth into the cobble, gives an indication of the level of bleaching that occurred into the sub-surfaces and illustrates which cobbles to analyse further for equivalent dose and age determination. The variation in luminescence with depth was investigated for (1) a cobble with a high L_n/T_n ratio for its bottom face, (2) a cobble which had an intermediate L_n/T_n ratio for its top face, and (3) two cobbles with low L_n/T_n ratios (see Figure 5.1) (Cobbles ORS04-1 and ORS04-3).

Figure 5.2 illustrates the L_n/T_n ratios, as far as ~ 25 mm into the sub-surface, for the cobble with a high and intermediate L_n/T_n ratio and for two cobbles with a low surface L_n/T_n ratio. In Figure 5.2 both the $IRSL_{50}$ and post-IR $IRSL_{225}$ signals are illustrated along

with model fitting from Freiesleben *et al*. (2015) (Equation 4.1 in this thesis), however, as discussed previously, these are used to illustrate the bleaching patterns only and are not used to estimate exposure lengths for the cobbles. The variation in L_n/T_n ratios with depth into the cobble with a high surface L_n/T_n ratio (ORS02-1) is illustrated in Figure 5.2a. Triplicate cores have been taken (ORS02-1-C, D, E) and one of the cores reaches a depth of ~ 25 mm whilst two of the other cores broke at a depth of ~ 13 mm. The L_n/T_n ratios observed with depth remain relatively high for both signals and for all of three of the cores. In addition to this there is no obvious trend or pattern in the L_n/T_n values with depth. This is also in contrast to the luminescence-depth profile observed for ORS00-1, the exposed cobble taken from the foreshore of Orrisdale Head (see Section 4.4) which shows a gradual increase in L_n/T_n ratios with depth, particularly in the upper few millimetres. The high L_n/T_n ratios, and no clear patterns with depth are interpreted to show that no bleaching has occurred and also confirms that the initial measurement of L_n/T_n ratios for the surface slices provides an accurate reflection that this cobble had not been bleached.

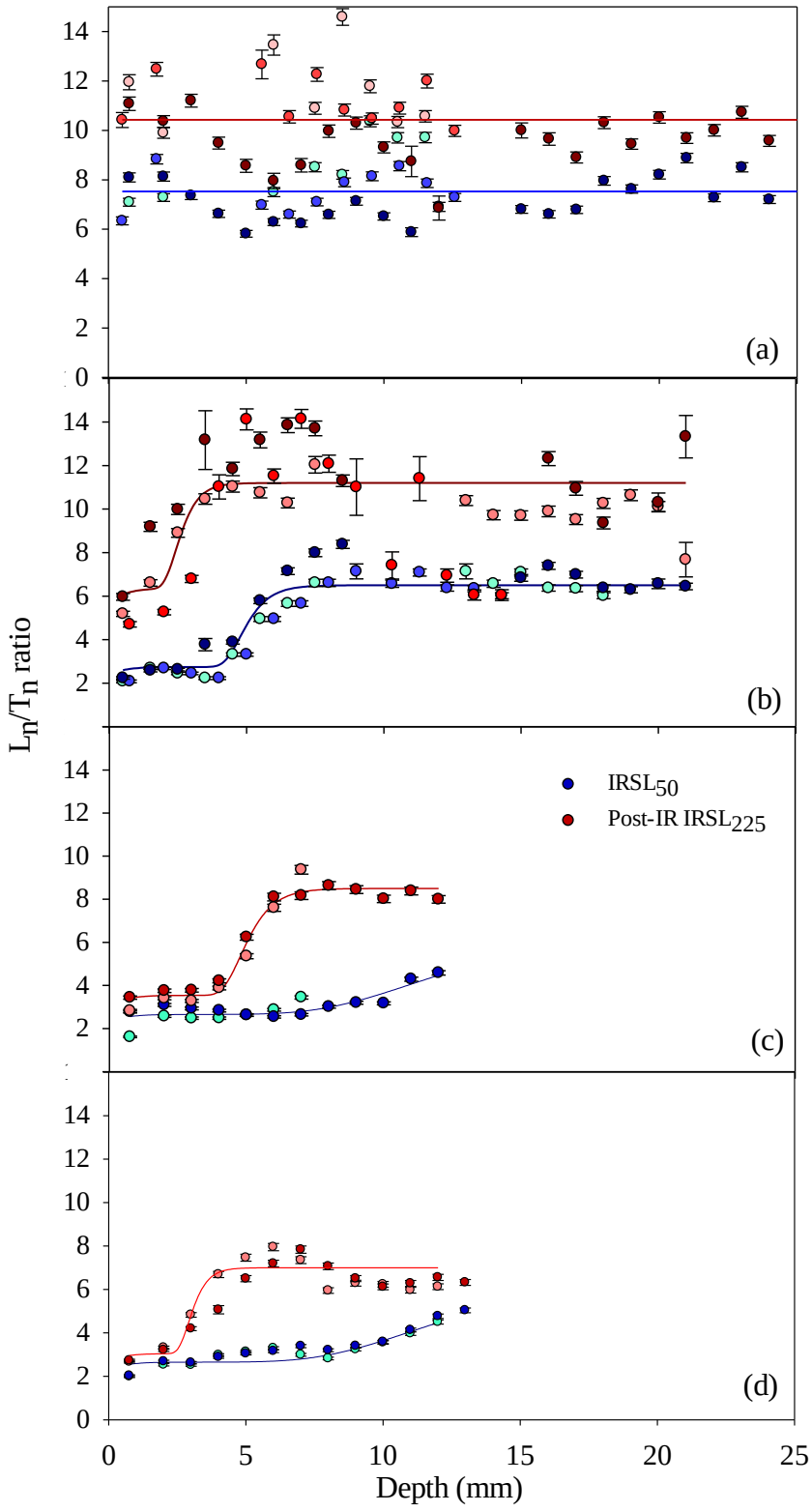

Figure 5.2. L_n/T_n ratios with depth for the cobble with a high surface L_n/T_n value and medium L_n/T_n value (a & b) (ORS02-1) and for cobbles with low surface L_n/T_n ratios (ORS04-3) (c) (ORS04-1) (d). Triplicates are provided in a & b (ORS02-1-C, D, E & ORS02-1-F, G, H) and duplicate cores in c and d (ORS04-3-A, B, ORS04-1-A, B) with duplicate and triplicate cores shown in a gradation of colours.

The variation in luminescence with depth into a cobble sub-surface that had an intermediate L_n/T_n value for its surface is given in Figure 5.2b. This luminescence-depth profile is taken from the same cobble as the profile illustrated in Figure 5.2a (ORS02-1), however, the triplicate cores are taken from the upper face of the cobble (Figure 5.2b) as opposed to the bottom face of the cobble (Figure 5.2a). Triplicate cores were taken (ORS02-1-F, G, H) and the surface slices give lower L_n/T_n values than the surface slices in Figure 5.2a. The lower L_n/T_n values remained consistent (for all three cores) until a depth of ~ 4 mm for the $IRSL_{50}$ signal and ~ 2 mm for the post-IR $IRSL_{225}$ signal. The $IRSL_{50}$ L_n/T_n ratios then gradually increase until they reach a plateau at a depth of ~ 7 mm (and reach the same L_n/T_n values as those observed for the cores in Figure 5.2a), whilst the post-IR $IRSL_{225}$ values show a more abrupt increase and then remain similar throughout the core. This is similar to the patterns of bleaching observed for the exposed cobble (Section 4.4) and shows that bleaching of the cobble sub-surface had occurred at deposition. The $IRSL_{50}$ L_n/T_n ratios are consistently lower than the post-IR $IRSL_{225}$ values and, in addition to this, the $IRSL_{50}$ values remain lower than the post-IR $IRSL_{225}$ values with depth into the sub-surface (which was also observed for the exposed cobble). This is due to the $IRSL_{50}$ signal bleaching more rapidly (Colarossi *et al*., 2015). Additionally, bleaching of the luminescence signal, with depth into cobble sub-surfaces of different lithologies has shown that the $IRSL_{50}$ signal consistently bleaches deeper than the post-IR $IRSL_{225}$ signal (Ou *et al*., 2018). Although the surface slice L_n/T_n ratio had an intermediate value (Figure 5.1), it is clear that sub-surface bleaching occurred in Figure 5.2b and therefore equivalent dose determination is undertaken for those cores. In addition to this, it is interesting to note that a difference in bleaching is observed from the top to the bottom of the same cobble and implies that bleaching occurred at final

deposition, with the emplaced cobble not being bleached during prior transportation phases.

The next cobble (ORS04-3; Figure 5.2c) shows the sub-surface luminescence profiles for a cobble which had low L_n/T_n ratios for the surface slice (Figure 5.1), for both signals. Having observed sub-surface bleaching for a cobble with an intermediate surface L_n/T_n ratio it is expected that the cobble in Figure 5.2c (ORS04-3) is the best bleached cobble. This is confirmed by the sub-surface $IRSL_{50}$ L_n/T_n ratios, which remain low to a depth of 8 mm, then gradually start to increase. Duplicate cores were taken for ORS04-3 and the longest core taken extends 12.5 mm into the cobble sub-surface, therefore, the $IRSL_{50}$ signal reaching saturation is not illustrated (Figure 5.2c). The post-IR $IRSL_{225}$ values also remain low to a depth of 4 millimetres and show that this is the best bleached cobble.

Figure 5.2d shows a second well-bleached cobble (ORS04-1) and shows similar sub-surface patterns to the other well-bleached cobble in Figure 5.2c. ORS04-1 shows low L_n/T_n values for the surface down to ~ 10 mm into the cobble for the $IRSL_{50}$ signal. However, a small increase in the $IRSL_{50}$ L_n/T_n ratios is observed at ~ 4 mm into the cobble, and an increase in the associated ages are discussed further in Section 5.6. Small changes in the L_n/T_n ratio, during an apparent well-bleached area of the cobble have been shown to illustrate multiple bleaching and exposure events (Freiesleben *et al*., 2015). Again, the $IRSL_{50}$ values are bleached to a greater depth than the post-IR $IRSL_{225}$ signals.

The changes in luminescence with depth shows that differences in bleaching are recorded within the cobble sub-surfaces with an increase in sub-surface bleaching, with depth, from Figure 5.2a through to Figure 5.2d. It is also illustrated that a difference in bleaching is recorded between two different faces of the same cobble (Figures 5.2a and

5.2b). Such changes in bleaching have so far not been illustrated in other studies, whereby cobble luminescence dating has focused on individual, well-bleached cobbles. Sub-surface changes in bleaching also indicate that the initial surface slice L_n/T_n ratio measurements are an accurate way of illustrating changes in bleaching across the population of granite cobbles.

5.4. Dose-recovery measurements on rock slices

Two dose-recovery tests were undertaken on granite rock slices to ensure that the SAR protocol is suitable for equivalent dose determination for the samples from Orrisdale Head. Dose-recovery tests were undertaken on rock slices taken from cores obtained from the exposed cobble from the foreshore of Orrisdale Head (ORS00-1).

In the first experiment, six cores were taken adjacent to each other from the cobble surface. Slices were taken from the cobble surface so as to use samples with the lowest remaining luminescence signal. Three rock slices were used to measure the residual signal in the rock slices whereas the other three rock slices were given a beta dose of ~ 86 Gy and then their equivalent dose was measured. The remaining residual $IRSL_{50}$ equivalent dose (4.36 ± 0.36 Gy) (Table 5.1) is much smaller than the post-IR $IRSL_{225}$ residual equivalent dose (13.12 ± 1.36 Gy). The dose-recovery ratios (with residual signals subtracted) for the $IRSL_{50}$ signal was 0.97 ± 0.09 and the post-IR $IRSL_{225}$ signal was 1.32 ± 0.15. This shows that the $IRSL_{50}$ signal, in this experiment, can recover a dose within 10 %, whereas the post-IR $IRSL_{225}$ signal cannot.

Table 5.1. Dose recovery data for the rock slices bleached naturally from cobble ORS00-1. The given dose is approximately equivalent to the expected natural equivalent dose.

	Residual dose (Gy)	Given dose (Gy)	Recovered dose (Gy)	Dose recovery ratio
$IRSL_{50}$	4.36 ± 0.36	85.86	87.74 ± 0.31	0.97 ± 0.09
pIR $IRSL_{225}$	13.12 ± 1.36	85.86	126.08 ± 5.32	1.32 ± 0.15

A second experiment used rock slices from the same exposed cobble (ORS00-1), however, rock slices were taken from deeper into the cobble sub-surface (Table 5.2). Because the rock slices were unlikely to have been bleached these were artificially bleached in a SOL2 solar simulator for 14 days (all 6 rock slices were turned over following 7 days to ensure that the trapped charge population was bleached entirely throughout the slice). Three rock slices then had their equivalent doses measured, following 14 days in the SOL2 solar simulator. The other three rock slices then received a dose of ~ 86 Gy and followed the same procedures as the first dose-recovery experiment. Following 14 days of bleaching in the SOL2 solar simulator, residual equivalent doses were lower than the natural measured equivalent doses from the cobble surface in the first experiment (Table 5.2). Residual subtracted dose-recovery ratios are 0.90 ± 0.11 Gy for the $IRSL_{50}$ signal and 0.97 ± 0.06 for the post-IR $IRSL_{225}$ signal.

Table 5.2. Dose-recovery ratios calculated from the second experiment, following 14 days of bleaching in the SOL2 solar simulator for all six rock slices.

	Residual dose (Gy)	Given dose (Gy)	Recovered dose (Gy)	Dose recovery ratio
$IRSL_{50}$	1.68 ± 0.17	85.86	79.01 ± 4.81	0.90 ± 0.11
pIR $IRSL_{225}$	3.38 ± 0.11	85.86	86.44 ± 4.85	0.97 ± 0.11

From both of the dose-recovery experiments, the $IRSL_{50}$ signal can recover a dose within 10 %. However, the post-IR $IRSL_{225}$ signal could only recover a dose following bleaching of the rock slices in the SOL2 solar simulator for 14 days. It is unclear as to why the post-IR $IRSL_{225}$ signal did not recover a dose for both experiments, however, when the residual luminescence signal was reduced, a dose could be recovered.

5.5. Anomalous fading

Anomalous fading can lead to age-underestimation when using feldspars in luminescence dating (Wintle, 1973). To assess the severity of this issue the feldspar minerals can be given a known dose and stored for a period of time, then subsequently re-measured to assess any loss in the luminescence signal over time. To quantify the anomalous fading that may be occurring for the rock slices, 20 different rock slices were measured, from three separate cobbles (ORS00-1, ORS04-1 and ORS04-3). All 20 rock slices were given a beta dose of 42.9 Gy and stored up to periods of 1 month. Preheating occurred in the final step before storage, following the method outlined by Auclair *et al*. (2003). An example of fading measurements performed for a rock slice for both the $IRSL_{50}$ and post-IR $IRSL_{225}$ signals are shown in Figure 5.3. Figure 5.3 shows measurements taken to establish fading rates at the time intervals of ~ 1 hour, ~ 7 hours, ~ 2 days, ~ 1 week and ~ 1 month. Figure 5.3 shows a steady and consistent decrease in the L_x/T_x values over time and illustrates that the measurements made for fading corrections are robust.

Average g-values for all 20 rock slices were 2.53 ± 0.65 % per decade for the $IRSL_{50}$ signal and 1.62 ± 0.69 % per decade for the post-IR $IRSL_{225}$ signal (Figure 5.4). For the samples at Orrisdale Head, fading corrections are made for the $IRSL_{50}$ signal (using the method outlined in Huntley and Lamothe (2001)). However, no correction is made for the post-IR $IRSL_{225}$ signal. This is because, although the g-values for the post-IR $IRSL_{225}$ signals are not zero (see Figure 5.4) the g-values are very low. Thiel *et al*. (2011) measured a fading rate for the OSL signal from quartz that is thought to be stable, but obtained a value of 1.3 ± 0.3 % per decade and this, therefore, shows the challenges involved with making and interpreting fading measurements.

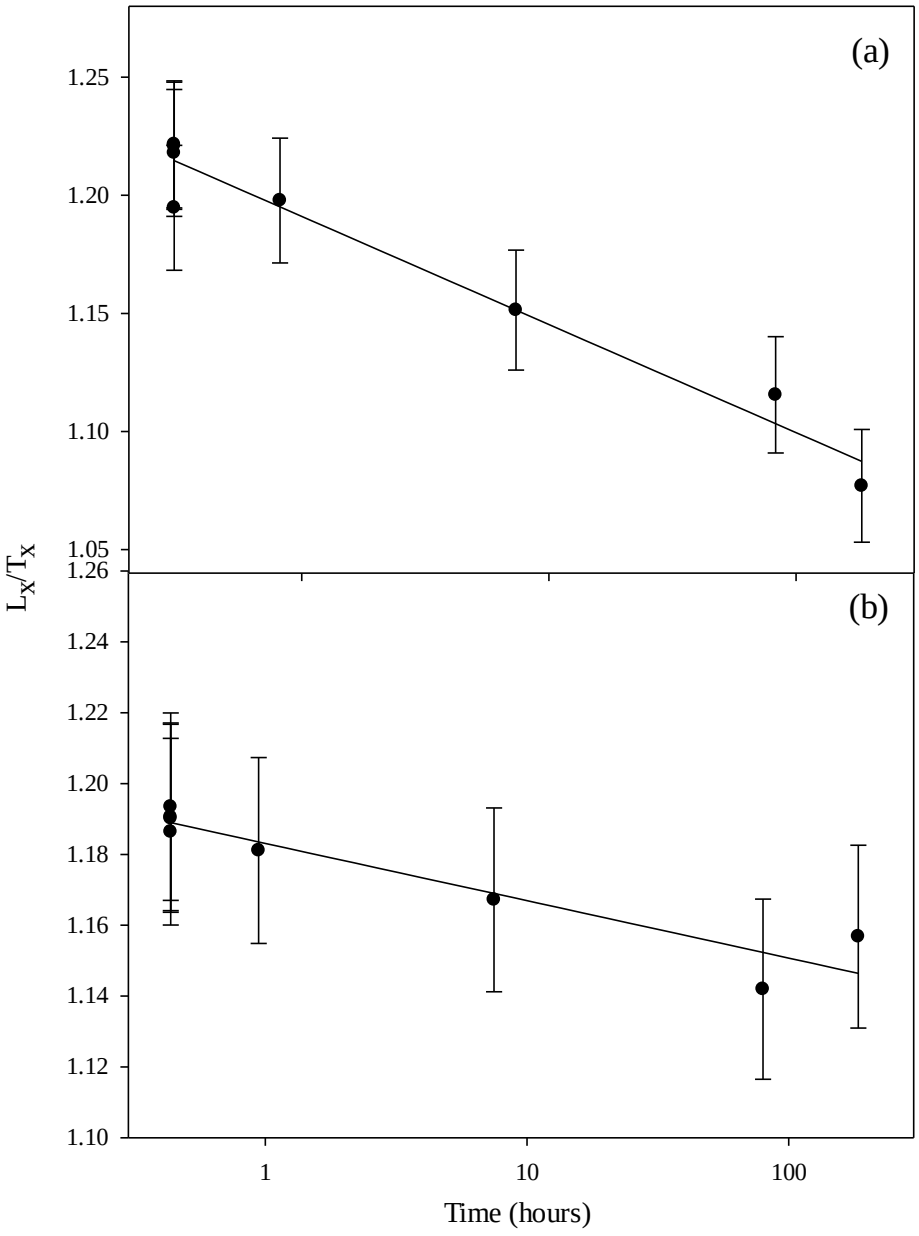

Figure 5.3. Changes in L_x/T_x up to a period of ~ 7 days for rock slice ORS04-3-B-2 for the $IRSL_{50}$ (a) and post-IR $IRSL_{225}$ signals (b). A higher fading rate for the $IRSL_{50}$ is apparent (g-value of 3.99 ± 0.72 % per decade compared to a g-value of 1.39 ± 0.77 % per decade for the post-IR $IRSL_{225}$ signal) for this individual rock slice and is also reflected in the overall higher average g-values for all 20 rock slices (see Figure 5.4).

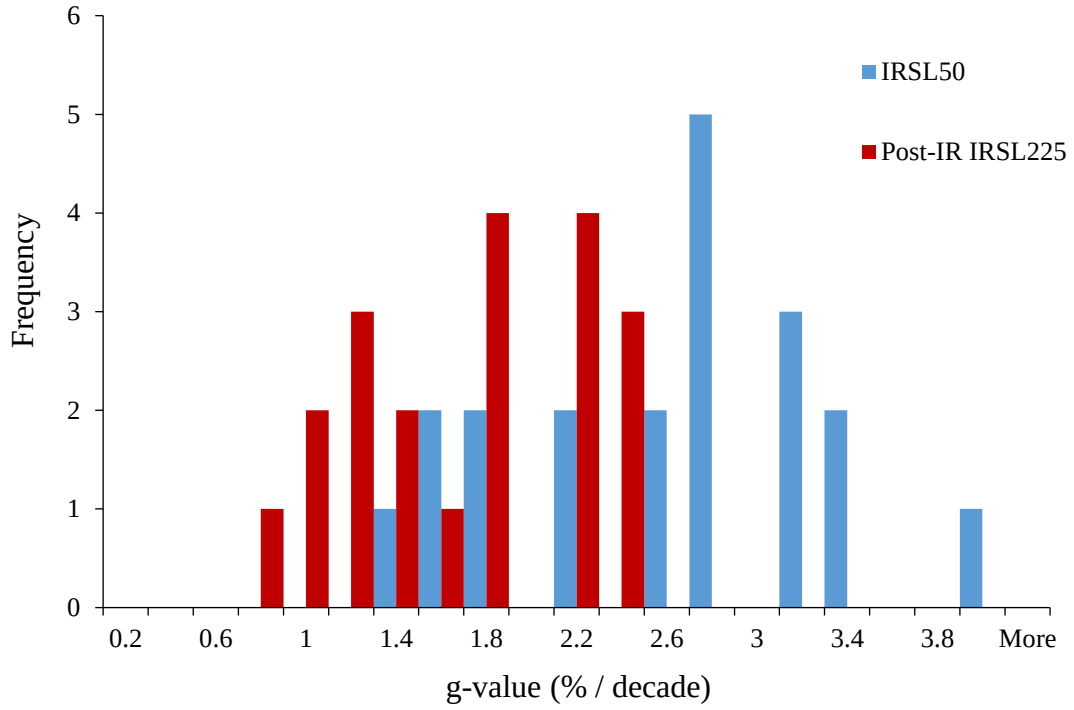

Figure 5.4. g-values for the $IRSL_{50}$ and post-IR $IRSL_{225}$ signals for 20 rock slices from Orrisdale Head with a higher $IRSL_{50}$ fading rate resulting in correction for that signal only.

As previously discussed in Section 5.3., a SAR protocol was undertaken on three rock slices to measure the $IRSL_{50}$ and post-IR $IRSL_{225}$ laboratory saturation levels (Figure 5.5). These rock slices were selected as they showed no signs of being bleached in the L_n/T_n with depth profiles (Figure 5.2a). The $IRSL_{50}$ signal again appears to fade, as shown by the natural L_n/T_n ratio below the saturated laboratory level (natural saturated signal is 64 % of the laboratory saturated signal (Figure 5.5)). This further illustrates the need for fading corrections when establishing an age using that signal. However, there is a similarity between the natural post-IR $IRSL_{225}$ L_n/T_n ratio and the laboratory saturation level (natural saturated signal is 99 % of the laboratory saturated signal) (Figure 5.5).

This supports fading measurements that indicate that no correction of the post-IR $IRSL_{225}$ signal is required.

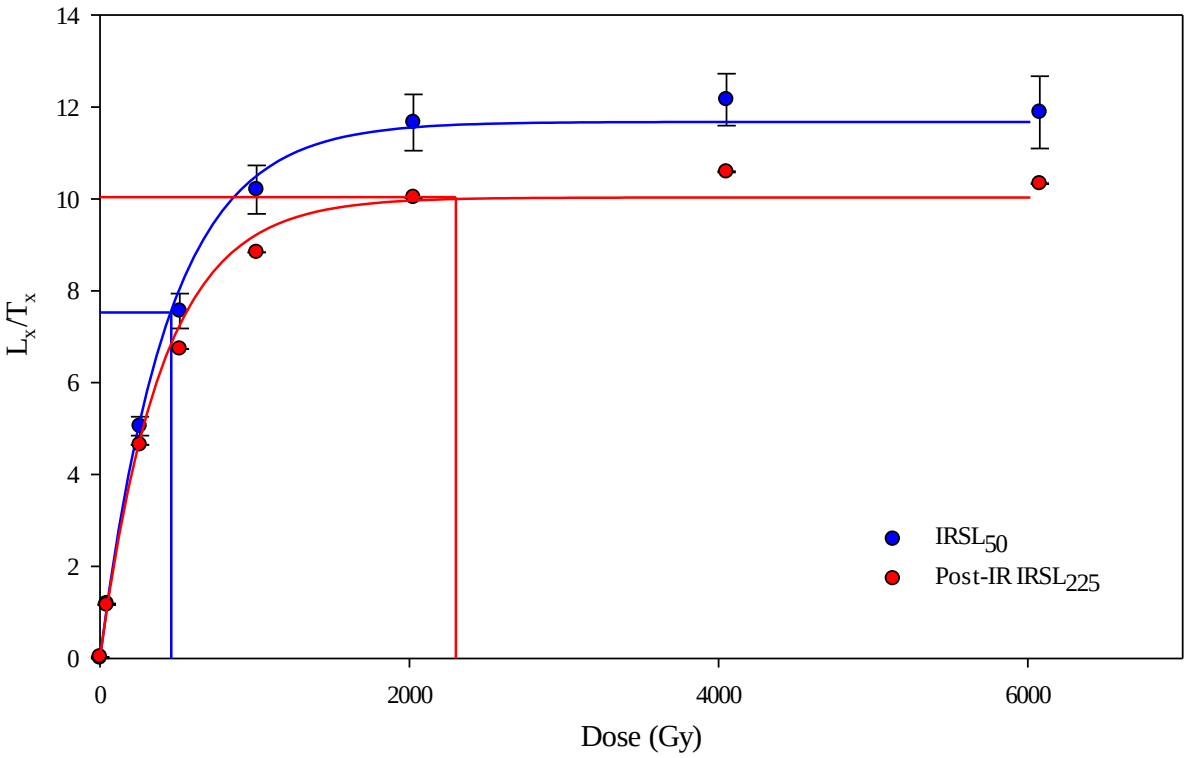

Figure 5.5. Dose response curves fitted with a double-saturating exponential for the $IRSL_{50}$ and post-IR $IRSL_{225}$ signals for an average of 3 rock slice (ORS02-1-E-4, 5 and 6). The difference between the natural L_n/T_n values and the saturated laboratory values are illustrated, with the post-IR $IRSL_{225}$ L_n/T_n values similar to the saturated laboratory values.

5.6. Luminescence ages from well-bleached cobbles

Equivalent dose measurements were undertaken on rock slices that showed signs (low surface L_n/T_n ratios) of sub-surface bleaching (e.g. Figures 5.2b, c and d) and a dose response curve and decay curve are illustrated in Figure 5.6. Each age data point, with depth into the cobble (Figure 5.7), are the combination of the average of two or three equivalent dose measurements which are divided by the dose rates. Information on how dose rates are calculated, with depth, is discussed in Section 3.4, and shows that dose rates to the rock slices vary with depth from 5.37 ± 0.72 Gy/ka at the surface to 6.78 ±

0.75 Gy/ka inside the cobble (for rock slice ORS04-1-A). A benefit of obtaining ages with an increasing depth into the cobbles is that because rapid changes in the dose rate occur at the surface of the cobble. Additionally, after ~ 2 mm into the cobble, dose rates to the rock slices are insensitive to uncertainty in water content of the sediment matrix surrounding the cobbles.

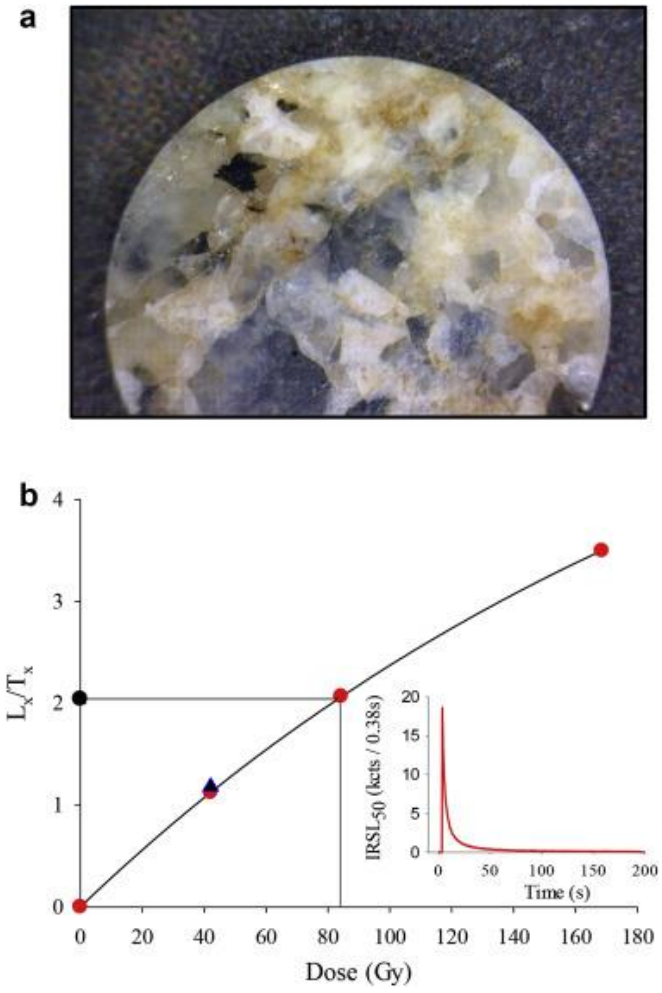

Figure 5.6. Magnified image of a single granite rock slice (with a diameter of ~ 0.8 cm) (from ORS04-3-C) used for identifying feldspar minerals present and establishing a grain size for the rock slice. (b) Dose response curve for the $IRSL_{50}$ signal for the rock slice shown in (a). The slice shows excellent recycling (blue triangle) and an inset shows the natural decay curve for the same rock slice.

Fading-corrected $IRSL_{50}$ ages and post-IR $IRSL_{225}$ ages, with depth, for three separate cobbles (ORS02-1, ORS04-3, and ORS04-1) are illustrated in Figure 5.7. Final

ages, for each individual cobble, are calculated by taking an overall average for those rock slices that were completely bleached. The completely bleached area is interpreted as the plateau of ages before an increase is observed. In addition to ages, with depth, illustrated for each individual cobble, independent age control is also shown in Figure 5.7. Independent age control for Orrisdale Head is described in Section 2.1 and age brackets (highlighted area in Figure 5.7) of 18.9 ± 1.0 – 20.3 ± 0.6 ka are given.

5.6.1. Fading-corrected $IRSL_{50}$ ages

Fading-corrected $IRSL_{50}$ ages remain lower, to greater depths into the cobble sub-surfaces, than post-IR $IRSL_{225}$ ages (Figure 5.7), as might be expected from initial L_n/T_n measurements with depth (as shown in Figure 5.2b, c, d). Fading-corrected $IRSL_{50}$ ages for the first cobble illustrated in Figure 5.7a (ORS02-1) are 21.2 ± 1.1 ka and this age is established by combining the top three rock slices. Fading-corrected $IRSL_{50}$ ages for the next cobble (ORS04-3) in Figure 5.2b are 20.6 ± 0.5 ka. This age is established for the uppermost 10 rock slices, with cobble ORS04-3 showing similar ages to a greater depth than all other cobbles analysed at Orrisdale Head. This is interpreted to indicate that cobble ORS04-3 was the best bleached. The final well-bleached cobble (ORS04-1 – Figure 5.7c) gives an average age of 20.8 ± 1.2 ka for the top 3 slices. However, $IRSL_{50}$ ages remain relatively low below these upper 3 rock slices and the potential for multiple bleaching and depositional events is discussed below in regards to these age differences (Section 5.6.3).

The fading-corrected $IRSL_{50}$ ages discussed above, from the three separate cobbles, give ages that are similar to each other and give an average age of 20.7 ± 1.3 ka. This depositional age agrees with the independent age provided (see Figure 5.7). It is clear, therefore, that initial L_n/T_n measurements with depth reflect those cobbles which

have the lowest ages, and such measurements are a good way of identifying which cobbles and rock slices to undertake equivalent dose measurements upon.

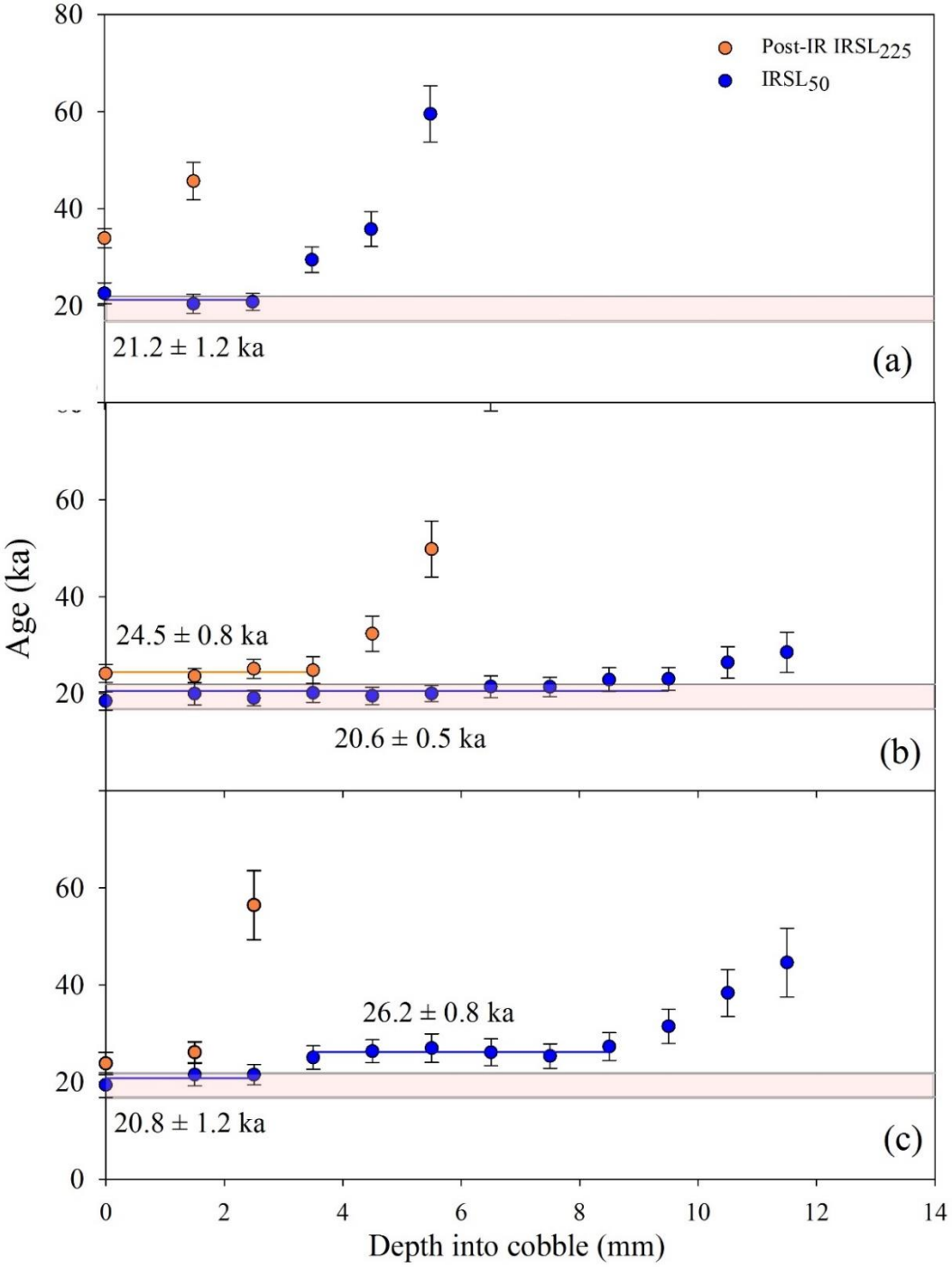

Figure 5.7. $IRSL_{50}$ and post-IR $IRSL_{225}$ ages with depth into cobbles (a) ORS02-1, (b) ORS04-3 , and (c) ORS04-1. Independent age control brackets are also provided (from Chiverrell *et al*., 2018; Smedley *et al*., 2017b) and give bracketing ages of 18.9 ± 1.0 – 20.3 ± 0.6 ka. A separate event is identified in the $IRSL_{50}$ data in 5.7c.

5.6.2. Post-IR IRSL$_{225}$ ages

Post-IR IRSL$_{225}$ ages show a different pattern with depth, as was the case for initial L_n/T_n measurements (Section 5.3.2). For 2 of the 3 cobbles, a monotonic increase with depth is observed for the post-IR IRSL$_{225}$ ages (for example Figure 5.7a & c). This is interpreted to show that complete bleaching has not occurred for that signal and therefore it is not possible to be confident in those ages. However, one cobble (Figure 5.7b) does show consistently low post-IR IRSL$_{225}$ ages, up to a depth of ~ 4 mm. Combined with the fact that this cobble (Figure 5.7b) has the lowest IRSL$_{50}$ ages, to the greatest depth, indicates that this cobble had been best bleached. The post-IR IRSL$_{225}$ ages for the top 4 slices in Figure 5.7b are consistent with each other, suggesting that they were well-bleached. These 4 slices give an average age of 24.5 ± 0.8 ka and are older than the IRSL$_{50}$ ages from the same cobble. However, the post-IR IRSL$_{225}$ signal still agrees with the independent age control within two standard deviations. A possible reason for the difference could be due to an unbleachable component in the post-IR IRSL$_{225}$ signal, however, the magnitude of this is has been suggested to be ~ 1 – 2 Gy (Thomsen *et al*., 2008). This would result in a difference of a few hundred years and, therefore, cannot explain the large difference between the IRSL$_{50}$ and post-IR IRSL$_{225}$ ages for the rock slices. However, as the IRSL$_{50}$ signal has been fading-corrected and is shown to be the more sensitive signal, this makes the IRSL$_{50}$ signal optimal for dating in the heterogeneously-bleached sandur environment.

5.6.3. Second plateau IRSL$_{50}$ ages – multiple exposure and burials?

It has been shown, in other studies (Freiesleben *et al*., 2015; Sohbati *et al*., 2015), that small changes in L_n/T_n ratios and ages in a well-bleached area of a cobble can indicate that multiple burial and exposure events are recorded in the cobble. In one of the

well-bleached cobbles from Orrisdale Head (ORS04-1) a small increase in L_n/T_n ratios, at a depth of ~ 3.5 mm is observed. This is also reflected in the fading-corrected $IRSL_{50}$ ages with depth for ORS04-1 (Figure 5.7c). Here, the upper 3 rock slices given an average age of 20.8 ± 1.2 ka whereas the rock slices from a depth of ~ 3.5 mm to 8 mm given a fading-corrected $IRSL_{50}$ age of 26.2 ± 0.8 ka. This plateau of increased ages is very different to the obvious increase in ages in Figure 5.7a, which indicates that sub-surface bleaching did not occur to greater extents.

The consistency in ages from ~ 3.5 – 8.5 mm is interpreted to show that complete bleaching occurred to this depth. The cobble was then buried at 26.2 ± 0.8 ka. The cobble was exposed and moved for a second time (20.8 ± 1.2 ka) and the upper 3 rock slices show this second event. Finally the cobble was then buried until time of sampling. However, as the deposits at Orrisdale Head are interpreted to record final deglaciation only, it is difficult to be confident of this earlier bleaching event. Modelling of the Irish Sea ice stream by Chiverrell *et al*. (2013) shows that the Irish Sea ice stream advanced across the Isle of Man, and this advance episode correlates to the second plateau of ages observed in the cobble sub-surface. It is suggested, therefore, that this cobble potentially shows two exposure and burial events within its sub-surface, and could possibly show two depositional phases for the same ice stream.

5.7. Conclusions

It is apparent that cobbles can be used to obtain reliable depositional ages for the glaciofluvial sediments at Orrisdale Head, Isle of Man. Initial L_n/T_n measurements from the surface of every cobble collected provides a reliable way of establishing which cobbles were better bleached (Figure 5.1). This is then followed by sub-surface L_n/T_n

measurements, which show that the cobbles with the lowest surface L_n/T_n ratios are those cobbles best bleached with depth (as might be expected). Initial surface L_n/T_n measurements, combined with L_n/T_n measurements with depth into the cobbles have illustrated that bleaching is not uniform across a single cobble (e.g. ORS02-1). This is interpreted as evidence that bleaching occurred at final deposition of the cobble in the sandur deposit.

As has been observed in other studies (e.g. Sohbati *et al*., 2015) the $IRSL_{50}$ signal is reset to greater depths than the post-IR $IRSL_{225}$ signal, however, for one cobble, consistently low post-IR $IRSL_{225}$ ages have been observed. Consistent age values, with depth, provides compelling evidence that the luminescence signal was completely reset at the time of deposition. This means that equivalent doses from rock slices do not suffer from any sample partial bleaching issues (as may occur for sand-sized material).

Fading-corrected $IRSL_{50}$ ages from three separate cobbles are similar and provide a weighted mean age of 20.7 ± 1.3 ka. This age agrees with independent age control provided by Chiverrell *et al*. (2018) and Smedley *et al*. (2017b). In addition to an age provided for final deglaciation of the Irish Sea ice stream, a fading-corrected $IRSL_{50}$ age of 26.2 ± 0.8 ka is provided from the sub-surface of one of the well-bleached cobbles (which illustrates the potential for multiple exposure events). This single clast may potentially record both the advance and retreat of the Irish Sea ice stream.

As outlined in Section 3.4, a major advantage of using cobbles over sand-sized material is that dose rates to the rock slices, after ~ 2 mm, are almost completely independent of external water content. Secondly, and as outlined in this section, consistent ages with depth into the cobble sub-surface indicate that the luminescence signal was completely reset. Sand-sized luminescence dating analyses distributions in the

equivalent doses to identify which grains had their signal reset. However, issues such as microdosimtery make the analysis of equivalent dose data difficult. This type of analysis is avoided when using ages taken from cobble sub-surfaces as the cobbles themselves illustrate that they were completely bleached and therefore cobbles can provide a significant advantage in these types of environments. Additionally, due to the consolidated nature of the cobbles, changes in the microdosimetry are avoided when using this type of material. The investigation at Orrisdale Head, therefore, has shown the potential for using cobbles in the glaciofluvial, sandur environment. However, to establish if this technique can be used consistently, application to multiple deposits may be required to identify how common the bleaching of cobbles may be.

6. Testing high-precision cobble-dating at an additional ice retreat location (Llyn Peninsula, north Wales)

6.1. Introduction

Following the successful trial of the luminescence dating of cobbles at Orrisdale Head, Isle of Man (see Chapter 5) this chapter applies this approach to two additional glaciofluvial sequences that were deposited during the retreat of the Irish Sea Ice Stream. Cobbles from two glaciofluvial exposures, Nefyn and Bryn-yr-Eryr, along the Llyn Peninsula in north Wales were collected (see Chapter 2.5). The two sites record deposition from the same retreat stage as each other as described by Chiverrell *et al*. (2013) and Smedley *et al*. (2017b). A total of 40 cobbles were collected from the two sites, and the sequence of tests described in Chapter 5 were applied. These tests were designed to assess if any cobbles had been bleached, if they were exposed for sufficient time for their sub-surfaces to bleach and if reliable depositional ages can be obtained. Age control is provided for the location by both Chiverell *et al*., (2013) and Smedley *et al*. (2017b) (see Chapter 2.5) and control for the site provides a fantastic opportunity to duplicate the trial of cobble luminescence dating.

6.2. Were the surface of the cobbles bleached in the glacial deposits at north Wales?

The L_n/T_n ratios for the $IRSL_{50}$ and post-IR $IRSL_{225}$ signals were measured for a surface slice from the topside of every cobble (Figure 6.1). The same test dose (~ 34 Gy) was used for these measurements as had been used at Orrisdale Head to make a comparison to the data more straightforward. This screening process is undertaken to

identify those cobbles which are most likely to have been bleached at deposition and then allows the targeting of specific cobbles to analyse bleaching with depth (as was undertaken at Orrisdale Head). Unlike Figure 5.1, from Orrisdale Head, the surface slice L_n/T_n ratios in Figure 6.1 are provided for the upper faces of the cobbles only – not from different sides of the cobbles. This is because Figure 5.1 shows that slices from the upper side of the cobbles are better bleached than the other faces.

The L_n/T_n ratios for Nefyn and Bryn-yr-Eryr are given on the same figure. As observed at Orrisdale Head, there is a range in L_n/T_n ratios (for both sites on the Llyn Peninsula). Values of L_n/T_n cover a wide range from 2.45 ± 0.1 to 7.61 ± 0.16 for Nefyn (for the $IRSL_{50}$ signal and with a test dose of ~ 34 Gy), and from 0.40 ± 0.0 to 8.68 ± 0.18 for Bryn-yr-Eryr and this range presumably reflects differences in the exposure of the cobbles to daylight at the time when the sediments were deposited. The L_n/T_n ratios for Nefyn and Bryn-yr-Eryr show a population of cobbles with low ratios and there are more slices with lower L_n/T_n values for Bryn-yr-Eryr than for Nefyn. As was undertaken in Section 5.3 at Orrisdale Head, to establish if the cobbles were completely bleached, the cobbles with the lowest L_n/T_n ratios were targeted for sub-surface L_n/T_n measurements. Figure 6.1 shows that there is a range in bleaching between the cobbles and this was also observed at Orrisdale. Although cobble size was recorded at the time of sampling there was not a significant population of cobbles to assess which size may be best for cobble luminescence dating. As all cobbles were obtained from a glaciofluvial setting, all cobbles were well-rounded and therefore it was not possible to discriminate which cobbles to collected based on size or shape.

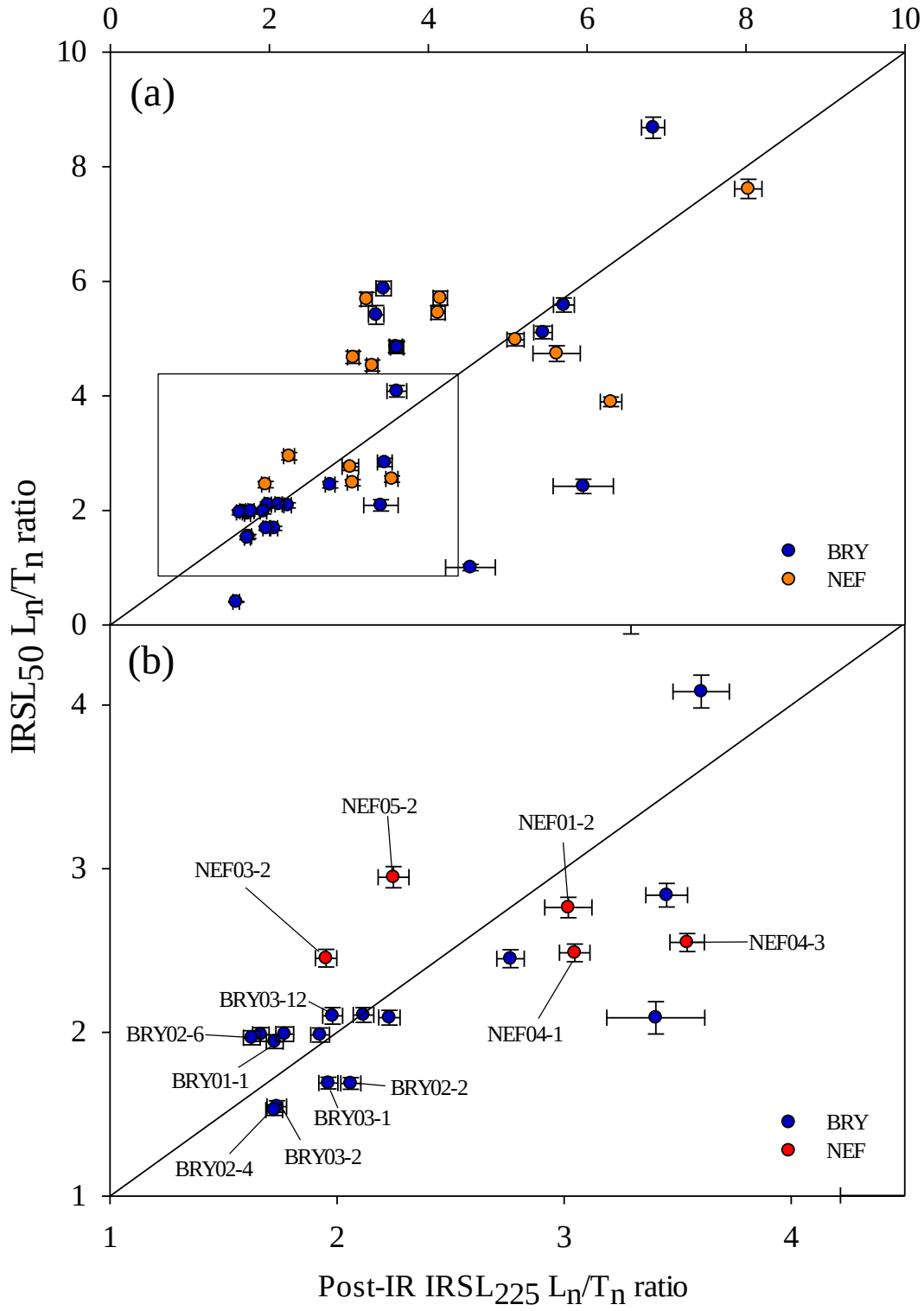

Figure 6.1. $IRSL_{50}$ and post-IR $IRSL_{225}$ L_n/T_n ratios for surface slices from the upper face of 40 cobbles from Nefyn (orange) and Bryn-yr-Eryr (blue) (with a box outlining those illustrated in b). A 1:1 line is given to guide the eye with the $IRSL_{50}$ signal expected to be lower than the post-IR $IRSL_{225}$ signal. Figure 6.1b shows a more detailed image of those cobbles with low L_n/T_n values with cobble names indicated.

6.3. Sub-surface luminescence measurements

As at Orrisdale Head, those cobbles with the lowest surface L_n/T_n ratios at their surface had their cores sliced completely to investigate their natural luminescence signal as a function of depth. Initially, one core was sliced and measured to establish if any pattern of bleaching is observed (the core that provided the surface slice). If a pattern of bleaching was observed from this initial core, duplicate and triplicate cores are then taken and sliced entirely to provide duplicate and triplicate measurements of L_n/T_n. This will then confirm if the cobbles were well-bleached and indicate which rock slices to measure equivalent doses. Figures 6.2 and 6.3 show L_n/T_n, with depth, for nine of the cobbles with low L_n/T_n ratios at their surface. Four cobbles with low L_n/T_n ratios were not included in Figure 6.2 and this is because when obtaining the cores only the surface slice could be obtained due to the breaking of the cobble and remainder of the core.

The L_n/T_n with depth data can be roughly split into a number of groups of similar patterns. The first group (Group I), whereby low surface L_n/T_n ratios increase at the next rock slice and then remain stable with depth, is illustrated in Figure 6.2a-c. For the first cobble illustrated in Figure 6.2(a) the $IRSL_{50}$ L_n/T_n ratio increases from 2.5 ± 0.1 to an L_n/T_n ratio of 5.1 ± 0.1 which then remains stable to a depth of 7.5 mm. This also happens for the post-IR $IRSL_{225}$ signal which increases from an L_n/T_n ratio of 3.05 ± 0.1 to a value of 4.97 ± 0.1 which also remains stable to 7.5 mm deep into the cobble. The same pattern is observed for cobbles BRY02-4 (Figure 6.2b) and BRY03-1 (Figure 6.2c).

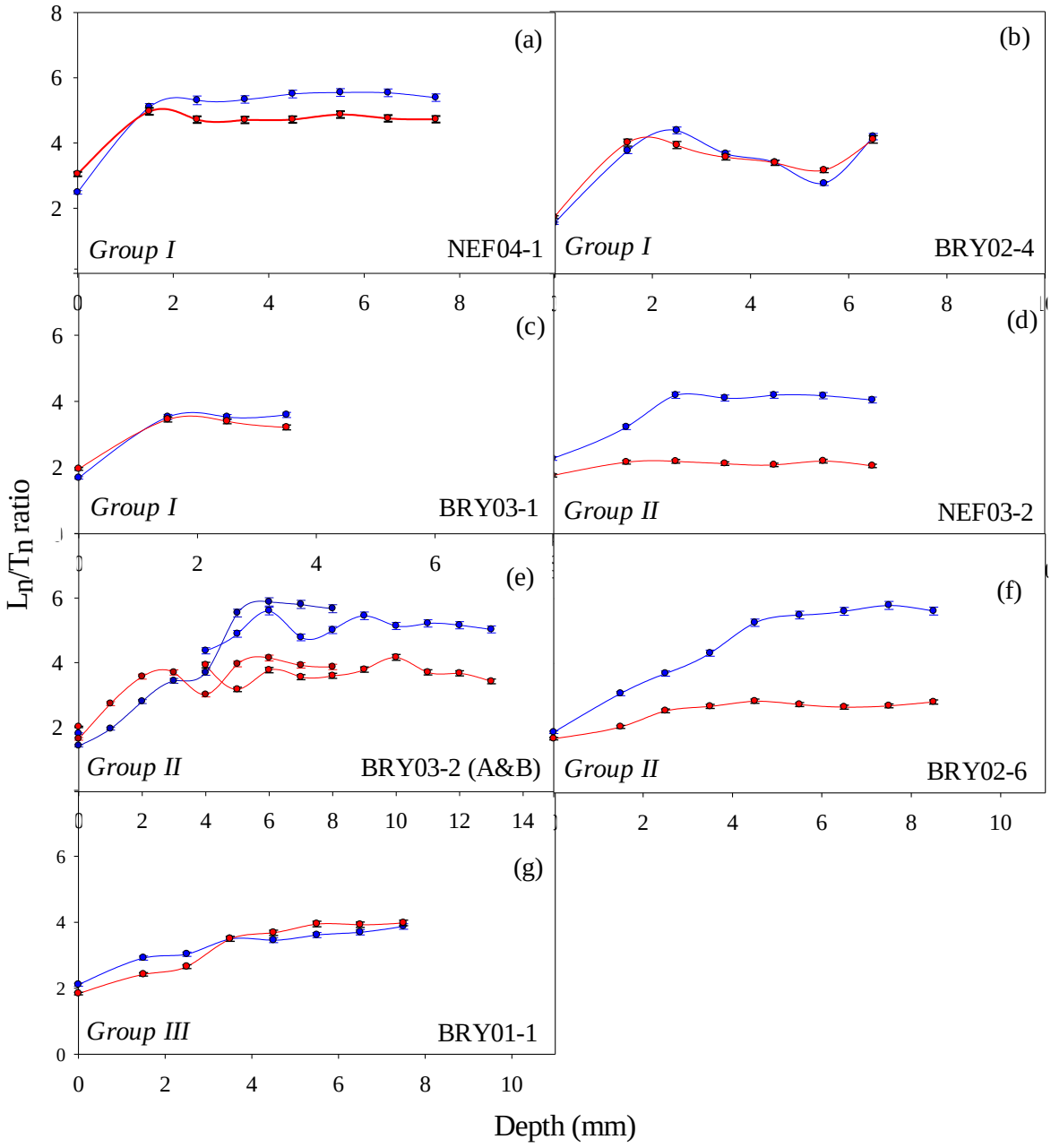

Figure 6.2. Measurements of L_n/T_n ratios, for the $IRSL_{50}$ (blue) and post-IR $IRSL_{225}$ (red) signals for 7 different cobbles from both Nefyn and Bryn-yr-Eryr. These 7 cobbles illustrate the different patterns of L_n/T_n ratios, with depth, and do not show the typical bleaching patterns that were observed at Orrisdale Head, in Section 5.3.

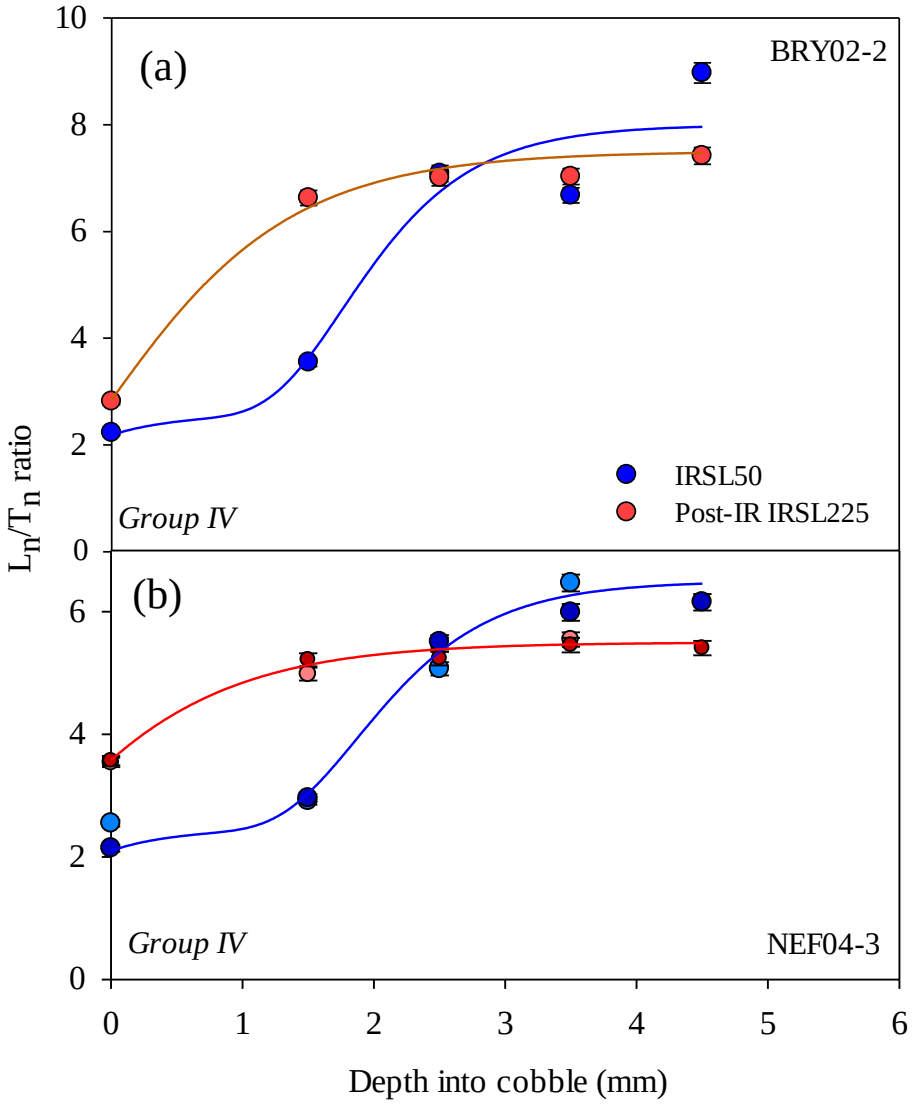

Figure 6.3. L_n/T_n ratios, with depth, for the cobbles BRY02-2 (a) and NEF04-3 (b) which show the most extensive sub-surface bleaching from the population of 40 cobbles from north Wales. The solid lines are the fitting of a bleaching model (Freiesleben *et al*. 2015) to quantify exposure length. Duplicate cores are taken for NEF04-3 whereas only a single core was taken for BRY02-2 due to the cobble breaking when taking the first core. Uncertainties for the surface slices are within the symbol size.

The second group (Group II) (Figure 6.2d - f) are three cobbles with increasing $IRSL_{50}$ L_n/T_n ratios with depth, however, a stable pattern of post-IR $IRSL_{225}$ values is apparent. For cobble NEF03-2 (Figure 6.2d), the post-IR $IRSL_{225}$ signal remains stable with depth, at low L_n/T_n values, which could suggested that the cobble was well-bleached, however the $IRSL_{50}$ signal increases into the next most slices and stabilises at

a higher L_n/T_n ratio than the post-IR $IRSL_{225}$ signal. The same pattern is observed for BRY02-6 (Figure 6.2f) whereby a higher saturating $IRSL_{50}$ L_n/T_n value is observed and a flat post-IR $IRSL_{225}$ pattern is present. BRY03-2 shows a slightly different bleaching pattern, with depth, however it is also clear that significant sub-surface bleaching has not occurred. This is because L_n/T_n values increase on a slice-by-slice basis, with depth into the cobble, and do not show the steady and low L_n/T_n values observed for cobbles at Orrisdale Head. However, BRY03-2 shows a gradually increasing L_n/T_n ratio pattern, with L_n/T_n values slowly increasing for the top 5 – 6 rock slices. The presence of low surface L_n/T_n ratios, with no further sub-surface bleaching occurring may be due a short bleaching episode, with partial bleaching occurring (as might be expected in this type of environment). The final cobble in Figure 6.2 (g) shows low gradually increasing L_n/T_n values, which do not increase dramatically (as might be expected for a bleaching profile).

A fourth group (Figure 6.3a-b) shows the $IRSL_{50}$ signal remaining stable for the upper two slices, with an increase following this. The post-IR $IRSL_{225}$ signal is also low at the surface, and then increases with depth into the next slice. Low surface $IRSL_{50}$ L_n/T_n ratios gradually increase into the next most slice (at 1.5 mm) for both cobbles and are similar L_n/T_n ratios to well-bleached cobbles seen at Orrisdale Head (e.g. ORS04-1 has an $IRSL_{50}$ L_n/T_n ratio of 1.99 ± 0.04 at its surface whilst BRY02-2 has an $IRSL_{50}$ L_n/T_n ratio of 2.22 ± 0.04). The post-IR $IRSL_{225}$ signal increases to saturation for the next slice, and again illustrates (as was the case at Orrisdale Head) that the post-IR $IRSL_{225}$ signal bleaches slower than the $IRSL_{50}$ signal. Stable and high L_n/T_n ratios for the $IRSL_{50}$ signal (6.2 ± 0.2 for NEF04-3) are similar to those observed at Orrisdale Head, Isle of Man (7.5 ± 1.1 for ORS02-1-E). The post-IR $IRSL_{225}$ saturated values are lower than the $IRSL_{50}$ saturated values and also lower than those observed at Orrisdale Head. However, it is

clear that both the $IRSL_{50}$ and post-IR $IRSL_{225}$ signals do not remain low, with depth, as was observed at Orrisdale with only two slices giving similar L_n/T_n values.

Cobbles in Group I of L_n/T_n patterns with depth (Figure 6.2a-c) could be a result of limited exposure at the cobble surface, with no subsequent bleaching occurring below this. A more complicated pattern is apparent for cobbles in Group II and Group III of L_n/T_n with depth patterns and the exposure context is hard to establish from these. The forth group of L_n/T_n with depth patterns (Figure 6.3a-b), which show low L_n/T_n ratios in the upper few slices, could be a result of either shorter bleaching periods within the deposition environment, limited exposure within the deposits or potential differences in lithology restricting light penetration into the cobble sub-surface (as illustrated by Ou *et al*., 2018). The pattern of L_n/T_n ratios with depth, however, appears similar to the L_n/T_n ratios with depth for the exposed cobble at Orrisdale Head (see Figure 4.7), and possibly indicates that these cobbles were exposed, but not for extensive periods. It is interesting to note that a similar pattern of bleaching with depth (with only the few upper millimetres giving low L_n/T_n values) were observed by Sohbati *et al*. (2012b) for buried quartzite cobbles in an alluvial fan (Figure 6.4).

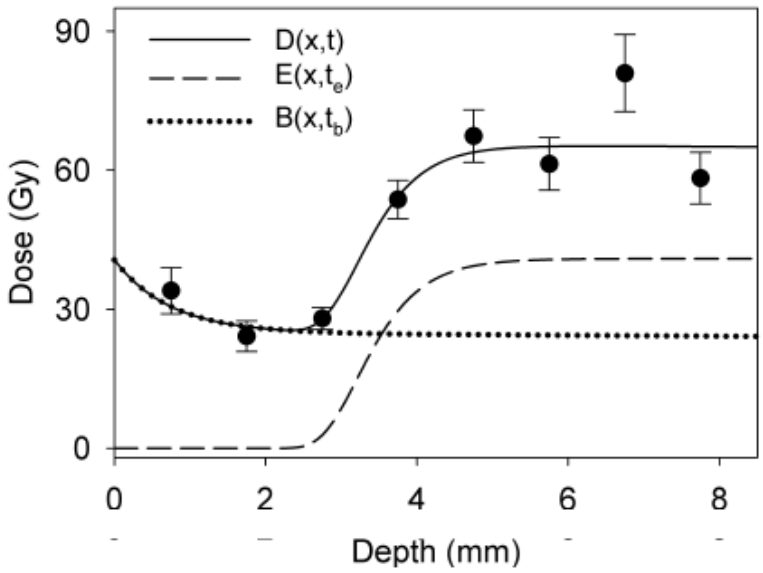

Figure 6.4. Limited sub-surface bleaching illustrated by Sohbati *et al*. (2012b) which shows that only the upper 3 rock slices have been bleached.

Although granite cobbles were targeted from the glacial deposits at north Wales, the different patterns of L_n/T_n ratios with depth into their sub-surfaces may indicate different characteristics for each individual cobble. This was not observed at the trial location of Orrisdale Head (see Section 5.3.2) whereby L_n/T_n ratio patterns (with the $IRSL_{50}$ signal bleaching to greater depths than the post-IR $IRSL_{225}$ signal) and saturation characteristics were similar for different cobbles. The upper slices from the fourth group of cobbles were targeted for subsequent D_e measurements and age determination.

6.4. Variability in dose response curves from different cobbles

A dose response curve is shown for the surface rock slice from each of the cobbles, to explore the range in L_x/T_x values with given doses (Figure 6.5 & 6.6). The dose response curves for the 8 different rock slices from 8 different cobbles show a range in L_x/T_x values for the same given dose of ~ 171 Gy from 2.58 ± 0.06 to 4.21 ± 0.08 (for the $IRSL_{50}$ signal) and from 2.38 ± 0.05 to 3.52 ± 0.07 for the post-IR $IRSL_{225}$ signal.

One of the groups identified in Figure 6.2 (d-f) (Group II) has post-IR $IRSL_{225}$ values that are flat and of a low value (L_n/T_n values of ~ 2). This would normally imply that the cobble was bleached at some point in the past. However, the $IRSL_{50}$ L_n/T_n values do not support that interpretation. Figure 6.6 shows L_x/T_x data for cobbles from this group and the dose response curves appear close to saturation even after ~ 171 Gy. Thus, the flat L_n/T_n values, with depth, seen for the post-IR $IRSL_{225}$ signal suggests that the signal has not been reset with depth. Additionally, the $IRSL_{50}$ dose response curves for those samples have some of the lowest values at ~ 171 Gy (Figure 6.5) and this could be why the $IRSL_{50}$ data appear to flatten, with depth and saturated at an L_n/T_n value of only ~ 4. The data in Figures 6.5 and 6.6 shows a lot of variability and the straighter the dose response curve (the higher the values of L_x/T_x for a given dose) the better suited the cobble. This is well illustrated by the dose response curves shown in Figure 6.6 for the post-IR $IRSL_{225}$ signal, with the two dose response curves with the highest L_x/T_x values (BRY02-2 and NEF04-3) belonging to rock slices which show the most extensive sub-surface bleaching (Group IV). In addition to dose response curves for rock slices from north Wales, dose response curves are also given for rock slices from Orrisdale Head, Isle of Man, for cobbles which show significant sub-surface bleaching (Figures 6.5 and 6.6). Although these dose response curves do not show the highest L_x/T_x values, they do not show very early saturation and are not highly variable. This is especially the case for the post-IR $IRSL_{225}$ signal, with L_x/T_x values for these being some of the highest. High L_x/T_x values for the post-IR $IRSL_{225}$ signal from rock slices from Orrisdale Head also correspond to those from north Wales, with the highest L_x/T_x values belonging to cobbles that showed the most extensive sub-surface bleaching.

A wide range in dose response curve characteristics has also been observed for feldspar samples by Li *et al*. (2015) with different L_x/T_x values for the same given doses.

In Li *et al*. (2015) normalising the L_x/T_x values to a given dose allowed the use of a global standardised growth curve (see Figure 6.7). Due to the large variability of the dose response curves observed here (Figures 6.5 and 6.6) it would be difficult to produce a standardised growth curve and this shows the large variability between the different cobbles. The change in dose-response curve characteristics for the different cobble slices shows the variability between the different samples (which were interpreted in the laboratory to be of the same lithology). The variability in L_x/T_x values could be a result of the variability in the minerals or type of feldspars being analysed. Therefore, to attempt to establish the composition of the cobbles, digital microscope images are taken.

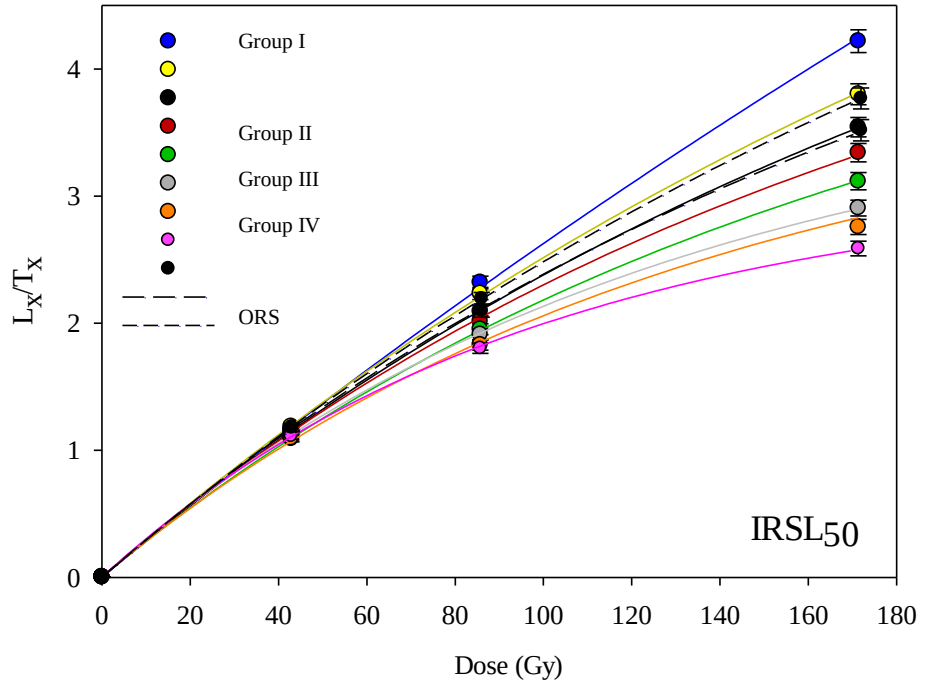

Figure 6.5. Dose response curves up to ~ 171 Gy for 8 different rock slices, from different cobbles from Nefyn and Bryn-yr-Eryr for the $IRSL_{50}$ signal.

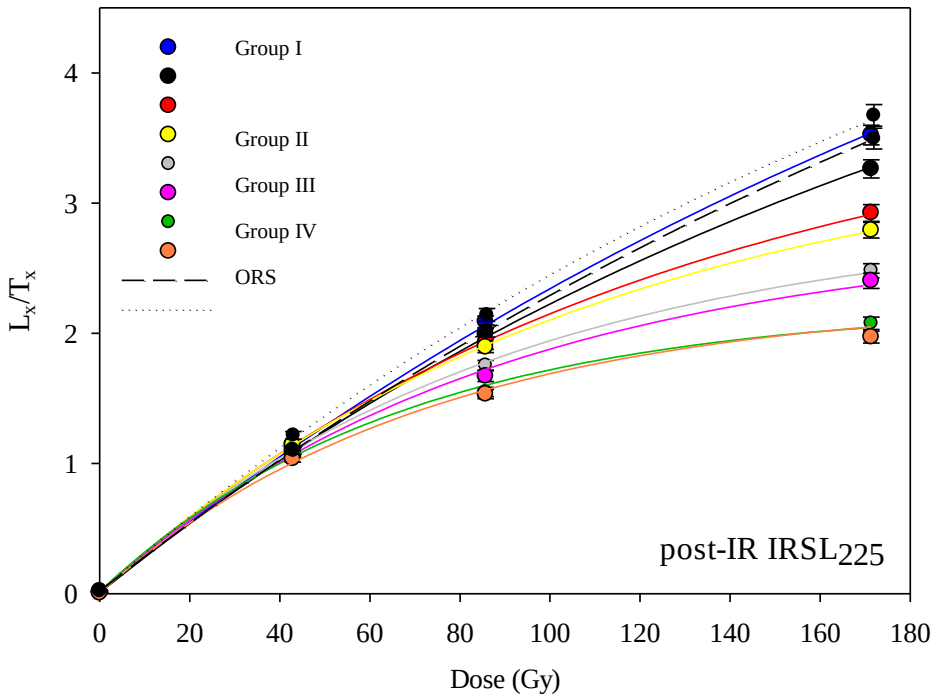

Figure 6.6. Dose-response curves up to ~ 171 Gy (for the post-IR $IRSL_{225}$ signal) for 8 rock slices, each from a different cobble from Nefyn and Bryn-yr-Eryr. A large difference in the L_x/T_x values, for the same dose, is apparent for the different rock slices and shows that the dose response curves grow differently for the different cobbles.

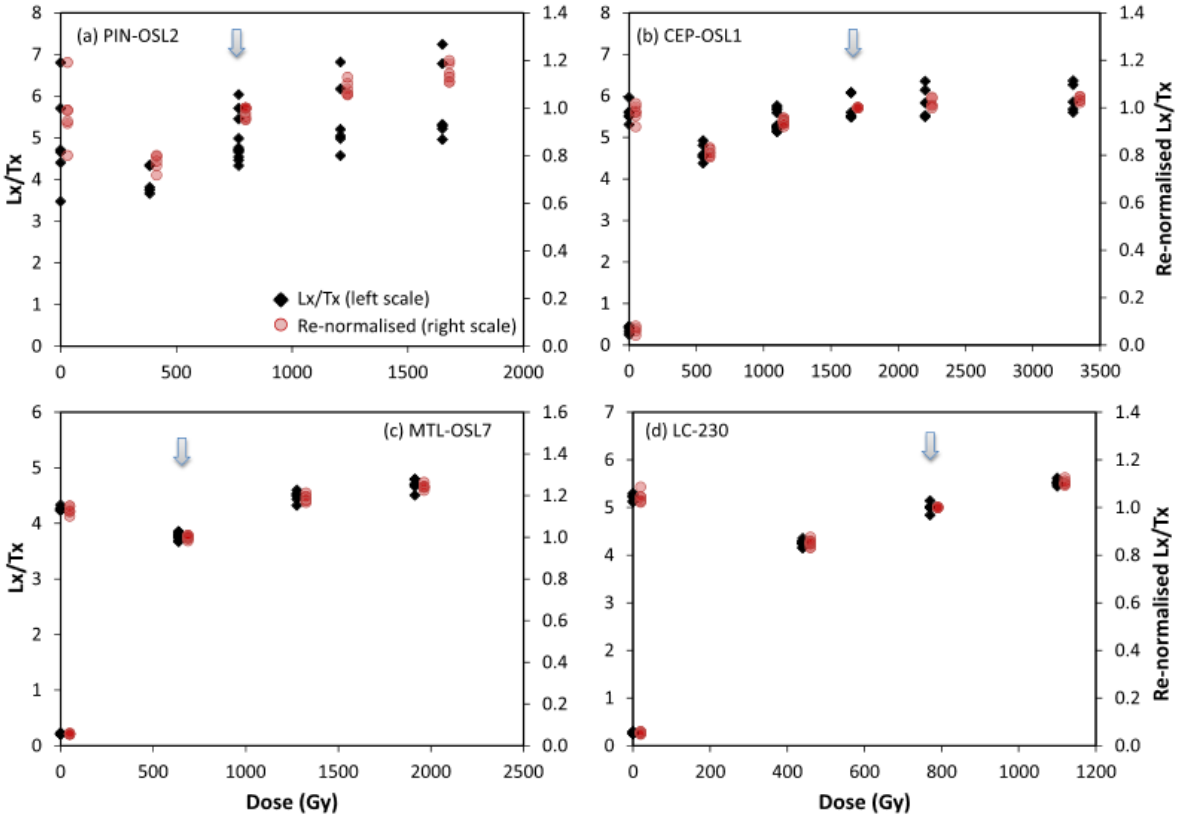

Figure 6.7. Dose response curve SAR data from four samples of feldspar. For each sample of feldspar a number of aliquots were measured by Li *et al*. (2015) and this gives multiple L_x/T_x values at each regeneration dose (black diamonds). Greater scatter is seen for sample PIN-OSL2 and the re-normalised L_x/T_x values given as red circles and show the normalising of the dose response curve.

6.5. Variability in the lithology of cobbles from the Llyn Peninsula

The glaciofluvial sediments along the Llyn Peninsula, north Wales, have a more variable lithological content than those sampled at Orrisdale Head, with a complex local geology contributing to this. This includes the local lithologies of granites, schists, quartzites, gneiss, greywacke, psammites and pelites (White and Beamish, 2014). Therefore, the rock slices taken from each cobble were optically analysed using a digital microscope to assess the different properties of each rock slice. At the time of sampling, crystalline igneous cobbles were targeted, however, due to mixing with numerous

lithologies, it was not always possible to identify these under subdued red light in the field.

NEF03-2-A (Figure 6.8) is relatively fine-grained and contains light coloured minerals with quartz grains identifiable. NEF04-1 is pink in colour, with an iron-stained matrix with single quartz grains within this. Both NEF04-3-A and NEF04-3-B are taken from the same cobble, with the slices coming from duplicate cores (Figure 6.8). NEF04-3 shows the most extensive sub-surface bleaching into the cobble observed at north Wales (Figure 6.3). Feldspar grains were identified in these rock slices and gave an average grain size of 0.390 mm ± 0.104 mm. Megacrysts of what appear to be quartz grains are also observed to grain sizes of up to ~ 1 mm. BRY02-2 and BRY02-4 appear similar with both having a very fine matrix with intermittent large quartz grains. BRY02-6 and BRY03-1 also have similar characteristics with very fine grains and a brownish hue. The L_n/T_n v depth plots look different for each of the rock slices however, (as shown later in Chapter 6.4), with BRY02-6 showing an increasing $IRSL_{50}$ L_n/T_n ratio up to a value of ~ 6 and BRY03-1 showing flat and low L_n/T_n ratios for both signals. BRY03-2-A and BRY03-2-B are both from same cobble and show larger quartz grains in a fine grained matrix. BRY01-1 appears much more equigranular with quartz and feldspar both identified. A range of textures were observed for the rock slices, however, one of the cobbles with the most extensive sub-surface bleaching, with depth, had the largest quartz grains present. The rock slices illustrated in Figure 6.8 are those rock slices from Figure 6.2 and 6.3 which give the lowest L_n/T_n ratios for the surface slices.


~ 0.8 cm
NEF03-2-A
NEF04-1-A
NEF04-3-A
NEF04-3-B
BRY02-2-B
BRY02-4-A

Figure 6.8. Digital microscope images of rock slices from Nefyn and Bryn-yr-Eryr, taken from cobbles with low surface L_n/T_n ratios (Figure 6.2; 6.3) and showing a range of characteristics between the cobbles that were initially thought to be granite lithologies under subdued red-light in-field.

The rock slices taken from cobbles from north Wales can be compared to those obtained from cobbles at Orrisdale Head which gave extensive sub-surface bleaching (Figure 6.9). The rock slices from Orrisdale Head (Figure 6.9) show relatively large crystalline grains (with ORS04-1 having a larger average grain size than ORS04-3). However both rock slices from Orrisdale Head show a clear crystalline texture, and this is in contrast to that observed for north Wales rock slices. Visually, rock slices from Orrisdale Head appear similar to the rock slice NEF04-3 (see Figure 6.8) which is a cobble from north Wales showing the most extensive sub-surface bleaching.

Figure 6.9. Rock slices of granite lithologies taken from two separate cobbles from Orrisdale Head, which both gave extensively bleached sub-surface values.

6.6. Anomalous Fading

Despite the lithological complexity of the samples from north Wales, further analysis was undertaken to see if reliable ages could be obtained. As at Orrisdale Head, two approaches were taken to try to assess the stability of the $IRSL_{50}$ and post-IR $IRSL_{225}$ signals. Firstly, storage experiments were undertaken to measure the g-value of the two signals. Secondly, a comparison is undertaken of the signal from a part of a cobble that

has not been exposed to daylight and is in field saturation with the saturation level measured in the laboratory (Buylaert *et al*., 2012). Fading measurements were made on 20 rock slices (10 from Nefyn and 10 from Bryn-yr-Eryr) for periods of up to ~ 2 months and for 4 different cobbles (NEF04-3, NEF03-2, BRY03-2, BRY02-2) (Figure 6.10 & Table 6.1). An example of the change in L_x/T_x, over time, is illustrated in Figure 6.10 for rock slice NEF04-3-A-2. Average g-values for Nefyn for the $IRSL_{50}$ signal are 0.33 ± 0.48 %/decade and for the post-IR $IRSL_{225}$ signal are 0.34 ± 0.22 %/decade (Figure 6.11 & Table 6.1). For Bryn-yr-Eryr, the g-value for the $IRSL_{50}$ signal is 0.68 ± 1.32 %/decade and for the post-IR $IRSL_{225}$ signal is 0.35 ± 0.54 %/decade (Figure 6.11). This indicates that no fading corrections are required for either of the signals at either of the locations in north Wales.

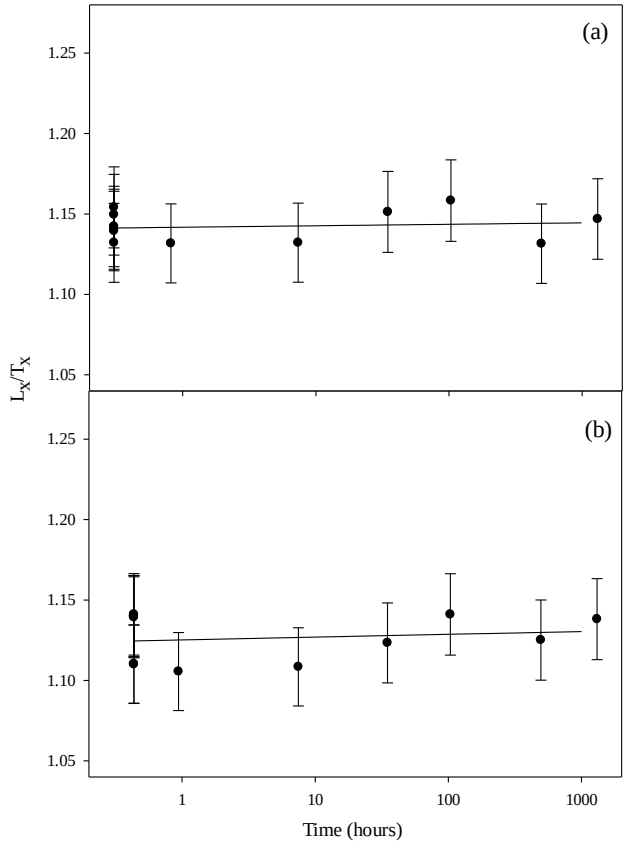

Figure 6.10. Changes in L_x/T_x up to ~ 1 month for rock slice NEF04-3-A-2 for the $IRSL_{50}$ (a) and post-IR $IRSL_{225}$ signals (b).

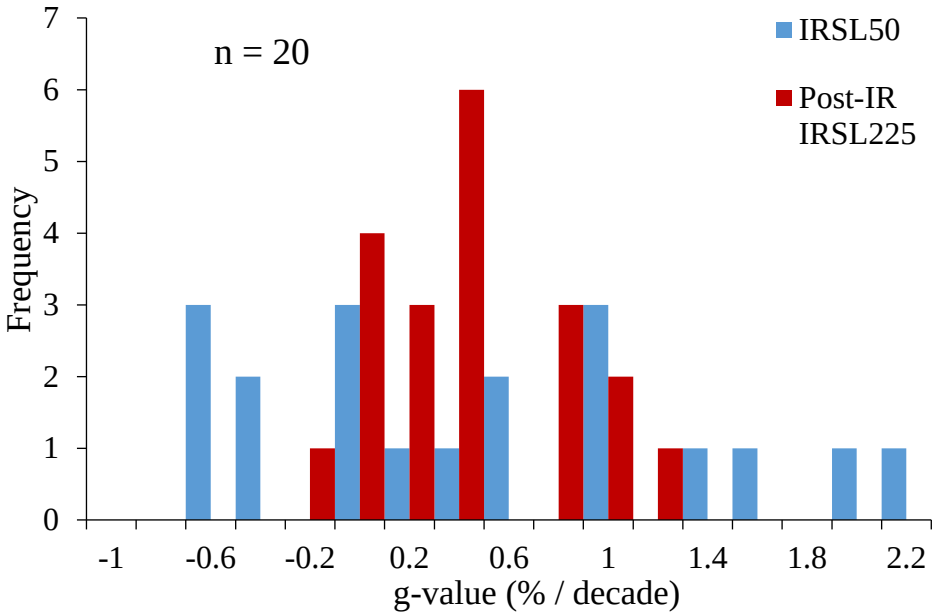

Figure 6.11. g-values for all rock slices from both Nefyn and Bryn-yr-Eryr, showing a larger deviation between the $IRSL_{50}$ g-values compared to the post-IR $IRSL_{225}$ g-values. G-values for the $IRSL_{50}$ and post-IR $IRSL_{225}$ signal for both locations indicate that ages did not need fading correcting.

Table 6.1. g-values for the $IRSL_{50}$ and post-IR $IRSL_{225}$ signals for each individual cobble showing the low $IRSL_{50}$ and post-IR $IRSL_{225}$ g-values for all samples from north Wales compared to a g-value which required fading corrections from Orrisdale Head.

Cobble	$IRSL_{50}$ g-value (% / decade)	Post-IR $IRSL_{225}$ g-value (% / decade)
NEF04-3	0.41 ± 0.54	0.20 ± 0.13
NEF03-2	0.24 ± 0.44	0.45 ± 0.22
BRY03-2	- 0.56 ± 0.25	- 0.13 ± 0.08
BRY02-2	1.87 ± 0.55	0.84 ± 0.23
Orrisdale Head	2.53 ± 0.65	1.62 ± 0.69

The second approach used to assess whether the two signals are stable over geological time is to compare the field saturated value with the laboratory saturation level. A single rock slice (NEF04-3-B-5) was given doses up to ~ 2741 Gy (Figure 6.12). This rock slice was selected as it was interpreted that it was in field saturation due to the

high and consistent values. Figure 6.12 shows a laboratory saturated L_x/T_x value of 7.78 ± 0.16 for the $IRSL_{50}$ signal and 6.49 ± 0.14 for the post-IR $IRSL_{225}$ signal. The natural signal is 76 % of the laboratory saturated signal for the $IRSL_{50}$ signal and 84 % for the post-IR $IRSL_{225}$ signal. This data can be compared with measurements made for 3 rock slices from Orrisdale Head which gave a naturally saturated percentage of 64 % for the $IRSL_{50}$ and 99 % for the post-IR $IRSL_{225}$ signal. It is interesting to note that the lower naturally saturated $IRSL_{50}$ signal (64 %) at Orrisdale Head also correlates to a higher g-value (2.53 ± 0.65 %/decade). The fact that the post-IR $IRSL_{225}$ naturally saturated value (84 %) from the rock slice from Nefyn shows a loss of signal (which is not expected from the stable post-IR IRSL signal) potentially illustrates that this rock slice was not entirely saturated, as was initially interpreted (and could also explain why there is a loss in the $IRSL_{50}$ signal).

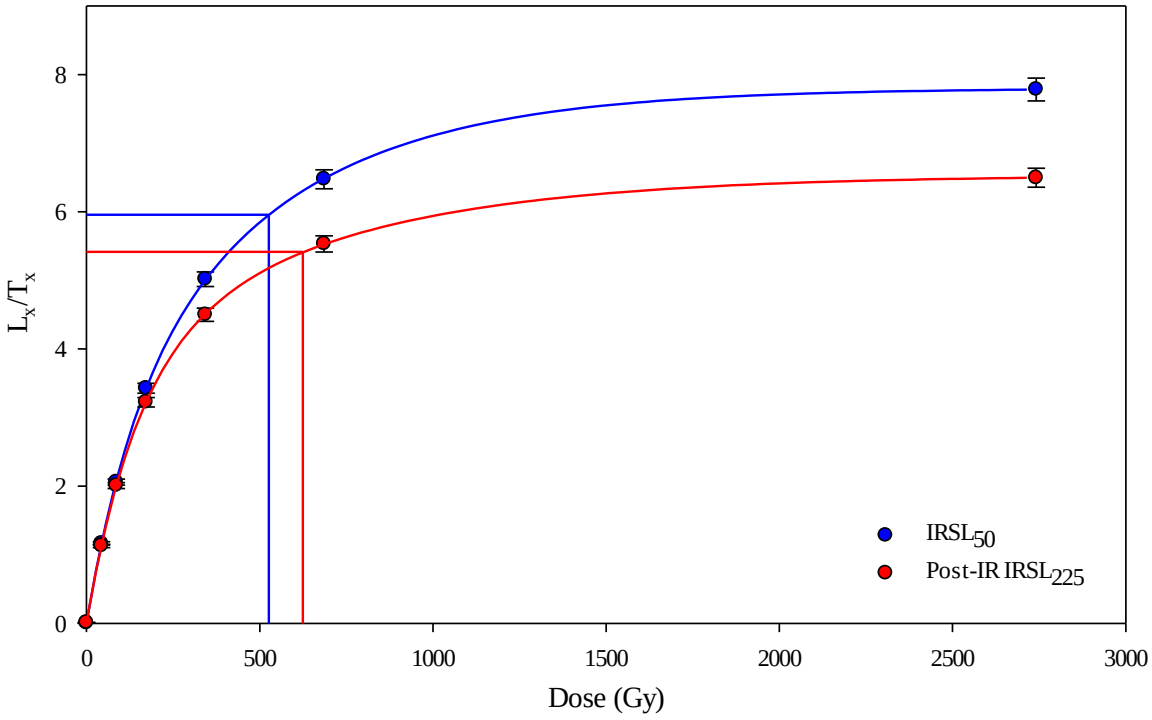

Figure 6.12. $IRSL_{50}$ and post-IR $IRSL_{225}$ dose response curves for NEF04-3-B-5 with a double-saturating exponential fitted. Dose-response curves show the saturated laboratory L_n/T_n values in addition to the saturated natural values.

6.7. Dose Recovery

Dose recovery measurements were undertaken on 4 cobbles, the two in Group IV which give the strongest indication of bleaching at deposition (BEY02-2 and NEF04-2) and one other cobble from each site (NEF04-1 and BRY01-1). In Chapter 5 (Section 5.4) it was observed that bleaching slices in the SOL2 solar simulator prior to dose recovery experiments ensured that the residual dose was reduced to a low level. Therefore, this procedure was used for the samples from north Wales and 24 rock slices (6 from each sample) were placed into the SOL2 solar simulator for 14 days (7 days on each side of the rock slice). Three rock slices were used to measure the residual signal in the rock slices whereas the other three rock slices were given a beta dose of ~ 86 Gy and then their equivalent dose was measured using the sequence in Table 3.1. Dose recovery ratios for all 4 samples are given in Table 6.2. For both NEF04-1 and BRY01-1, the $IRSL_{50}$ and post-IR $IRSL_{225}$ signals can recover a dose within 5 % showing that a post-IR $IRSL_{225}$ protocol is suitable to use for D_e determinations. It is interesting to note that the post-IR $IRSL_{225}$ residual doses are similar to those observed for samples bleached in the SOL-2 solar simulator from Orrisdale Head (3.38 ± 0.11 Gy). NEF04-3 also recovers a dose within ~ 10 %, however for sample BRY02-2, the $IRSL_{50}$ signal dose not recover a dose. It is unclear why this sample does not recover a dose for the $IRSL_{50}$ signal, and this is the first time that rock slice samples bleached in the SOL-2 solar simulator do not recover a dose for the $IRSL_{50}$ signal.

Table 6.2. Dose-recovery data for the 4 samples from north Wales. Here, the residual dose values and recovered dose values are the mean and standard error of three separate rock slices.

	Residual dose (Gy)	Given dose (Gy)	Recovered dose (Gy)	Dose recovery ratio
NEF04-1				
$IRSL_{50}$	1.10 ± 0.04	85.86	89.02 ± 4.07	1.02 ± 0.06
pIR $IRSL_{225}$	2.18 ± 0.06	85.86	85.95 ± 3.46	0.98 ± 0.05
NEF04-3				
$IRSL_{50}$	1.09 ± 0.03	85.86	81.78 ± 1.40	0.94 ± 0.02
pIR $IRSL_{225}$	2.18 ± 0.05	85.86	80.22 ± 7.38	0.91 ± 0.09
BRY01-1				
$IRSL_{50}$	0.71 ± 0.13	85.86	89.73 ± 5.53	1.04 ± 0.06
pIR $IRSL_{225}$	1.44 ± 0.11	85.86	85.44 ± 3.64	0.98 ± 0.04
BRY02-2				
$IRSL_{50}$	1.18 ± 0.08	85.86	73.34 ± 1.23	0.84 ± 0.01
pIR $IRSL_{225}$	3.00 ± 0.17	85.86	80.02 ± 0.86	0.90 ± 0.01

6.8. Luminescence ages from cobbles

The two cobbles in Group IV that showed consistent L_n/T_n values, with depth (see Figure 6.3) had equivalent dose measurements made for those slices that showed signs of bleaching, and age with depth for these cobbles is shown in Figures 6.13 and 6.14 (for the cobbles NEF04-3 and BRY02-2). Figure 6.13 shows age with depth for cobble NEF04-3. The surface slice gives an uncorrected $IRSL_{50}$ age of 23.92 ± 1.71 ka, which agrees with independent age control (21.2 – 23.4 ka), but for the surface slice only. The next slice gives an $IRSL_{50}$ age of 30.65 ± 1.88 ka and suggests that this cobble was not completely bleached with depth (due to the increase in the age for the next slice). The post-IR $IRSL_{225}$ age for the surface slice does not agree with the independent age control (Figure 6.13) and shows a difference in age from the $IRSL_{50}$ signal for the same rock slice.

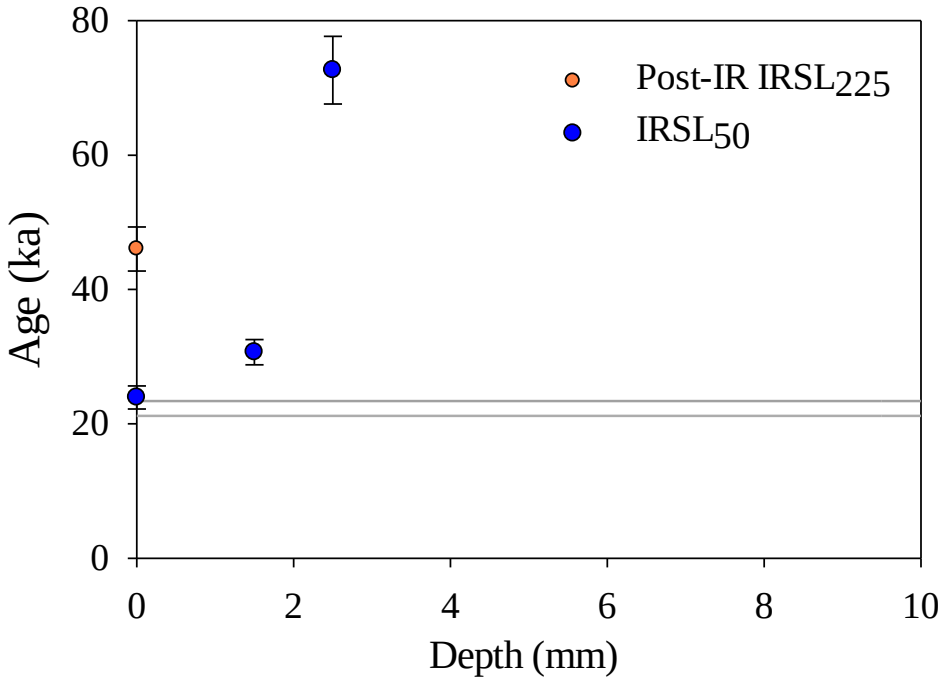

Figure 6.13. Age with depth into cobble NEF04-3 showing that for the cobble with the most extensive sub-surface bleaching only the surface slice gives an uncorrected $IRSL_{50}$ age that agrees with independent age control (21.2 – 23.4 ka).

For the cobble at Bryn-yr-Eryr, that appeared to show sub-surface bleaching (from the L_n/T_n values (BRY02-2) – see Section 6.2), the surface slice gives an uncorrected $IRSL_{50}$ age of 11.27 ± 0.74 ka and a post-IR $IRSL_{225}$ age of 15.5 ± 1.04 ka neither of which agree with the independent control (Figure 6.14). The uncorrected $IRSL_{50}$ age at the next slice for BRY02-2 (at a depth of 1.5 mm) increases rapidly (27.8 ± 1.60 ka) implying that this slice was not well-bleached. It is interesting that the ages for the surface slices are, for both IRSL signals, younger than the independent age control.

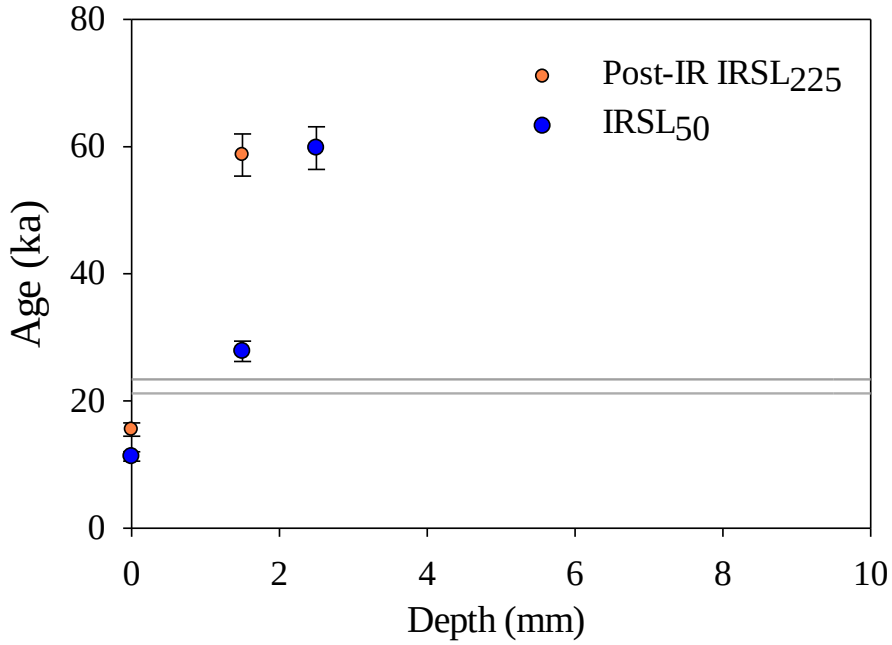

Figure 6.14. Age with depth for cobble BRY02-2, which is a cobble that showed L_n/T_n ratios remaining consistent for the upper two slices. The age-depth profiles indicates, as in Figure 6.13, that age does not remain consistent with depth, and none of the $IRSL_{50}$ or post-IR $IRSL_{225}$ ages agree with the independent age control.

Neither of the cobbles that appeared to have been bleached (Figure 6.3) give ages for the sub-surface that are within uncertainties of the age of the surface slice. For cobble NEF04-3 the surface gives an age consistent with the independent age control, but what if we did not have that control? Is there any other way that we could see if the surface bad been reset sufficiently at deposition to give an accurate age? At these sites there are several surface slices which gave low L_n/T_n values (Figure 6.1) even if it does not appear that the sub-surface is bleached (Figure 6.2). Therefore, the D_e was measured for the surface slices from multiple cobbles to provide ages for the surface only. This approach (only measuring the surface and no sub-surface data) has also been applied by Simms *et al*. (2012) who analysed quartz taken from the surface of granite cobbles from a raised-beach in Antarctica. Figure 6.15 illustrates the distribution of ages for both the $IRSL_{50}$

and post-IR $IRSL_{225}$ signals for the surface slices from cobbles from Nefyn and Bryn-yr-Eryr. This data is also given in Table 6.3.

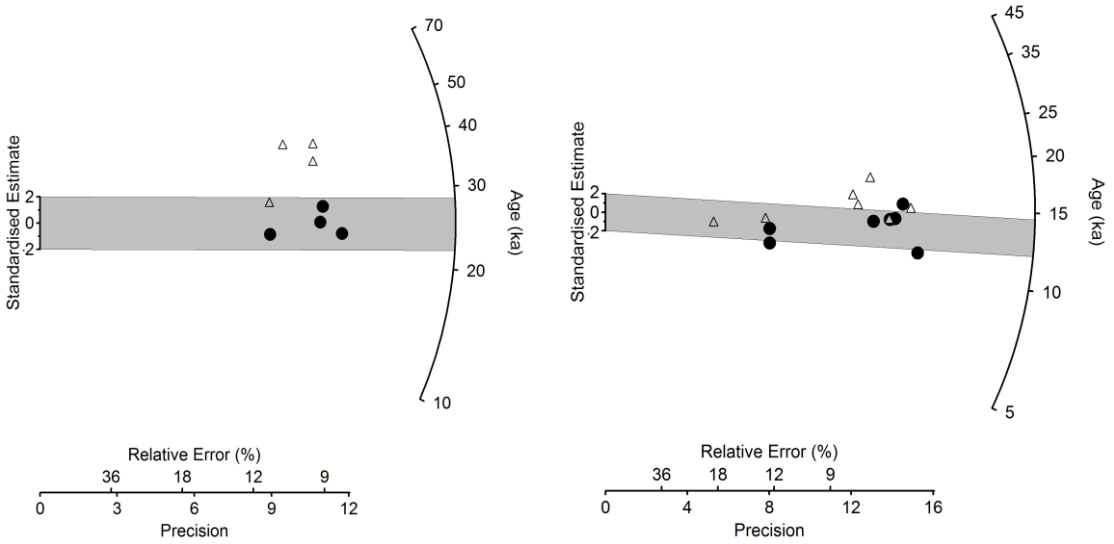

Figure 6.15. Radial plots for the $IRSL_{50}$ (black circles) and post-IR $IRSL_{225}$ (grey triangles) uncorrected ages for surface slices from Nefyn (left) and Bryn-yr-Eryr (right).

The average uncorrected $IRSL_{50}$ age from 4 surface slices from Nefyn give an age of 24.84 ± 2.53 ka which agrees with independent age control (see Figure 6.14 and Table 6.3). Therefore, even though the benefits of sub-surface ages are not obtained from these samples, surface slices can produce an average uncorrected $IRSL_{50}$ age that agrees with independent control. The average uncorrected post-IR $IRSL_{225}$ age (40.29 ± 7.7 ka), even for the surface slices, does not agree with the independent age control.

The average uncorrected $IRSL_{50}$ age from the surface slices from Bryn-yr-Eryr is 13.08 ± 2.08 ka whilst the post-IR $IRSL_{225}$ age is 15.7 ± 2.55 ka. Neither the uncorrected $IRSL_{50}$ nor post-IR $IRSL_{225}$ ages agree with independent age control and are in fact younger than the independent age control. It is unclear why both IRSL ages are younger than the independent age control, with the glaciofluvial sediments at Bryn-yr-Eryr

located upstream from Nefyn and recent luminescence ages by Smedley *et al*. (2017) confirm that ice retreat along this section of the Llyn Peninsula at ~ 21.7 ± 0.8 ka. It is possible that post-depositional reworking may have occurred at the site. Additionally, it is interesting to note that rock slices from Bryn-yr-Eryr appeared to have a smaller grain-sized than that observed at Nefyn. This may result in overestimation of the internal beta dose-rate and therefore underestimate the age.

Table 6.3. Uncorrected $IRSL_{50}$ and post-IR $IRSL_{225}$ ages from the surface slices from cobbles at both Nefyn and Bryn-yr-Eryr.

Sample	$IRSL_{50}$ age	Uncertainty (±)	Post-IR $IRSL_{225}$ age	Uncertainty (±)
NEF03-2-A	28.23	2.57	29.97	3.36
NEF04-1-A	23.32	1.99	39.14	3.69
NEF04-3-A	25.28	2.32	44.49	4.20
NEF04-3-B	22.55	2.52	47.56	5.04
BRY01-1-A	14.28	1.01	14.28	1.03
BRY02-2-A	11.27	0.74	15.50	1.04
BRY02-4-A	13.87	1.06	17.65	1.46
BRY02-6-A	15.99	1.10	16.17	1.31
BRY03-1-A	14.17	1.02	20.07	1.55
BRY03-2-A	12.03	1.50	13.85	1.77
BRY03-2-B	9.95	1.24	12.47	2.36

6.9. Conclusions

L_n/T_n measurements for the surface of the cobbles collected at Nefyn and Bryn-yr-Eryr show a range in values and appear to show a range of bleaching occurring across the population of cobbles (as also occurred at Orrisdale Head). However, only two cobbles show any indication of sub-surface bleaching. The remainder show L_n/T_n remaining consistent with depth, or showing a low L_n/T_n for the surface, followed by the

L_n/T_n values reaching saturation immediately. This has been interpreted to be a result of either a lack of exposure, or the potential for a different lithology not allowing extensive sub-surface bleaching (Ou *et al*., 2018). Due to such a difference in depth profiles, due to lithological variations, resulted in the final application (at Bridgwalton) targeting only granite cobbles and avoiding complex lithologies. A large difference in the L_x/T_x values, for the same dose, is apparent for the different rock slices and shows that the dose response curves grow differently for the different cobbles. To overcome this, it may help to undertake L_n/T_n measurements for each rock slice and an additional regenerative dose, as suggested by Li *et al*. (2015).

Dose recovery measurements show that for one rock slice (BRY02-2) the $IRSL_{50}$ signal cannot recover the given dose, however, comparison to other rock slices ages (Table 6.6) suggest that this impact is small and dose recovery measurements are successful for a another rock slice from Bryn-yr-Eryr (BRY01-1). Measurements were also undertaken on a saturated rock slice to compare the natural saturated signal to the laboratory saturated signal. However, due to the post-IR $IRSL_{225}$ naturally saturated values being lower than the laboratory saturated values it is suggested that this rock slice may have been bleached over geological time.

For one of the cobbles (NEF04-3), even though the cobble shows sub-surface bleaching, NEF04-3 has only 1 rock slice (the surface) with an age (23.92 ± 1.71 ka) that agrees with independent age control (21.2 – 23.4 ka). To overcome this lack of sub-surface bleaching the average age from the surface slices of the cobbles from Nefyn was calculated and gives an $IRSL_{50}$ age (24.84 ± 2.53 ka) that agrees with independent age control (21.2 – 23.4 ka). Such an approach of measuring ages from the surface of the cobbles only has also been applied by Simms *et al*. (2011). However, both the cobble that shows sub-surface bleaching and the average of all surface slices from Bryn-yr-Eryr

give an $IRSL_{50}$ age (13.08 ± 2.07 ka) and post-IR $IRSL_{225}$ age (15.70 ± 2.55 ka) below the expected age. It is unclear why the ages from cobble surfaces do not agree with independent age control from Bryn-yr-Eryr.

A potential reason for ages from cobbles at Bryn-yr-Eryr not agreeing with independent control could be due to the assumption of a 12 % K content. The K content has not been measured directly for these samples, therefore, a difference in K content could result in a discrepancy between given ages and independent control. Although cobbles from the two sites at north Wales do not show as extensive sub-surface bleaching as those cobbles from Orrisdale Head, it is clear that measurements of the surface of multiple cobbles can (in the case of the deposits at Nefyn) provide an age which agrees with the independent age control. Additionally, the general depositional environment differs at Bryn-yr-Eryr in comparison to Nefyn. The sediment deposits at Bryn-yr-Eryr are bounded by higher terrain to the east and this could result in a potential down-hill movement of sediment or reworking since deposition. Although the sediment deposit has been interpreted as an ice-marginal sediment sequence, there is potential for distal deposition during final sedimentation at Bryn-yr-Eryr, potentially resulting in ages younger than the independent age control.

7. Luminescence dating of cobbles from a glaciofluvial deposit with limited independent age control

7.1. Introduction

Following the application of the luminescence dating of cobbles at locations with independent age control, a location at Bridgwalton, Shropshire (see Section 2.6) was selected where there is little independent age control. As previously outlined in Section 2.6 the glacial deposit at Bridgwalton, Shropshire, marks the furthest extent of a separate, independent ice lobe, that occupied the Cheshire-Shropshire basin (at the LGM). Establishing the timing of deposition is vital as this location marks the furthest extent of the only land terminating ice-stream of the BIIS. In addition to this, it is important to understand if the maximum extent of ice streams occurred synchronously, and if not, what impact this had on the dynamics of the BIIS.

7.2. Routine tests to assess if cobbles have been bleached

As was undertaken at both locations used to trial the cobble luminescence dating technique, the surface slice from a separate core from each individual cobble was taken and the L_n/T_n ratio was measured for this rock slice. As undertaken at the sites from north Wales, rock cores were only obtained from the topside of the cobbles because results from Orrisdale Head (Figure 5.1) showed that the topside of the cobbles were better

bleached than the side or bottom of the cobbles. At Bridgwalton, two cobbles (out of a population of 21 cobbles sampled) had low surface L_n/T_n ratios (Figure 7.1).

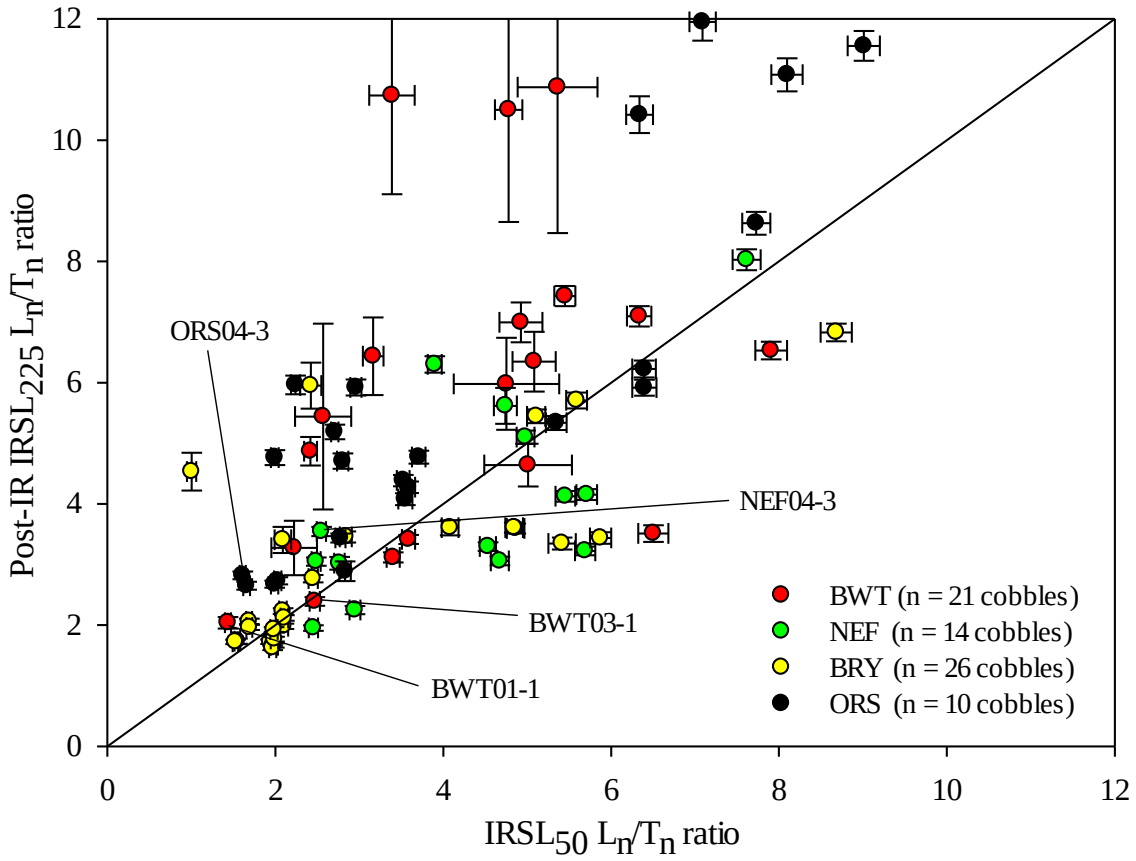

Figure 7.1. L_n/T_n ratios for the $IRSL_{50}$ and post-IR $IRSL_{225}$ signals for samples from Bridgwalton (red) in comparison to the L_n/T_n ratios for cobbles from Nefyn (green), Bryn-yr-Eryr (yellow) and Orrisdale Head (black). This figure shows that cobbles from Bridgwalton show a range of L_n/T_n ratios, similar to the other locations, and indicates that a possible range in bleaching occurred across the population of cobbles. Cobbles that showed signs of sub-surface bleaching at the other locations (ORS04-3, NEF04-3) are also indicated.

For the two cobbles (BWT01-1 and BWT03-1) that gave low L_n/T_n ratios (Figure 7.1), the cores were sliced entirely, with depth, to observe the patterns of L_n/T_n. This was undertaken routinely in the two previous trial locations (e.g. Section 6.3) and has shown cobbles with well-bleached sub-surfaces. However, it has also shown cobbles with low

L_n/T_n ratios at the surface, but increase immediately into the next slice (e.g. Figures 6.2 and 6.3 in Chapter 6). It is clear that this analysis of the sub-surface information indicates which rock slices to undertaken equivalent dose measurements upon.

L_n/T_n with depth for one of the cobbles with a low surface slice L_n/T_n ratio is illustrated in Figure 7.2. The L_n/T_n values for BWT01-1 show initial low $IRSL_{50}$ values, which increase slice-by-slice until a depth of ~ 4 mm is reached. The L_n/T_n values do not remain consistently low, and indicate limited sub-surface bleaching. The post-IR $IRSL_{225}$ signal gradually increases from the surface to ~ 3 mm deep where it remains consistently low. A consistently low L_n/T_n ratio is usually indicative of bleaching occurring, however the easier to bleach $IRSL_{50}$ signal shows that this is not the case for BWT01-1. The L_n/T_n with depth profile appears similar to those observed at north Wales (Figure 6.2d, e, f) which also indicated a lack of sub-surface bleaching.

L_n/T_n ratios, with depth, for the second cobble with a low surface L_n/T_n ratio (BWT03-1) are illustrated in Figure 7.3. The $IRSL_{50}$ L_n/T_n ratios remain consistently low to a depth of ~ 6 mm. In addition to this, the post-IR $IRSL_{225}$ signal also remains low, until a depth of ~ 4 mm, where the values gradually increase. The pattern of L_n/T_n with depth for BWT03-1 is similar to measurements at Orrisdale Head (Figure 5.2), that shows L_n/T_n values consistently low with depth, which then provide reliable depositional ages for the location. However, only a single core was obtained from BWT03-1 as the cobble broke during the drilling process. It is clear from this population of cobbles that some cobbles show limited sub-surface bleaching (as was similar at north Wales) whilst one cobble shows extensive sub-surface bleaching (as was similar at Orrisdale Head). Equivalent dose measurements were undertaken on those rock slices that were bleached with depth (7 rock slices from BWT03-1).

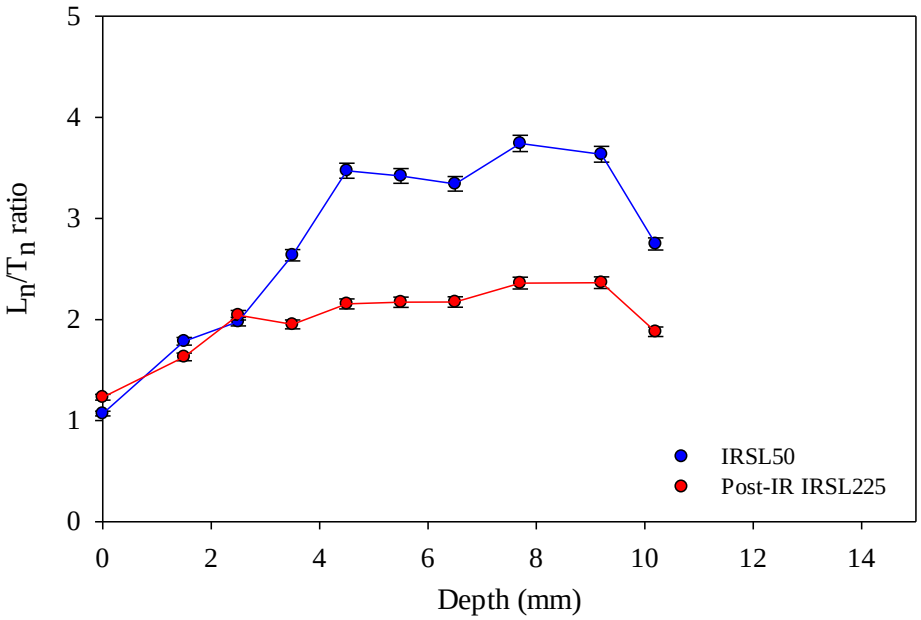

Figure 7.2. Example of L_n/T_n with depth, into cobble BWT01-1, a cobble that gave a low surface L_n/T_n value and assumed to be well-bleached. The sub-surface L_n/T_n values show an increasing $IRSL_{50}$ value in the few upper millimetres.

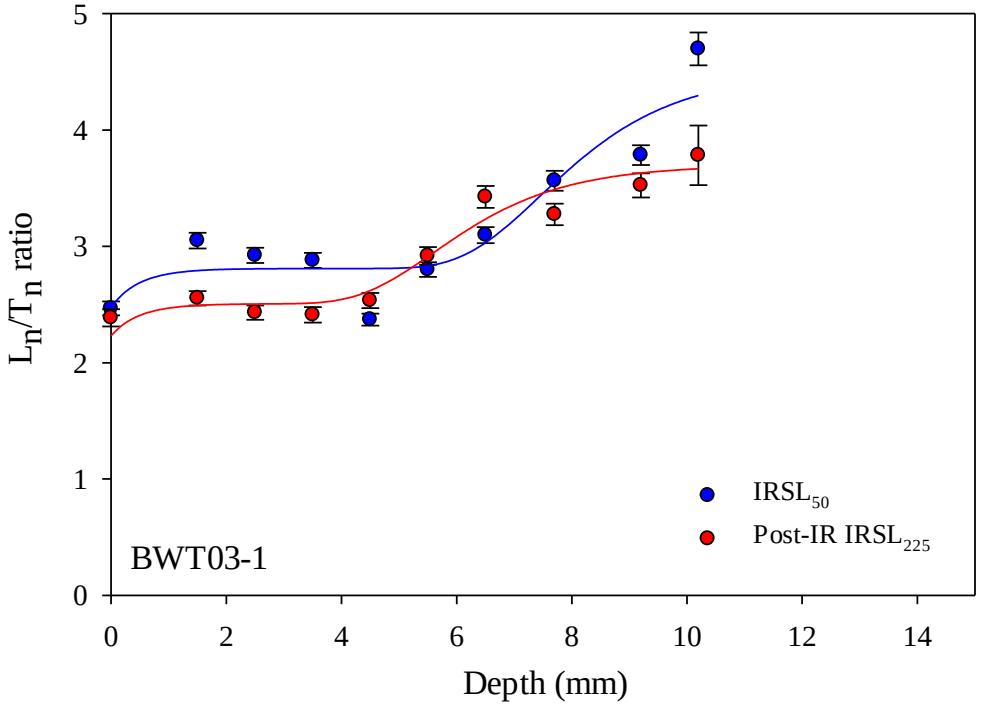

Figure 7.3. L_n/T_n with depth for the $IRSL_{50}$ and post-IR $IRSL_{225}$ signals for cobble BWT03-1, with only a single core taken from this cobble.

7.3. Rock slice characteristics

Analysis of rock slices from cobbles from north Wales showed that different patterns of L_n/T_n ratios with depth into the cobble sub-surfaces were associated with different characteristics (texture, grain size, and colour) for each individual cobble. A change in the L_n/T_n characteristics, with depth, for different cobbles was also observed at north Wales and was interpreted to be due to the potential variability in the lithologies analysed. Images were taken for one rock slice from the two cobbles at Bridgwalton (Figure 7.4). BWT03-1-A-2 is relatively coarse grained crystalline lithology with some translucent minerals present (Figure 7.4). As shown above, this lithology shows the most extensive sub-surface bleaching (Figure 7.3). BWT01-1-A-2 appears to have a relatively smaller grain size and a crystalline texture cannot be discerned from the image. The cobble from which this rock slice was obtained (BWT01-1) shows limited sub-surface bleaching (Figure 7.2).

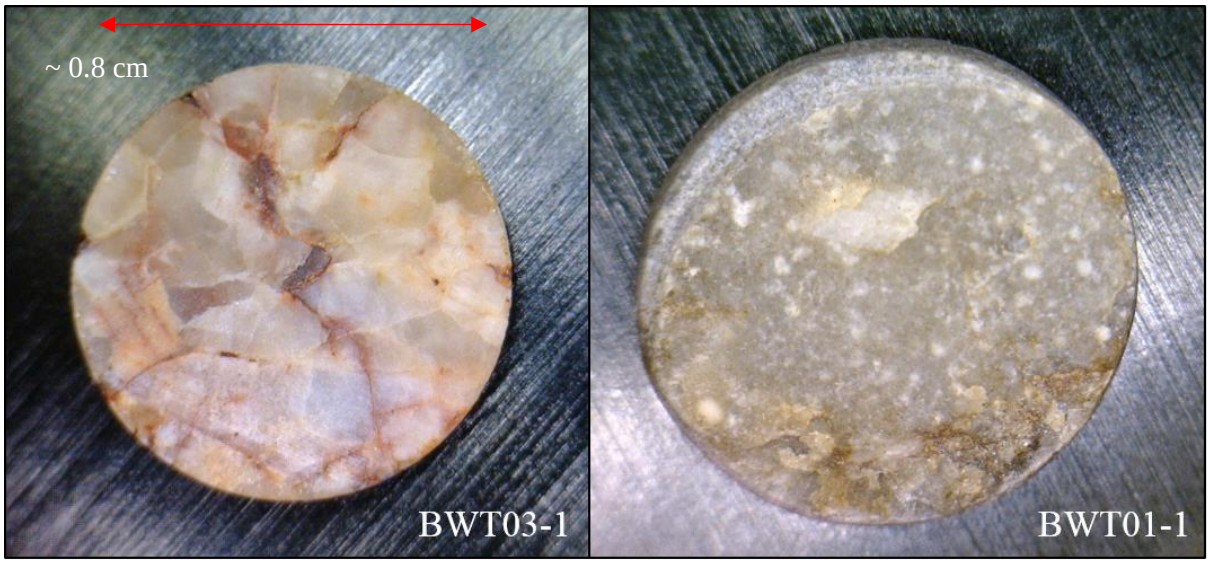

Figure 7.4. Digital microscope images of rock slices BWT03-1-A-2 and BWT01-1-A-2. Both are rock slices which gave low L_n/T_n ratios for the surface of the cobbles, however, BWT03-1 shows the most extensive sub-surface bleaching.

7.4. Dose-rate with depth into the cobble sub-surface

For the well-bleached cobble (BWT03-1) the dose rate, with depth into its subsurface, is illustrated in Figure 7.5. The dose rates are established and modelled as previously outlined in Section 3.2.1. A grain size of 590 ± 250 mm was measured for this rock slice and was used for the internal dose-rate calculations. Figure 7.5 illustrates that, similar to the dose-rate configuration at Orrisdale Head, Isle of Man, (see Figure 3.5 in Section 3.2.8) the dose rate to the rock slices becomes almost entirely (but not wholly) independent from the external dose rate of the surrounding sediment matrix. At depths ≥ 2 mm below the surface 93 % of the dose rate comes from the cobbles at Orrisdale, whilst at Bridgwalton the value is 89 %. This dose-rate configuration observed for cobble BWT03-1 shows that the previously observed advantage of avoiding external dose rates (and therefore water contents) is replicated at Bridgwalton. Although cobble sub-surface bleaching was not observed at north Wales it is interesting to see if the proportion of the dose rate from the cobbles is consistent between the different individual cobbles. Table 7.1 illustrates the variability in the dose rates for each cobble that was used for dating in this thesis (from all locations) and the percentage of the dose rate that comes from the cobble itself, at a depth of 2 mm. This illustrates that even the cobble with the highest dependence on external, matrix dose rate, ~ 68 % of the dose originates from the cobble and is therefore independent of water content uncertainties. The cobble from Bridgwalton has 89 % of its dose from the cobble and is therefore independent of the external dose rates. This corresponds to a higher internal beta dose rate (due to the larger grain size of the cobble).

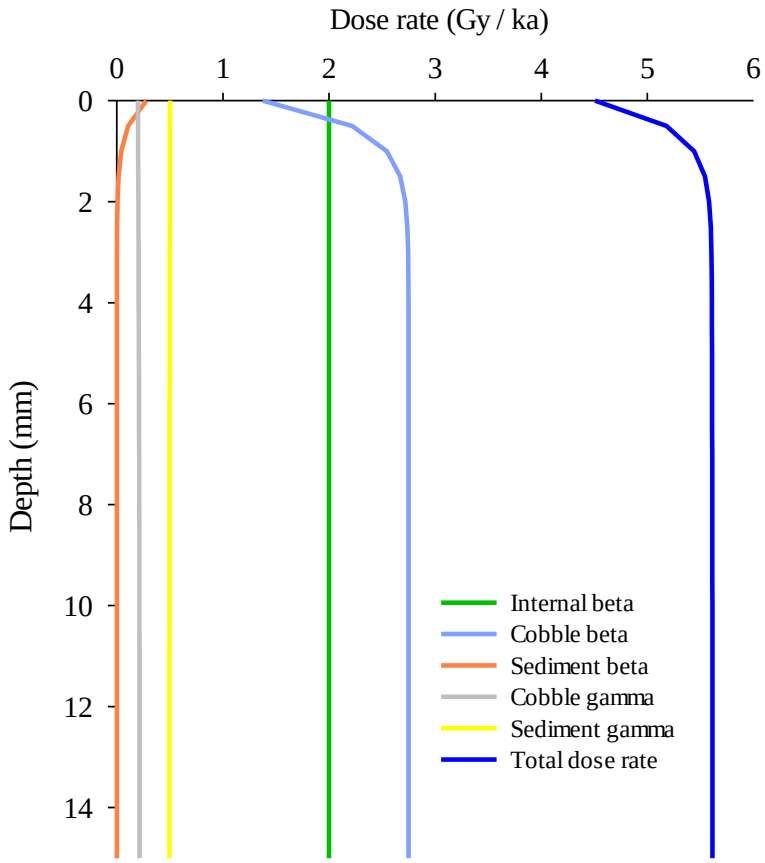

Figure 7.5. Dose rate data, with depth, for BWT03-1 showing that at a depth of 2 mm into the cobble sub-surface 89 % of the dose rate to rock slices comes from the cobble itself, making the dose rate, and age, insensitive to the surrounding sediment matrix.

Table 7.1. Dose rates for the sediment matrix and cobbles for all samples used to establish an age in this thesis. In addition to this, the final column illustrates the percentage of the dose rate which originates from the cobble itself, and not the surrounding sediment matrix (and therefore independent of water content).

Cobble	***Beta Matrix (Gy/ka)***	***Gamma matrix (Gy/ka)***	***Beta cobble (Gy/ka)***	***Gamma cobble (Gy/ka)***	***Internal beta (cobble) (Gy/ka)***	***% of dose rate from cobble at 2 mm deep***
ORS02-1	0.861 ± 0.079	0.621 ± 0.045	3.292 ± 0.243	3.029 ± 0.200	2.250 ± 0.702	93 %
ORS04-1	0.782 ± 0.072	0.549 ± 0.040	3.586 ± 0.265	2.406 ± 0.131	2.250 ± 0.702	92 %
ORS04-3	0.782 ± 0.072	0.549 ± 0.040	3.854 ± 0.285	2.643 ± 0.131	2.250 ± 0.702	93 %
NEF04-1	1.348 ± 0.093	0.820 ± 0.041	3.179 ± 0.143	1.708 ± 0.077	1.399 ± 0.367	68 %
NEF04-3	1.348 ± 0.093	0.820 ± 0.041	2.270 ± 0.103	1.598 ± 0.101	1.399 ± 0.367	69 %
NEF03-2	1.312 ± 0.092	0.892 ± 0.062	2.335 ± 0.103	2.042 ± 0.151	1.399 ± 0.367	71 %
BRY03-2	1.300 ± 0.089	1.144 ± 0.057	3.160 ± 0.234	2.002 ± 0.860	1.189 ± 0.328	86 %
BRY02-2	1.300 ± 0.089	1.144 ± 0.057	3.803 ± 0.161	2.187 ± 0.111	1.189 ± 0.328	88 %
BRY02-4	1.300 ± 0.089	1.144 ± 0.057	2.773 ± 0.118	1.498 ± 0.061	1.189 ± 0.328	86 %
BRY03-1	1.300 ± 0.089	1.144 ± 0.057	3.666 ± 0.155	1.965 ± 0.143	1.189 ± 0.328	84 %
BRY01-1	1.776 ± 0.119	1.052 ± 0.062	3.261 ± 0.138	1.718 ± 0.079	1.189 ± 0.328	82 %
BRY02-6	1.300 ± 0.089	1.144 ± 0.057	3.678 ± 0.156	2.045 ± 0.077	1.189 ± 0.328	82 %
BWT03-1	0.554 ± 0.056	0.576 ± 0.038	2.749 ± 0.240	1.537 ± 0.069	2.000 ± 0.849	89 %

7.5. Fading measurements

As significant sub-surface bleaching was observed for one cobble at Bridgwalton (BWT03-1) the rock slices from that cobble were measured to assess the potential impact of anomalous fading. As at Orrisdale Head and north Wales two approaches are undertaken to try to assess the stability of the $IRSL_{50}$ and post-IR $IRSL_{225}$ signals. Firstly, storage experiments are undertaken to measure the g-value and then a comparison is undertaken of the signal that is in field saturation with the saturation level measured in the laboratory (Buylaert *et al*., 2012). Measurements were undertaken on 5 rock slices, all taken from the same cobble which showed sub-surface bleaching (BWT03-1). Rock slices were irradiated (42.9 Gy) and preheated prior to storage for periods up to 1 month, following the method of Auclair *et al*. (2003). An example of fading measurements performed for a rock slice from Bridgwalton are show in Figure 7.6. The average g-values were 1.41 ± 0.63 % per decade (n = 5) for the $IRSL_{50}$ signal, and 0.67 ± 0.62 % per decade for the post-IR $IRSL_{225}$ signal (n = 5) (Figure 7.7). Given the similarity of the fading rate measured for the $IRSL_{50}$ signal and the apparent quartz OSL fading rates of Thiel *et al*., (2011) (1.3 ± 0.3% per decade), no correction is made for the Bridgwalton ages for fading of either the $IRSL_{50}$ or the post-IR $IRSL_{225}$ signal.

In addition to anomalous fading measurements, a SAR protocol was undertaken on a single rock slice to measure the $IRSL_{50}$ and post-IR $IRSL_{225}$ laboratory saturation levels (Figure 7.8) (rock slice BWT03-1-A-9). The $IRSL_{50}$ natural saturated signal is 66 % of the laboratory saturated signal and 83 % for the post-IR $IRSL_{225}$ signal (Figure 7.8). It is interesting to note that the post-IR $IRSL_{225}$ signal is not in complete saturation (as would be expected for this stable IRSL signal). It is interpreted that the rock slice used for saturation measurements was not completely saturated, and had experienced some

bleaching in the geological past. However, as this rock slice was one of the lowest from the entire core, there were no further opportunities to assess saturated values.

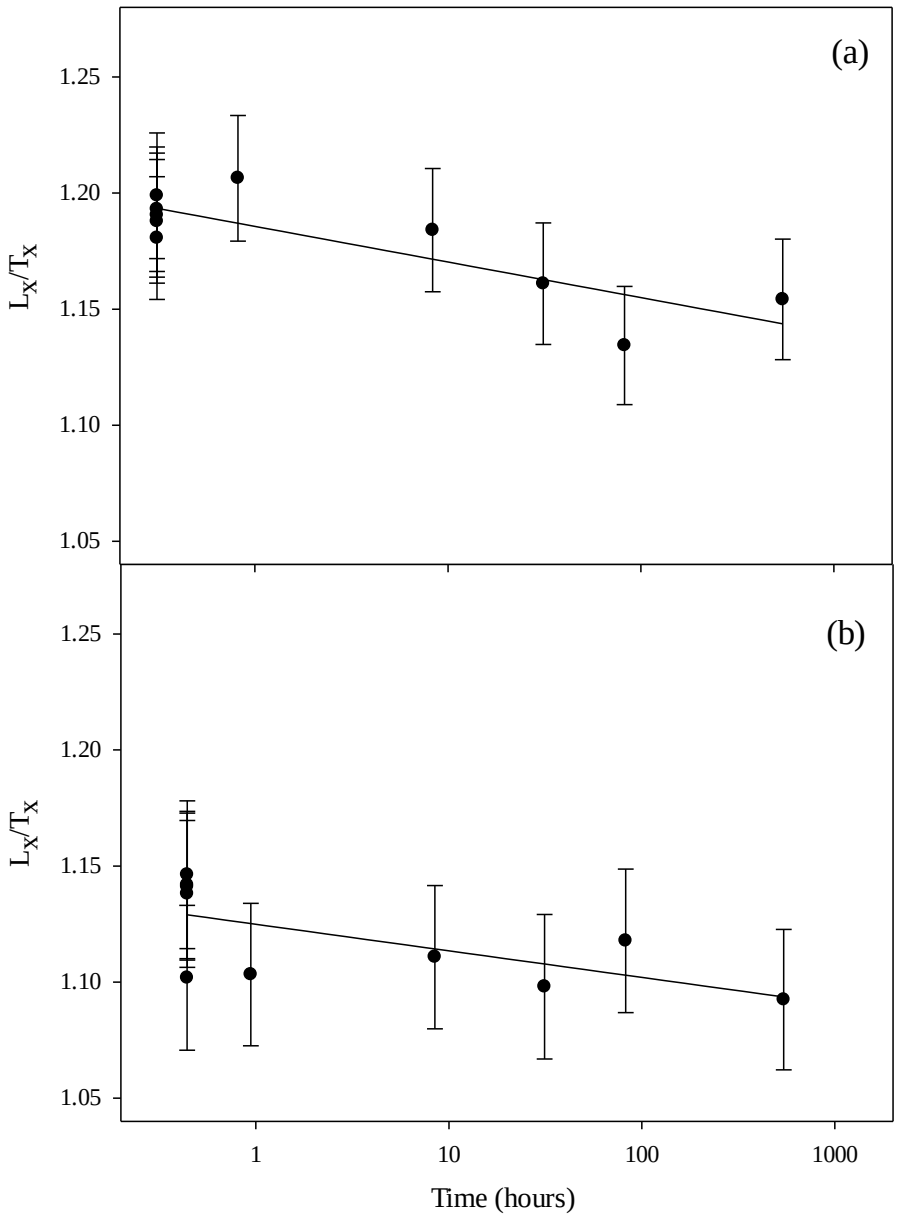

Figure 7.6. Example of the changes in L_x/T_x over time for rock slice BWT03-1-A-4 for the $IRSL_{50}$ (a) and post-IR $IRSL_{225}$ (b) signals.

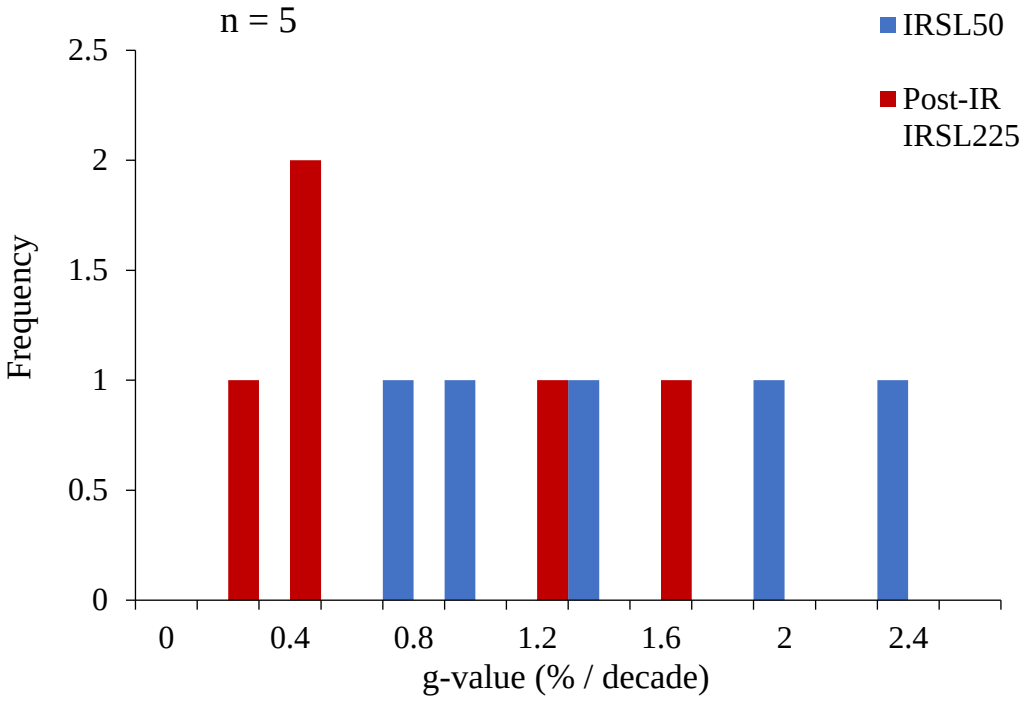

Figure 7.7. g-values for the $IRSL_{50}$ and post-IR $IRSL_{225}$ signals for the 5 rock slices measured showing a lower average g-value for the post-IR $IRSL_{225}$ signal than the $IRSL_{50}$ signal.

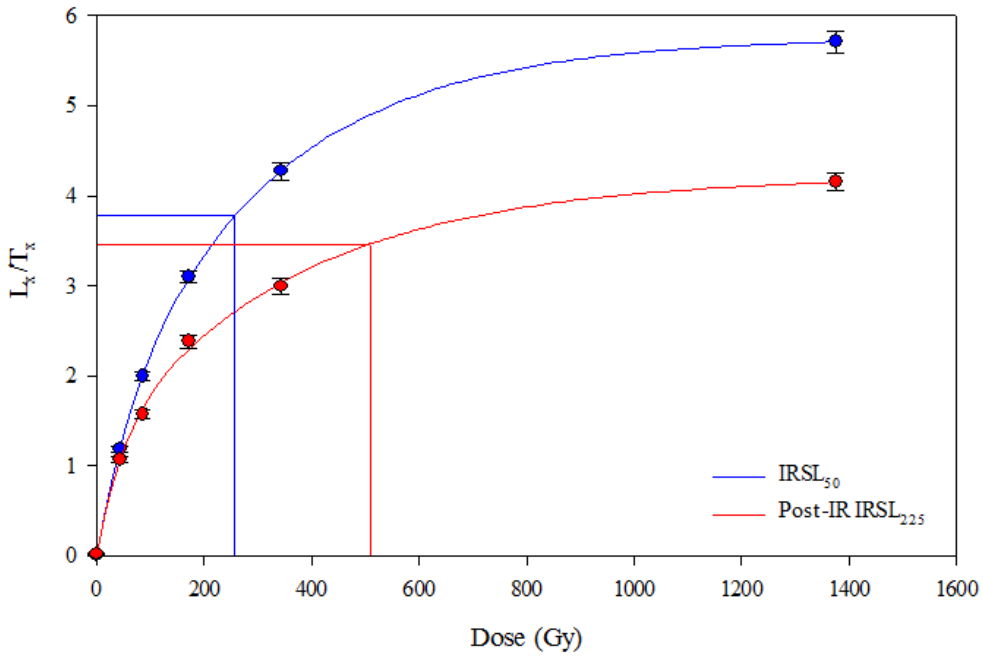

Figure 7.8. Dose response curves for the $IRSL_{50}$ and post-IR $IRSL_{225}$ signals for rock slice BWT03-1-A-9.

7.6. Dose recovery measurements

Dose-recovery measurements were performed on rock slices to ensure that the SAR protocol is suitable for rock slices from Bridgwalton. Any residual signal within the rock slices was reset using a SOL-2 solar simulator for 7 days. This was undertaken at Orrisdale Head (Table 5.3), and as this successfully reset the residual signal the process of using the SOL-2 solar simulator was undertaken for all locations. The 6 rock slices used for dose recovery measurements (3 used for residual measurements and 3 given a known dose of 85.6 Gy) were taken from the same cobble as those rock slices that were used to determine an age (BWT03-1). Measurements show that the $IRSL_{50}$ signal gives a residual-subtracted ratio of 0.90 ± 0.02 and post-IR $IRSL_{225}$ residual-subtracted dose-recovery ratio of 0.97 ± 0.03 (Table 7.2). These ratios show that both signals recover a dose within 10 % and that the SAR protocol is suitable.

Table 7.2. Dose recovery ratios for the six rock slices from Bridgwalton showing that both IRSL signals can recover a dose within 10 %.

	Residual dose (Gy)	Given dose (Gy)	Recovered dose (Gy)	Dose recovery ratio
$IRSL_{50}$	0.17 ± 0.03	85.86	77.17 ± 4.07	0.90 ± 0.02
Post-IR $IRSL_{225}$	0.99 ± 0.09	85.86	83.27 ± 2.52	0.97 ± 0.03

7.7. Age for the furthest extent of the ice stream in the Cheshire-Shropshire basin

Age-depth profiles were determined for BWT03-1 using both the $IRSL_{50}$ and post-IR $IRSL_{225}$ signal from the rock slices (Figure 7.9). In previous applications each age data point is the average of 2 or 3 rock slices, however, at Bridgwalton, the well-bleached cobble broke during the drilling process and only one rock core could be used to determine an age. L_n/T_n with depth measurements (Figure 7.3) confirm that sample

BWT03-1 was well-bleached, with depth, with low $IRSL_{50}$ and post-IR $IRSL_{225}$ L_n/T_n ratios at the surface gradually increasing at a depth of ~ 6 mm.

$IRSL_{50}$ ages are consistent to a depth of ~ 7 mm which confirms that the cobble had been well-bleached at deposition (Figure 7.9). The average age of the upper 7 rock slices from BWT03-1 for the $IRSL_{50}$ signal is 25.3 ± 1.6 ka. The post-IR $IRSL_{225}$ age for the upper 4 rock slices (29.3 ± 2.4 ka) is greater than the $IRSL_{50}$ age and this has also been observed at Orrisdale Head. It is unclear, why there is a difference between the two signals, however, the $IRSL_{50}$ ages are thought to be more reliable based on the agreement of $IRSL_{50}$ ages from cobbles and independent age control at Orrisdale Head, Isle of Man. In addition to this, bleaching experiments confirm that the $IRSL_{50}$ signal bleaches more quickly, with depth, than the post-IR $IRSL_{225}$ signal.

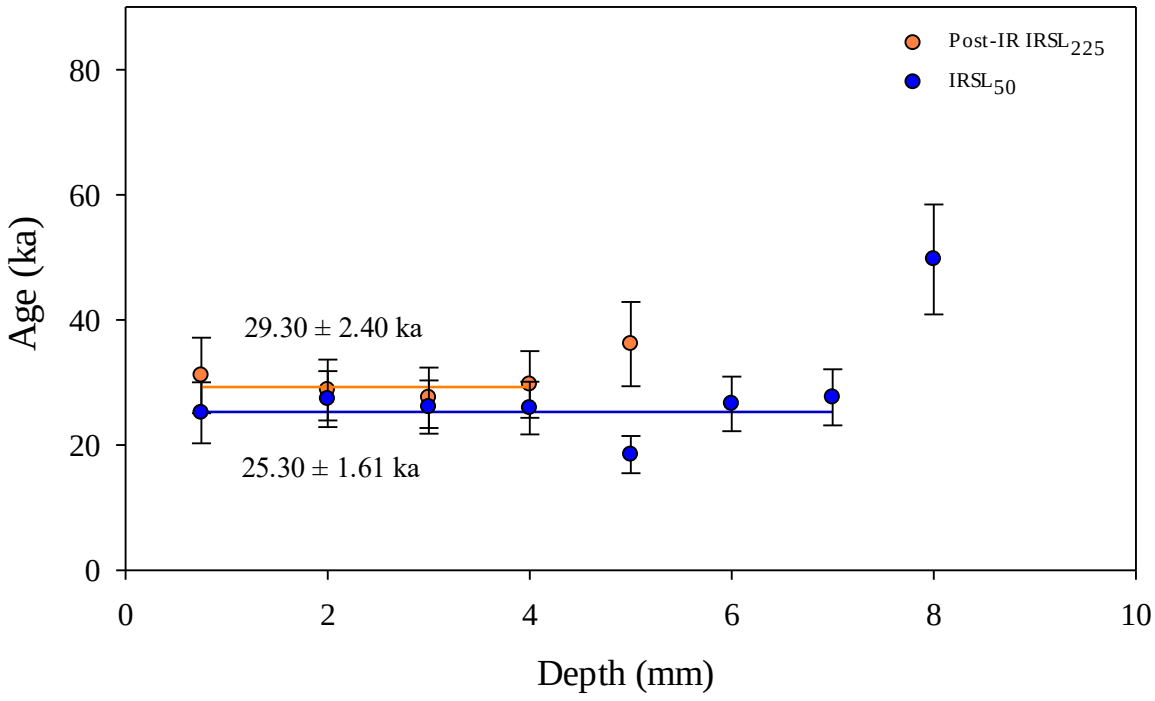

Figure 7.9. Age with depth into cobble BWT03-1 showing consistent $IRSL_{50}$ ages across the upper ~ 7 mm of the cobble surface, indicating that the cobble was well-bleached at deposition.

7.9. Conclusions

L_n/T_n measurements from the surface of 21 different cobbles shows a range of L_n/T_n measurements and indicated that a difference in bleaching occurred across the population of cobbles. One of the cobbles (BWT03-1) shows extensive sub-surface bleaching, similar to that which was observed at Orrisdale Head, Isle of Man, and was not present for north Wales cobbles. Dose-rate configurations are similar to that at Orrisdale Head, and shows that the advantage of cobble luminescence dating (the dose rate coming primarily from the cobble) is also seen at this location. Uncorrected $IRSL_{50}$ ages (25.3 ± 1.6 ka (n = 7 slices)) provide the first depositional ages for the furthest extent of the ice lobe that occupied the Cheshire-Shropshire Basin. These ages indicate that the furthest extent of the ice lobe was synchronous with the furthest extent of the Irish Sea Ice Stream at the Scilly Isles (Smedley *et al*., 2017a).

8. Summary & Conclusions

This thesis is the first application of cobble luminescence dating to heterogeneously bleached glacial sediments. Additionally, this thesis is the first to analyse a large population of cobbles (as opposed to individual cobbles) with more cobbles analysed (~ 90) than all the other past research publications combined (< 30). The analysis of a larger population allows the observation of the distribution of bleaching across the population of cobbles and selection of those cobbles that showed signs of being bleached. A number of innovations and refinements to the dating of cobbles have been made in this thesis which include rock slices cut thinner to provide more measurements of D_e with depth. A modified SAR protocol is developed to ensure that the thicker rock slices heat sufficiently. Rock slices with smaller diameters are produced to allow placement into planchettes as opposed to placing the rock slices directly into the disc holes. Finally, sub-surface L_n/T_n measurements are used to confirm that generally heterogeneously bleached sediments are in fact well-bleached with depth.

Bleaching experiments of individual rock slices show that the thicker rock slices and unseparated feldspar minerals within the rock slices bleach in a similar fashion to those observed in the literature (Chapter 4) for sand-sized material. In addition to this, the bleaching model of Sohbati *et al*. (2012c) fits well to the values of L_n/T_n with depth obtained by bleaching a saturated cobble for increasing time periods (Chapter 4).

The initial trial at Orrisdale Head, Isle of Man (Chapter 5), shows that cobbles can provide accurate depositional ages (consistent with independent age control). In addition to this, the cobble sub-surfaces provide evidence that the cobbles were completely bleached at deposition and this is a significant advantage over sand-sized luminescence dating. An additional benefit at Orrisdale Head is that, after 2 mm deep into the cobble, the dose rate is almost entirely (~ 92 %) independent of water content (see Chapter 5). A third benefit is that, at Orrisdale Head, a cobble appears to record both the advance (26.2 ± 0.8 ka) and retreat (20.7 ± 1.3 ka) of the Irish Sea ice stream and is shown by two distinct age populations, with depth.

Forty five rock slices gave tightly clustered ages and gave a recessional age of 20.7 ± 1.3 ka for Orrisdale Head. The age of 20.7 ± 1.3 ka derived from the average of the $IRSL_{50}$ ages from the 3 cobbles is almost identical to the revised retreat age (20.3 ± 0.6 ka; Smedley *et al*. 2017b) for the margin of the Irish Sea Ice Stream as it crossed the Isle of Anglesey ~70 km to the south. This implies that, once retreat of the ice stream passed the pinning point formed by the Isle of Anglesey, retreat occurred very rapidly. This study is also the first to outline the specific lithofacies (bar-top lithofacies) targeted to maximise the chances that the cobbles were bleached in the glacial sediments. This targeting was highly effective and the top an individual cobble from Orrisdale Head was bleached better than its bottom-side.

When testing this novel technique at additional locations in north Wales (Chapter 6), patterns of L_n/T_n do not show significant sub-surface bleaching, even though initial measurements from the surface of the cobbles showed that they were likely to have been bleached. A lack of sub-surface bleaching was attributed to the variable and complex lithology at north Wales, with a complex source area up-stream of the ice. However, due to the precise ages obtained at Orrisdale Head, and the fact that some surface slices from

cobbles from north Wales give accurate ages, cobble luminescence dating was then undertaken at a location with no independent age control (Chapter 7).

In Chapter 7 data were obtained from a single cobble from the site at Bridgwalton, but the pattern of bleaching is more like that seen at Orrisdale Head than north Wales. Bridgwalton marks the furthest extent of the ice stream which occupied the Cheshire-Shropshire basin and is the only land-terminating ice stream of the entire British Irish Ice Sheet. The ages produced from a cobble from Bridgwalton (25.3 ± 1.6 ka) show that the furthest extent of the ice stream at this location is synchronous with the furthest extent of the Irish Sea Ice Stream at the Scilly Isles (Smedley *et al*., 2017a). The cobble from Bridgwalton also showed that the advantage of ages being almost entirely independent of water content is replicated.

8.1. Areas for future work

Following the measurements and objectives addressed in this thesis, it is clear that this novel dating method has potential areas for future research and some questions remain unanswered. One question is why there is an apparent difference between the $IRSL_{50}$ and post-IR $IRSL_{225}$ L_n/T_n values and ages for rock slices that appear to be well-bleached (e.g. Figure 5.7). One cobble at Orrisdale Head was well-bleached with depth, with 4 post-IR $IRSL_{225}$ ages remaining consistent with depth (Figure 5.7). However, the post-IR $IRSL_{225}$ ages were consistently higher than the $IRSL_{50}$ ages. This has also been observed in other studies (when using the post-IR $IRSL_{290}$ protocol (Freiesleben *et al*., 2015) and the post-IR $IRSL_{225}$ protocol (Sohbati *et al*., 2015)). Recent measurements by Thomsen *et al*. (2018) suggest that this might be a result of the $IRSL_{50}$ signal and post-

IR $IRSL_{225}$ signals originating from feldspar grains with a different internal chemical composition to each other.

Another potential area for future research, which could reduce uncertainties in the luminescence ages, is the more precise quantification of grain-sizes within rock slices. This is because uncertainties in grain-sizes impact upon the uncertainty in the internal beta dose of the individual grains themselves.

It has been shown in this thesis that cobbles from a relatively poorly-bleached glacial environment can give precise luminescence ages and that the cobble sub-surfaces show whether the sample was well-bleached. It may be interesting in future studies to consider the bleaching regimes of cobbles from even more poorly-bleached environments (moraines, glaciomarine and even potentially esker style sediments) and the potential to date glacial moraines could be incredibly exciting when attempting to define glacier extents. It may also be interesting to see how other styles of luminescence signal resetting (pressure) may reset the signal, with depth, into cobble sub-surfaces.

8.2. Summary

- Cobbles were collected from glaciofluvial sediments, with specific lithofacies targeted (those interpreted to have been exposed for longer periods before burial)
- Rock cores are taken from cobbles and sliced in the laboratory to provide luminescence-depth measurements
- Feldspar minerals from granite cobbles were analysed due to high sensitivity and reproducible measurements
- A single rock slice from each individual cobble from a location is measured to see how bleaching changes across the population of cobbles

- Those with low L_n/T_n ratios are used for sub-surface measurements
- Sub-surface measurements show which slices to use for age calculations and show if cobbles were completely bleached at deposition
- Dose-rates were determined for each cobble used for age calculations
- Ages from each rock slice that were completed bleached at deposition are averaged to provide a depositional age for the location sampled
- Fading and dose-recovery measurements are undertaken to assess stability and reproducibility of the luminescence signal from rock slices
- Application to a location with a very well developed independent age control shows that this cobble luminescence dating technique is a highly precise and accurate method for dating glacial sediments

9. Reference List

Aitken, M. J. (1985) *Thermoluminescence Dating*. London: Academic Press

Armitage, S. J. and Bailey, R. M. (2005) 'The measured dependency of laboratory beta dose rates on sample grain size.' *Radiation Measurements*, **39**, 123 – 127.

Auclair, M., Lamothe, M. and Huot, S. (2003) 'Measurement of anomalous fading for feldspar IRSL using SAR.' *Radiation Measurements*, **37** (4), 487 – 492.

Ballantyne, C. K., McCarroll, D. and Stone, J. O. (2006) 'Vertical dimensions and age of the Wicklow Mountains ice dome, Eastern Ireland, and implications for the extent of the last Irish Ice Sheet.' *Quaternary Science Reviews*, **25**, 2048 – 2058.

Bateman, M. D., Swift, D. A., Piotrowski, J. A. and Sanderson, D. C. (2012) 'Investigating the effects of glacial shearing of sediment on luminescence.' *Quaternary Geochronology*, **10**, 230 – 236.

Bateman, M. D., Swift, D. A., Piotrowski, J. A., Rhodes, E. J. and Damsgaard, A. (2018) 'Can glacial shearing of sediment reset the signal used for luminescence dating?' *Geomorphology*, **306**, 90 – 101.

Bøtter-Jensen, L. and Mejdahl, V. (1988) 'Assessment of beta dose-rate using a GM multicounter system.' *Nuclear Tracks and Radiation Measurements*, **14**, 187 – 191.

Bøtter-Jensen, L., Andersen, C. E., Duller, G. A. T. and Murray, A. S. (2003) 'Developments in radiation, stimulation and observation facilities in luminescence measurements.' *Radiation Measurements*, **37**, 535 – 541.

Bowen, D. Q., Phillips, F. M., McCabe, A. M., Knutz, P. C. and Sykes, G. A. (2002) 'New data for the last glacial maximum in Great Britain and Ireland.' *Quaternary Science Reviews*, **21**, 89 – 101.

Bowen, D. Q., Rose, J., McCabe, A. M. and Sutherland, D. G. (1986) ‘Correlation of quaternary glaciations in England, Ireland, Scotland and Wales.’ *Quaternary Science Reviews,* **5**, 299 - 340.

Buylaert, J. P. and Jain, M., Murray, A. S., Thomsen, K. J., Thiel, C. and Sohbati, R. (2012) ‘A robust feldspar luminescence dating method for Middle and Late Pleistocene sediments.’ *Boreas,* **41**, 435 – 451.

Buylaert, J. P., Murray, A. S., Thomsen, K. J. and Jain, M. (2009) ‘Testing the potential of an elevated temperature IRSL signal from K-feldspar.’ *Radiation Measurements,* **44**, 560 – 565.

Chapot, M. S., Sohbati, R., Murray, A. S., Pederson, J. L. and Rittenour, T. M. (2012) ‘Constraining the age of rock art by dating a rockfall event using sediment and rock-surface luminescence dating techniques.’ *Quaternary Geochronology*, **13**, 18 – 25.

Chiverrell, R. C. and Thomas, G. S. P. (2010) ‘Extent and timing of the Last Glacial Maximum (LGM) in Britain and Ireland: a review.’ *Journal of Quaternary Science,* **25**, 535 – 549.

Chiverrell, R. C., Thrasher, I. M., Thomas, G. S. P., Lang, A., Scourse, J. D., van Landeghem, K. J. J., McCarroll, D., Clark, C. D., O’Cofaigh, C., Evans, D. J. A. and Ballantyne, C. K. (2013) ‘Bayesian modelling the retreat of the Irish Sea Ice Stream.’ *Journal of Quaternary Science*, **28**, 200 – 209.

Chiverrell, R. C., Thomas, G. S. P., Smedley, R. K., Bateman, M. D., Burke, M. J., Clark, C. D., Duller, G. A. T., Jenkins, G. T. H. and Medialdea, A. (in prep) ‘Deglaciation of the terrestrial-terminating sector of the Irish Sea Ice Stream.

Clark, C. D., Ely, J. C., Greenwood, S. L., Hughes, A. L., Meehan, R., Barr, I. D., Bateman, M. D., Bradwell, T., Doole, J., Evans, D. J. and Jordan, C. J. (2017) ‘BRITICE Glacial Map, version 2: a map and GIS database of glacial landforms of the last British-Irish Ice Sheet.’ *Boreas*, **47**, 11 – e8

Clark, C. D., Hughes, A. L., Greenwood, S. L., Jordan, C. and Sejrup, H. P. (2012) 'Pattern and timing of retreat the last British-Irish Ice Sheet.' *Quaternary Science Reviews,* **44**, 112 – 146.

Colarossi, D., Duller, G. A. T., Roberts, H. M., Tooth, S. and Lyons, R. (2015) 'Comparison of paired quartz OSL and feldspar post-IR IRSL dose distributions in poorly bleached fluvial sediments from South Africa.' *Quaternary Geochronology*, **30**, 233 – 238.

Duller, G. A. T. (1994) 'Luminescence dating of poorly bleached sediments from Scotland.' *Quaternary Science Reviews,* **13**, 521 – 524

Duller, G. A. T. (2006) 'Single grain optical dating of glacigenic deposits.' Quaternary *Geochronology,* **1**, 296 – 304.

Duller, G. A. T. (2008a) 'Luminescence Dating: guidelines on using luminescence dating in archaeology.' English Heritage.

Duller, G. A. T. (2008b) 'Single-grain optical dating of Quaternary sediments: why aliquot size matters in luminescence dating.' *Boreas*, **37**, 589 – 612.

Duller, G. A. T., Tooth, S., Barham, L. and Tsukamoto, S. (2015) 'New investigations at Kalambo Falls, Zambia: Luminescence chronology, site formation, and archaeological significance.' *Journal of Human Evolution*, **85**, 111 - 125.

Evans, D. J., Bateman, M. D., Roberts, D. H., Medialdea, A., Hayes, L., Duller, G. A. T., Fabel, D. and Clark, C. D. (2017) 'Glacial Lake Pickering: stratigraphy and chronology of a proglacial lake dammed by the North Sea Lobe of the British-Irish Ice Sheet.' *Journal of Quaternary Science,* **32**, 295 – 310.

Evans, D. J., Clark, C. D. and Mitchell, W. A. (2005) 'The last British Ice Sheet: A review of the evidence utilised in the compilation of the Glacial Map of Britain.' *Earth-Science Reviews,* **70**, 235 – 312.

Freiesleben, T., Sohbati, R., Murray, A., Jain, M., al Khasawneh, S., Hvidt, S. and Jakobsen, B. (2015) 'Mathematical model quantifies multiple daylight exposure and burial events for rock surfaces using luminescence dating.' *Radiation Measurements*, **81**, 16 – 22.

Fuchs, M. and Owen, L. A. (2008) 'Luminescence dating of glacial and associated sediments: review, recommendations and future directions.' *Boreas*, **37**, 636 – 659

Galbraith, R. F. and Roberts, R. G. (2012) 'Statistical aspects of equivalent dose and error calculation and display in OSL dating: an overview and some recommendations.' *Quaternary Geochronology*, **11**, 1 - 27.

Galbraith, R. F., Roberts, R. G., Laslett, G. M., Yoshida, H. and Olley, M. (1999) 'Optical dating of single and multiple grains of quartz from Jinmium rock shelter, northern Australia: part I, experimental design and statistical models.' *Archaeometry*, **41**, 339 – 364.

Gemmell, A. M. D. (1997) 'Fluctuations in the thermoluminescence signal of suspended sediment in an alpine glacial meltwater stream.' *Quaternary Geochronology*, **16**, 281 – 290.

Guérin, G., Mercier, N. and Adamiec, G. (2011) 'Dose-rate conversion factors: update.' *Ancient TL*, **29**, 5 – 8.

Habermann, J., Schilles, T., Kalchgruber, R., and Wagner, G. A. (2000) 'Steps towards surface dating using luminescence.' *Radiation Measurements*, **32**, 847-851.

Hansen, V., Murray, A., Buylaert, J. P., Yeo, E. Y. and Thomsen, K. (2015) 'A new irradiated quartz for beta source calibration.' *Radiation Measurements*, **81**, 123 - 127.

Hubbard, A., Bradwell, T., Golledge, N., Hall, A., Patton, H., Sugden, D. and Stoker, M. (2009) 'Dynamic cycles, ice streams and their impact on the extent, chronology and

deglaciation of the British-Irish ice sheet.' *Quaternary Science Reviews*, **28** (7), 758 – 776.

Huntley, D. J. and Baril, M. R. (1997) 'The K content of the K-feldspars being measured in optical dating or in thermoluminescence dating.' *Ancient TL*, **15**, 11 - 13.

Huntley, D. J. and Lamothe, M. (2001) 'Ubiquity of anomalous fading in K-feldspars and the measurement and correction for it in optical dating.' *Canadian Journal of Earth Sciences*, **38**, 1093 – 1106.

Jain, M. and Ankjærgaard, C. (2011) 'Towards a non-fading signal in feldspar: insights into charge transport and tunnelling from time-resolved optically stimulated luminescence.' *Radiation Measurements*, **46**, 292 – 309.

Jansson, K. N. and Glasser, N. F. (2005) 'Palaeoglaciology of the Welsh sector of the British-Irish Ice Sheet.' *Journal of the Geological Society*, **162**, 25 – 37.

Lehmann, B., Valla, P. G., King, G. E. and Herman, F. (2018) 'Investigation of OSL surface exposure dating to reconstruct post-LIA glacier fluctuations in the French Alps (Mer de Glace, Mont Blanc massif).' *Quaternary Geochronology*, **44**, 63 – 74

Li, B., Roberts, R. G., Jacobs, Z., Li, S. H. and Guo, Y. J. (2015) 'Construction of a 'global standardised growth curve'(gSGC) for infrared stimulated luminescence dating of K-feldspar.' *Quaternary Geochronology*, **27**, 119 - 130.

Liritzis, I. (2011) 'Surface dating by luminescence: an overview.' *Geochronometria*, **38**, 292 - 302.

Liritzis, I., Guibert, P., Foti, F., and Schvoerer, M. (1997) 'The temple of Apollo (Delphi) strengthens novel thermoluminescence dating method.' *Geoarchaeology*, **12**, 479-496.

McCabe, A. M., Clark, P. U., Clark, J. and Dunlop, P. (2007) 'Radiocarbon constraints on readvances of the British-Irish Ice Sheet in the northern Irish Sea Basin during the last deglaciation.' *Quaternary Science Reviews*, **26**, 1204 – 1211.

McCarroll, D., Stone, J. O., Ballantyne, C. K., Scourse, J. D., Fifield, L. K., Evans, D. J and Hiemstra, J. F. (2010) 'Exposure-age constraints on the extent, timing and rate of retreat of the last Irish Sea ice stream.' *Quaternary Science Reviews*, **29**, 1844 – 1852.

Olley, J. M., Roberts, R. G. and Murray, A. S. (1997) 'Disequilibria in the uranium decay series in sedimentary deposits at Allen's Cave, Nullarbor Plain, Australia: implications for dose rate determinations.' *Radiation Measurements*, **27**, 433 - 443.

Ou, X. J., Roberts, H. M., Duller, G. A. T., Gunn, M. D. and Perkins, W. T. (2018) 'Attenuation of light in different rock types and implications for rock surface luminescence dating.' *Radiation Measurements*.

Polikreti, K. (2007) 'Detection of ancient marble forgery: techniques and limitations.' *Archaeometry*, **49**, 603-619.

Poolton, N. R. J., Ozanyan, K. B., Wallinga, J., Murray, A. S. and Bøtter-Jensen, L. (2002) 'Electrons in feldspar II: a consideration of the influence of conduction band-tail states on luminescence processes.' *Physics and Chemistry of Minerals*, **29**, 217 – 225.

Prescott, J. R. and Hutton, J. T. (1994) 'Cosmic ray contributions to dose rates for luminescence and ESR dating: large depths and long-term time variations.' *Radiation Measurements*, **23**, 497 - 500.

Preusser, F., Chithambo, M. L., Gotte, T., Martini, M., Ramseyer, K., Sendezera, E. J., Susino, G. J. and Wintle, A. G. (2009) 'Quartz as a natural luminescence dosimeter.' *Earth Science Reviews*, **97**, 184 – 214.

Rhodes, E. (2011) 'Optically Stimulated Luminescence Dating of Sediments over the Past 200,000 Years.' *Annual Review of Earth and Planetary Sciences*, **39**, 461 – 488.

Rhodes, E. J. and Schwenninger, J. L. (2007) ‘Dose rates and radioisotope concentrations in the concrete calibration blocks at Oxford.’ *Ancient TL*, **25**, 5 – 8.

Richards, B. W., Owen, L. A. and Rhodes, E. J. (2000) ‘Timing of Late Quaternary glaciations in the Himalayas of northern Pakistan.’ *Journal of Quaternary Science*, **15**, 283 – 297.

Richards, M. (1994) *Luminescence dating of quartzite from the Diring Yuriakh site* (MA dissertation, Arts and Social Sciences: Archaeology).

Roberts, D. H., Dackombe, R. V. and Thomas, G. S. P. (2007) ‘Palaeo-ice streaming in the central sector of the British-Irish Ice Sheet during the Last Glacial Maximum: evidence from the northern Irish Sea Basin.’ *Boreas*, **36**, 115 – 129.

Scourse, J. D. (1991) ‘Glacial deposits of the Isles of Scilly.’ In: *Glacial deposits in Great Britain and Ireland*. (eds.) Ehlers, J., Gibbard, P. L. and Rose, J.

Simkins, L. M., DeWitt, R., Simms, A. R., Briggs, S. and Shapiro, R. S. (2016) ‘Investigation of optically stimulated luminescence behaviour of quartz from crystalline rock surfaces: A look forward.’ *Quaternary Geochronology*, **36**, 161 – 173.

Simms, A. R., DeWitt, R., Kouremones, P. and Drewry, A. M. (2011) ‘A new approach to reconstructing sea levels in Antarctica using optically stimulated luminescence of cobble surfaces.’ *Quaternary Geochronology*, **6**, 50 – 60.

Smedley, R. K., Glasser, N. F. and Duller, G. A. T. (2016) ‘Luminescence dating of glacial advances at Lago Buenos Aires (~ 46 ^{o} S), Patagonia.’ *Quaternary Science Reviews*, **134**, 59 – 73.

Smedley, R. K., Scourse, J. D., Small, D., Hiemstra, J. F., Duller, G. A. T., Bateman, M. D., Burke, M. J., Chiverrell, R. C., Clark, C. D., Davies, S. M. and Fabel, D. (2017a) ‘New age constraints for the limit of the British-Irish Ice Sheet on the Isles of Scilly.’ *Journal of Quaternary Science*, **32** (1), 48 – 62.

Smedley, R. K., Chiverrell, R. C., Ballantyne, C. K., Burke, M. J., Clark, C. D., Duller, G. A. T., Fabel, D., McCarroll, D., Scourse, J. D., Small, D. and Thomas, G. S. P. (2017b) 'Internal dynamics condition centennial-scale oscillations in marine-based ice-stream retreat.' *Geology*, **45**, 787 - 790.

Sohbati, R., Murray, A. S., Jain, M., Buylaert, J. P. and Thomsen, K. J. (2011) 'Investigating the resetting of OSL signals in rock surfaces.' *Geochronometria*, **38**, 249 – 258.

Sohbati, R., Murray, A. S., Buylaert, J. P., Almeida, N. A. C. and Cunha, P. P. (2012a) 'Optically stimulated luminescence (OSL) dating of quartzite cobbles from the Tapada do Montinho archaeological site (east-central Portugal).' *Boreas*, **41**, 452 – 462.

Sohbati, R., Jain, M. and Murray, A. (2012b) 'Surface exposure dating of non-terrestrial bodies using optically stimulated luminescence: A new method.' *Icarus*, **221**, 160 – 166.

Sohbati, R., Murray, A. S., Chapot, M., Jain, M. and Pederson, J. (2012c) 'Optically stimulated luminescence (OSL) as a chronometer for surface exposure dating.' *Journal of Geophysical Research*, **117**, 7 pp.

Sohbati, R., Murray, A. S., Porat, N., Jain, M. and Avner, U. (2015) 'Age of a prehistoric 'Rodedian' cult site constrained by sediment and rock surface luminescence dating techniques.' *Quaternary Geochronology*, **30**, 90 – 99

Stokes, C. R. and Clark, C. D. (2001) 'Palaeo-ice streams.' *Quaternary Science Reviews*, **20**, 1437 – 1457

Svendsen, J. I., Alexanderson, H., Astakhov, V. I., Demidov, I., Dowdeswell, J. A., Funder, S., Gataullin, V., Henriksen, M., Hjort, C., Houmark-Nielsen, M., Hubberten, H. W., Ingolfsson, O., Jakobsson, M., Kjaer, K. H., Larsen, E., Lokrantz, H., Lunkka, J. P., Lysa, A., Mangerud, J., Matiouchkov, A., Murray, A., Moller, P., Niessen, F., Nikolskaya, O., Polyak, L., Saarnisto, M., Siegert, C., Siegert, M.J., Spielhagen, R. F.

and Stein, R. (2004) ‘Late Quaternary ice sheet history of northern Eurasia.’ *Quaternary Science Reviews*, **23**, 1229-1271.

Thiel, C., Buylaert, J. P., Murray, A., Terhorst, B., Hofer, I., Tsukamoto, S. and Frechen, M. (2011) ‘Luminescence dating of the Stratzing loess profile (Austria)–Testing the potential of an elevated temperature post-IR IRSL protocol.’ *Quaternary International*, **234**, 23 - 31.

Thomas, G. S. (1989) ‘The Late Devensian glaciation along the western margin of the Cheshire-Shropshire Lowland.’ *Journal of Quaternary Science*, **4**, 167 - 181.

Thomas, G. S. and Chiverrell, R. C. (2007) ‘Structural and depositional evidence for repeated ice-marginal oscillation along the eastern margin of the Late Devensian Irish Sea Ice Stream.’ *Quaternary Science Reviews*, **26**, 2375 – 2405.

Thomas, G. S. P. (1989) ‘The late Devensian glaciation along the western margin of the Cheshire-Shropshire lowland.’ *Journal of Quaternary Science*, **4**, 167 – 181.

Thomas, G. S., Chiverrell, R. C. and Huddart, D. (2004) ‘Ice-marginal depositional responses to readvance episodes in the Late Devensian deglaciation of the Isle of Man.’ *Quaternary Science Reviews*, **23**, 85 – 106.

Thomas, P. J., Murray, A. S., Kjaer, K. H., Funder, S., Larsen, E. (2006a) ‘Optically stimulated luminescence (OSL) dating of glacial sediments from Arctic Russia - depositional bleaching and methodological aspects.’ *Boreas*, **35**, 587 - 599.

Thomas G. S. P., Chiverrell R. C., Huddart D., Long D., Roberts, D. (2006b) The Ice Age. In: *A New History of the Isle of Man: The Evolution of the Natural Landscape*, Chiverrell R.C., Thomas G.S.P. (eds). Liverpool University Press: Liverpool; 100 – 150.

Thomsen, K. J., Murray, A. S., Jain, M. and Botter-Jensen, L. (2008) ‘Laboratory fading rates of various luminescence signals from feldspar-rich sediment extracts.’ *Radiation Measurements*, **43**, 1474 – 1486.

Thomsen, K. J., Kook, M., Murray, A. S. and Jain, M. (2018) ‘Resolving luminescence in spatial and compositional domains.’ *Radiation Measurements*.

Thrasher, I. M., Mauz, B., Chiverrell, R. C. and Lang, A. (2009b) ‘Luminescence dating of glaciofluvial deposits: a review.’ *Earth-Science Reviews*, **97** (1), 133 – 146.

Thrasher, I. M., Mauz, R. C., Chiverrell, R. C., Lang, A. and Thomas, G. S. P. (2009a) ‘Testing an approach to OSL dating of Late Devensian glaciofluvial sediments of the British Isles.’ *Journal of Quaternary Science*, **24**, 785 – 801.

Van Landeghem, K. J., Wheeler, A. J. and Mitchell, N. C. (2009) ‘Seafloor evidence for palaeo-ice streaming and calving of the grounded Irish Sea Ice Stream: Implications for the interpretation of its final deglaciation phase.’ *Boreas*, **38**, 119 – 131.

White, J. C. and Beamish, D. (2014) ‘A lithological assessment of the resistivity data acquired during the airborne geophysical survey of Anglesey, North Wales.’ *Proceedings of the Geologists' Association*, **125**, 170 - 181.

Wintle, A. G. (1973) ‘Anomalous fading of thermo-luminescence in mineral samples.’ *Nature*, **245**, 143 – 144.

Wintle, A. G. and Aitken, M. J. (1977) ‘Absorbed dose from a beta source as shown by thermoluminescence dosimetry.’ *International Journal of Applied Radiation and Isotopes*, **28**, 625 – 627.

Wintle, A. G. and Huntley, D. J. (1979) ‘Thermoluminescence dating of a deep-sea sediment core.’ *Nature*, **279**, 710.

Wintle, A. G. and Murray, A. S. (2006) ‘A review of quartz optically stimulated luminescence characteristics and their relevance in single-aliquot regeneration dating protocols.’ *Radiation Measurements*, **41**, 369 – 391.

Appendix A

Publication of data and interpretations from Chapter 5 – ‘A new approach for luminescence dating glaciofluvial deposits – High precision optical dating of cobbles’

Quaternary Science Reviews 192 (2018) 263–273

Contents lists available at ScienceDirect

Quaternary Science Reviews

journal homepage: www.elsevier.com/locate/quascirev

A new approach for luminescence dating glaciofluvial deposits - High precision optical dating of cobbles

G.T.H. Jenkins [a, *], G.A.T. Duller [a], H.M. Roberts [a], R.C. Chiverrell [b], N.F. Glasser [a]

[a] Department of Geography and Earth Sciences, Aberystwyth University, Ceredigion, SY23 3DB, UK
[b] Department of Geography and Planning, University of Liverpool, Liverpool, L69 3BX, UK

ARTICLE INFO

Article history:
Received 6 February 2018
Received in revised form
24 May 2018
Accepted 24 May 2018
Available online 15 June 2018

Keywords:
Quaternary
Glaciation
Europe
Optical methods
Clasts
Feldspar
Heterogeneous bleaching

ABSTRACT

In recent years luminescence dating has increasingly been applied to date glaciofluvial sediments, but uncertainties about the degree of bleaching of the luminescence signal at deposition make dating of such sediments challenging. Here we test a new approach for luminescence dating of glaciofluvial sediments, based on the analysis of rock cores drilled from granite cobbles, and compare the luminescence ages generated against independent age control.

Luminescence measurements from rock slices in cobble-sized clasts can be used to reconstruct the extent of bleaching, thereby giving greater confidence in the ages produced. This study illustrates that another important advantage of using cobbles is that at depths of 2 mm or more below the cobble surface >90% of the total dose rate arises from the cobble itself, making the dose rate insensitive to the water content of the sediment matrix. Ordinarily, uncertainties in estimating water content during burial are one of the largest sources of uncertainty in luminescence dating methods, and hence reducing the reliance upon the dose rate could be particularly advantageous for glacial deposits, where water contents can potentially be large and highly variable.

Measurements of cobbles from Orrisdale Head, Isle of Man, demonstrate that the luminescence signal was completely bleached to depths of up to 12 mm into the cobble. Sampling of orientated cobbles from lithofacies diagnostic of bar-top environments was used to maximise the chances of exposure to sunlight. The upper-faces of these orientated cobble surfaces appear to be bleached to a greater depth than the lowermost faces. Data from 45 rock slices from these cobbles were tightly clustered, yielding a mean age of 20.7 ± 0.3 ka that is in agreement with independent age control. One of the well-bleached cobbles shows evidence of two discrete exposure events, potentially recording both the advance at 26.2 ± 0.8 ka, and retreat at 20.7 ± 0.3 ka, of the Irish Sea Ice Stream.

1. Introduction

Glacigenic sediments are amongst the most challenging Quaternary deposits for dating. Optically stimulated luminescence (OSL) dating using sand-sized grains of quartz or feldspar has been applied in recent years, and whilst many ages have been determined that underpin our understanding of ice sheet dynamics over the last glacial cycle (e.g. Svendsen et al., 2004; Ou et al., 2015; Smedley et al., 2016, 2017a; b), the method is challenging (cf Thomas et al., 2006b; Duller, 2008). In recent years a new luminescence method has been developed, dating buried clasts varying in size from centimetres to tens of centimetres in diameter (Sohbati et al., 2012, 2015; Freiesleben et al., 2015), building upon earlier research (e.g. Habermann et al., 2000; Polikreti et al., 2002; Vafiadou et al., 2007). These clasts are much larger than the sand- and silt-sized grains normally used in luminescence dating (Duller, 2004). One of the benefits of using large clasts for dating is that the degree of bleaching that occurred before burial can be assessed using information encoded within the clast itself (Sohbati et al., 2015). It has also been shown that variations in the luminescence signal with depth into a clast can reveal multiple episodes of bleaching and subsequent burial (Freiesleben et al., 2015). In glacial environments, where heterogeneous bleaching is likely to be a significant problem, the ability to determine whether or not a clast was completely bleached on deposition, prior to subsequent burial, offers a significant advantage over dating sand-sized grains. This is

* Corresponding author.
E-mail address: gej11@aber.ac.uk (G.T.H. Jenkins).

https://doi.org/10.1016/j.quascirev.2018.05.036

because when using sand-sized grains, statistical models are required to identify which equivalent dose (D_e) values are derived from sediment grains that were bleached at deposition, and to exclude those that were not bleached (Galbraith et al., 1999). The choice of statistical model, and estimation of parameters such as sigma-b for use in the minimum age model (Galbraith and Roberts, 2012), is complex (Smedley et al., 2017a) and the most appropriate approach is not yet agreed upon.

This study is the first to apply the newly developed cobble dating method to glaciofluvial sedimentary deposits, and aims to see whether it can be used to circumvent many of the issues associated with luminescence dating of sediments in this environment. Critically, the ability of buried clasts to record the extent of bleaching at deposition within a heterogeneously bleached (in this case, glacial) environment will be considered.

2. Materials and methods

2.1. Study area & sample selection

The Orrisdale area, in the north of the Isle of Man, UK (Fig. 1), comprises a complex sequence of ice-front moraines and lateral ice-marginal sandur or outwash systems deposited as the former Irish Sea Ice Stream retreated northwards (Thomas et al., 1985, 2006a; Thrasher et al., 2009). Orrisdale Head was selected because of the extensive (>8 km) exposure in coastal cliff sections and the independent age control available from multiple geochronological techniques in the wider region. The geomorphology around Orrisdale shows a series of repeating packages of proglacial sandur and ice-contact moraine ridges that are also reflected in the coastal exposures (Fig. 1b). Previously, OSL dating constrained the outwash deposits at Orrisdale (Thrasher et al., 2009) to 16.4 to 14.1 ka, but those ages were calculated using the water contents measured at the time of sampling (5–16%) and do not account for water table lowering with coastal cliff retreat (rates typically 1–2 m per year). Recalculating the Thrasher et al. (2009) ages with water contents of 20–23% revises these ages to 18.3 ± 3.5 and 14.2 ± 2.3 ka. Single grain OSL dating of quartz and cosmogenic nuclide dating of the ice retreat sequence in the wider Irish Sea Basin shows ice limits were 500 km to the south on the Isles of Scilly at ~26 ± 1.6 ka (Smedley et al., 2017a), to the south coast of Ireland by 25.1 ± 1.2ka (Small et al., 2018, in press) and pulling back north from Anglesey by 20.3 ± 0.6 ka (Smedley et al., 2017b). Further north, Chiverrell et al. (submitted) have added 11 single grain quartz OSL ages and 8 cosmogenic isotope ages to further define the ice retreat sequence in the northern Irish Sea Basin, and using a Bayesian model were able to constrain deglaciation of the Isle of Man before 18.9 ± 1.0 ka. This chronology is similar to, but refines, previous Bayesian modelling of the ice retreat dynamics (Chiverrell et al., 2013) and also suggests that the small aliquot OSL ages (Thrasher et al., 2009) for the Orrisdale ice marginal complex underestimate the age by 2–6 ka.

Orrisdale Head forms part of an 8 km long coastal section, giving near continuous exposure of glaciofluvial deposits in cliffs up to 30 m in height. At 54.3194°N 4.5727°W a series of gravel bars fining upwards into sand units are seen, and are indicative of deposition in a sandur with repeated packages superimposed upon each other (Fig. 2). Four gravel packages (ORS01, 02, 03, 04) were sampled, lying within 20 m of each other laterally and between ~3 and 7 m below the current surface. Stratified planar crossbeds of back-bar gravels (Gp), and massive, clast-supported imbricated bar-top gravel lithofacies (Gm) were targeted for sampling (Fig. 2b and c). These have been interpreted as ice-proximal bar-forms deposited within a dynamic environment of migrating bars and channels (Thomas et al., 1985, 2006a), with the bar-tops potentially emergent above the water, thus maximising the probability that clasts were exposed to daylight before burial.

Forty-five clasts of varying lithologies were obtained from

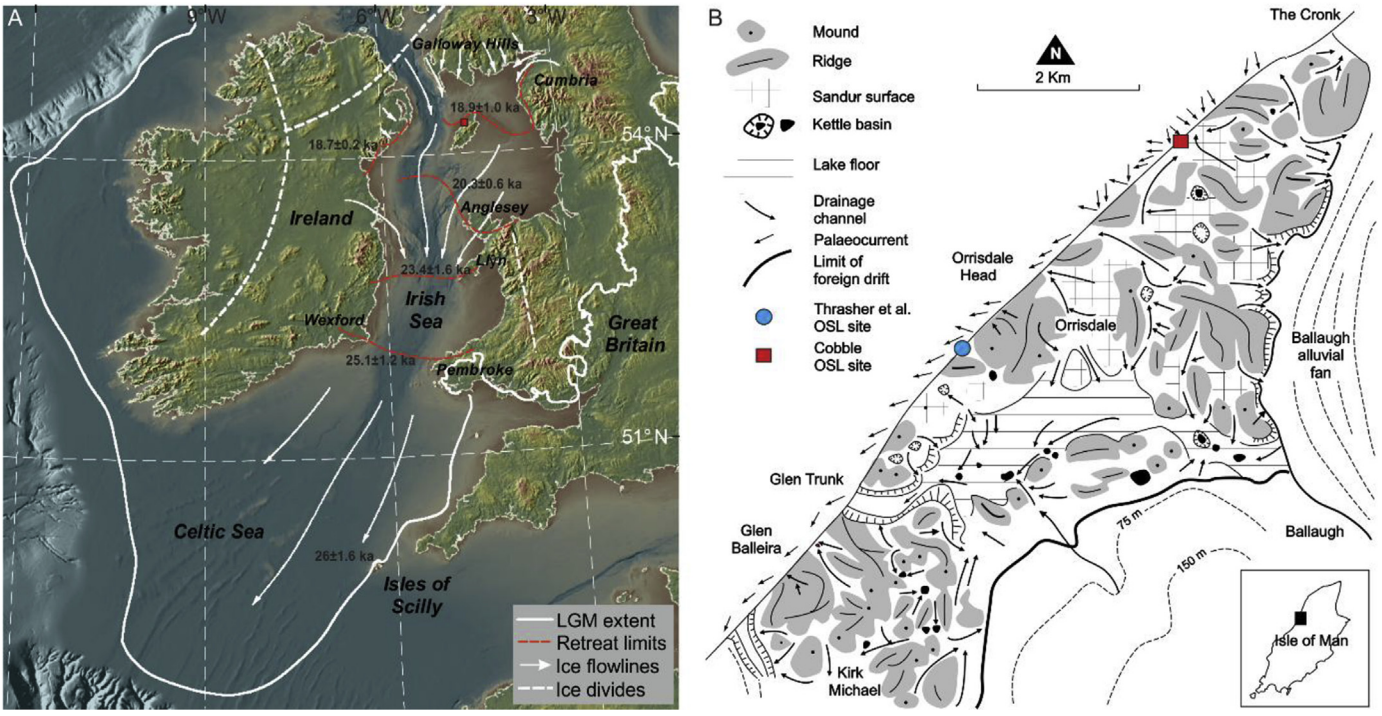

Fig. 1. (a) Location of Orrisdale on the Isle of Man (red square), and its relation to various retreat stages of the Irish Sea Ice Stream and ages for those as discussed in the text. The location of places mentioned in the text are also shown. (b) Geomorphological map of the sandur at Orrisdale Head sampled for this study (shown by a red square). Adapted from Thomas et al. (2006a). (For interpretation of the references to colour in this figure legend, the reader is referred to the Web version of this article.)

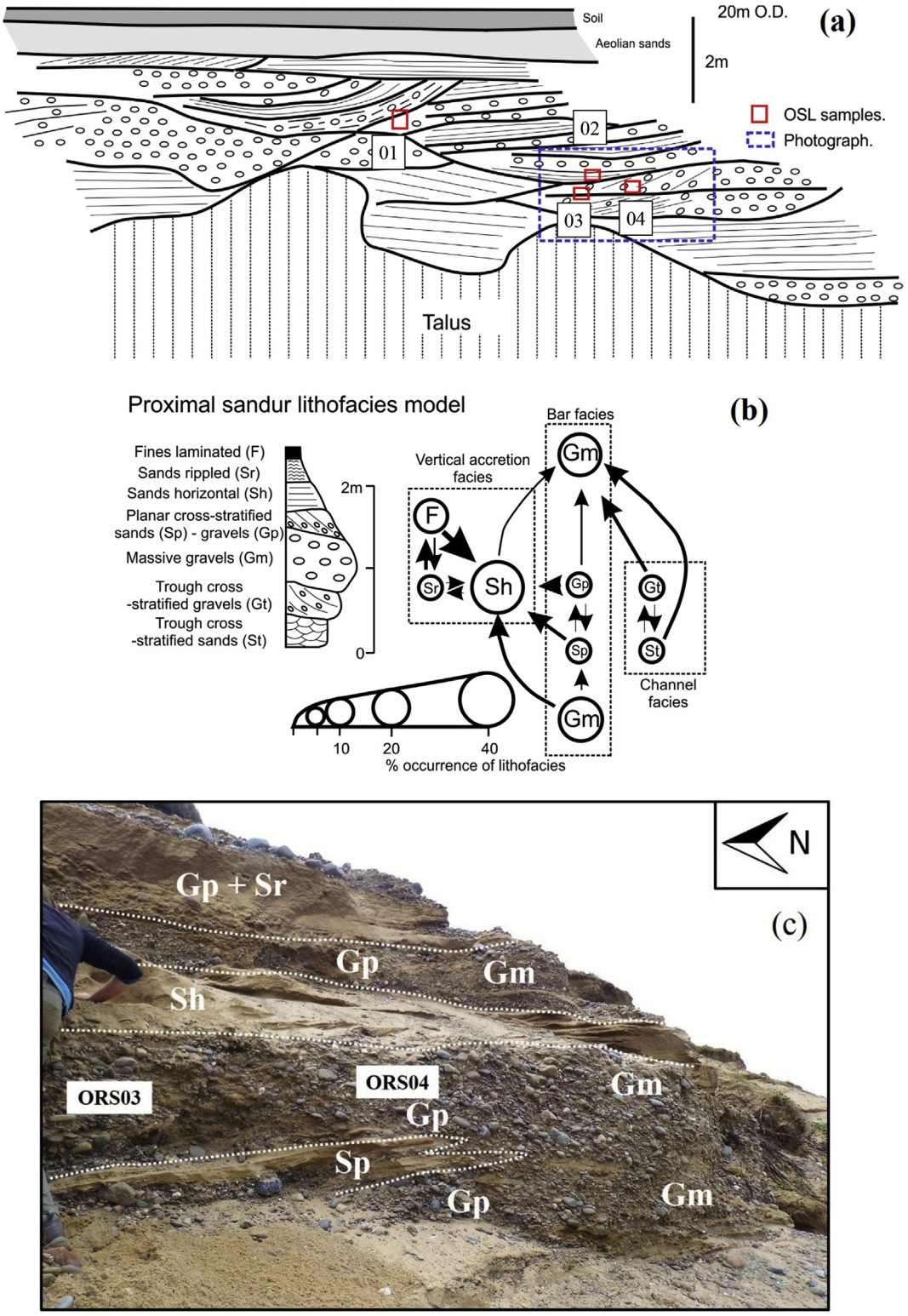

Fig. 2. (a) Schematic of the coastal glaciofluvial sediment exposures at Orrisdale Head with the location of 4 sampled gravel units illustrated (ORS01 - 04). (b) Model of ice-proximal bar formations (Thomas et al., 1985) and key for lithofacies. (c) Example image of the stratified planar cross beds (Gp) and massive, matrix-supported (Gm) gravel lithofacies exposed at Orrisdale Head. The locations where samples ORS03 and ORS04 were collected are also shown.

across the four gravel packages (ORS01 to ORS04). These were collected from sediment exposures which were cleaned and sampled underneath a black, light-tight plastic sheet held against the section to shield the freshly-exposed clasts from daylight. Cobbles with b-axes varying from ~3.5–10 cm were identified within the sediment with the help of a red LED head torch, and collected into light-safe bags. The orientation of each clast within the section was recorded by marking the upper and lower surfaces.

Individual clasts from each package were numbered sequentially to give them a unique name (e.g. ORS03-4 is the fourth cobble from package ORS03). Two samples of the matrix material from each gravel package were also collected for dosimetry, and combined to give a single representative sample of the matrix for each package (samples OH01, 02, 03, 04). The gamma dose rate for each gravel package was also measured in the field by inserting an Ortec Dig-iDART gamma spectrometer equipped with a 2 inch NaI (Tl) crystal into the sediment profile.

2.2. Sample selection, preparation, and measurement protocols

The 45 cobbles sampled were identified in the laboratory as being derived from three lithologies: granites, sandstones and quartz. Following initial investigations, ten granite cobbles were identified as the most appropriate materials for detailed investigation, as the sandstone was too friable to drill and the quartz, thought to be hydrothermal in origin, yielded very little optically stimulated luminescence signal.

Under subdued red light in the laboratory, cores of ~8 mm diameter and of varying lengths (up to ~ 20 mm long) were obtained from the 10 granite cobbles, using a water-cooled, low-speed diamond-tipped drill. Each core drilled from a cobble was given a unique letter code (e.g. core C from ORS03-4 is the third core from cobble ORS03-4). As required, the granite cores were subsequently sliced using a Buehler IsoMet 11–4254 water-cooled, diamond-edged wafering blade (0.3 mm thickness), and rock slices of ~0.7 mm thickness (mean value = 0.71 ± 0.19 mm (n = 116 slices)) were produced. The granite rock slices were washed in distilled water in an ultrasonic bath to remove the rock flour produced during the drilling and slicing process. The clean rock slices were dried and subsequently placed into stainless steel planchettes for luminescence measurements.

All luminescence measurements were made using a Risø TL/OSL-DA-20 reader (Bøtter-Jensen et al., 2003), originally manufactured in 1989 but refurbished with new electronics and a new optical stimulation head in 2010. All measurements, including thermal pretreatments, were carried out in a nitrogen-rich atmosphere. Infrared stimulation (880 nm) was achieved with 22 TSFF5210 LEDs delivering 160 mW/cm^2 at the sample, and photon detection was undertaken with an EMI 9635QA photomultiplier tube filtered by 2 mm thickness each of Schott BG39 and Corning 7–59 filter combined with a neutral density 2.0 filter. A^{90}Sr/^{90}Y beta source mounted on the reader was used for sample irradiation. This beta source was calibrated specifically for rock slices of 0.7 mm thickness, using rock slices from a quartzite cobble sampled from the glaciofluvial sediments at Orrisdale Head. These quartzite rock slices were sensitised and stabilised by giving repeated cycles of irradiation (42.9 Gy) and heating (up to 500 °C), prior to receiving a known gamma dose of 4.90 Gy delivered in a scatter free geometry using a calibrated ^{137}Cs source at DTU, Denmark. The subsequent calibration measurements used the blue-stimulated OSL signal from the gamma-irradiated quartzite rock slices obtained as part of a single-aliquot regenerative dose protocol, and gave a dose rate of 0.031 Gy s^{-1}. This is 82% of the dose rate to sand-sized grains mounted on aluminium discs (but note that the ratio of dose rates will vary depending upon sample-source distance, and this was 11 mm for this instrument).

A post-IR IRSL$_{225}$ SAR protocol based on the approach of Buylaert et al. (2009) was used to study the granite cobble samples from Orrisdale Head (Table 1). To reduce the impact of thermal lag within the ~0.7 mm thick rock slices, a slow heating rate of 1 °C/s was used, coupled with extended preheats held for 100s duration (instead of the more common 60s used when dating sand-sized grains), and the sample was also held at its measurement temperature of 50 °C or 225 °C for 100s before IR stimulation began. A typical decay-curve and dose-response curve for the IRSL$_{50}$ signal are shown in Fig. 3, illustrating the excellent recycling and the intense IRSL$_{50}$ signal typical of the data derived from the granite cobbles in this study.

To assess whether the post-IR IRSL$_{225}$ protocol was appropriate for these samples, two dose-recovery tests were performed on rock slices taken from a single cobble (ORS00-1) collected from the foreshore of Orrisdale Head that had been exposed to daylight for an unknown period of time. In the first dose recovery experiment, the surface slices from each of six cores drilled adjacent to each other on this single cobble were used; three slices were given a beta dose of ~86 Gy on top of their natural D$_e$ prior to measurement of the apparent D$_e$ using the protocol in Table 1. The remaining three slices were used to assess the natural D$_e$ value from the surface of the cobble at the time of sampling, thereby providing a residual D$_e$ value. The resultant residual-subtracted dose recovery values are given in Table 2. The natural D$_e$ ('residual dose', Table 2) derived from the post-IR IRSL$_{225}$ signal is much larger (13.12 ± 1.36 Gy) than that derived from the IRSL$_{50}$ signal (4.36 ± 0.38 Gy). The IRSL$_{50}$ signal recovers the given dose (residual-subtracted dose recovery ratio = 0.97 ± 0.01; Table 2), whilst the post-IR IRSL$_{225}$ signal does not recover the given dose, yielding a residual-subtracted dose recovery ratio of 1.32 ± 0.06 for these naturally-bleached surface-slices (Table 2, Experiment 1).

The second dose recovery experiment used rock slices from the same cores used in dose recovery experiment 1, but taken from deeper into the cobble. Given the relatively high D$_e$ values measured for the surface slices in experiment 1, slices from deeper in the cores were unlikely to have been bleached. For experiment 2, these deeper slices were bleached in a SOL2 solar simulator for 14 days (with the rock slices turned over after 7 days) to reduce the trapped charge population; the same experimental procedure as used in experiment 1 was then applied, with three slices having their apparent D$_e$ measured to provide a residual D$_e$ value, and three slices receiving a dose of 86 Gy prior to D$_e$ determination. The residual D$_e$ values observed following 14 days SOL2 bleaching (1.68 ± 0.17 Gy for the IRSL$_{50}$ signal; 3.38 ± 0.11 Gy for the post-IR IRSL$_{225}$ signal), are significantly lower than observed in the first experiment for natural, sunlight bleaching (60% and 74% lower IRSL$_{50}$ and post-IR IRSL$_{225}$ residuals, respectively). The residual-subtracted dose recovery ratio in experiment 2 is 0.90 ± 0.06 for the IRSL$_{50}$ signal, and 0.97 ± 0.06 for the post-IR IRSL$_{225}$ signal (Table 2).

The IRSL$_{50}$ signal recovered a dose within 10% (allowing for uncertainties) in both experiments (Table 2), whilst the post-IR IRSL$_{225}$ signal only recovered a given dose when the residual signal was lowered by an extended exposure to a solar simulator prior to delivery of the dose to be recovered (Table 2, experiment 2). The reason for this difference in performance is not clear.

3. Dose rate determination

The dose rate to individual rock slices originates from radionuclides in the cobble itself, in the surrounding matrix, and from cosmic rays. A sample of each cobble and a sample of the surrounding matrix were milled to a fine powder prior to dosimetry measurements. Dose rates were determined from thick source alpha counting (TSAC, using a Daybreak 583 instrument) and beta counting datasets (using a Risø GM-25-5 instrument; Bøtter-Jensen and Mejdahl, 1988) (Table 3a). TSAC was used to calculate the U and Th concentrations (Table 3b), and a combination of beta counting and TSAC were used to calculate the K concentration. The U, Th and K concentrations were then combined to establish the external gamma dose rate with the conversion factors of Guérin et al. (2011).

Table 1
Modified Single Aliquot Regenerative dose (SAR) procedure used to measure ~ 0.7 mm thick granite rock slices.

Step	Description	Signal
1	No dose in cycle 1 – different regenerative doses in later cycles	
2	Preheat to 250 °C at 1 °C/s and hold for 100 s	
3	Heat to 50 °C at 1 °C/s, pause for 100 s, and measure IRSL for 200 s	Lx_{50}
4	Heat to 225 °C at 1 °C/s, pause for 100 s, and measure IRSL for 200 s	Lx_{225}
5	Test dose (34 Gy)	
6	Preheat to 250 °C at 1 °C/s and hold for 100 s	
7	Heat to 50 °C at 1 °C/s, pause for 100 s, and measure IRSL for 200 s	Tx_{50}
8	Heat to 225 °C at 1 °C/s, pause for 100 s, and measure IRSL for 200 s	Tx_{225}
9	Heat to 280 °C at 1 °C/s, pause for 100 s, and measure IRSL for 200 s	
10	Repeat cycles 1–9 for different regenerative doses in step 1	

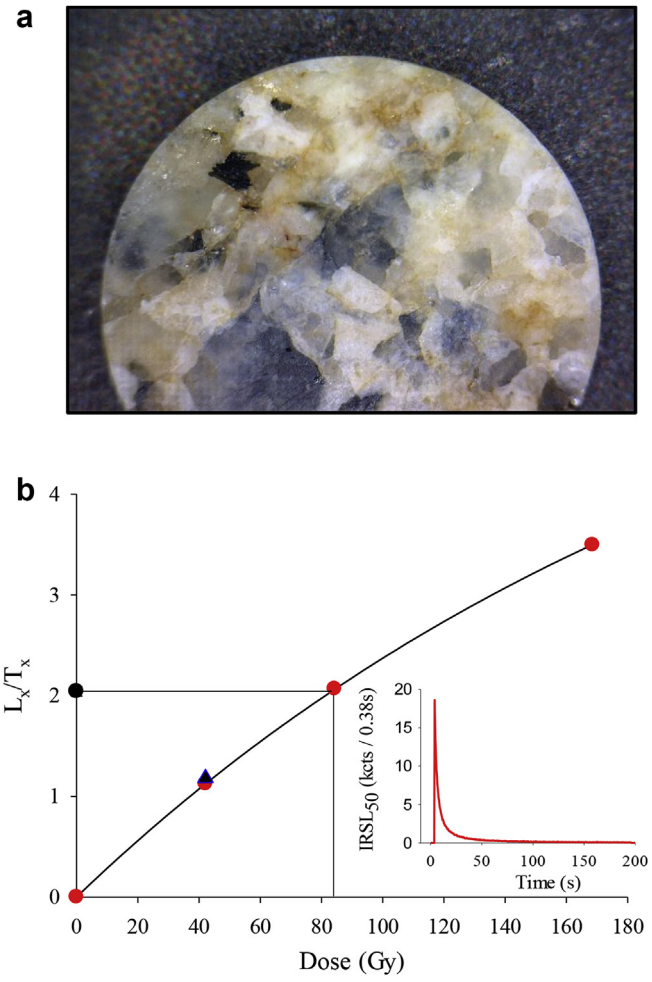

Fig. 3. (a) An example of a rock slice (8 mm diameter) as used for luminescence measurements (from core B of cobble ORS04-1). (b) Dose response curve for the $IRSL_{50}$ signal for the rock slice shown in (a). This slice was from 1.5 to 2.2 mm into the cobble sub-surface. The slice shows excellent recycling (blue triangle). The inset shows the natural decay curve of the same rock slice. For equivalent dose determination, the signal was summed over the first 9 channels (3.4 s) of optical stimulation, and the last 50 channels (19 s) were used to define the background. (For interpretation of the references to colour in this figure legend, the reader is referred to the Web version of this article.)

In-situ measurements of the external gamma contribution (Table 3a) were also made, as described in section 2.1. A water content during burial of 15 ± 5% was estimated for the surrounding sediment matrix, based on saturated water content measurements in the laboratory. In previous studies (e.g. Sohbati et al., 2015) the water content of the cobble itself has been assumed to be negligible. In this study a water content of <0.1% was measured for cobble ORS04–1 demonstrating that the water content is indeed negligible. The internal beta dose rate from K-feldspar grains was calculated assuming a 12.5% K content (Huntley and Baril, 1997). The sizes of feldspar grains within the rock slices were measured using a digital hand-lens and ranged from 320 to 1500 μm and gave a mean value of 647 ± 235 μm. The internal beta dose rate calculated for this grain size was 2.250 ± 0.702 Gy/ka (Table 3a). The dose rate contribution from cosmic radiation was also calculated following Prescott and Hutton (1994).

Freiesleben et al. (2015) calculated the variation of dose rate with depth into a cobble, making use of the approach outlined by Aitken (1985, Appendix H). In Freiesleben et al. (2015), the cobble was part of a rubble layer, and the calculations assumed that the cobble being dated was part of a flat layer, of thickness h and of infinite lateral extent. Equation (1) describes the variation in the beta dose rate with depth (x) into a cobble sub-surface that is buried within a sediment matrix (Freiesleben et al., 2015).

$$\dot{D}(x)_{\beta}^{\text{Cobble}} = \dot{D}_{\text{Rock},\beta}^{\text{inf}}\left[1 - 0.5\left(e^{-bx} + e^{-b(h-x)}\right)\right] + \dot{D}_{\text{Sed},\beta}^{\text{inf}} 0.5\left(e^{-bx} + e^{-b(h-x)}\right). \quad (1)$$

Here, b is the beta attenuation factor (1.9 mm^{-1} following Sohbati et al., 2015) and $\dot{D}_{\text{Rock},\beta}^{\text{inf}}$ and $\dot{D}_{\text{Sed},\beta}^{\text{inf}}$ are the infinite matrix beta dose rates for the cobble and sediment respectively (Table 3a). For cobbles that are typically ~40–90 mm in diameter, the approximation of Freiesleben et al. (2015) is appropriate for the beta dose rate. An equation of the same form is used for the gamma contribution $\dot{D}(x)_{\gamma}^{\text{Cobble}}$ but with an attenuation factor of 0.01 mm^{-1}. For the alpha contribution to the equation $\dot{D}(x)_{\alpha}^{\text{Cobble}}$, the sediment alpha contribution is ignored, due to the short distances (~10 μm) travelled by alpha particles. The alpha contribution arising from the cobble itself is calculated using an a-value of 0.08 ± 0.02 (Rees-Jones, 1995). The dose rate at a specific depth (x) is then calculated by summing the alpha $\dot{D}(x)_{\alpha}^{\text{Cobble}}$, beta $\dot{D}(x)_{\beta}^{\text{Cobble}}$ and gamma $\dot{D}(x)_{\gamma}^{\text{Cobble}}$ contributions, the internal alpha and beta dose, and the cosmic ray dose.

The dose rate to feldspar grains in rock slices in core A from cobble ORS04-1 varies from 5.37 ± 0.72 Gy/ka at the surface to 6.78 ± 0.75 Gy/ka inside the cobble (Fig. 4). The dose rate changes rapidly in the outer 2 mm of the cobble due to the large difference in the beta dose rate from the matrix and the cobble and the limited penetration of beta particles (Fig. 4). The gamma dose varies little, and is much lower (0.31 ± 0.02 Gy/ka at the cobble surface) than the beta dose. At depths of 2 mm or more into the cobble, the internal beta dose arising from K in the feldspar grains is 33% of the total dose rate, and the external beta dose to the grains arising from the

Table 2
Two sets of dose recovery data for slices from cobble ORS00-1 with a given dose approximately equivalent to the expected natural D_e. Cobble ORS00-1 was collected from the modern beach, and assumed to have been bleached to at least some degree due to its location at the time of sampling. Experiment 1 applied the beta dose to be recovered direct to untreated slices prepared from the surface of this cobble, while experiment 2 applied the dose to be recovered to rock slices that had been bleached for 14 days in a SOL2 solar simulator.

	Residual dose (Gy)	Given dose (Gy)	Recovered dose (Gy)	Dose recovery ratio
	Experiment 1: Samples bleached in nature			
$IRSL_{50}$	4.36 ± 0.38	85.86	87.74 ± 0.31	0.97 ± 0.01
pIR $IRSL_{225}$	13.12 ± 1.36	85.86	126.08 ± 5.32	1.32 ± 0.06
	Experiment 2: Sample bleached in a solar simulator			
$IRSL_{50}$	1.68 ± 0.17	85.86	79.01 ± 4.81	0.90 ± 0.06
pIR $IRSL_{225}$	3.38 ± 0.11	85.86	86.44 ± 4.85	0.97 ± 0.06

Table 3a
Measured dosimetry data for cobble and matrix samples from Orrisdale Head. Each individual rock slice will receive a different dose rate as outlined in Section 3.

Attenuated[a] and water corrected dose rates									
Sample name	Sample type	Depth (m)	TSAC[b] (cts/ks/cm^2)	Infinite matrix beta dose rate (Gy/ka)	Beta (Gy/ka)	Gamma (Gy/ka)	In-situ gamma (Gy/ka)	Cosmic (Gy/ka)	Internal beta (Gy/ka)
OH02	Matrix		0.375 ± 0.007	1.383 ± 0.047	0.861 ± 0.079	0.621 ± 0.045	0.687 ± 0.035	–	–
ORS02-1	Cobble	6	1.840 ± 0.032	4.454 ± 0.142	3.292 ± 0.243	3.029 ± 0.200	–	0.104 ± 0.05	2.250 ± 0.702
OH04	Matrix		0.305 ± 0.006	1.257 ± 0.044	0.782 ± 0.072	0.549 ± 0.040	0.799 ± 0.040	–	–
ORS04-1	Cobble	7	1.080 ± 0.019	4.852 ± 0.154	3.586 ± 0.265	2.406 ± 0.131	–	0.094 ± 0.05	2.250 ± 0.702
ORS04-3	Cobble	7	1.460 ± 0.023	5.215 ± 0.166	3.854 ± 0.285	2.643 ± 0.131	–	0.094 ± 0.05	2.250 ± 0.702

Notes.
[a] Beta and gamma dose rates attenuated for grain size within the cobble. Correction for water content is applied to doses arising from the matrix, but not the cobble.
[b] TSAC – Thick-Source Alpha Counting.

Table 3b
Dosimetry data calculated for cobble and matrix samples from Orrisdale Head.

Sample name	Sample type	Cobble Size (mm) (a:b:c)	Depth (m)	K (%)	U (ppm)	Th (ppm)
OH02	Matrix	–		0.62 ± 0.05	1.09 ± 0.18	4.49 ± 0.58
ORS02-1	Cobble	86:57:56	6	3.03 ± 0.20	6.65 ± 1.11	29.66 ± 3.72
OH04	Matrix	–		0.55 ± 0.04	1.33 ± 0.16	4.15 ± 0.52
ORS04-1	Cobble	60:32:30	7	2.41 ± 0.13	4.67 ± 0.60	14.85 ± 2.00
ORS04-3	Cobble	73:39:38	7	2.64 ± 0.13	8.97 ± 0.60	10.76 ± 1.98

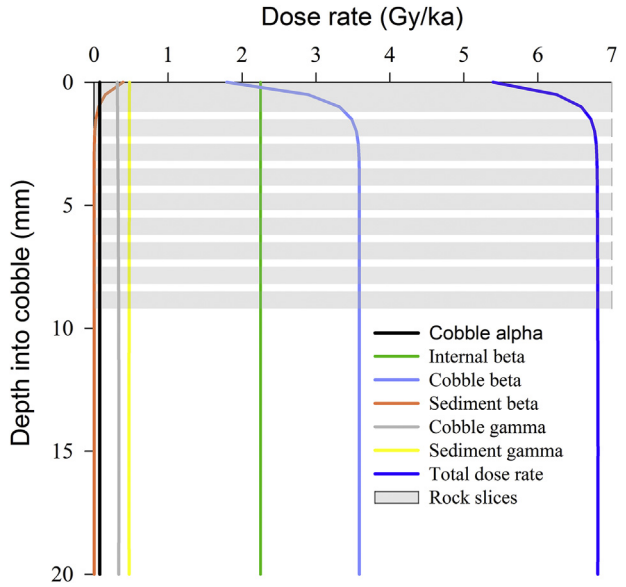

Fig. 4. Dose rate variations with depth into the sub-surface of core A of cobble ORS04-1. The horizontal grey bars show the position of the rock slices, with breaks in these illustrating material lost during the slicing process.

cobble is 53% of the total dose rate. When combined with the gamma dose arising from the cobble itself, this means that 93% of the total dose rate arises from the cobble itself at depths ≥2 mm below the surface. This dose rate is insensitive to the water content of the matrix, and also to potential changes due to post-depositional migration of radionuclides, and hence studying cobbles offers major advantages compared to more conventional dating using sand- or silt-sized sediments. However, care must be taken when assessing the dose rate to the outermost ~2 mm of the cobbles because the dose rate changes rapidly through this upper layer (i.e. the outer 1 or 2 slices in this study, Fig. 4), meaning that small uncertainties in the assessment of the depth will result in large uncertainties in the dose rate (cf. Simkins et al., 2016).

4. Rapid assessment of the degree of bleaching of cobble surfaces

To maximise efficiency, a method was devised to screen cobble samples for suitability for further measurements by rapidly assessing whether or not a cobble face had been exposed to light prior to deposition. This initial screening involved extracting a core of material from each cobble face of interest, and removing a single slice from the surface of each core taken. A total of 23 cores were drilled from 10 cobbles, to assess the variability between different faces of the same cobble, and between cores taken adjacent to each other. The L_n/T_n ratio of these surface slices was determined using

both the $IRSL_{50}$ and post-IR $IRSL_{225}$ signals obtained during a single initial cycle of the SAR measurement procedure shown in Table 1 and using a test dose of ~34 Gy (Fig. 5). As might be expected, the L_n/T_n ratios measured using the $IRSL_{50}$ signals are normally lower than those measured using the post-IR $IRSL_{225}$ signal, both because the $IRSL_{50}$ signal bleaches more rapidly in daylight (e.g. Colarossi et al., 2015), and because the $IRSL_{50}$ signal is expected to suffer from anomalous fading more strongly than the post-IR $IRSL_{225}$ signal (Thomsen et al., 2008).

The 23 L_n/T_n values obtained (Fig. 5) span a wide range from 1.61 ± 0.04 to 9.01 ± 0.19 for the $IRSL_{50}$ signal, presumably reflecting differences in the exposure of the cobbles to daylight at the time when the sandur was deposited. Where two or more cores were taken from the same face of a well-bleached cobble, the L_n/T_n values were consistent for a given signal (e.g. L_n/T_n for $IRSL_{50}$ for core A of ORS04-1 is 1.99 ± 0.04 and for core B of the same cobble is 2.03 ± 0.04). Replicate measurements of unbleached surfaces showed greater scatter (e.g. data for ORS02-1 shown as blue diamonds in Fig. 5); this scatter is also observed when looking at L_n/T_n values for cores where the signal is at saturation (e.g. Fig. 6a). In some instances large differences were observed between different faces of the same cobble (e.g. cobble ORS02-1, Fig. 5), and within the small data set available the upper cobble surfaces were significantly better bleached than the lower cobble surfaces, implying that much of the bleaching of the cobbles occurred after deposition. The data shown in Fig. 5 suggest that the measurement of L_n/T_n ratios from the outer surface of cores removed from a cobble face is sufficient to serve as a rapid, initial screening test to infer the degree of bleaching of the cobbles prior to deposition, and hence to identify the suitability of the core material for further measurements. The validity of this rapid screening test is assessed in Section 5, by selecting a range of natural L_n/T_n ratios identified for surface slices in Fig. 5, and exploring how this signal changes with depth into the cobble.

5. Verifying bleaching by measuring changes in luminescence with depth into the cobble

Following the initial screening to identify those cobbles that were best bleached at deposition (Section 4), the variation in luminescence signal with depth was investigated, to explore whether the inferred pattern of bleaching at deposition had been correctly identified from the measurements of surface L_n/T_n ratios alone (Section 4). The remaining material from ten cores drilled from four of the cobble faces tested in Fig. 5 was sliced and used for this experiment. The cores were selected to span the range of surface L_n/T_n ratios observed in Section 4: duplicate cores were examined for surface slices with low L_n/T_n ratios, taken from the upper face of two different cobbles (cores A and B from cobble ORS04-1, and cores A and B from cobble ORS04-3); three cores were examined from across one cobble face with an intermediate L_n/T_n ratio for the surface slices (cores F, G and H from cobble ORS02-1), and three further cores were examined from the same cobble but taken from the lowermost face, which had a high L_n/T_n ratio for the surface slices (cores C, D and E from ORS02-1). The L_n/T_n ratios with depth into each of these ten cores was investigated, up to a maximum depth of ~25 mm into the cobbles.

Fig. 6a shows the variation in L_n/T_n ratio with depth for both the $IRSL_{50}$ and post-IR $IRSL_{225}$ signals, derived from triplicate cores (C,

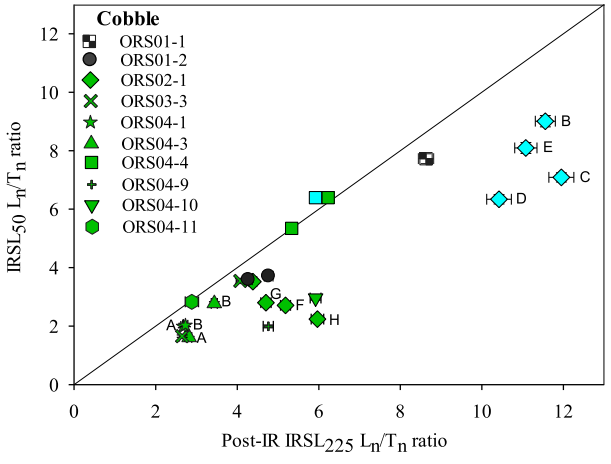

Fig. 5. A comparison of the $IRSL_{50}$ and post-IR $IRSL_{225}$ L_n/T_n ratios for 23 different granite surfaces with the location of the rock slices on the cobbles also illustrated (green – upper-face, black – side-face and blue – bottom-face of the cobbles). Individual cores from cobbles ORS02-1, ORS04-1 and ORS04-3 discussed in the text are labelled with their core letter. The large difference in bleaching from one face of a cobble to another is also illustrated here (see data for different faces of ORS02-1, green and blue diamond symbols). (For interpretation of the references to colour in this figure legend, the reader is referred to the Web version of this article.)

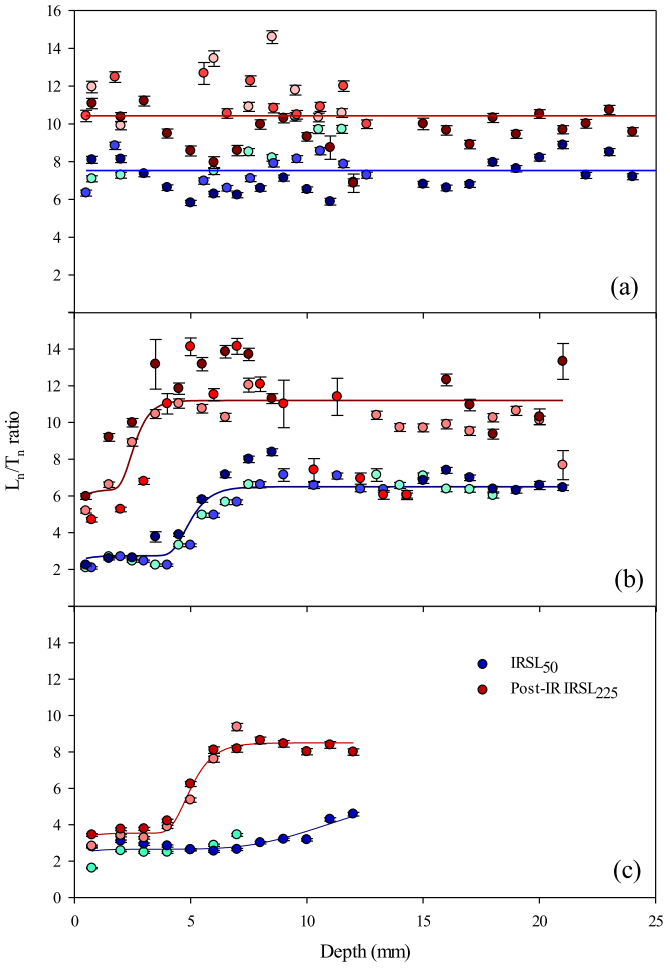

Fig. 6. L_n/T_n ratios for $IRSL_{50}$ (red shaded symbols) and post-IR $IRSL_{225}$ (blue shaded symbols) shown for each individual rock slice, with depth into cobbles with a range of sub-surface characteristics. Triplicate cores from cobble ORS02-1 (cores C, D and E in Fig. 6a, and cores F, G and H in Fig. 6b), and duplicate cores from cobble ORS04-3 (cores A and B, Fig. 6c) were taken, and illustrate similar L_n/T_n ratios with depth for rock slices from different cores. The solid lines in Fig. 6a–c illustrates the fitting of a bleaching model used by Freiesleben et al. (2015) to quantify exposure periods. (For interpretation of the references to colour in this figure legend, the reader is referred to the Web version of this article.)

D and E from ORS02-1), each of which had a high L_n/T_n ratio for the surface slices shown in Fig. 5 (Section 4). There is no obvious trend in the L_n/T_n data for either signal with depth (Fig. 6a), and the L_n/T_n ratios observed are relatively high, which is consistent with neither the $IRSL_{50}$ signal or the post-IR $IRSL_{225}$ signals having been bleached (Fig. 5), as also inferred from examination of the surface slices alone. The laboratory-saturation levels for the $IRSL_{50}$ and post-IR $IRSL_{225}$ signals were assessed for three slices from core E of ORS02-1 using a SAR protocol (Fig. 7), giving an L_x/T_x value of 10.4 ± 0.7 ($n = 3$ slices) for post-IR $IRSL_{225}$ signal saturation in the laboratory, similar to the level observed for the L_n/T_n values through the core (mean value $= 10.4 \pm 1.5$, $n = 3$ slices; Fig. 6a), which is also consistent with the idea that this surface of the cobble was not bleached prior to deposition. The similarity between the L_n/T_n ratio from the natural slices and the laboratory-determined L_x/T_x saturation values, also implies that the post-IR $IRSL_{225}$ signal in this study is not affected by anomalous fading. In contrast, the L_n/T_n values for the $IRSL_{50}$ signal from the same cores (average value 7.53 ± 1.06, $n = 3$ slices; Fig. 6a) are significantly lower than the laboratory-determined L_x/T_x saturation values for the $IRSL_{50}$ signal (11.9 ± 0.7, $n = 3$ slices; Fig. 7), implying that the $IRSL_{50}$ signal is subject to anomalous fading (see section 6).

The change in L_n/T_n ratio with depth for triplicate cores F, G and H from cobble ORS02-1 which had intermediate surface L_n/T_n values (Fig. 5; section 4), are shown in Fig. 6b. The L_n/T_n ratios for both the $IRSL_{50}$ and post-IR $IRSL_{225}$ signals for this face of cobble ORS02-1 (cores F, G and H) are lower than those observed for the un-bleached face of this same cobble, discussed above (cores C, D and E from ORS02-1; Fig. 6a). Additionally, the L_n/T_n values for the $IRSL_{50}$ signal are consistently lower than those from the post-IR $IRSL_{225}$ signal, partly due to the greater bleachability of the $IRSL_{50}$ signal (e.g. as demonstrated by Colarossi et al., 2015), but also likely due to the greater rate of anomalous fading for the $IRSL_{50}$ signal compared to the post-IR $IRSL_{225}$ signal. The enhanced bleachability of the $IRSL_{50}$ signal also results in the $IRSL_{50}$ signal being bleached to a greater depth than the post-IR $IRSL_{225}$ signal. However, at depths below ~7 mm and ~4 mm for $IRSL_{50}$ and post-IR $IRSL_{225}$ signals respectively (cores F, G, H in Fig. 6b), the L_n/T_n ratios are the same as those observed for the face that has not been bleached (cores C, D, and E in Fig. 6a). It is interesting to note that the change in L_n/T_n with depth in Fig. 6b is derived from the same cobble (ORS02-1) as the poorly-bleached cores shown in Fig. 6a, but from a different surface, showing the heterogeneous pattern of bleaching that is possible for a single clast. This emphasises the importance of recording the orientation of clasts on sampling, and considering the geomorphological processes at work prior to deposition.

The two cores (A and B) from cobble ORS04-3 (Fig. 6c) yielded low L_n/T_n ratios at their surfaces (Fig. 5), implying this surface of the cobble had been well-bleached on deposition. Here, both the $IRSL_{50}$ and post-IR $IRSL_{225}$ signals give low L_n/T_n ratios to much greater depths into the cobble sub-surface than for the cobble face considered in Fig. 6b. It is apparent, therefore, that there are significant differences recorded in these bleaching profiles (even for different faces of the same clast c.f. Fig. 6a and b), and the cobble surface in Fig. 6c has been exposed for a longer period of time than either of the surfaces shown in Fig. 6a and b. The bleaching profile in Fig. 6b is in-turn better bleached than that in Fig. 6a. This consideration of the bleaching profiles with depth, indicates that the initial L_n/T_n surface slice analysis effectively identified the well-bleached cobbles within the population at Orrisdale Head. To calculate an age, the data from those cores that show signs of having been bleached were selected, but the extent to which anomalous fading affects the $IRSL_{50}$ and post-IR $IRSL_{225}$ signals needs consideration.

6. Assessment of anomalous fading

Anomalous fading can be a significant issue when dating using feldspars (e.g. Huntley and Lamothe, 2001). The similarity between the laboratory saturation level for the post-IR $IRSL_{225}$ signal (Fig. 7; 10.4 ± 0.7) and the L_n/T_n ratio obtained from an unbleached cobble (Fig. 6a; 10.4 ± 1.5) imply that this signal is not affected by anomalous fading. In contrast, the $IRSL_{50}$ signal does appear to fade, based on the laboratory L_x/T_x versus natural L_n/T_n saturation values (cf. Figs. 7 and 6a). To quantify rates of fading, measurements were undertaken on 20 different granite rock slices, from cores taken from three different clasts (from two well-bleached cobbles (ORS04-1 and ORS04-3) and an exposed cobble from the foreshore of Orrisdale Head (ORS00-1)). Rock slices were irradiated (42.9 Gy) and preheated prior to storage for periods up to 1 month, following the method of Auclair et al. (2003). The average g-values were $2.53 \pm 0.65\%$ per decade ($n = 20$ slices) for the $IRSL_{50}$ signal, and $1.62 \pm 0.69\%$ per decade for the post-IR $IRSL_{225}$ signal ($n = 20$ slices) (Fig. 8). It is interesting to note that the g-value for the post-IR $IRSL_{225}$ signal is not zero, as was implied from the similarity between the natural and laboratory saturation values (Figs. 7 and 6a), although the measured g-value is within uncertainties of a value of

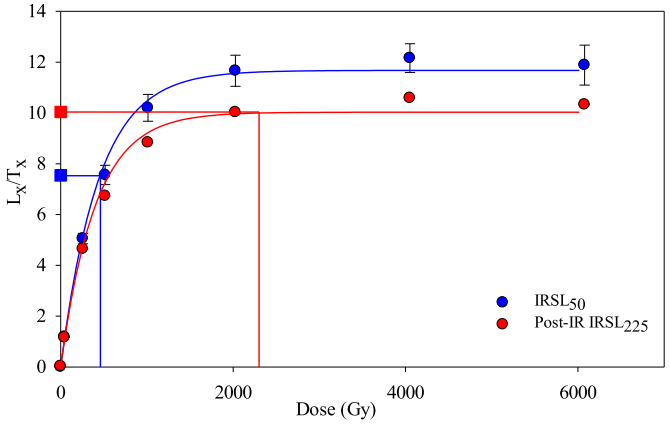

Fig. 7. $IRSL_{50}$ and post-IR $IRSL_{225}$ dose response curves for three rock slices (with each data point the average of these three slices) fitted with a double-saturating exponential equation. The dose-response curves show the saturated laboratory L_x/T_x values and allow comparison to the natural saturated signals (square symbols). The $IRSL_{50}$ signal yields an apparent D_e of 518 ± 40 Gy.

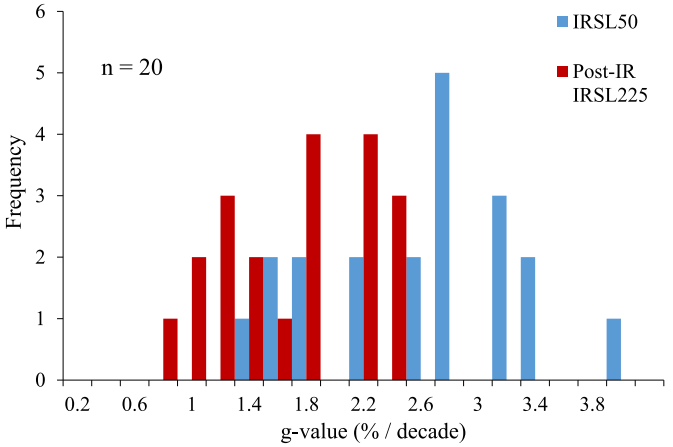

Fig. 8. g-values (%/decade) for both the $IRSL_{50}$ and post-IR $IRSL_{225}$ signals, showing a lower post-IR $IRSL_{225}$ fading value.

1.3 ± 0.3% per decade measured for quartz OSL by Thiel et al. (2011), a signal that is widely accepted not to fade. Both of these measurements illustrate the challenge of making and interpreting fading measurements in the laboratory, particularly where fading rates are low. Given the similarity of the fading rate measured for the post-IR $IRSL_{225}$ signal in this study and the apparent quartz OSL fading rates of Thiel et al. (2011), no correction is made in this study for fading of the post-IR $IRSL_{225}$ signal. The $IRSL_{50}$ age of each slice has been corrected using the method outlined in Huntley and Lamothe (2001) using the average measured fading rate of 2.53 ± 0.65% per decade. As discussed in the next section, even without correcting the post-IR $IRSL_{225}$ ages for fading, they consistently yield older ages than those derived from the $IRSL_{50}$ signal after correcting for fading.

7. Luminescence ages from cobbles and comparison with independent age control

Ages for rock slices from three cobbles are shown in Fig. 9a–c; the post-IR $IRSL_{225}$ ages are not corrected for fading, but the $IRSL_{50}$ ages are corrected as described in section 6. Each data point in Fig. 9 is the average D_e of two, or typically three slices from the same depth on the same clast face, divided by the dose rate for that specific slice-depth calculated following the method described in section 3. Independent age control (18.9 ± 1.0 to 20.3 ± 0.6 ka; Chiverrell et al., submitted; Smedley et al., 2017b) described previously (Section 2.1) is included on Fig. 9 as a light red horizontal bar. To calculate an age for the deposition of each cobble, the ages from different depths into the cobble sub-surface are combined as shown in Fig. 9.

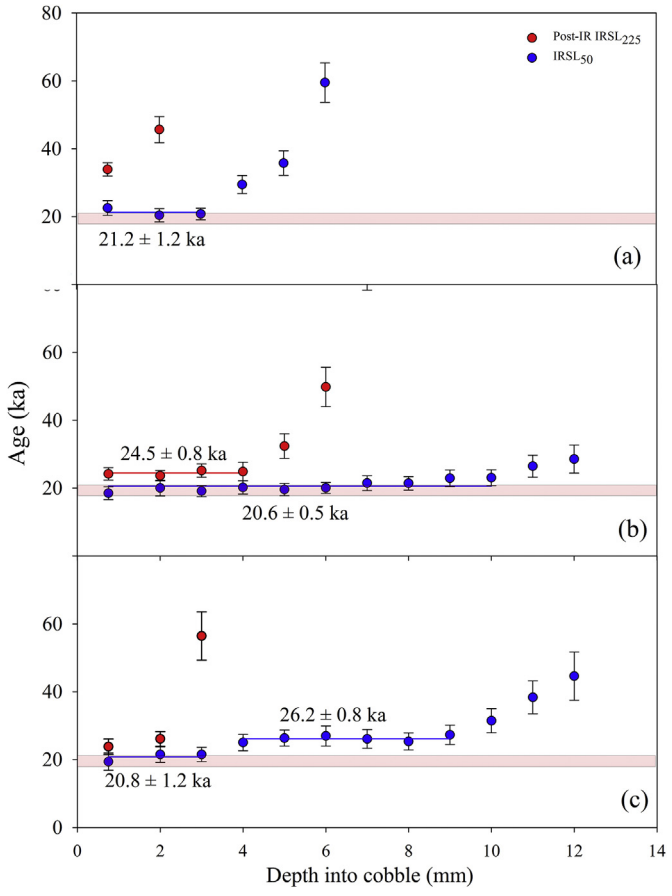

Fig. 9. Post-IR $IRSL_{225}$ (red) ages and fading-corrected $IRSL_{50}$ ages (blue) with depth into cobbles (a) ORS02-1, (b) ORS04-3, and (c) ORS04-1. The independent age control derived from Smedley et al. (2017b) and Chiverrell et al. (submitted) is also given in the light red shaded area (18.9 ± 1.0 ka to 20.3 ± 0.6 ka). (For interpretation of the references to colour in this figure legend, the reader is referred to the Web version of this article.)

The differences seen in the depth to which L_n/T_n ratios appear to be well bleached (Fig. 6) are reflected in the data in Fig. 9 when apparent ages are calculated for each slice. As expected, the $IRSL_{50}$ signal is seen to bleach to a greater depth into each of the three cobbles than the post-IR-$IRSL_{225}$ signal. For all three cobbles, slices from the outermost portion of each core give $IRSL_{50}$ ages which are consistent with one another. For cobble ORS02-1 (Fig. 9a) slices from the uppermost 2.8 mm (3 slices from each of 3 cores on the same cobble face) give an average fading-corrected $IRSL_{50}$ age of 21.2 ± 1.2 ka (n = 9 slices); for cobble ORS04-3 (Fig. 9b) the uppermost ~9 mm (10 slices from each of 3 cores) give a fading-corrected $IRSL_{50}$ age of 20.6 ± 0.5 ka (n = 27 slices, as 3 slices were lost at the base of one core); and the uppermost 3 slices of cobble ORS04-1 (Fig. 9c) give a fading-corrected $IRSL_{50}$ age of 20.8 ± 1.2 ka (n = 9 slices). These slices nearest the surface of these three cores (Fig. 9a–c) give ages that are similar to one another, yielding a mean age for the deposit of 20.7 ± 0.3 ka (n = 45 slices).

The post-IR $IRSL_{225}$ ages show a monotonic increase with depth into the core for two of the three samples (cobbles ORS02-1 and ORS04-1; Fig. 9a and c), and so it is not possible to be confident from these data alone that the surface post-IR $IRSL_{225}$ signals were bleached. The fading-corrected $IRSL_{50}$ ages show that cobble ORS04-3 is the clast that has been bleached to the greatest depth (>9 mm; Fig. 9b), and the post-IR $IRSL_{225}$ ages from the uppermost ~4 mm of this cobble are also consistent with one another, suggesting that this clast was well bleached at deposition. The mean post-IR $IRSL_{225}$ age for cobble ORS04-3 is 24.5 ± 0.8 ka (n = 9 slices), whilst the corresponding mean fading-corrected $IRSL_{50}$ age is significantly younger, being 20.6 ± 0.5 ka (n = 27 slices). These paired age determinations, measured for the same slices, do not agree with each other within two sigma uncertainties, and only the $IRSL_{50}$ age is in agreement with the independent age control for the site of 18.9 ± 1.0 to 20.3 ± 0.6 ka (Chiverrell et al., submitted; Smedley et al., 2017b). The disagreement between the $IRSL_{50}$ and post-IR $IRSL_{225}$ ages is intriguing. The consistency in the post-IR $IRSL_{225}$ ages with depth imply that although this signal is harder to bleach than the $IRSL_{50}$ signal, nevertheless it was uniformly reset to a depth of almost 4 mm at deposition (see also Fig. 6c). Some research has suggested that there could be an unbleachable component in the post-IR $IRSL_{225}$ signal, but the magnitude of this appears to be ~1–2 Gy (Thomsen et al., 2008; Smedley et al., 2015) and would equate to less than a few hundred years in the present study. It is also noteworthy that an overestimate of D_e was observed in the post-IR $IRSL_{225}$ signal dose-recovery experiment using a dose applied to a naturally-bleached cobble from the beach (32% overestimate, Table 2), though this effect was not seen when a sample was artificially bleached in the laboratory (Table 2). At present, the reason for the difference between the ages from the $IRSL_{50}$ and post-IR $IRSL_{225}$ signals is not known, but the greater sensitivity to daylight exposure of the $IRSL_{50}$ signal makes it the optimal signal for dating in this type of environment, and the fading-corrected $IRSL_{50}$ ages generated are shown to agree with the available independent age control.

In cobble ORS04-1 (Fig. 9c) the $IRSL_{50}$ ages are consistent for the three uppermost slices, a pattern similar to that seen in the other two sets of measurements in Fig. 9 (a & b). If the cobble records a single episode of sunlight exposure then one would expect the D_e (and apparent age) to increase monotonically below some point in the cobble. This is seen for cobble ORS02-1 (Fig. 9a) which rises steeply until the samples are in field saturation (as seen in Fig. 6c).

In contrast, the ages for cobble ORS04-1 rise to a second plateau (Fig. 9c), giving an average age of 26.2 ± 0.8 ka (n = 12 slices) from a depth of ~3.5–8.5 mm. The consistency in the age implies that the cobble had been bleached fully to a depth of ~8.5 mm at that time and then buried. Subsequently the cobble was moved a second time (re-worked), but this time only exposed for sufficient time such that the upper ~3 mm was fully bleached, and then deposited finally at 20.8 ± 1.2 ka. Since the depositional context in which this earlier event took place is not known, it is difficult to be confident of the palaeoenvironmental significance of this earlier resetting event. However, it is possible that this earlier event may relate to the advance of the Irish Sea Ice Stream, as modelled by Chiverrell et al. (2013) using the limited radiocarbon evidence available from the Irish Sea Basin.

The age of 20.7 ± 0.3 ka derived from the average of the fading-corrected $IRSL_{50}$ ages (n = 45 slices) from the 3 cobbles shown in Fig. 9 is almost identical to the revised retreat age (20.3 ± 0.6 ka; Smedley et al., 2017b) for the margin of the Irish Sea Ice Stream as it crossed the Isle of Anglesey ~70 km to the south of the study site, and implies that once the Irish Sea Ice Stream retreated past the pinning point formed by the Isle of Anglesey, recession then occurred very rapidly.

8. Conclusions

This paper examined the application of luminescence dating to cobbles from a glaciofluvial environment. The importance of careful sample site selection and of recording the orientation of cobbles was highlighted through the targeted sampling of bar-top lithofacies to maximise the likelihood of exposure to sunlight, which demonstrated that the up-orientated surfaces of the cobbles were the best-bleached on deposition, some to depths of up to 12 mm in granite. A procedure was developed to rapidly identify the best-bleached cobbles by measuring the L_n/T_n ratio of the surface rock slices from cobbles, without the need for further slicing or analysis of the deeper material drilled from the cobbles. The variable nature of the bleaching opportunities within a glaciofluvial deposit was demonstrated, with some cobbles giving a consistent value for age across several mm depth into the cobble implying that the luminescence signal had been fully-reset on deposition, whilst others showed little sign of resetting at deposition, giving a rapid increase in apparent age with depth from the surface. In accordance with studies on sand-sized grains, the $IRSL_{50}$ signal is reset more rapidly and to a greater depth than the post-IR $IRSL_{225}$ signal, with only one cobble showing evidence of the post-IR $IRSL_{225}$ signal being well-bleached on deposition. Only cobbles offer this clear assessment of whether the luminescence signal was completely reset at deposition, thereby avoiding the need for application of the complex statistical models used when dating sand-sized sediment grains in similar glaciofluvial settings. A further advantage to working with cobbles is that the dose rate is much less sensitive to variations in water content than is the dose to sand-sized grains. This is clearly advantageous in glacial or glaciofluvial settings where water contents can reach high values, and can vary over the time since deposition. At a depth of 2 mm or more into the surface, more than 90% of the dose rate arises from the cobble itself rather than its surroundings, and this dose rate is not influenced by water in the surrounding sediment.

The fading-corrected $IRSL_{50}$ ages from three well-bleached cobble faces yield reproducible ages, giving a mean age of 20.7 ± 0.3 ka (n = 45 slices), in agreement with independent age control provided by Chiverrell et al. (submitted) and Smedley et al. (2017b). In one of the well-bleached cobbles, the $IRSL_{50}$ data shows evidence of two discrete exposure events and this single clast potentially records both the advance of the Irish Sea ice stream at 26.2 ± 0.8 ka, as well as its retreat at 20.7 ± 0.3 ka, providing further constraint on the pace of rapid ice marginal retreat in the northern Irish Sea basin. This study is the first to successfully date glaciofluvial sediments using cobbles, demonstrating a number of advantages of working with cobbles as a substrate for dating and highlighting the potential for the use of cobbles in future dating studies of glacial sediments.

Acknowledgments

This paper was supported by a Natural Environment Research Council consortium grant (BRITICE-CHRONO NE/J008672/1). We thank Professor Andrew Murray and Vicki Hansen at the Nordic Laboratory for Luminescence Dating for gamma irradiating rock slices for calibration. GTHJ thanks Aberystwyth University for a DCDS Postgraduate Scholarship, DGES for contributing to fieldwork costs, and the QRA for a conference award to allow the work to be presented at the International Luminescence and Electron Spin Resonance dating conference in 2017. We also thank Dr Rachel Smedley for assistance in the field and Miss Hollie Wynne for assistance in the laboratory. Two anonymous referees are thanked for their comments which improved this paper.

Appendix A. Supplementary data

Supplementary data related to this article can be found at https://doi.org/10.1016/j.quascirev.2018.05.036.

References

Aitken, M.J., 1985. Thermoluminescence Dating. Academic press.
Auclair, M., Lamothe, M., Huot, S., 2003. Measurement of anomalous fading for feldspar IRSL using SAR. Radiat. Meas. 37, 487–492.
Bøtter-Jensen, L., Mejdahl, V., 1988. Assessment of beta dose-rate using a GM multicounter system. Nucl. Tracks Radiat. Meas. 14, 187–191.
Bøtter-Jensen, L., Andersen, C.E., Duller, G.A.T., Murray, A.S., 2003. Developments in radiation, stimulation and observation facilities in luminescence measurements. Radiat. Meas. 37, 535–541.
Buylaert, J.P., Murray, A.S., Thomsen, K.J., Jain, M., 2009. Testing the potential of an elevated temperature IRSL signal from feldspar. Radiat. Meas. 44, 560–565.
Chiverrell, R.C., Thrasher, I.M., Thomas, G.S., Lang, A., Scourse, J.D., van Landeghem, K.J.J., McCarroll, D., Clark, C.D., O'Cofaigh, C., Evans, D.J.A., Ballantyne, C.K., 2013. Bayesian modelling the retreat of the Irish Sea ice stream. J. Quat. Sci. 28, 200–209.
Chiverrell, R.C., Smedley, R.K., Small, D., Ballantyne, C.K., Burke, M.J., Callard, L., Clark, C., Duller, G.A.T., Evans, D.J.A., Fabel, D., Van Landeghem, K.J.J., Livingstone, S., O Cofaigh, C., Thomas, G.S.P., Roberts, D., Saher, M., Scourse, J.D., Wilson, P., Submitted. Ice margin oscillations during deglaciation of the northern Irish Sea basin. J. Quat. Sci..
Colarossi, D., Duller, G.A.T., Roberts, H.M., Tooth, S., Lyons, R., 2015. Comparison of paired quartz OSL and feldspar post-IR IRSL dose distributions in poorly bleached fluvial sediments from South Africa. Quat. Geochronol. 30, 233–238.
Duller, G.A.T., 2004. Luminescence dating of Quaternary sediments: recent advances. J. Quat. Sci. 19, 183–192.
Duller, G.A.T., 2008. Single grain optical dating of Quaternary sediments: why aliquot size matters in luminescence dating. Boreas 37, 589–612.
Freiesleben, T., Sohbati, R., Murray, A., Jain, M., Al Khasawneh, S., Hvidt, S., Jakobsen, B., 2015. Mathematical model quantifies multiple daylight exposure and burial events for rock surfaces using luminescence dating. Radiat. Meas. 81, 16–22.
Galbraith, R.F., Roberts, R.G., 2012. Statistical aspects of equivalent dose and error calculation and display in OSL dating: an overview and some recommendations. Quat. Geochronol. 11, 1–27.
Galbraith, R.F., Roberts, R.G., Laslett, G.M., Yoshida, H., Olley, J.M., 1999. Optical dating of single and multiple grains of quartz from Jinmium rock shelter, northern Australia: Part I, experimental design and statistical models. Archaeometry 41, 339–364.
Guérin, G., Mercier, N., Adamiec, G., 2011. Dose-rate conversion factors: update. Ancient TL 29, 5–8.
Habermann, J., Schilles, T., Kalchgruber, R., Wagner, G.A., 2000. Steps towards surface dating using luminescence. Radiat. Meas. 32, 847–851.
Huntley, D.J., Baril, M.R., 1997. The K content of the K-feldspars being measured in optical dating or in thermoluminescence dating. Ancient TL 15, 11–13.
Huntley, D.J., Lamothe, M., 2001. Ubiquity of anomalous fading in K-feldspars and the measurement and correction for it in optical dating. Can. J. Earth Sci. 38,

Appendix A

1093–1106.
Ou, X.J., Duller, G.A.T., Roberts, H.M., Zhou, S.Z., Lai, Z.P., Chen, R., Chen, R., Zeng, L., 2015. Single grain optically stimulated luminescence dating of glacial sediments from the Baiyu Valley, southeastern Tibet. Quat. Geochronol. 30, 314–319.
Polikreti, K., Michael, C.T., Maniatis, Y., 2002. Authenticating marble sculpture with thermoluminescence. Ancient TL 20, 11–18.
Prescott, J.R., Hutton, J.T., 1994. Cosmic ray contributions to dose rates for luminescence and ESR dating: large depths and long-term time variations. Radiat. Meas. 23, 497–500.
Rees-Jones, J., 1995. Optical dating of young sediments using fine-grain quartz. Ancient TL 13, 9–14.
Simkins, L.M., DeWitt, R., Simms, A.R., Briggs, S., Shapiro, R.S., 2016. Investigation of optically stimulated luminescence behavior of quartz from crystalline rock surfaces: a look forward. Quat. Geochronol. 36, 161–173.
Small, D., Smedley, R.K., Chiverrell, R.C., Scourse, J.D., O Cofaigh, C., Duller, G.A.T., McCarron, S., Burke, M.J., Evans, D.J.A., Fabel, D., Gheorghiu, D.M., Thomas, G.S.P., Xu, S., Clark, C.D., 2018. Trough geometry was a greater influence than climate-ocean forcing in regulating retreat of the marine-based Irish-Sea Ice Stream. Geol. Soc. Am. Bull. Accepted: https://doi.org/10.1130/B31852.1.
Smedley, R.K., Duller, G.A.T., Roberts, H.M., 2015. Bleaching of the post-IR IRSL signal from individual grains of K-feldspar: implications for single-grain dating. Radiat. Meas. 79, 33–42.
Smedley, R.K., Glasser, N.F., Duller, G.A.T., 2016. Luminescence dating of glacial advances at Lago Buenos Aires (~46 °S), Patagonia. Quat. Sci. Rev. 134, 59–73.
Smedley, R.K., Scourse, J.D., Small, D., Hiemstra, J.F., Duller, G.A.T., Bateman, M.D., Burke, M.J., Chiverrell, R.C., Clark, C.D., Davies, S.M., Fabel, D., Gheorghiu, D.M., McCarroll, D., Medialdea, A., Xu, S., 2017a. New age constraints for the limit of the British–Irish ice sheet on the Isles of Scilly. J. Quat. Sci. 32, 48–62.
Smedley, R.K., Chiverrell, R.C., Ballantyne, C.K., Burke, M.J., Clark, C.D., Duller, G.A.T., Fabel, D., McCarroll, D., Scourse, J.D., Small, D., Thomas, D.S.G., 2017b. Internal dynamics condition centennial-scale oscillations in marine-based ice-stream retreat. Geology 45, 787–790.
Sohbati, R., Murray, A.S., Buylaert, J.P., Almeida, N.A., Cunha, P.P., 2012. Optically stimulated luminescence (OSL) dating of quartzite cobbles from the Tapada do Montinho archaeological site (east-central Portugal). Boreas 41, 452–462.
Sohbati, R., Murray, A.S., Porat, N., Jain, M., Avner, U., 2015. Age of a prehistoric "Rodedian" cult site constrained by sediment and rock surface luminescence dating techniques. Quat. Geochronol. 30, 90–99.
Svendsen, J.I., Alexanderson, H., Astakhov, V.I., Demidov, I., Dowdeswell, J.A., Funder, S., Gataullin, V., Henriksen, M., Hjort, C., Houmark-Nielsen, M., Hubberten, H.W., Ingolfsson, O., Jakobsson, M., Kjaer, K.H., Larsen, E., Lokrantz, H., Lunkka, J.P., Lysa, A., Mangerud, J., Matiouchkov, A., Murray, A., Moller, P., Niessen, F., Nikolskaya, O., Polyak, L., Saarnisto, M., Siegert, C., Siegert, M.J., Spielhagen, R.F., Stein, R., 2004. Late Quaternary ice sheet history of northern Eurasia. Quat. Sci. Rev. 23, 1229–1271.
Thiel, C., Buylaert, J.P., Murray, A., Terhorst, B., Hofer, I., Tsukamoto, S., Frechen, M., 2011. Luminescence dating of the Stratzing loess profile (Austria)–Testing the potential of an elevated temperature post-IR IRSL protocol. Quat. Int. 234, 23–31.
Thomas, G.S.P., Connaughton, M., Dackombe, R.V., 1985. Facies variation in a Late Pleistocene supraglacial outwash sandur from the Isle of Man. Geol. J. 20, 193–213.
Thomas, G.S.P., Chiverrell, R.C., Huddart, D., Long, D., Roberts, D., 2006a. The ice age. In: Chiverrell, R.C., Thomas, G.S.P. (Eds.), A New History of the Isle of Man: the Evolution of the Natural Landscape. Liverpool University Press, Liverpool, pp. 100–150.
Thomas, P.J., Murray, A.S., Kjaer, K.H., Funder, S., Larsen, E., 2006b. Optically stimulated luminescence (OSL) dating of glacial sediments from Arctic Russia - depositional bleaching and methodological aspects. Boreas 35, 587–599.
Thomsen, K.J., Murray, A.S., Jain, M., Bøtter-Jensen, L., 2008. Laboratory fading rates of various luminescence signals from feldspar-rich sediment extracts. Radiat. Meas. 43, 1474–1486.
Thrasher, I.M., Mauz, B., Chiverrell, R.C., Lang, A., Thomas, G.S.P., 2009. Testing an approach to OSL dating of Late Devensian glaciofluvial sediments of the British Isles. J. Quat. Sci. 24, 785–801.
Vafiadou, A., Murray, A.S., Liritzis, I., 2007. Optically stimulated luminescence (OSL) dating investigations of rock and underlying soil from three case studies. J. Archaeol. Sci. 34, 1659–1669.

Supplementary Information

This document contains supplementary information for the article:

Jenkins, G.T.H., Duller, G.A.T., Roberts, H.M., Chiverrell, R.C. and Glasser, N.F. “A new approach for luminescence dating glaciofluvial deposits - high precision optical dating of cobbles” published in Quaternary Science Reviews

Table S1: L_n/T_n values for rock slices from Orrisdale, Data are shown graphically in Figure 6a.

ORS02-1-C					***ORS02-1-D***					***ORS02-1-E***				
Depth (mm)	*$IRSL_{50}$*		*Post-IR $IRSL_{225}$*		*Depth (mm)*	*$IRSL_{50}$*		*Post-IR $IRSL_{225}$*		*Depth (mm)*	*$IRSL_{50}$*		*Post-IR $IRSL_{225}$*	
0.75	7.09	± 0.15	11.95	± 0.31	0.5	6.34	± 0.16	10.42	± 0.30	0.75	8.10	± 0.19	11.08	± 0.27
2	7.28	± 0.15	9.90	± 0.22	1.5	8.84	± 0.19	12.48	± 0.28	2	8.13	± 0.18	10.36	± 0.23
6	7.51	± 0.18	13.46	± 0.41	5.5	6.97	± 0.16	12.67	± 0.58	3	7.36	± 0.16	11.21	± 0.26
7.5	8.51	± 0.18	10.90	± 0.24	6.5	6.59	± 0.15	10.55	± 0.25	4	6.62	± 0.15	9.49	± 0.24
8.5	8.20	± 0.17	14.59	± 0.34	7.5	7.10	± 0.15	12.27	± 0.28	5	5.82	± 0.14	8.57	± 0.26
9.5	10.37	± 0.22	11.79	± 0.26	8.5	7.90	± 0.18	10.83	± 0.24	6	6.29	± 0.14	7.95	± 0.31
10.5	9.70	± 0.21	10.34	± 0.23	9.5	8.14	± 0.18	10.48	± 0.23	7	6.23	± 0.14	8.59	± 0.27
11.5	9.71	± 0.21	10.57	± 0.23	10.5	8.55	± 0.19	10.90	± 0.24	8	6.58	± 0.15	9.97	± 0.25
					11.5	7.86	± 0.17	12.00	± 0.28	9	7.13	± 0.16	10.30	± 0.25
					12.5	7.28	± 0.16	9.98	± 0.23	10	6.52	± 0.15	9.31	± 0.23
										11	5.88	± 0.18	8.74	± 0.62
										12	6.91	± 0.18	6.86	± 0.49
										15	6.80	± 0.15	10.00	± 0.31
										16	6.61	± 0.15	9.65	± 0.25
										17	6.79	± 0.15	8.91	± 0.23
										18	7.96	± 0.17	10.31	± 0.24
										19	7.63	± 0.17	9.45	± 0.21
										20	8.21	± 0.18	10.52	± 0.23
										21	8.88	± 0.19	9.69	± 0.21
										22	7.27	± 0.16	10.00	± 0.23
										23	8.51	± 0.19	10.74	± 0.24
										24	7.20	± 0.16	9.58	± 0.22

Table S2: L_n/T_n values for rock slices from Orrisdale, Data are shown graphically in Figure 6b.

ORS02-1-F					***ORS02-1-G***					***ORS02-1-H***				
Depth					*Depth*					*Depth*				
(mm)	*$IRSL_{50}$*		*Post-IR $IRSL_{225}$*		*(mm)*	*$IRSL_{50}$*		*Post-IR $IRSL_{225}$*		*(mm)*	*$IRSL_{50}$*		*Post-IR $IRSL_{225}$*	
0.5	2.71	± 0.04	5.19	± 0.12	0.75	2.08	± 0.07	4.70	± 0.13	0.5	2.24	± 0.05	5.97	± 0.15
1.5	2.69	± 0.06	6.61	± 0.15	2	2.69	± 0.06	5.26	± 0.12	1.5	2.58	± 0.06	9.19	± 0.21
2.5	2.90	± 0.06	8.91	± 0.20	3	2.45	± 0.06	6.79	± 0.16	2.5	2.63	± 0.06	9.99	± 0.24
3.5	3.19	± 0.07	10.46	± 0.24	4	2.23	± 0.07	11.02	± 0.56	3.5	3.77	± 0.29	13.17	± 1.35
4.5	4.29	± 0.07	11.03	± 0.25	5	3.31	± 0.08	14.12	± 0.48	4.5	3.89	± 0.09	11.85	± 0.31
5.5	6.11	± 0.07	10.75	± 0.24	6	4.95	± 0.11	11.52	± 0.33	5.5	5.79	± 0.13	13.18	± 0.36
6.5	7.34	± 0.07	10.28	± 0.22	7	5.66	± 0.13	14.15	± 0.43	6.5	7.15	± 0.16	13.85	± 0.34
7.5	7.06	± 0.06	12.04	± 0.38	8	6.61	± 0.17	12.09	± 0.39	7.5	7.99	± 0.18	13.71	± 0.34
13	9.05	± 0.07	10.39	± 0.23	9	7.14	± 0.35	11.01	± 1.30	8.5	8.38	± 0.19	11.30	± 0.26
14	8.37	± 0.08	9.72	± 0.21	10.3	6.57	± 0.17	7.41	± 0.62	15	6.84	± 0.15	17.36	± 0.62
15	7.56	± 0.09	9.70	± 0.22	11.3	7.09	± 0.16	11.40	± 1.01	16	7.39	± 0.16	12.32	± 0.32
16	6.49	± 0.10	9.89	± 0.24	12.3	6.37	± 0.15	6.94	± 0.30	17	6.99	± 0.15	10.95	± 0.32
17	6.82	± 0.15	9.52	± 0.23	13.3	6.35	± 0.14	6.05	± 0.24	18	6.37	± 0.15	9.36	± 0.27
18	6.81	± 0.15	10.26	± 0.23	14.3	6.02	± 0.14	6.04	± 0.25	19	6.29	± 0.14	20.28	± 1.40
19	7.30	± 0.16	10.63	± 0.25						20	6.57	± 0.22	10.31	± 0.43
20	6.93	± 0.15	10.12	± 0.23						21	6.44	± 0.15	13.33	± 0.97
21	6.16	± 0.22	7.67	± 0.79										

Table S2: L_n/T_n values for rock slices from Orrisdale, Data are shown graphically in Figure 6c.

ORS04-3-A					***ORS04-3-B***				
Depth (mm)	*$IRSL_{50}$*		*Post-IR $IRSL_{225}$*		*Depth (mm)*	*$IRSL_{50}$*		*Post-IR $IRSL_{225}$*	
0.75	1.61	± 0.04	2.82	± 0.07	0.75	2.78	± 0.06	3.44	± 0.07
2	2.57	± 0.06	3.41	± 0.07	2	3.10	± 0.07	3.76	± 0.08
3	2.48	± 0.06	3.28	± 0.07	3	2.93	± 0.06	3.78	± 0.08
4	2.49	± 0.06	3.88	± 0.08	4	2.83	± 0.06	4.21	± 0.09
5	2.62	± 0.06	5.36	± 0.12	5	2.63	± 0.06	6.24	± 0.14
6	2.87	± 0.06	7.60	± 0.16	6	2.54	± 0.06	8.10	± 0.18
7	3.44	± 0.07	9.37	± 0.20	7	2.64	± 0.06	8.17	± 0.18
					8	3.01	± 0.07	8.63	± 0.19
					9	3.20	± 0.07	8.45	± 0.18
					10	3.17	± 0.07	8.02	± 0.17
					11	4.29	± 0.09	8.38	± 0.18
					12	4.58	± 0.10	7.99	± 0.17